VIRTUAL ELEMENT METHODS FOR GENERAL LINEAR SECOND-ORDER HYPERBOLIC PROBLEMS ON POLYGONAL MESHES

by

GOURANGA PRADHAN

DEPARTMENT OF MATHEMATICS

INDIAN INSTITUTE OF TECHNOLOGY GUWAHATI

GUWAHATI-781039, INDIA

July, 2023

VIRTUAL ELEMENT METHODS FOR GENERAL LINEAR SECOND-ORDER HYPERBOLIC PROBLEMS ON POLYGONAL MESHES

A thesis submitted

in partial fulfillment of the requirements

for the degree of

DOCTOR OF PHILOSOPHY

by

GOURANGA PRADHAN

(Roll No. 186123008)

Under the supervision of
Prof. Bhupen Deka

Department of Mathematics

INDIAN INSTITUTE OF TECHNOLOGY GUWAHATI

July, 2023

This thesis

is dedicated

to

my family

CERTIFICATE

It is certified that the work contained in this thesis entitled **"Virtual Element Methods for General Linear Second-Order Hyperbolic Problems on Polygonal Meshes"** by **Gouranga Pradhan**, a student of Department of Mathematics, Indian Institute of Technology Guwahati, for the award of the degree of Doctor of Philosophy has been carried out under my supervision and that this work has not been submitted elsewhere for a degree.

July, 2023

Prof. Bhupen Deka
Professor
Department of Mathematics
Indian Institute of Technology Guwahati

ACKNOWLEDGEMENT

This thesis would not have been possible without the love and support of some people, who are always with me directly or indirectly. I take this opportunity to acknowledge them and extend my sincere gratitude.

First and foremost, I want to give my warmest thanks to my supervisor Prof. Bhupen Deka who made this work possible. His guidance and advice carried me through all the stages of writing my thesis. I would like to express sincere gratitude to my doctoral committee: Prof. R. K. Sinha, Prof. D.C. Dalal and Prof. S.N. Bora, Department of Mathematics, for their thoughtful comments and suggestions during the progress of my research.

I sincerely acknowledge IIT Guwahati for providing me various facilities necessary to carry out my research. I am most grateful to Council of Scientific & Industrial Research (CSIR), Government of India, for providing me financial assistance during my PhD work.

I am also grateful to all the faculty members, staff members and research scholars of the Department of Mathematics for their kind support and help. I would like to thank my seniors Naresh, Jogen, Kuldeep, Shyam, Shamik, Uttam and Deepak for helping and encouraging me like an elder brother. I would also like to thank my friends Sutapa, Raman, Arun, Monu, Khyodeno, Shiva, Gaurav, Sunil, Mahesh and Rahul for easing my life at IIT Guwahati with their presence.

I also want to give special thanks to my family for their continuous support and understanding during this period. Your prayer for me was what sustained me this far.

Finally, I would like to thank God for letting me through all the difficulties. You are the one who let me finish my degree.

June, 2023

Gouranga Pradhan

Department of Mathematics

Indian Institute of Technology Guwahati

ABSTRACT

Virtual element method (VEM) is a recently developed numerical technique that provides accurate and flexible solutions to complex problems in various fields of engineering and science. This thesis focuses on the development of VEM for the general second-order hyperbolic problems on polygonal meshes. The main objective of this research is to explore the capabilities of VEM for solving various hyperbolic problems and to compare its performance with other existing methods. These problems involve additional damping terms (weak damping and/or strong damping terms) in addition to the standard wave equations and require further analysis to derive optimal convergence results.

The collection of existing literature suggests that finite element methods (FEMs) are the most suitable approximation techniques on simple geometries due to their wide applicability. But, in the case of complex geometries that use general polytopal (polygonal or polyhedral) discretization, implementing higher order methods becomes very complicated. Use of general polytopal meshes provides greater flexibility in both numerical approximation and mesh generation. The polygonal FEM can handle hybrid meshes using generalized non-polynomial shape functions. But the use of such non-polynomial shape functions requires higher computational cost. Another method that can handle polytopal discretization is the mimetic finite difference method, which uses only degrees of freedom and doesn't have test and trial functions inside the elements leading to complexity in analysis and implementation. The increasing popularity of polytopal elements in scientific and engineering literature has encouraged the development of numerical methods which can efficiently deal with such type of element discretization. In this race VEM has came out as a suitable numerical technique for solving partial differential equations (PDEs) on polytopal meshes.

At first, we develop the virtual element methods for weakly damped wave equations on polygonal meshes. In both the L^2 norm and the H^1 semi-norm optimal convergence rates are established for the semi-discrete approximation. We employ the Crank-Nicolson temporal discretization scheme for the fully discrete problem and derive the convergence

analysis. Next, we proceed to discuss the virtual element method for pulsed electric field model problems on polygonal meshes. We have presented both the spatially semi-discrete approximation and Crank-Nicolson based fully discrete approximation, and derived the convergence analysis for both the approximations. We define a new non-standard projection operator motivated from the finite element solution of the pulsed electric field model problems. In our third and fourth problem, we design and analyse the virtual element methods for second-order Sobolev equations and viscoelastic wave equations, respectively. For these problems with distinct variable coefficients for diffusion and damping terms, obtaining optimal error estimates in L^2 norm is not possible without the use of the newly defined non-standard projection operator. For the time discretization, we have used implicit second-order Newmark scheme and optimal convergence rates in both the L^2 norm and the H^1 semi-norm are established. Fully discrete virtual element methods with second-order accuracy in temporal direction require to choose smaller time steps in order to preserve the higher accuracy provided by spatial direction. To overcome this restriction higher-order time stepping methods are needed. In our last work the general Newmark scheme for temporal discretization is considered along with the virtual element discretization in space for the wave equations on polygonal meshes. Rigorous analysis has been done on the stability and convergence of the proposed method. Optimal convergence is obtained in spatial direction along with up to fourth-order convergence in time for some special cases.

The research will include the development of algorithms and codes for the implementation of VEM, and several numerical experiments have been performed to demonstrate the accuracy, efficiency, flexibility and robustness of each proposed algorithms. All the mesh generations and computations are carried out using the MATLAB software. The results of this research are expected to provide valuable insights into the use of VEM for time-dependent hyperbolic problems and to contribute to the advancement of numerical techniques in this field.

Contents

List of Figures

List of Tables

1 Introduction

This chapter is introductory and includes a description of the problems, some notations, and preliminary material. It also includes a brief survey of the relevant literature and motivation behind the current study. The chapter-wise description of the thesis is reported in the last section of this chapter.

1.1 Problem Description

In this work, we study and analyse the virtual element methods for general second-order hyperbolic equations of the following form:

$$\gamma(x)u_{tt} + \kappa(x)u_t + \delta(x)u - \nabla.(\sigma(x)\nabla u + \epsilon(x)\nabla u_t) = f(x,t) \text{ for } (x,t) \in \Omega \times (0,T], \quad (1.1.1)$$

with initial and boundary conditions

$$u(x,0) = u_0, \quad u_t(x,0) = v_0 \text{ for } x \in \Omega \ \ \& \ \ u(x,t) = 0 \text{ for } (x,t) \in \partial\Omega \times (0,T], \qquad (1.1.2)$$

where Ω is a convex polygonal domain in $\mathbb{R}^2$ with a Lipschitz boundary $\partial\Omega$ and $T < \infty$ is the finite terminal observation time. Here, the physical coefficients $\gamma, \kappa, \delta, \sigma, \epsilon \in L^\infty(\Omega)$ are positive real-valued functions on Ω, and f denotes the forcing function. Further, $u_0,\ v_0 : \Omega \to \mathbb{R}$ are initial data. The physical coefficients, forcing function and initial data are assumed to be smooth functions in their respective domains of definition. Additional regularity assumptions were made throughout the thesis to carry out the convergence analysis.

Equation (1.1.1) is interesting as it represents different classes of physical problems for different choices of the coefficients. Our objective will be to apply virtual element methods for each problem separately.

Weakly Damped Wave Equation: For $\gamma = 1$ and $\delta = 0 = \epsilon$, we have the following weakly damped wave equation:

$$u_{tt} + \kappa(x)u_t - \nabla.(\sigma(x)\nabla u) = f(x,t) \text{ for } (x,t) \in \Omega \times (0,T], \tag{1.1.3}$$

with initial and boundary conditions

$$u(x,0) = u_0, \;\; u_t(x,0) = v_0 \text{ for } x \in \Omega \;\; \& \;\; u(x,t) = 0 \text{ for } (x,t) \in \partial\Omega \times (0,T].$$

Equation (1.1.3) also represents a special case of general second-order telegraph equation in two-dimensional space which governs the models in telegraphic transmission and different wave phenomena [21, 98]. More interestingly, equation (1.1.3) models the propagation of heat in biological media [32, 130] and is well-known as Maxwell-Cattaneo equation or hyperbolic heat equation. The modeling of heat propagation in biological media has numerous applications in biological and biomedical technologies [20, 23].

Pulsed Electric Field Model: For $\gamma = \kappa = \delta = 0$, we have the following pulsed electric field model problem:

$$-\nabla.(\sigma(x)\nabla u + \epsilon(x)\nabla u_t) = f(x,t) \text{ for } (x,t) \in \Omega \times (0,T], \tag{1.1.4}$$

with initial and boundary conditions

$$u(x,0) = u_0 \text{ for } x \in \Omega \;\; \& \;\; u(x,t) = 0 \text{ for } (x,t) \in \partial\Omega \times (0,T].$$

Numerical solutions of the model (1.1.4)-(1.1) draw significant attention in a variety of fields such as neural activation during deep brain simulations [27, 68], debacterization of liquids, food processing [136], bio-fouling prevention [113], and selective spectroscopic imaging of the electrical properties of biological media [10].

Second Order Sobolev Equation: For $\gamma = 0 = \delta$ and $\kappa = 1$, we have the following second-order Sobolev equation:

$$u_t - \nabla.(\sigma(x)\nabla u + \epsilon(x)\nabla u_t) = f(x,t) \text{ for } (x,t) \in \Omega \times (0,T], \tag{1.1.5}$$

with initial and boundary conditions

$$u(x,0) = u_0 \text{ for } x \in \Omega \;\; \& \;\; u(x,t) = 0 \text{ for } (x,t) \in \partial\Omega \times (0,T].$$

Equation (1.1.5) comes to light in many mathematical physics models and mechanical engineering. They are used to study moisture transport problems in soil [115], heat conduction

problems in different media [125], homogeneous fluid flow in fissile materials such as soil and rock [15], and other physical models.

Viscoelastic Wave Equation: For $\gamma = 1$ and $\kappa = 0 = \delta$, we have the following viscoelastic wave equation:

$$u_{tt} - \nabla.(\sigma(x)\nabla u + \epsilon(x)\nabla u_t) = f(x,t) \text{ for } (x,t) \in \Omega \times (0,T], \tag{1.1.6}$$

with initial and boundary conditions

$$u(x,0) = u_0, \;\; u_t(x,0) = v_0 \text{ for } x \in \Omega \;\; \& \;\; u(x,t) = 0 \text{ for } (x,t) \in \partial\Omega \times (0,T],$$

Equation (1.1.6) represents the wave propagation through a viscoelastic medium [71, 85, 122] and hence called as viscoelastic wave equation. This equation arises in the field of viscoelastic mechanics [83], nuclear reaction kinetics, biology mechanics [119], geophysics [7] and so on.

Acoustic Wave Equation For $\gamma = 1$ and $\kappa = \delta = \epsilon = 0$, we have the following acoustic wave equation:

$$u_{tt} - \nabla.(\sigma(x)\nabla u) = f(x,t) \text{ for } (x,t) \in \Omega \times (0,T], \tag{1.1.7}$$

with initial and boundary conditions

$$u(x,0) = u_0, \;\; u_t(x,0) = v_0 \text{ for } x \in \Omega \;\; \& \;\; u(x,t) = 0 \text{ for } (x,t) \in \partial\Omega \times (0,T],$$

Wave equation (1.1.7) is of fundamental importance in the modelling of many real life problems such as time dependent acoustic, electromagnetic [75], or elastic wave phenomena [66]. In geophysics, it helps for the prediction of earthquakes and other seismic activity [81, 87].

1.2 Preliminaries

1.2.1 Basic notations

In this section, we will introduce the basic notations and results that are used in this thesis. Let $x = (x_1, x_2, \ldots, x_n) \in \mathbb{R}^n$ and $\alpha = (\alpha_1, \alpha_2, \ldots, \alpha_n)$, α_i non-negative integers, be a multi-index symbol with the notations

$$|\alpha| = \alpha_1 + \alpha_2 + \cdots + \alpha_n \text{ and } x^\alpha = x_1^{\alpha_1} x_2^{\alpha_2} \cdots x_n^{\alpha_n}.$$

We set

$$D^{\alpha}u = \frac{\partial^{|\alpha|}u}{\partial x_1^{\alpha_1}\partial x_2^{\alpha_2}\cdots\partial x_n^{\alpha_n}}.$$

For $|\alpha| = m$, $D^{\alpha}u$ denotes the m-th partial derivatives of the function $u = u(x_1, x_2, \ldots, x_n)$. For simplicity, we write only x for $(x_1, x_2) \in \mathbb{R}^2$.

Now, we introduce some function spaces which will be used frequently thorough out the discussion. Let $\mathcal{D}$ be an open bounded domain in $\mathbb{R}^2$ with smooth boundary $\partial\mathcal{D}$. $\mathbb{P}_m(\mathcal{D})$, $m \geq -1$, denotes the space of polynomials of degree up to m restricted to $\mathcal{D}$ with $\mathbb{P}_{-1}(\mathcal{D}) = \{0\}$. For $1 \leq p \leq \infty$, we denote $L^p(\mathcal{D})$ to be the space of equivalence classes of measurable functions u on $\mathcal{D}$ such that $\|u\|_{L^p(\mathcal{D})}$ is finite, where

$$\|u\|_{L^p(\mathcal{D})} = \left(\int_{\mathcal{D}} |u(x)|^p dx\right)^{\frac{1}{p}}, 1 \leq p < \infty \text{ and } \|u\|_{L^\infty(\mathcal{D})} = \operatorname{ess\,sup}_{x\in\mathcal{D}} |u(x)|.$$

Particularly, when $p = 2$, $L^2(\mathcal{D})$ is a Hilbert space with norm $\|\cdot\|_{L^2(\mathcal{D})}$ and inner product $(\cdot,\cdot)_{L^2(\mathcal{D})}$ defined as

$$(u, v)_{L^2(\mathcal{D})} = \int_{\mathcal{D}} u(x)v(x)dx.$$

For simplicity, we write $\|\cdot\|_{L^2(\mathcal{D})}$ by $\|\cdot\|_{\mathcal{D}}$ and $(\cdot,\cdot)_{L^2(\mathcal{D})}$ by $(\cdot,\cdot)_{\mathcal{D}}$. For $m \geq 0$, we denote $H^m(\mathcal{D})$ to be the Sobolev space of order m, and is defined by

$$H^m(\mathcal{D}) := \left\{u \in L^2(\mathcal{D}) : D^{\alpha}u \in L^2(\mathcal{D}), |\alpha| \leq m\right\},$$

with norm $\|u\|_{m,\mathcal{D}} = \left(\sum_{|\alpha|\leq m} \|D^{\alpha}u\|_{\mathcal{D}}^2\right)^{\frac{1}{2}}$ and semi-norm $|u|_{m,\mathcal{D}} = \left(\sum_{|\alpha|=m} \|D^{\alpha}u\|_{\mathcal{D}}^2\right)^{\frac{1}{2}}$. Again, $H_0^1(\mathcal{D}) \subset H^1(\mathcal{D})$ such that

$$H_0^1(\mathcal{D}) = \{v \in H^1(\mathcal{D}) : v = 0 \text{ on } \partial\mathcal{D}\}.$$

When $\mathcal{D} = \Omega$, we remove the subscript $\mathcal{D}$ in the notations of norms and inner products. For more detail on Sobolev spaces, we refer to [5]. For a Banach space $\mathbb{B}$ of real-valued functions and time interval $\mathcal{J} = [0, T]$, the Bôchner spaces are given by

$$L^p(\mathcal{J};\mathbb{B}) = \{u : \mathcal{J} \to \mathbb{B} : \|u\|_{L^p(\mathcal{J};\mathbb{B})} \text{ is finite}\},$$

where $\|u\|_{L^p(\mathcal{J};\mathbb{B})} = \left(\int_0^T \|u(t)\|_{\mathbb{B}}^p \, dt\right)^{\frac{1}{p}}$, for $1 \leq p < \infty$ and $\|u\|_{L^\infty(\mathcal{J};\mathbb{B})} = \operatorname{ess\,sup}_{t\in\mathcal{J}} \|u(t)\|_{\mathbb{B}}$. Similarly, for $1 \leq m < \infty$, we define

$$H^m(\mathcal{J};\mathbb{B}) = \{u : \mathcal{J} \to \mathbb{B} : \|u\|_{H^m(\mathcal{J};\mathbb{B})} \text{ is finite}\},$$

where $\|u\|_{H^m(\mathcal{J};\mathbb{B})} = \left(\sum_{j=0}^{m}\int_0^T \left\|\frac{\partial^j u(t)}{\partial t^j}\right\|_{\mathbb{B}}^2 dt\right)^{\frac{1}{2}}$.

Throughout this thesis, the generic constant C is always positive and doesn't dependent on the mesh size and time step. However, it may change its value at different occurrence and generally dependent on the physical coefficients. Whenever required, we shall use C_δ to denote a constant depending on parameter δ.

1.2.2 Basic results

Now we shall recall some important inequalities for our subsequent use [74].

Young's inequality: For $a, b \geq 0$ and $\epsilon > 0$, the following inequality holds

$$ab \leq \frac{a^2}{2\epsilon} + \frac{\epsilon b^2}{2}.$$

An important consequence of the Young's inequality is the Hölder's inequality. The discrete version of Hölder's inequality is stated below.

Hölder's inequality: Let $p > 1$ and q be such that $\frac{1}{p} + \frac{1}{q} = 1$. Then, for any real numbers $a_i, b_i \in \mathbb{R}$, $i = 1, 2, \ldots, n$,

$$\sum_{i=1}^{n} |a_i b_i| \leq \left(\sum_{i=1}^{n} |a_i|^p\right)^{\frac{1}{p}} \left(\sum_{i=1}^{n} |b_i|^q\right)^{\frac{1}{q}}.$$

In particular, for $p = q = 2$, the above inequality is known as the **Cauchy-Schwarz inequality** in $\mathbb{R}^n$.

The integral analogue of Hölder's inequality is as follows: Let $p > 1$ and q be such that $\frac{1}{p} + \frac{1}{q} = 1$. Then, for any measurable functions $\phi, \psi : \Omega \to \mathbb{R}$

$$\|\phi\psi\|_{L^1(\Omega)} \leq \|\phi\|_{L^p(\Omega)} \|\psi\|_{L^q(\Omega)}.$$

For $p = q = 2$, the above inequality is known as the **Cauchy-Schwarz inequality**.

Poincaré inequality: Let Ω be a bounded open domain in $\mathbb{R}^n$. Then there exists a positive constant $C = C(\Omega)$ such that

$$\|\phi\| \leq C\|\nabla\phi\| \quad \forall \phi \in H_0^1(\Omega).$$

In view of the Poincaré inequality, $\|\nabla\phi\|$ defines a norm on $H_0^1(\Omega)$.

Gronwall's lemma: Let $G(t)$ be a continuous function and $H(t)$ a non-negative continuous function on its interval $t_0 \leq t \leq t_0 + a$. If a continuous function $F(t)$ has the property

$$F(t) \leq G(t) + \int_{t_0}^{t} F(s)H(s)ds \text{ for } t_0 \leq t \leq t_0 + a.$$

Then

$$F(t) \leq G(t) + \int_{t_0}^{t} G(s)H(s)exp\left(\int_{s}^{t} H(\tau)d\tau\right) ds \text{ for } t_0 \leq t \leq t_0 + a.$$

In particular, when $G(t) = C$, an non-negative constant, we have

$$F(t) \leq Cexp\left(\int_{t_0}^{t} H(s)ds\right) \text{ for } t_0 \leq t \leq t_0 + a.$$

Lemma 1.2.1. *For any Banach space $\mathbb{B}$, we have (cf. [110], Proposition 7.1)*

$$\sup_{0\leq t\leq T} \|v(t)\|_{\mathbb{B}} \leq C\|v\|_{H^1(\mathcal{J};\mathbb{B})}, \quad v \in H^1(\mathcal{J};\mathbb{B}). \tag{1.2.1}$$

1.3 Background and Motivation

This section briefly explains the existing relevant literature, including our contributions and the motivation behind the present study.

It has always been an interesting topic among scientists and numerical analysts developing advanced numerical techniques to solve various partial differential equations (PDEs) arising in the field of science and engineering. Numerical solutions to such problems draw significant attention in various fields of applied sciences, engineering and medicines like acoustics, fluid mechanics, astrophysics, aerodynamics, and high-intensity focused ultrasound etc. The key features of a good numerical method are its cost efficiency and higher-order accuracy. Several numerical methods, like finite difference methods (FDMs) and finite element methods (FEMs) in the literature, are intended for numerical approximation of such problems on simple geometry. FEMs are one of the most accurate, efficient and reliable approximation schemes in scientific computing due to their significant applications for real-world physical phenomena. However, in the case of polygonal or polyhedral (polytopal) discretization, it becomes very difficult to implement higher-order methods due to the complexity in basis construction and requires various Gauss quadratures for the evaluation of integrals. In recent years, the use of polytopal elements in scientific and engineering literature has seen significant growth due to their wide applications.

Several attempts were made in order to generalize the traditional FEMs that allow the use of arbitrary polygonal elements, rather than just triangles or quadrilaterals such as generalized FEM [12], composite FEM [73], rational function approach [132], extended FEM [57], and others [22, 38, 90, 109, 124, 131]. Methods like polygonal finite element method (PFEM) have been developed, which can handle polygonal or polyhedral meshes by using

generalized non-polynomial shape function [120, 123]. Moreover, it can provide a more accurate approximation of the solution for problems that exhibit singularities or discontinuities. But the use of such a non-polynomial shape function leads to higher computational cost as it needs to be integrated inside each local element, and that too approximately. Alternatively, we can construct relatively simple (polygonal) discrete spaces by relaxing the continuity requirements along the inter-element boundary. Discontinuous Galerkin (DG) [29, 35] and weak Galerkin (WG) [92] FEM impose weak continuity requirements along the inter-element boundary and are able to use general polygonal or polyhedral meshes.

Mimetic finite difference (MFD) is one of the promising techniques among the techniques that can handle complex geometries [25, 43, 44]. It is a FDM that evolved from the classical finite difference or finite volume method, along with some similarities to FEMs and is named "mimetic" as it preserves the underlying mathematical structure of the PDE. Unlike FEM, this method uses only the degrees of freedom and doesn't have a trial function inside the elements. Higher-order MFD has been introduced using some additional degrees of freedom such as moments on faces, edges and elements [19, 45, 72]. However, the analyses and implementation of the method become complicated due to the unavailability of test and trial functions inside the elements.

The virtual element method (VEM) is a recent numerical technique developed for solving PDEs which can efficiently deal with polygonal or polyhedral mesh discretizations. This method is motivated by MFD and can be seen as the most suitable generalization of FEM for complex geometries. In VEM, the local basis function space in each element contains polynomials (as FEM) as well as some non-polynomial functions, which are the solution of some PDE in that element. The explicit construction of the basis functions is not required, and one needs to define suitable degrees of freedom to represent any function in the space uniquely. The basic framework of VEM is to use suitable projections from the local space onto the space of polynomials, which can be computed using the degrees of freedom associated with the local space. Thus, for the computation of the stiffness matrix, particularly the discrete bilinear form, we need only the integration of polynomials over the element and a suitable stabilization term of the right order of magnitude. The method was designed to handle arbitrarily shaped polygonal discretizations, which are convenient for handling complex geometries. This is by far the most appealing feature of the method, not only because VEM has been shown to be robust to mesh distortion but also because it can handle non-conforming discretizations in standard FEM (i.e., meshes containing

hanging nodes) in a straightforward manner. VEM simply interprets a hanging node in a non-conforming mesh as a division of an edge at a 180° angle, effectively increasing by one the number of edges in elements sharing this node. This requires no modification whatsoever to the VEM formulation, and the element is treated normally, thereby resulting in a conforming virtual element mesh. Handling non-conforming discretizations gives VEM an edge over standard FEM. Another important property of VEM is that it satisfies the patch-test required by engineers and scientists.

In literature, VEM was first introduced in 2013 by Beirão Da Veiga et al., where a conforming method was discussed for the Poisson equation in two-dimension [16]. In [48] a non-conforming VEM was presented by Dios et al.. Next, Ahmad et al. gave an alternative construction of the discrete space using L^2 projection onto the space of polynomial of degree m (where m is the order of accuracy of the method) instead of $m-2$ (as in original VEM [16]) [6]. This new formulation allowed us to extend the method to elliptic problems involving lower-order differential terms, such as reaction-diffusion problems. Further, it was extended to elliptic problems with variable coefficients [2, 46] and general elliptic problems [18, 31]. The extension to the variable coefficient is not so trivial because the discrete bilinear forms, in this case, do not satisfy the polynomial consistency and stability results as in the case of constant coefficients. VEM has been successfully applied to solve a wide range of stationary problems such as linear elasticity problems [41, 59], plate-bending problems [26], eigenvalue problems [63, 91], system of equations [28, 30] etc. Some works on the practical implementation of the method are presented in [17, 42, 121].

VEM is also being used as the discretizing tool for spatial direction in time-dependent initial-boundary value problems. In [129], Vacca et al. developed the conforming VEM for parabolic problems considering the standard time-dependent diffusion equations and the non-conforming counterpart was developed by Zhao et al. in [139]. In addition to the discrete bilinear form that approximates the grad-grad form in the elliptic case [16], another discrete bilinear form is introduced to approximate the L^2 inner product using the L^2 projection defined in [6]. The error analysis was worked out using an energy projection onto the discrete space, which bridges the discrete and original grad-grad form. Vacca also extended the previous work to hyperbolic problems in [128], where they considered the standard wave equation as the model problem. Conforming VEMs for semi-linear parabolic and hyperbolic problems were studied by Adak et al. in [3] and [4], respectively, where the discrete counterpart of the non-linear source term was constructed using the modified L^2

projection.

In the majority of literature on time-dependent problems, the coefficients were taken to be constant and hyperbolic problems with damping terms are not studied. The main focus of the study is to develop the VEM for the general linear second-order problems (1.1.1)-(1.1.2) with variable coefficients. In particular, we consider the different classes of problems obtained for different choice of coefficients in (1.1.1) and develop the VEM for each separately. These problems contain either weak or strong damping terms (or both), making the convergence study more difficult and requiring additional analyses to obtain optimal convergence estimates. Our first work discussed the VEM for the weakly damped wave equations (1.1.3) with variable coefficients on polygonal meshes with homogeneous Dirichlet boundary conditions. These are hyperbolic-type equations with an additional weak damping term. Thus, these problems can be seen as a mixture of standard hyperbolic and parabolic problems, also known as hyperbolic heat equations. The coefficients are assumed to be smooth enough to satisfy the necessary requirements in the convergence analysis. The virtual semi-discrete approximation of the model problem is constructed using three approximated bilinear forms. The fully discrete scheme is obtained by first reformulating the governing equation into a system of first-order equations and then employing the Crank-Nicolson discretization. We present rigorous error analysis for the semi-discrete and fully discrete schemes and derive optimal convergence estimates. Numerical examples justifying the theoretical results for high-order VEM with different polygonal meshes show the flexibility of the proposed method with respect to arbitrary mesh discretizations. Next, we analyze the VEM for the pulsed electric field model problems (1.1.4) with variable coefficients on polygonal meshes. These problems contain the strong damping term and do not come under the standard classification of time-dependent problems. Optimal error estimates are derived for both semi-discrete and fully discrete schemes in L^2 and H^1 norms. The fully discrete scheme can be reinterpreted as the Crank-Nicolson discretization of the reformulation of the governing equation in the first-order system, as in Baker [13]. Further, in support of our theoretical findings, some numerical examples are presented with different meshes. The convergence analysis for the pulsed electric field model problems plays a vital role while discussing the optimal order convergence in L^2 norm for our next two works. In our next two works, we develop optimal order VEM for second-order Sobolev equation (1.1.5) and viscoelastic wave equations (1.1.6). Recently, VEM has been discussed for the second-order Sobolev equations (1.1.5) in [135, 138]. Error analysis in [138] uses an elliptic

projection operator for constant coefficients. Then the convergence results in [138] have been extended for variable coefficients by Xu et al. [135] assuming $\sigma = \epsilon$. In [18], the authors have shown that in the case of variable coefficients, the usual choice of approximated bilinear forms (as in the case of constant coefficients [128, 129, 138]) is insufficient to produce optimal convergence results. Following the idea in [18], modified approximated bilinear forms are used to construct the semi-discrete virtual element approximation of the model problem. The modified discrete bilinear forms generally do not follow the polynomial consistency property and stability estimates with respect to the original bilinear forms. Thus, additional analysis is required to deal with the consistency error and its consequences. It is observed that although the standard elliptic projection leads to an optimal error estimate in the energy norm, it is difficult to achieve an optimal convergence rate in the L^2 norm. This is due to the fact that the elliptic projection operator can only take care of either $\nabla \cdot (\sigma \nabla u)$ or $\nabla \cdot (\epsilon \nabla u_t)$ in the error analysis. The approximation properties of a newly introduced non-standard projection operator (motivated by the semi-discrete solution of pulsed electric model problems) play a crucial role in the derivation of the a priori error bound in the L^2 norm. We introduce an auxiliary variable to reformulate the second-order governing equation into a first-order system. The fully discrete virtual element approximation of the model problem is obtained by employing the Crank-Nicolson discretization to the first-order system of equations. The temporal method can be seen as a particular case of the Newmark method for wave equations (cf. [67]), which has been used extensively in applications. Rigorous analysis has been carried out for semi-discrete convergence and fully discrete schemes, and the optimal order of convergence is derived. Numerical examples are presented with different types of meshes and different polynomial degrees to support our theoretical findings.

In our final work, we present higher-order time-stepping VEMs for the wave equations with variable coefficients on polygonal meshes. The VEM for the wave equation (1.1.7) with constant coefficients on polygonal meshes in [128] mainly focuses on the semi-discrete error analysis of the proposed method, while for the fully-discrete approximation, both Newmark and Bathe method has been used. But a detailed analysis of stability and convergence for the proposed methods is missing. Also, the methods are shown to be at most second-order accurate in temporal discretization. While using the higher-order FEMs for spatial discretization, second-order temporal schemes are insufficient to produce a higher-order method together and require choosing smaller time steps in order to preserve the higher

accuracy provided by spatial direction. To preserve higher accuracy, we should use higher-order time schemes as well. Such a scheme can be obtained by the modified equation approach, where appropriate modification is done on the existing second-order schemes by looking at the truncation error [36, 37, 117]. In this work, we have developed a fully discrete VEM using a general Newmark scheme and obtained up to fourth-order convergence in time for some special cases. We present a full theoretical analysis for the semi-discrete error and derive optimal convergence estimates. We analyze the stability of the fully discrete scheme and show that the method converges the discrete energy. Further, in support of theoretical findings, numerical examples are presented.

1.4 Virtual Element Framework

In this section, we will discuss the construction of virtual element approximation for numerical solution of an elliptic problem with variable coefficients. We refer to the papers [6, 16, 18] for more details. We consider the following elliptic boundary value problem

$$\begin{cases} \delta(x)u - \nabla \cdot (\sigma(x)\nabla u) = f(x) \text{ for } x \in \Omega, \\ u(x) = 0 \text{ for } x \in \partial\Omega. \end{cases} \tag{1.4.1}$$

Here $f(x)$ is the forcing function and the coefficients $\delta(x), \sigma(x) \in L^\infty(\Omega)$ such that

$$\underline{M} \leq \delta(x), \sigma(x) \leq \overline{M} \quad \forall x \in \bar{\Omega}$$

for some positive constants $\underline{M}$ and $\overline{M}$.

Let $\{\mathcal{T}_h\}$ be a partition of the domain Ω into elements (arbitrary polygons) E. For any element E, h_E denotes the element diameter and $h = \max_{E \in \mathcal{T}_h} h_E$ represents the mesh size of $\mathcal{T}_h$. Further, $n(E)$ and $|E|$ are the number of sides and area of E, respectively, and V_i's are the vertices of E. The discretization $\mathcal{T}_h$ of domain Ω is demonstrated in Figure 1.4.1. We assume the following regularity conditions on the mesh decomposition [16]:

Assumption 1.4.1.

$\mathcal{A}1$. We assume that there exists a $\gamma \geq 0$ such that, for all h, each element E in $\mathcal{T}_h$ is star-shaped with respect to a ball of radius γh_E.

$\mathcal{A}2$. We assume that there exists a $\rho \geq 0$ such that, for all h, each element E in $\mathcal{T}_h$ the distance between any two vertices of E is ρh_E.

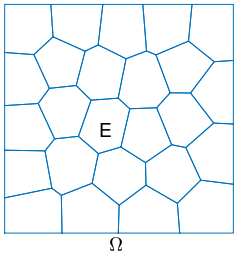

Figure 1.4.1: Partition of Ω.

The mesh assumptions for the family of meshes $\mathcal{T}_h$ in [16] implies the following mesh regularity condition [33].

Assumption 1.4.2. *There exists a uniformly shape regular and quasi-uniform virtual triangulation $\mathcal{T}_E$ of each element E in $\mathcal{T}_h$ with mesh size proportional to h_E.*

For any element $E \in \mathcal{T}_h$ with boundary ∂E, we define the auxiliary local space $V_h^m(E)$ by

$$V_h^m(E) = \left\{ v \in H^1(E) \cap C^0(\partial E) : \ v|_{\mathcal{E}} \in \mathbb{P}_m(\mathcal{E}) \text{ for all edge } \mathcal{E} \ \in \partial E, \ \Delta v \in \mathbb{P}_m(E) \right\}.$$

Here $m \geq 1$ is an integer and called as the polynomial order of accuracy of the method. We define the elliptic projection operator $\Pi_{m,E}^{\nabla} : H^1(E) \to \mathbb{P}_m(E)$ by

$$\begin{cases} (\nabla \Pi_{m,E}^{\nabla} v, \nabla q)_E = (\nabla v, \nabla q)_E & \forall q \in \mathbb{P}_m(E), \\ P_E^a(\Pi_{m,E}^{\nabla} v) = P_E^a v, \end{cases}$$

where P_E^a is the averaging operator

$$P_E^a v = \begin{cases} \frac{1}{n(E)} \sum_{i=1}^{n(E)} v(V_i), & m = 1 \\ \frac{1}{|E|} \int_E v dx, & m > 1. \end{cases}$$

Then the virtual local space $W_h^m(E)$ can be defined as

$$W_h^m(E) = \left\{ w \in V_h^m(E) : \int_E (\Pi_{m,E}^{\nabla} w) q dx = \int_E w q dx \ \ \forall q \in \mathbb{M}_m(E)/\mathbb{M}_{m-2}(E) \right\}.$$

Symbol $\mathbb{M}_m(E)$ represents the space of scaled monomials defined by

$$\mathbb{M}_m(E) = \left\{ \left(\frac{x - x_E}{h_E} \right)^{\boldsymbol{s}}, |s| \leq m \right\}.$$

For a multi-index $\boldsymbol{s}$, we write $|\boldsymbol{s}| := s_1 + s_2$ and $x^{\boldsymbol{s}} := x_1^{s_1} x_2^{s_2}$. Again, $\mathbb{M}_m(E)/\mathbb{M}_{m-2}(E)$ denotes the scaled monomials of degree m on E that are L^2- orthogonal to all the scaled monomials of degree $m-2$ on E.

Any $w \in W_h^m(E)$ can be uniquely determined by the following degrees of freedom (D) associated with local virtual space $W_h^m(E)$ (cf. [16]):

(D1) $w(V_i)$,

(D2) $w(E_i)$, where E_i's are the $n(E) \times (m-1)$ distinct points on the edges of E,

(D3) for all $\mu \in \mathbb{M}_{m-2}(E)$, the values $\frac{1}{|E|} \int_E w \ \mu \ dx$.

With the Assumption 1.4.2, we have the following inverse inequality [33].

Lemma 1.4.1. *For $v \in W_h^m(E)$, we have*

$$\|\nabla v\|_E \leq C h_E^{-1} \|v\|_E. \tag{1.4.2}$$

Next, we define the L^2 projection operators $\Pi_{m,E}^0 : L^2(E) \to \mathbb{P}_m(E)$ and $\boldsymbol{\Pi}_{m-1,E}^0 : [L^2(E)]^2 \to [\mathbb{P}_{m-1}(E)]^2$ by

$$(\Pi_{m,E}^0 v, q)_E = (v, q)_E \quad \forall q \in \mathbb{P}_m(E)$$

and

$$(\boldsymbol{\Pi}_{m-1,E}^0 \nabla v, \mathbf{q})_E = (\nabla v, \mathbf{q})_E \quad \forall \mathbf{q} \in [\mathbb{P}_{m-1}(E)]^2,$$

respectively. It is easy to note that

$$\|\boldsymbol{\Pi}_{m-1,E}^0 \nabla v\|_E \leq \|\nabla v\|_E, \quad \|\nabla v - \boldsymbol{\Pi}_{m-1,E}^0 \nabla v\|_E \leq \|\nabla v - \nabla \Pi_{m,E}^{\nabla} v\|_E. \tag{1.4.3}$$

Also, for the projection operators $\Pi_{m,E}^0$ and $\Pi_{m,E}^{\nabla}$, we have the following bounds:

$$\|\Pi_{m,E}^0 v\|_E \leq \|v\|_E, \quad \|v - \Pi_{m,E}^0 v\|_E \leq \|v\|_E, \tag{1.4.4}$$

and

$$|\Pi_{m,E}^{\nabla} v|_{1,E} \leq |v|_{1,E}, \quad |v - \Pi_{m,E}^{\nabla} v|_{1,E} \leq |v|_{1,E}, \tag{1.4.5}$$

respectively. We have the following estimates for the projection errors [24].

Lemma 1.4.2. *For $m \geq 0$ and $v \in H^{m+1}(E)$, it holds*

$$\|v - \Pi^{\nabla}_{m,E} v\|_E + h_E |v - \Pi^{\nabla}_{m,E} v|_{1,E} \leq C h_E^{m+1} |v|_{m+1,E},$$
$$\|v - \Pi^{0}_{m,E} v\|_E + h_E |v - \Pi^{0}_{m,E} v|_{1,E} \leq C h_E^{m+1} |v|_{m+1,E},$$
$$\|\nabla v - \mathbf{\Pi}^{0}_{m-1,E} \nabla v\|_E \leq C h_E^{m} |\nabla v|_{m,E},$$

where C is a positive constant independent of h_E.

Following the standard way, we easily obtain the variational problem for the model problem (1.4.1) as : Find $u \in H^1_0(\Omega))$ so that for all $v \in H^1_0(\Omega)$

$$m(u, v) + a(u, v) = (f, v), \tag{1.4.6}$$

where $m(u, v) = (\delta(x)u, v)$ and $a(u, v) = (\sigma(x)\nabla u, \nabla v)$ for all $u, v \in H^1_0(\Omega)$.

The bilinear forms $m(\cdot, \cdot)$ and $a(\cdot, \cdot)$ can be splited into their local counterparts in the following manner

$$m(u, v) := \sum_{E \in \mathcal{T}_h} m^E(u, v) \quad \& \quad a(u, v) := \sum_{E \in \mathcal{T}_h} a^E(u, v) \ \forall \ u, v \in H^1_0(\Omega).$$

Remark 1.4.1. *In the case of constant-coefficients, the following discrete bilinear forms are usually considered in order to approximate the original bilinear forms (see, [16]):*

$$a^E_h(v, w) := \left(\nabla \Pi^{\nabla}_{m,E} v, \nabla \Pi^{\nabla}_{m,E} w\right)_E + \left((I - \Pi^{\nabla}_{m,E})v, (I - \Pi^{\nabla}_{m,E})w\right)_E,$$
$$m^E_h(v, w) := (\Pi^{0}_{m,E} v, \Pi^{0}_{m,E} w)_E + \left((I - \Pi^{0}_{m,E})v, (I - \Pi^{0}_{m,E})w\right),$$

for $v, w \in W^m_h(E)$. For variable coefficients as in (1.4.1), a natural extension of the above choices would suggest considering the discrete bilinear forms as

$$a^E_h(v, w) := \left(\sigma \nabla \Pi^{\nabla}_{m,E} v, \nabla \Pi^{\nabla}_{m,E} w\right)_E + \tilde{S}^E_\sigma \left((I - \Pi^{\nabla}_{m,E})v, (I - \Pi^{\nabla}_{m,E})w\right),$$
$$m^E_h(v, w) := \left(\delta \Pi^{0}_{m,E} v, \Pi^{0}_{m,E} w\right)_E + \tilde{S}^E_\delta \left((I - \Pi^{0}_{m,E})v, (I - \Pi^{0}_{m,E})w\right) \tag{1.4.7}$$

for $v, w \in W^m_h(E)$, where $\tilde{S}^E_\sigma, \tilde{S}^E_\delta$ are stabilizer terms. For $m = 1$, this choice works fine. However, for $m \geq 2$, it fails to deliver optimal order of convergence (see, [18]).

In order to overcome the sub-optimal convergence, we require to modify discrete bilinear forms (1.4.7) according to [18]. For all $E \in \mathcal{T}_h$, by making use of $\Pi^{\nabla}_{m,E}$, $\Pi^{0}_{m,E}$ and $\mathbf{\Pi}^{0}_{m-1,E}$,

we introduce the local bilinear forms $a_h^E(\cdot,\cdot) : W_h^m(E) \times W_h^m(E) \to \mathbb{R}$ and $m_h^E(\cdot,\cdot) : W_h^m(E) \times W_h^m(E) \to \mathbb{R}$ that approximate the exact forms $a^E(\cdot,\cdot)$ and $m(\cdot,\cdot)_E$, respectively, in the following manner

$$\begin{aligned} a_h^E(v,w) &:= \left(\sigma \boldsymbol{\Pi}^0_{m-1,E}\nabla v, \boldsymbol{\Pi}^0_{m-1,E}\nabla w\right)_E + S_\sigma^E\left((I-\Pi^\nabla_{m,E})v,(I-\Pi^\nabla_{m,E})w\right) \quad \& \\ m_h^E(v,w) &:= (\delta \Pi^0_{m,E}v, \Pi^0_{m,E}w)_E + S_\delta^E\left((I-\Pi^0_{m,E})v,(I-\Pi^0_{m,E})w\right), \end{aligned} \tag{1.4.8}$$

where S_σ^E, S_δ^E are symmetric positive definite bilinear forms such that there exist positive constants $\alpha_\sigma, \alpha_\delta, \beta_\sigma, \beta_\delta$ independent of h satisfying

$$\alpha_\sigma a^E(w,w) \le S_\sigma^E(w,w) \le \beta_\sigma a^E(w,w), \tag{1.4.9}$$

for all $w \in W_h^m(E)$ with $\Pi^\nabla_{m,E}w = 0$ and

$$\alpha_\delta m^E(w,w) \le S_\delta^E(w,w) \le \beta_\delta m^E(w,w) \tag{1.4.10}$$

for all $w \in W_h^m(E)$ with $\Pi^0_{m,E}w = 0$.

We note that symmetric properties of S_σ^E, S_δ^E and the relations (1.4.9)-(1.4.10) yield

$$S_\sigma^E(v,w) \le \left(S_\sigma^E(v,v)\right)^{\frac{1}{2}}\left(S_\sigma^E(w,w)\right)^{\frac{1}{2}} \le \beta_\sigma\left(a^E(v,v)\right)^{\frac{1}{2}}\left(a^E(w,w)\right)^{\frac{1}{2}}, \tag{1.4.11}$$

for all $v,w \in W_h^m(E)$ with $\Pi^\nabla_{m,E}v = \Pi^\nabla_{m,E}w = 0$ and

$$S_\delta^E(v,w) \le \left(S_\delta^E(v,v)\right)^{\frac{1}{2}}\left(S_\delta^E(w,w)\right)^{\frac{1}{2}} \le \beta_\delta\left(m^E(v,v)\right)^{\frac{1}{2}}\left(m^E(w,w)\right)^{\frac{1}{2}} \tag{1.4.12}$$

for all $v,w \in W_h^m(E)$ with $\Pi^0_{m,E}v = \Pi^0_{m,E}w = 0$. We choose the stabilizing terms in (1.4.8) as follows:

$$\begin{aligned} S_\sigma^E(v,w) &= \beta_\sigma^E \sum_{r=1}^{N^E} dof_r(v)dof_r(w) \quad \& \\ S_\delta^E(v,w) &= \beta_\delta^E |E| \sum_{r=1}^{N^E} dof_r(v)dof_r(w), \end{aligned}$$

where $\beta_\sigma^E = P_E^a(\sigma)$, $\beta_\delta^E = P_E^a(\delta)$ and $N^E = \dim W_h^m(E)$. Here, $dof_r(w)$ denotes the r-th local degree of freedom of w in $W_h^m(E)$.

Next, we present some results for the modified bilinear forms (1.4.8) which are important for our further analysis. The results are derived following the idea in [18] with necessary modifications. We have presented the proofs for the completeness of this works.

Lemma 1.4.3. *For any $v, w \in L^2(E)$, we have*

$$\begin{aligned}
&a^E(v,w) - \left(\sigma\boldsymbol{\Pi}^0_{m-1,E}\nabla v, \boldsymbol{\Pi}^0_{m-1,E}\nabla w\right)_E \\
&\leq \left\|\sigma\nabla v - \boldsymbol{\Pi}^0_{m-1,E}(\sigma\nabla v)\right\|_E \left\|\nabla w - \boldsymbol{\Pi}^0_{m-1,E}\nabla w\right\|_E \\
&\quad + \left\|\nabla v - \boldsymbol{\Pi}^0_{m-1,E}\nabla v\right\|_E \left(\overline{M}\left\|\nabla w - \boldsymbol{\Pi}^0_{m-1,E}\nabla w\right\|_E + \left\|\sigma\nabla w - \boldsymbol{\Pi}^0_{m-1,E}(\sigma\nabla w)\right\|_E\right).
\end{aligned}$$

Proof. Use projection operator $\boldsymbol{\Pi}^0_{m-1,E}$ and Cauchy-Schwarz inequality to obtain

$$\begin{aligned}
&a^E(v,w) - \left(\sigma\boldsymbol{\Pi}^0_{m-1,E}\nabla v, \boldsymbol{\Pi}^0_{m-1,E}\nabla w\right)_E \\
&= \left(\sigma\nabla v, \nabla w - \boldsymbol{\Pi}^0_{m-1,E}\nabla w\right)_E + \left(\nabla v - \boldsymbol{\Pi}^0_{m-1,E}\nabla v, \sigma\boldsymbol{\Pi}^0_{m-1,E}\nabla w\right)_E \\
&= \left(\sigma\nabla v - \boldsymbol{\Pi}^0_{m-1,E}(\sigma\nabla v), \nabla w - \boldsymbol{\Pi}^0_{m-1,E}\nabla w\right)_E \\
&\quad + \left(\nabla v - \boldsymbol{\Pi}^0_{m-1,E}\nabla v, \sigma\boldsymbol{\Pi}^0_{m-1,E}\nabla w - \boldsymbol{\Pi}^0_{m-1,E}(\sigma\nabla w)\right)_E \\
&= \left(\sigma\nabla v - \boldsymbol{\Pi}^0_{m-1,E}(\sigma\nabla v), \nabla w - \boldsymbol{\Pi}^0_{m-1,E}\nabla w\right)_E \\
&\quad + \left(\nabla v - \boldsymbol{\Pi}^0_{m-1,E}\nabla v, \sigma\boldsymbol{\Pi}^0_{m-1,E}\nabla w - \sigma\nabla w\right)_E \\
&\quad + \left(\nabla v - \boldsymbol{\Pi}^0_{m-1,E}\nabla v, \sigma\nabla w - \boldsymbol{\Pi}^0_{m-1,E}(\sigma\nabla w)\right)_E \\
&\leq \left\|\sigma\nabla v - \boldsymbol{\Pi}^0_{m-1,E}(\sigma\nabla v)\right\|_E \left\|\nabla w - \boldsymbol{\Pi}^0_{m-1,E}\nabla w\right\|_E \\
&\quad + \left\|\nabla v - \boldsymbol{\Pi}^0_{m-1,E}\nabla v\right\|_E \left(\overline{M}\left\|\nabla w - \boldsymbol{\Pi}^0_{m-1,E}\nabla w\right\|_E + \left\|\sigma\nabla w - \boldsymbol{\Pi}^0_{m-1,E}(\sigma\nabla w)\right\|_E\right),
\end{aligned}$$

which completes the proof of Lemma 1.4.3. □

The following consistency error estimate is a direct consequence of the Lemma 1.4.3.

Lemma 1.4.4. *For $v \in H^{m+1}(E)$ and $w \in W_h^m(E)$, we have*

$$a^E(\Pi^0_{m,E}v, w) - a_h^E(\Pi^0_{m,E}v, w) \leq Ch_E^m|v|_{m+1,E}|w|_{1,E}.$$

Proof. Since $\Pi^0_{m,E}v \in \mathbb{P}_m(E)$ implies $\Pi^\nabla_{m,E}(\Pi^0_{m,E}v) = \Pi^0_{m,E}v$ and $\boldsymbol{\Pi}^0_{m-1,E}\nabla(\Pi^0_{m,E}v) = \nabla(\Pi^0_{m,E}v)$, we have

$$\begin{aligned}
a^E(\Pi^0_{m,E}v, w) - a_h^E(\Pi^0_{m,E}v, w) &= a^E(\Pi^0_{m,E}v, w) - \left(\sigma\boldsymbol{\Pi}^0_{m-1,E}\nabla(\Pi^0_{m,E}v), \boldsymbol{\Pi}^0_{m-1,E}\nabla w\right)_E \\
&\leq \left\|\sigma\nabla(\Pi^0_{m,E}v) - \boldsymbol{\Pi}^0_{m-1,E}(\sigma\nabla(\Pi^0_{m,E}v))\right\|_E \left\|\nabla w - \boldsymbol{\Pi}^0_{m-1,E}\nabla w\right\|_E \\
&\leq Ch_E^m\left|\sigma\nabla(\Pi^0_{m,E}v)\right|_{m,E}\|\nabla w\|_E \leq Ch_E^m\overline{M}|v|_{m+1,E}|w|_{1,E}.
\end{aligned}$$

Here, we have used the projection error estimates in Lemma 1.4.2. □

For $u \in H^{m+1}(\Omega)$, we define the interpolant $u_I \in W_h^m$ of u as

$$dof_r(u_I) = dof_r(u), \quad r = 1, 2, \ldots, N_h,$$

where $N_h = \dim W_h^m$. Then, we have the following interpolation error estimate [33].

$$\|u - u_I\|_E + h_E|u - u_I|_{1,E} \leq Ch_E^{m+1}|u|_{m+1,E} \quad \forall E \in \mathcal{T}_h. \tag{1.4.13}$$

Remark 1.4.2. *In particular if $w = u_I$, for some $u \in H_0^1(E) \cap H^2(E)$, the above result can be improved. We can have*

$$\begin{aligned}
&a^E(\Pi_{m,E}^0 v, u_I) - a_h^E(\Pi_{m,E}^0 v, u_I) \\
&\leq \left\|\sigma\nabla(\Pi_{m,E}^0 v) - \boldsymbol{\Pi}_{m-1,E}^0(\sigma\nabla(\Pi_{m,E}^0 v))\right\|_E \left\|\nabla u_I - \boldsymbol{\Pi}_{m-1,E}^0 \nabla u_I\right\|_E \\
&\leq Ch_E^m \left|\sigma\nabla(\Pi_{m,E}^0 v)\right|_{m,E} \left\|\nabla u_I - \boldsymbol{\Pi}_{m-1,E}^0 \nabla u\right\|_E \\
&\leq Ch_E^{m+1}\overline{M}|v|_{m+1,E}|u|_{2,E}.
\end{aligned}$$

Now, we define the global discrete space and the corresponding global bilinear forms by assembling the local counterpart as

$$W_h^m = \left\{w \in H_0^1(\Omega) : w|_E \in W_h^m(E) \quad \forall E \in \mathcal{T}_h\right\}$$

and

$$a_h(v, w) := \sum_{E \in \mathcal{T}_h} a_h^E(v, w) \quad \& \quad m_h(v, w) := \sum_{E \in \mathcal{T}_h} m_h^E(v, w) \quad \forall v, w \in W_h^m.$$

Regarding the continuity and coercivity of the discrete bilinear forms, we have the following result.

Lemma 1.4.5. *The bilinear forms a_h and m_h satisfies*

$$a_h(v, w) \leq (1 + \beta_\sigma)\overline{M}|v|_1|w|_1 \quad \& \quad m_h(v, w) \leq (1 + \beta_\delta)\overline{M}\|v\|\|w\| \quad \forall v, w \in W_h^m$$

and

$$a_h(w, w) \geq \min\{1, \alpha_\sigma\}\underline{M}|w|_1^2 \quad \& \quad m_h(w, w) \geq \min\{1, \alpha_\delta\}\underline{M}\|w\|^2 \quad \forall w \in W_h^m.$$

Proof. From (1.4.3), we have

$$\left(\sigma\boldsymbol{\Pi}^0_{m-1,E}\nabla v, \boldsymbol{\Pi}^0_{m-1,E}\nabla w\right)_E \leq \overline{M}\left\|\boldsymbol{\Pi}^0_{m-1,E}\nabla v\right\|\left\|\boldsymbol{\Pi}^0_{m-1,E}\nabla w\right\|_E \leq \overline{M}|v|_{1,E}|w|_{1,E}.$$

Again from (1.4.11) and (1.4.5), we get

$$\begin{aligned} S^E_\sigma\left((I-\Pi^\nabla_{m,E})v,(I-\Pi^\nabla_{m,E})w\right) &\leq \beta_\sigma\overline{M}|(I-\Pi^\nabla_{m,E})v|_{1,E}|(I-\Pi^\nabla_{m,E})w|_{1,E} \\ &\leq \beta_\sigma\overline{M}|v|_{1,E}|w|_{1,E}. \end{aligned}$$

Combining the above two estimates, we obtain

$$\begin{aligned} a^E_h(v,w) &= \left(\sigma\boldsymbol{\Pi}^0_{m-1,E}\nabla v, \boldsymbol{\Pi}^0_{m-1,E}\nabla w\right)_E + S^E_\sigma\left((I-\Pi^\nabla_{m,E})v,(I-\Pi^\nabla_{m,E})w\right) \\ &\leq (1+\beta_\sigma)\overline{M}|v|_{1,E}|w|_{1,E}. \end{aligned}$$

Now summing over $E\in\mathcal{T}_h$ results in

$$a_h(v,w)=\sum_{E\in\mathcal{T}_h}a^E_h(v,w)\leq(1+\beta_\sigma)\overline{M}|v|_1|w|_1 \quad \forall v,w\in W^m_h.$$

Similarly, we have

$$\begin{aligned} m^E_h(v,w) &= \left(\delta\Pi^0_{m,E}v, \Pi^0_{m,E}w\right)_E + S^E_\delta\left((I-\Pi^0_{m,E})v,(I-\Pi^0_{m,E})w\right) \\ &\leq (1+\beta_\delta)\overline{M}\|v\|_E\|w\|_E. \end{aligned}$$

Here, we have used the bounds in (1.4.4) and (1.4.12). Consequently,

$$m_h(v,w)\leq(1+\beta_\delta)\overline{M}\|v\|\|w\| \quad \forall v,w\in W^m_h.$$

For the coercivity part using (1.4.9) and (1.4.3), we have

$$\begin{aligned} a^E_h(w,w) &= \left(\sigma\boldsymbol{\Pi}^0_{m-1,E}\nabla w, \boldsymbol{\Pi}^0_{m-1,E}\nabla w\right)_E + S^E_\sigma\left((I-\Pi^\nabla_{m,E})w,(I-\Pi^\nabla_{m,E})w\right) \\ &\geq \underline{M}\left\|\boldsymbol{\Pi}^0_{m-1,E}\nabla w\right\|^2_E + \alpha_\sigma\underline{M}\left|(I-\Pi^\nabla_{m,E})w\right|^2_{1,E} \\ &\geq \underline{M}\left\|\boldsymbol{\Pi}^0_{m-1,E}\nabla w\right\|^2_E + \alpha_\sigma\underline{M}\left\|\nabla w-\boldsymbol{\Pi}^0_{m-1,E}\nabla w\right\|^2_E \\ &\geq \min\{1,\alpha_\sigma\}\underline{M}\|\nabla w\|^2_E \\ &= \min\{1,\alpha_\sigma\}\underline{M}|w|^2_{1,E}. \end{aligned}$$

Now summing over $E \in \mathcal{T}_h$ results in

$$a_h(w,w) = \sum_{E\in\mathcal{T}_h} a_h^E(w,w) \geq \min\{1,\alpha_\sigma\}\underline{M}|w|_1^2 \quad \forall w \in W_h^m.$$

For m_h proceeding in a similar manner, we obtain

$$\begin{aligned} m_h^E(w,w) &= \left(\delta\Pi_{m,E}^0 w, \Pi_{m,E}^0 w\right)_E + S_\delta^E\left((I-\Pi_{m,E}^0)w, (I-\Pi_{m,E}^0)w\right) \\ &\geq \underline{M}\left\|\Pi_{m,E}^0 w\right\|_E^2 + \alpha_\delta \underline{M}\left\|(I-\Pi_{m,E}^0)w\right\|_E^2 \\ &\geq \min\{1,\alpha_\delta\}\underline{M}\|w\|_E^2. \end{aligned}$$

Here, we have used the stability estimate (1.4.10). Hence,

$$m_h(w,w) = \sum_{E\in\mathcal{T}_h} m_h^E(w,w) \geq \min\{1,\alpha_\delta\}\underline{M}\|w\|^2 \quad \forall w \in W_h^m.$$

□

We set the discrete form of the source function f as

$$f_h := \Pi_m^0 f, \tag{1.4.14}$$

with the notation $(\Pi_m^0 g)|_E = \Pi_{m,E}^0(g|_E)$ for all $g \in L^2(\Omega)$ and $\forall E \in \mathcal{T}_h$. Then, due to the approximation property of $\Pi_{m,E}^0$, we have the following result.

Lemma 1.4.6. *Let $f \in H^{m+1}(\Omega)$. Then, for f_h defined in (1.4.14), we have*

$$\|f_h - f\| \leq Ch^{m+1}|f|_{m+1}.$$

Now, we can have the virtual element discrete problem to the variational problem (1.4.6) defined by: Find $u_h \in W_h^m$ such that

$$m_h(u_h, w_h) + a_h(u_h, w_h) = (f_h, w_h) \quad \forall w_h \in W_h^m. \tag{1.4.15}$$

We have the following theorem for the discrete problem.

Theorem 1.4.1. *The problem (1.4.15) has a unique solution $u_h \in W_h^m$, and satisfies the following error estimates:*

$$\begin{aligned} |u_h - u|_1 &\leq Ch^m(|u|_{m+1} + |f|_m) \quad \& \\ \|u_h - u\| &\leq Ch^{m+1}(|u|_{m+1} + |f|_{m+1}), \end{aligned}$$

where C is a constant independent of h but depending on the coefficients δ and σ.

1.5 Projection Operators

In this section, we will define some projection operators that will be used in the analysis of the proposed problems.

We will need the following elliptic projection operator $R_h : H_0^1(\Omega) \to W_h^m$ defined by

$$a_h(R_h u, w) = a(u, w) \ \ \forall w \in W_h^m. \tag{1.5.1}$$

For the estimate of the projection errors of the operator R_h, we have the following result.

Lemma 1.5.1. *For $u \in H^{m+1}(\Omega)$, we have*

$$|R_h u - u|_1 \leq C_\sigma h^m |u|_{m+1}$$

and if Ω is a convex domain

$$\|R_h u - u\| \leq C_\sigma h^{m+1} |u|_{m+1}.$$

Proof. The existence and uniqueness of R_h follows from the fact that a_h is continuous and coercive and the continuity of a. Setting $\delta_h := R_h u - u_I$ and using the definition of R_h, we derive

$$\begin{aligned}
a_h(\delta_h, \delta_h) &= a_h(R_h u, \delta_h) - a_h(u_I, \delta_h) \\
&= \sum_{E \in \mathcal{T}_h} \left[a^E(u, \delta_h) - a_h^E(u_I, \delta_h) \right] \\
&= \sum_{E \in \mathcal{T}_h} a^E(u - \Pi_{m,E}^0 u, \delta_h) + \sum_{E \in \mathcal{T}_h} \left(a^E(\Pi_{m,E}^0 u, \delta_h) - a_h^E(\Pi_{m,E}^0 u, \delta_h) \right) \\
&\quad + \sum_{E \in \mathcal{T}_h} a_h^E(\Pi_{m,E}^0 u - u_I, \delta_h) \\
&= I_1 + I_2 + I_3.
\end{aligned} \tag{1.5.2}$$

From continuity of a and Lemma 1.4.2, we have

$$I_1 \leq \sum_{E \in \mathcal{T}_h} \overline{M} |u - \Pi_{m,E}^0 u|_{1,E} |\delta_h|_{1,E} \leq \sum_{E \in \mathcal{T}_h} \overline{M} C h_E^m |u|_{m+1,E} |\delta_h|_{1,E} \leq C_\sigma h^m |u|_{m+1} |\delta_h|_1. \tag{1.5.3}$$

For I_2, using Lemma 1.4.4, we obtain

$$I_2 \leq \sum_{E\in\mathcal{T}_h} \overline{M}Ch_E^m|u|_{m+1,E}|\delta_h|_{1,E} \leq C_\sigma h^m|u|_{m+1}|\delta_h|_1. \tag{1.5.4}$$

Again for I_3, continuity of a_h, Lemma 1.4.2 and interpolation error estimate (1.4.13) imply

$$\begin{aligned} I_3 &\leq \sum_{E\in\mathcal{T}_h} (1+\beta_\sigma)\overline{M}|\Pi^0_{m,E}u - u_I|_{1,E}|\delta_h|_{1,E} \\ &\leq \sum_{E\in\mathcal{T}_h} (1+\beta_\sigma)\overline{M}Ch_E^m|u|_{m+1,E}|\delta_h|_{1,E} \\ &\leq C_\sigma h^m|u|_{m+1}|\delta_h|_1. \end{aligned} \tag{1.5.5}$$

Plugging (1.5.3)-(1.5.5) in (1.5.2) and using the coercivity of a_h results in

$$|\delta_h|_1 \leq C_\sigma h^m|u|_{m+1}.$$

Thus by interpolation error estimate (1.4.13) and triangle inequality, we obtain

$$|R_h u - u|_1 \leq C_\sigma h^m|u|_{m+1}. \tag{1.5.6}$$

For the L^2 norm estimate, we will use the following dual problem: Find $\varphi \in H_0^1(\Omega)$ such that

$$-\Delta\varphi = u - R_h u.$$

If Ω is convex, we have the regularity result

$$|\varphi|_2 \leq C\|u - R_h u\|. \tag{1.5.7}$$

Let $\varphi_I \in W_h^m$ be the interpolant of φ. Then, we have

$$|\varphi - \varphi_I|_1 \leq Ch|\varphi|_2 \leq Ch\|u - R_h u\|. \tag{1.5.8}$$

Again from the definition of R_h, we derive

$$\begin{aligned} (\sigma(u - R_h u), u - R_h u) &= (\sigma(u - R_h u), -\Delta\varphi) \\ &= a(u - R_h u, \varphi) \\ &= a(u - R_h u, \varphi - \varphi_I) + a(u - R_h u, \varphi_I) \\ &= a(u - R_h u, \varphi - \varphi_I) + a(u, \varphi_I) - a(R_h u, \varphi_I) \\ &= a(u - R_h u, \varphi - \varphi_I) + a_h(R_h u, \varphi_I) - a(R_h u, \varphi_I) \\ &= T_1 + T_2. \end{aligned} \tag{1.5.9}$$

For T_1, using (1.5.6) and (1.5.8), we have

$$T_1 = a(u - R_h u, \varphi - \varphi_I) \leq \overline{M}|u - R_h u|_1 |\varphi - \varphi_I|_1 \leq C_\sigma h^{m+1}|u|_{m+1}\|u - R_h u\|.$$

The second term T_2 can be written as

$$\begin{aligned} T_2 =& a_h(R_h u, \varphi_I) - a(R_h u, \varphi_I) \\ &= \sum_{E\in\mathcal{T}_h} \left[a_h^E(R_h u, \varphi_I) - a^E(R_h u, \varphi_I)\right] \\ &= \sum_{E\in\mathcal{T}_h} \left[a_h^E(R_h u - \Pi^0_{m,E} u, \varphi_I) - a^E(R_h u - \Pi^0_{m,E} u, \varphi_I)\right] \\ &\quad + \sum_{E\in\mathcal{T}_h} \left[a_h^E(\Pi^0_{m,E} u, \varphi_I) - a^E(\Pi^0_{m,E} u, \varphi_I)\right] \\ &= J_1 + J_2. \end{aligned} \tag{1.5.10}$$

For J_1, using Remark 1.4.2, Lemma 1.4.2 and (1.5.6)-(1.5.7), we have

$$\begin{aligned} J_1 &= \sum_{E\in\mathcal{T}_h} \left[a_h^E(R_h u - \Pi^0_{m,E} u, \varphi_I) - a^E(R_h u - \Pi^0_{m,E} u, \varphi_I)\right] \\ &\leq C_\sigma \sum_{E\in\mathcal{T}_h} h_E |R_h u - \Pi^0_{m,E} u|_{1,E} |\varphi|_{2,E} \\ &\leq C_\sigma \sum_{E\in\mathcal{T}_h} h_E^{m+1} |u|_{m+1,E} |\varphi|_{2,E} \\ &\leq C_\sigma h^{m+1} |u|_{m+1} |\varphi|_2 \\ &\leq C_\sigma h^{m+1} |u|_{m+1} \|u - R_h u\|. \end{aligned}$$

Similarly for J_2, using Remark 1.4.2 and (1.5.7), we obtain

$$\begin{aligned} J_2 &= \sum_{E\in\mathcal{T}_h} \left[a_h^E(\Pi^0_{m,E} u, \varphi_I) - a^E(\Pi^0_{m,E} u, \varphi_I)\right] \\ &\leq C_\sigma \sum_{E\in\mathcal{T}_h} h_E^{m+1} |u|_{m+1,E} |\varphi|_{2,E} \\ &\leq C_\sigma h^{m+1} |u|_{m+1} |\varphi|_2 \\ &\leq C_\sigma h^{m+1} |u|_{m+1} \|u - R_h u\|. \end{aligned}$$

Substituting the above two estimate in (1.5.10), it yields

$$T_2 \leq C_\sigma h^{m+1}|u|_{m+1}\|u - R_h u\|.$$

Plugging the bounds for T_1 and T_2 in (1.5.9), we get

$$\|u - R_h u\| \leq C_\sigma h^{m+1}|u|_{m+1}.$$

This completes the proof. □

We will also require the L^2 projection operator $L_h : L^2(\Omega) \to W_h^m$ define by

$$m_h(L_h u, w) = (u, w) \ \ \forall w \in W_h^m. \tag{1.5.11}$$

The operator L_h has the following projection error [128].

Lemma 1.5.2. *For $u \in H^{m+1}(\Omega)$, we have*

$$\|L_h u - u\| \leq C h^{m+1}|u|_{m+1}.$$

1.6 Layout of the Thesis

This thesis is composed of seven chapters, which are listed below.

Chapter 1 contains the description of the problems, basic notations and preliminary results to be used in the thesis. It also provides a brief literature survey on the numerical techniques for the concern problems on polytopal meshes and the motivations behind the present study. Finally, the basic frame work of VEM for an elliptic problem with variable coefficients is discussed.

In **Chapter 2**, we describe the VEM for the weakly damped wave equations with variable coefficients on polygonal meshes. Very general polygonal meshes are used for the spatial discretization. In both L^2 norm and H^1 semi-norm, optimal order of convergence is obtained for the spatially discrete approximation. We employ the Crank-Nicolson temporal discretization scheme for the fully discrete problem and derive the convergence analysis. Numerical experiments are illustrated to confirm our theoretical findings. Results and findings of this chapter are published in [103].

Chapter 3 concerns with the VEM for pulsed electric field model problems with variable coefficients on polygonal meshes. We have presented the spatially semi-discrete approximation and derive optimal order error estimates in L^2 norm and H^1 norm for the spatially

discrete approximation. We have also developed the fully discrete approximation based on Crank-Nicolson temporal discretization and derived the convergence analysis. The numerical experiments are consistent with the theoretical results. Results and findings of this chapter are published in [102].

In **Chapter 4**, a VEM for second-order Sobolev equations on polygonal meshes is discussed. We propose both semi-discrete and fully discrete schemes to numerically solve the linear Sobolev equations. For the time discretization, we have used implicit second-order Newmark scheme. Optimal convergence rates in both the L^2 norm and the H^1 semi-norm are established using a new non-standard projection operator. Numerical experiments are illustrated to confirm our theoretical findings. Results and findings of this chapter are communicated in [100].

Chapter 5 is devoted to studying the VEM for viscoelastic wave equations on polygonal meshes. We present both semi-discrete and fully discrete approximation to the linear viscoelastic wave equations. We employed the implicit second-order Newmark method for the time discretization. A new non-standard projection operator is used to establish the optimal convergence rates in both the L^2 norm and the H^1 semi-norm. Numerical simulations justify the accuracy, efficiency, and robustness of the proposed algorithms. Results and findings of this chapter are communicated in [101].

In **Chapter 6**, we discuss the high-order time stepping VEMs for the wave equations. Fully discrete VEMs with second-order accuracy in temporal direction require to choose smaller time steps in order to preserve the higher accuracy provided by spatial direction. To overcome this restriction, higher-order time stepping methods are needed. In this work, the general Newmark scheme for temporal discretization is considered along with the virtual element discretization in space for the wave equations on polygonal meshes. Rigorous analysis has been done on the stability and convergence of the proposed method. Optimal convergence is obtained in spatial direction along with up to fourth-order convergence in time for some special cases. Numerical experiments are illustrated to confirm our theoretical findings. Results and findings of this chapter are communicated in [99].

Finally, **Chapter 7** discusses the critical interpretation of the results, trying to emphasize the contributions made by this thesis and the scope of future studies.

2

VEMs for Weakly Damped Wave Equations

This chapter provides a virtual element method for weakly damped wave equations with variable coefficients on polygonal meshes. In both L^2 norm and H^1 semi-norm, optimal order of convergence is obtained for the spatially discrete approximation. We employ the Crank-Nicolson temporal discretization scheme for the fully discrete problem and derive the convergence analysis. Numerical experiments are illustrated to confirm our theoretical findings.

2.1 Introduction

We consider the following hyperbolic type equations with weak damping as our model problem (cf. [76, 105])

$$u_{tt} + \kappa(x)u_t - \nabla \cdot (\sigma(x)\nabla u) = f(x,t) \text{ for } (x,t) \in \Omega \times (0,T] \tag{2.1.1}$$

with ICs and BCs

$$u(x,0) = u_0 \ \ \& \ \ u_t(x,0) = v_0 \text{ for } x \in \Omega; \ \ u(x,t) = 0 \text{ for } (x,t) \in \partial\Omega \times (0,T], \tag{2.1.2}$$

where $\Omega \subset \mathbb{R}^2$ is a polygonal domain with smooth boundary $\partial\Omega$ and $T < \infty$. Here, f denotes the source function, $\kappa(x)$ and $\sigma(x)$ are the damping coefficient and the diffusion coefficient, respectively. Further, we assume that there exists two positive constants $\underline{M}$ and $\overline{M}$ such that $\underline{M} \leq \kappa(x),\ \sigma(x) \leq \overline{M}$ a. e. in Ω.

In the past years, many numerical methods has been developed for solving the hyperbolic heat equation (2.1.1) (see [82, 86, 89, 93, 118] and references therein). Recently, a finite

Results of this Chapter are published in [103]

element method (FEM) with interface is developed in [49, 50]. But, in case of polygonal or polyhedral meshes employing FEM becomes very difficult task due to the complexity in basis construction and it demands higher computational cost to evaluate the integrals using Gauss quadrature. To avoid above difficulties associated with numerical approximation of the model problem (2.1.1), we will propose a novel VEM.

The virtual semi-discrete approximation of the model problem is constructed using three approximated bilinear forms. The fully discrete scheme is obtained by first reformulating the governing equation into a system of first-order equations and then employing the Crank-Nicolson discretization. We present rigorous error analysis for the semi-discrete as well as fully discrete scheme and also derive optimal convergence estimates. Further, in support of theoretical findings numerical examples are presented for high-order VEMs with different polygonal meshes.

The remainder of the content is divided as follows. We present the semi-discrete virtual element approximation in Section 2.2. Next, while Section 2.3 deals with the semi-discrete error analysis, Section 2.4 discusses fully discrete approximation and its convergence. Numerical examples and the conclusion are presented in Section 2.5 and Section 2.6, respectively.

2.2 Semi-discrete Virtual Element Approximation

This section deals with construction of semi-discrete virtual element approximation for the model problem (2.1.1)-(2.1.2).

The variational problem for the model problem (2.1.1)-(2.1.2) is given by : Find $u \in L^2(0,T;H_0^1(\Omega)) \cap H^2(0,T;L^2(\Omega))$ so that for a.e. $t \in (0,T]$

$$\begin{cases} (u_{tt},v) + s(u_t,v) + a(u,v) = (f,v), \ \forall v \in H_0^1(\Omega), \\ u(0) = u_0, u_t(0) = v_0, \end{cases} \tag{2.2.1}$$

where $s(u,v) = (\kappa(x)u,v)$, and $a(u,v) = (\sigma(x)\nabla u, \nabla v)$ $\forall u,v \in H_0^1(\Omega)$. The existence and uniqueness of a solution to the continuous problem follow from the coercivity and continuity of the bilinear forms $s(\cdot,\cdot)$ and $a(\cdot,\cdot)$ on $H_0^1(\Omega)$. In the absence of forcing function f, the continuous energy is given by

$$E(t) = \frac{1}{2}\left[(u_t,u_t) + a(u,u)\right].$$

We recall that due to the symmetry and coercivity of the bilinear form $a(\cdot,\cdot)$, the continuous energy $E(t)$ decreases when it is non-zero.

We recall the virtual element framework discussed in Chapter 1, Section 1.4. The bilinear forms $a(\cdot,\cdot)$ and $s(\cdot,\cdot)$ can be split into their local counterparts in the following manner:

$$a(u,v) := \sum_{E\in\mathcal{T}_h} a^E(u,v),\ s(u,v) := \sum_{E\in\mathcal{T}_h} s^E(u,v)\ \forall\ u,v \in H_0^1(\Omega).$$

As in (1.4.8), we now define the following local discrete bilinear forms on the local virtual element space $W_h^m(E)$:

$$\begin{aligned}
a_h^E(v,w) &:= \left(\sigma\boldsymbol{\Pi}^0_{m-1,E}\nabla v, \boldsymbol{\Pi}^0_{m-1,E}\nabla w\right)_E + S_\sigma^E\left((I-\Pi^\nabla_{m,E})v,(I-\Pi^\nabla_{m,E})w\right),\\
m_h^E(v,w) &:= (\Pi^0_{m,E}v,\Pi^0_{m,E}w)_E + S_0^E\left((I-\Pi^0_{m,E})v,(I-\Pi^0_{m,E})w\right) \quad \&\\
s_h^E(v,w) &:= (\kappa\Pi^0_{m,E}v,\Pi^0_{m,E}w)_E + S_\kappa^E\left((I-\Pi^0_{m,E})v,(I-\Pi^0_{m,E})w\right),
\end{aligned} \tag{2.2.2}$$

where

$$\begin{aligned}
S_\sigma^E(v,w) &= \beta_\sigma^E\sum_{r=1}^{N^E} dof_r(v)dof_r(w),\\
S_0^E(v,w) &= |E|\sum_{r=1}^{N^E} dof_r(v)dof_r(w) \quad \&\\
S_\kappa^E(v,w) &= \beta_\kappa^E|E|\sum_{r=1}^{N^E} dof_r(v)dof_r(w)
\end{aligned}$$

with $\beta_\sigma^E = P_E^a(\sigma)$, $\beta_\kappa^E = P_E^a(\kappa)$ and $N^E = \dim W_h^m(E)$.

The global bilinear forms on the global discrete space W_h^m can be obtained by assembling the local counterpart as: For all $v,w \in W_h^m$

$$a_h(v,w) := \sum_{E\in\mathcal{T}_h} a_h^E(v,w),\ m_h(v,w) := \sum_{E\in\mathcal{T}_h} m_h^E(v,w),\ s_h(v,w) := \sum_{E\in\mathcal{T}_h} s_h^E(v,w).$$

Following the proof in Lemma 1.4.5, we can show that the global bilinear forms a_h, m_h and s_h satisfies the following continuity and coercivity properties: For $v,w \in W_h^m$

$$\begin{aligned}
a_h(v,w) &\le (1+\beta_\sigma)\overline{M}|v|_1|w|_1,\\
m_h(v,w) &\le (1+\beta_0)\|v\|\|w\| \ \&\\
s_h(v,w) &\le (1+\beta_\kappa)\overline{M}\|v\|\|w\|
\end{aligned}$$

and for $w \in W_h^m$

$$a_h(w,w) \geq \min\{1,\alpha_\sigma\}\underline{M}|w|_1^2,$$
$$m_h(w,w) \geq \min\{1,\alpha_0\}\|w\|^2 \ \&$$
$$s_h(w,w) \geq \min\{1,\alpha_\kappa\}\underline{M}\|w\|^2,$$

where $\alpha_\sigma, \beta_\sigma, \alpha_0, \beta_0, \alpha_\kappa, \beta_\kappa$ are some positive constants.

Now, we have the following semi-discrete virtual element approximation to (2.2.1): Find $u_h \in L^2(0,T;W_h^m) \cap H^2(0,T;W_h^m)$ such that for a.e. $t \in (0,T]$

$$\begin{cases} m_h(u_{htt},w_h) + s_h(u_{ht},w_h) + a_h(u_h,w_h) = (f_h,w_h) \quad \forall w_h \in W_h^m, \\ u_h(0) = R_h u_0, \ \ u_{ht}(0) = R_h v_0, \end{cases} \tag{2.2.3}$$

where f_h is the discrete form of the source function f as defined in (1.4.14). Here, R_h is the elliptic projection as defined in (1.5.1).

We will need the following L^2- projections $L_{i,h} : L^2(\Omega) \to W_h^m$, $i = 1,2$ defined by

$$m_h(L_{1,h}u,w) = (u,w), \ \ s_h(L_{2,h}u,w) = s(u,w) \ \ \forall w \in W_h^m. \tag{2.2.4}$$

The operators $L_{i,h}$, $i = 1,2$ has the following projection errors [128].

Lemma 2.2.1. *For $u \in H^{m+1}(\Omega)$, we have*

$$\|L_{i,h}u - u\| \leq Ch^{m+1}|u|_{m+1},$$

where C is a constant independent of h.

2.3 Error Analysis for the Semi-discrete Problems

This section is dedicated to the derivation of error estimates related to the semi-discrete approximation (2.2.3) in both L^2 and H^1 semi-norm.

Before proceeding to the error estimates, we present the following results regarding the stability of the semi-discrete solution u_h with respect to the initial data and the source function.

Lemma 2.3.1. *Let $u_0 \in H_0^1(\Omega) \cap H^k(\Omega)$, $v_0 \in H_0^1(\Omega) \cap H^{k-1}(\Omega)$, and $f \in H^{k-1}(H^{k-2}(\Omega))$, $k = 2, 3, 4$. Then, we have*

$$\|D_t^k u_h(0)\| + \|D_t^{k-1} u_h(0)\|_1 \leq C\big(\|u_0\|_k + \|v_0\|_{k-1} + \|f\|_{H^{k-1}(H^{k-2})}\big),$$

where $D_t^k = \dfrac{\partial^k}{\partial t^k}$.

Proof. We take $t \to 0^+$ in (2.2.3) and then using definition of the elliptic projection operator R_h, we get

$$\begin{aligned} m_h(u_{htt}(0), w_h) &= -s_h(u_{ht}(0), w_h) - a_h(u_h(0), w_h) + (f_h(0), w_h) \\ &= -s_h(R_h v_0, w_h) - a_h(R_h u_0, w_h) + (f_h(0), w_h) \\ &= -s_h(R_h v_0, w_h) - a(u_0, w_h) + (f_h(0), w_h). \end{aligned} \tag{2.3.1}$$

From the continuity of the bilinear form s_h and the H^1-stability of R_h, we have

$$s_h(R_h v_0, w_h) \leq (1 + \beta_\kappa)\overline{M}\|R_h v_0\|\|w_h\| \leq C\|v_0\|\|w_h\|. \tag{2.3.2}$$

By using Green's formula and boundary condition the second term can be bounded as

$$-a(u_0, w_h) = (\nabla \cdot (\sigma(x)\nabla u_0), w_h) \leq C\|u_0\|_2\|w_h\|. \tag{2.3.3}$$

Again, from Lemma 1.4.6 and Lemma 1.2.1, we obtain

$$(f_h(0), w_h) \leq C\|f\|_{H^1(L^2)}\|w_h\|. \tag{2.3.4}$$

Now substituting $w_h = u_{htt}(0)$, using the coercivity of m_h and the estimates in (2.3.2), (2.3.3) and (2.3.4) in (2.3.1) yields

$$\|u_{htt}(0)\| \leq C(\|u_0\|_2 + \|v_0\| + \|f\|_{H^1(L^2)}). \tag{2.3.5}$$

Again, from the H^1-stability of R_h, we have

$$\|u_{ht}(0)\|_1 = \|R_h v_0\|_1 \leq C\|v_0\|_1.$$

This proves the result for $k = 2$. For $k = 3$, from (2.2.3) and (2.2.1) for $t \to 0^+$, we have

$$m_h(u_{htt}(0), w_h) - (u_{tt}(0), w_h) = s(v_0, w_h) - s_h(R_h v_0, w_h) + (f_h(0) - f(0), w_h).$$

Here, we have used the definition of R_h operator. Now, from the definition of L^2-projection operators $L_{i,h}$, $i = 1, 2$, we obtain

$$m_h(u_{htt}(0) - L_{1,h}u_{tt}(0), w_h) = s_h(L_{2,h}v_0 - R_h v_0, w_h) + (f_h(0) - f(0), w_h).$$

Setting $w_h = u_{htt}(0) - L_{1,h}u_{tt}(0)$, using coercivity of m_h, continuity of s_h, approximation properties of operators R_h and $L_{2,h}$, and definition of f_h, we obtain

$$\begin{aligned} \|u_{htt}(0) - L_{1,h}u_{tt}(0)\| \leq & C(\|L_{2,h}v_0 - R_h v_0\| + \|f_h(0) - f(0)\|) && (2.3.6)\\ \leq & Ch(\|v_0\|_1 + \|f\|_{H^1(H^1)}). && (2.3.7) \end{aligned}$$

Estimate (2.3.7) along with inverse inequality (1.4.2) and H^1-stability of $L_{1,h}$ yields

$$\begin{aligned} \|u_{htt}(0)\|_1 \leq & Ch^{-1}\|u_{htt}(0) - L_{1,h}u_{tt}(0)\| + \|L_{1,h}u_{tt}(0)\|_1 \\ \leq & C(\|v_0\|_1 + \|f\|_{H^1(H^1)} + \|u_{tt}(0)\|_1). && (2.3.8) \end{aligned}$$

From (2.1.1), we have

$$u_{tt}(0) = -\kappa(x)v_0 + \nabla \cdot (\sigma(x)\nabla u_0) + f(0). \tag{2.3.9}$$

Now, using Lemma 1.2.1, we get

$$\|u_{tt}(0)\|_1 \leq C(\|u_0\|_3 + \|v_0\|_1 + \|f\|_{H^1(H^1)}). \tag{2.3.10}$$

Hence, using (2.3.10), (2.3.8) reduces to

$$\|u_{htt}(0)\|_1 \leq C(\|u_0\|_3 + \|v_0\|_1 + \|f\|_{H^1(H^1)}).$$

Next, differentiating (2.2.3) partially with respect to variable t and then taking $t \to 0^+$, we obtain

$$\begin{aligned} m_h(u_{htt}(0), w_h) &= -s_h(u_{htt}(0), w_h) - a_h(R_h v_0, w_h) + (f_{ht}(0), w_h) \\ &= -s_h(u_{htt}(0), w_h) - a(v_0, w_h) + (f_{ht}(0), w_h). \end{aligned}$$

Following the arguments as in (2.3.5), we can easily derive

$$\|u_{htt}(0)\| \leq C(\|u_0\|_2 + \|v_0\|_2 + \|f\|_{H^2(L^2)}). \tag{2.3.11}$$

This proves the result for $k = 3$. For $k = 4$, we first observe that

$$\begin{aligned}
&m_h(u_{htttt}(0), w_h)\\
&= -s_h(u_{httt}(0), w_h) - a_h(u_{htt}(0), w_h) + (f_{htt}(0), w_h)\\
&= -s_h(u_{httt}(0), w_h) - a_h(u_{htt}(0) - R_h u_{tt}(0), w_h) - a(u_{tt}(0), w_h) + (f_{htt}(0), w_h)\\
&= -s_h(u_{httt}(0), w_h) - a_h(u_{htt}(0) - R_h u_{tt}(0), w_h) + (\nabla \cdot (\sigma(x)\nabla u_{tt}(0)), w_h) + (f_{htt}(0), w_h)\\
&\leq C\left(\|u_{httt}(0)\| + h^{-1}\|u_{htt}(0) - R_h u_{tt}(0)\|_1 + \|u_{tt}(0)\|_2 + \|f\|_{H^3(L^2)}\right)\|w_h\|. \qquad (2.3.12)
\end{aligned}$$

Now using inverse inequality (1.4.2) and (2.3.6), we have

$$\begin{aligned}
\|u_{htt}(0) - R_h u_{tt}(0)\|_1 \leq& Ch^{-1}\|u_{htt}(0) - L_{1,h}u_{tt}(0)\| + \|L_{1,h}u_{tt}(0) - R_h u_{tt}(0)\|_1\\
\leq& Ch(\|v_0\|_2 + \|f\|_{H^1(H^2)} + \|u_{tt}(0)\|_2). \qquad (2.3.13)
\end{aligned}$$

Similar to (2.3.10) from (2.3.9), we have

$$\|u_{tt}(0)\|_2 \leq C(\|u_0\|_4 + \|v_0\|_2 + \|f\|_{H^1(H^2)}). \qquad (2.3.14)$$

Substituting $w_h = u_{htttt}(0)$ and then using estimate (2.3.14) together with (2.3.11) and (2.3.13) in (2.3.12), gives us

$$\|u_{htttt}(0)\| \leq C(\|u_0\|_4 + \|v_0\|_2 + \|f\|_{H^3(H^2)}). \qquad (2.3.15)$$

Now, using the same argument employed in (2.3.8), we get

$$\begin{aligned}
\|u_{htt}(0)\|_1 \leq& Ch^{-1}\|u_{htt}(0) - L_{1,h}u_{ttt}(0)\| + \|L_{1,h}u_{ttt}(0)\|_1\\
\leq& C(\|u_0\|_3 + \|v_0\|_3 + \|f\|_{H^2(H^1)}).
\end{aligned}$$

□

Lemma 2.3.2. *For $u_0 \in H_0^1(\Omega) \cap H^k(\Omega)$, $v_0 \in H_0^1(\Omega) \cap H^{k-1}(\Omega)$, and $f \in H^{k-1}(H^{k-2}(\Omega))$, $k = 3, 4$, u_h satisfies*

$$\|D_t^k u_h\|^2_{L^2(L^2)} \leq C\left(\|u_0\|_k^2 + \|v_0\|_{k-1}^2 + \|f\|^2_{H^{k-1}(H^{k-2})}\right).$$

Proof. Differentiating (2.2.3) twice with respect to t and then substituting $w_h = u_{htt}$, we obtain

$$\frac{1}{2}\frac{d}{dt}m_h(u_{htt}, u_{htt}) + s_h(u_{htt}, u_{htt}) + \frac{1}{2}\frac{d}{dt}a_h(u_{htt}, u_{htt}) = (f_{htt}, u_{htt}).$$

Now integrating from 0 to T, application of Young's inequality and coercivity of m_h yields

$$\int_0^T \|u_{httt}(t)\|^2 dt \leq C\Big(\|u_{httt}(0)\|^2 + \|u_{htt}(0)\|_1^2 + \int_0^T \|f_{htt}(t)\|^2 dt\Big).$$

Further, using Lemma 2.3.1 in the above equation, we have

$$\|u_{httt}\|^2_{L^2(L^2)} \leq C(\|u_0\|_3^2 + \|v_0\|_2^2 + \|f\|^2_{H^2(H^1)}).$$

This proves for $k = 3$. For the case $k = 4$, proceeding in a similar manner, we obtain

$$\|u_{htttt}\|^2_{L^2(L^2)} \leq C(\|u_0\|_4^2 + \|v_0\|_3^2 + \|f\|^2_{H^3(H^2)}).$$

□

We derive the following result for the error estimate of the semi-discrete approximation (2.2.3) in H^1 semi-norm.

Theorem 2.3.1. *Assume that $u_0 \in H^{m+1}(\Omega)$ and $u_t, u_{tt}, f \in L^2(0,T;H^{m+1}(\Omega))$. Then for all $t \in (0,T]$, we have*

$$\begin{aligned}|u_h(t) - u(t)|_1 \leq & Ch^m(|u_0|_{m+1} + \|u_t\|_{L^1(H^{m+1})}) \\ & + Ch^{m+1}(\|u_t\|_{L^2(H^{m+1})} + \|u_{tt}\|_{L^2(H^{m+1})} + \|f\|_{L^2(H^{m+1})}).\end{aligned}$$

Proof. Let us divide the error $e_h(t) = u_h(t) - u(t)$ as

$$e_h(t) = \phi(t) + \psi(t), \tag{2.3.16}$$

where $\phi(t) =: u_h(t) - R_h u(t)$ and $\psi(t) =: R_h u(t) - u(t)$. Now, we have the following bounds for $\psi(t)$ due to Lemma 2.2.1:

$$|\psi(t)|_1 \leq Ch^m|u(t)|_{m+1} \leq Ch^m(|u_0|_{m+1} + \|u_t\|_{L^1(H^{m+1})}). \tag{2.3.17}$$

Therefore, we only need to estimate the bound for the term $\phi(t)$. From (2.2.3) and using the definition of the projection operator R_h, we have the following error equation for $\phi(t)$. For all $w_h \in W_h^m$ and for all $t \in (0,T]$

$$\begin{aligned}& m_h(\phi_{tt}(t), w_h) + s_h(\phi_t(t), w_h) + a_h(\phi(t), w_h) \\ &= (f_h(t), w_h) - m_h(R_h u_{tt}(t), w_h) - s_h(R_h u_t(t), w_h) - a_h(R_h u(t), w_h) \\ &= (f_h(t) - f(t), w_h) + (u_{tt}(t), w_h) - m_h(R_h u_{tt}(t), w_h) + s(u_t(t), w_h) - s_h(R_h u_t(t), w_h) \\ &=: T_1 + T_2 + T_3. \end{aligned} \tag{2.3.18}$$

For the term T_1, from Lemma 1.4.6, we have

$$T_1 = (f_h(t) - f(t), w_h) \leq Ch^{m+1}|f(t)|_{m+1}\|w_h\|. \tag{2.3.19}$$

Now for the term T_2, using the definition of projection operator $L_{1,h}$, continuity of m_h and approximation properties of $L_{1,h}$ and R_h, we obtain

$$\begin{aligned} T_2 &= (u_{tt}(t), w_h) - m_h(R_h u_{tt}(t), w_h) \\ &= m_h(L_{1,h}u_{tt}(t) - R_h u_{tt}(t), w_h) \\ &\leq (1+\beta_0)\|L_{1,h}u_{tt}(t) - R_h u_{tt}(t)\|\|w_h\| \\ &\leq Ch^{m+1}|u_{tt}(t)|_{m+1}\|w_h\|. \end{aligned} \tag{2.3.20}$$

Using similar arguments, we can write

$$T_3 = s(u_t(t), w_h) - s_h(R_h u_t(t), w_h) \leq Ch^{m+1}|u_t(t)|_{m+1}\|w_h\|. \tag{2.3.21}$$

Now, substituting the estimates for T_1, T_2 and T_3 from (2.3.19)-(2.3.21) and putting $w_h = \phi_t(t)$ in the error equation (2.3.18), we obtain

$$\begin{aligned} &m_h(\phi_{tt}(t), \phi_t(t)) + s_h(\phi_t(t), \phi_t(t)) + a_h(\phi(t), \phi_t(t)) \\ &\leq Ch^{m+1}(|u_t(t)|_{m+1} + |u_{tt}(t)|_{m+1} + |f(t)|_{m+1})\|\phi_t(t)\|. \end{aligned}$$

The above equation can be rewritten as

$$\begin{aligned} &\frac{1}{2}\frac{d}{dt}m_h(\phi_t(t), \phi_t(t)) + s_h(\phi_t(t), \phi_t(t)) + \frac{1}{2}\frac{d}{dt}a_h(\phi(t), \phi(t)) \\ &\leq Ch^{m+1}(|u_t(t)|_{m+1} + |u_{tt}(t)|_{m+1} + |f(t)|_{m+1})\|\phi_t(t)\|. \end{aligned}$$

Integrating from 0 to t and using the fact that $\phi(0) = \phi_t(0) = 0$, we get

$$\begin{aligned} &m_h(\phi_t(t), \phi_t(t)) + 2\int_0^t s_h(\phi_t(s), \phi_t(s))ds + a_h(\phi(t), \phi(t)) \\ &\leq \int_0^t Ch^{m+1}(|u_t(s)|_{m+1} + |u_{tt}(s)|_{m+1} + |f(s)|_{m+1})\|\phi_t(s)\|ds. \end{aligned} \tag{2.3.22}$$

Employing Young's inequality in (2.3.22) and neglecting the terms $\|\phi_t(t)\|^2$ and $\|\phi_t(t)\|^2_{L^2(L^2)}$, we obtain

$$|\phi(t)|_1^2 \leq Ch^{2(m+1)}(\|u_t\|^2_{L^2(H^{m+1})} + \|u_{tt}\|^2_{L^2(H^{m+1})} + \|f\|^2_{L^2(H^{m+1})}). \tag{2.3.23}$$

Now plugging (2.3.17) and (2.3.23) in (2.3.16), we get

$$\begin{aligned}|u_h(t)-u(t)|_1 \leq & Ch^m(|u_0|_{m+1}+\|u_t\|_{L^1(H^{m+1})}) \\ & + Ch^{m+1}(\|u_t\|_{L^2(H^{m+1})}+\|u_{tt}\|_{L^2(H^{m+1})}+\|f\|_{L^2(H^{m+1})}).\end{aligned}$$

□

Now, we will present the main result of this section. The semi-discrete approximation (2.2.3) has the following error estimate in L^2 norm.

Theorem 2.3.2. *Assume that $u_0, v_0 \in H^{m+1}(\Omega)$ and $u_t, f \in L^1(0,T;H^{m+1}(\Omega))$. Then, we have*

$$\|u_h(t)-u(t)\| \leq Ch^{m+1}(|u_0|_{m+1}+|v_0|_{m+1}+\|u_t\|_{L^1(H^{m+1})}+\|f\|_{L^1(H^{m+1})}) \quad \forall t \in (0,T].$$

Proof. As in (2.3.16), let us split the error $e_h(t) = u_h(t)-u(t) =: \phi(t)+\psi(t)$. Applying Lemma 2.2.1, we have the following bounds for $\psi(t)$ in L^2 norm

$$\|\psi(t)\| \leq Ch^{m+1}|u(t)|_{m+1} \leq Ch^{m+1}(|u_0|_{m+1}+\|u_t\|_{L^1(H^{m+1})}). \tag{2.3.24}$$

Now, in order to obtain the bounds for the term $\phi(t)$, using the definition of projection operators $L_{i,h}$, $i=1,2$ and then taking $\rho = L_{1,h}u - R_h u$, $\tilde{\rho} = L_{2,h}u - R_h u$ in the error equation (2.3.18), we have the following relation. For all $w_h \in W_h^m$ and for all $t \in (0,T]$

$$\begin{aligned}&\frac{d}{dt}m_h(\phi_t(t),w_h) - m_h(\phi_t(t),w_{ht}) + \frac{d}{dt}s_h(\phi(t),w_h) - s_h(\phi(t),w_{ht}) + a_h(\phi(t),w_h) \\ &= (f_h(t)-f(t),w_h) + \frac{d}{dt}(u_t(t),w_h) - (u_t(t),w_{ht}) - \frac{d}{dt}m_h(R_h u_t(t),w_h) \\ &\quad + m_h(R_h u_t(t),w_{ht}) + s(u_t(t),w_h) - s_h(R_h u_t(t),w_h) \\ &= (f_h(t)-f(t),w_h) + \frac{d}{dt}m_h(L_{1,h}u_t(t),w_h) - m_h(L_{1,h}u_t(t),w_{ht}) - \frac{d}{dt}m_h(R_h u_t(t),w_h) \\ &\quad + m_h(R_h u_t(t),w_{ht}) + s_h(L_{2,h}u_t(t),w_h) - s_h(R_h u_t(t),w_h) \\ &= (f_h(t)-f(t),w_h) + \frac{d}{dt}m_h(\rho_t(t),w_h) - m_h(\rho_t(t),w_{ht}) + s_h(\tilde{\rho}_t(t),w_h).\end{aligned} \tag{2.3.25}$$

Define,

$$\widehat{\phi}(\cdot,t) = \int_t^\zeta \phi(\cdot,s)ds, \quad 0 \leq t \leq T.$$

Then, clearly $\widehat{\phi}(\cdot,\zeta)=0$ and $\widehat{\phi}_t(\cdot,t)=-\phi(\cdot,t)$, $0\le t\le T$. Now, substituting $w_h=\widehat{\phi}(t)\in W_h^m$ in (2.3.25), we get

$$\begin{aligned}&\frac{d}{dt}m_h(\phi_t(t),\widehat{\phi}(t))+m_h(\phi_t(t),\phi(t))+\frac{d}{dt}s_h(\phi(t),\widehat{\phi}(t))+s_h(\phi(t),\phi(t))+a_h(\phi(t),\widehat{\phi}(t))\\&=\Big(f_h(t)-f(t),\widehat{\phi}(t)\Big)+\frac{d}{dt}m_h(\rho_t(t),\widehat{\phi}(t))+m_h(\rho_t(t),\phi(t))+s_h(\tilde{\rho}_t(t),\widehat{\phi}(t))\end{aligned}$$

which can be rewritten as

$$\begin{aligned}&\frac{1}{2}\frac{d}{dt}m_h(\phi(t),\phi(t))+\frac{d}{dt}s_h(\phi(t),\widehat{\phi}(t))+s_h(\phi(t),\phi(t))-\frac{1}{2}\frac{d}{dt}a_h(\widehat{\phi}(t),\widehat{\phi}(t))\\&=\Big(f_h(t)-f(t),\widehat{\phi}(t)\Big)+\frac{d}{dt}m_h(\rho_t(t)-\phi_t(t),\widehat{\phi}(t))+m_h(\rho_t(t),\phi(t))+s_h(\tilde{\rho}_t(t),\widehat{\phi}(t)).\end{aligned}$$

Integrating 0 to ζ and using $\widehat{\phi}(\cdot,\zeta)=0$, $\phi(0)=\phi_t(0)=0$, we get

$$\begin{aligned}&\frac{1}{2}m_h(\phi(\zeta),\phi(\zeta))+\int_0^\zeta s_h(\phi(s),\phi(s))ds+\frac{1}{2}a_h(\widehat{\phi}(0),\widehat{\phi}(0))\\&=\int_0^\zeta\Big(f_h(s)-f(s),\widehat{\phi}(s)\Big)\,ds-m_h(\rho_t(0),\widehat{\phi}(0))\\&+\int_0^\zeta m_h(\rho_t(s),\phi(s))ds+\int_0^\zeta s_h(\tilde{\rho}_t(s),\widehat{\phi}(s))ds\\&=I_1+I_2+I_3+I_4.\end{aligned}\tag{2.3.26}$$

Since $\phi(t)$ is continuous in the variable t, we let

$$\|\phi(\zeta)\|=\sup_{0\le t\le T}\|\phi(t)\|.$$

Then, one can easily see that $\|\widehat{\phi}(t)\|\le C\|\phi(\zeta)\|$ for all $t\in(0,T]$. Hence, Lemma 1.4.6 implies

$$\begin{aligned}I_1&=\int_0^\zeta\Big(f_h(s)-f(s),\widehat{\phi}(s)\Big)\,ds\\&\le\int_0^\zeta\|f_h(s)-f(s)\|\,\|\widehat{\phi}(s)\|ds\\&\le\int_0^\zeta Ch^{m+1}|f(s)|_{m+1}\|\widehat{\phi}(s)\|ds\\&\le Ch^{m+1}\|\phi(\zeta)\|\int_0^\zeta|f(s)|_{m+1}ds\\&\le Ch^{m+1}\|f\|_{L^1(H^{m+1})}\|\phi(\zeta)\|.\end{aligned}$$

Next, for I_2 using the continuity of the bilinear form m_h, we get

$$I_2 = m_h(\rho_t(0), \widehat{\phi}(0)) \leq Ch^{m+1}|v_0|_{m+1}\|\phi(\zeta)\|.$$

Similarly,

$$I_3 = \int_0^\zeta m_h(\rho_t(s), \phi(s))ds \leq Ch^{m+1}\|u_t\|_{L^1(H^{m+1})}\|\phi(\zeta)\|$$

and

$$I_4 = \int_0^\zeta s_h(\tilde{\rho}_t(s), \widehat{\phi}(s))ds \leq Ch^{m+1}\|u_t\|_{L^1(H^{m+1})}\|\phi(\zeta)\|.$$

Using all the estimates in (2.3.26), we get

$$\|\phi(\zeta)\|^2 \leq Ch^{m+1}(|v_0|_{m+1} + \|f\|_{L^1(H^{m+1})} + \|u_t\|_{L^1(H^{m+1})})\|\phi(\zeta)\|.$$

Hence,

$$\|\phi(t)\| \leq \|\phi(\zeta)\| \leq Ch^{m+1}(|v_0|_{m+1} + \|f\|_{L^1(H^{m+1})} + \|u_t\|_{L^1(H^{m+1})}). \tag{2.3.27}$$

Now, from (2.3.24) and (2.3.27), we get the theorem

$$\|u_h(t) - u(t)\| \leq Ch^{m+1}(|u_0|_{m+1} + |v_0|_{m+1} + \|u_t\|_{L^1(H^{m+1})} + \|f\|_{L^1(H^{m+1})}).$$

□

2.4 Error Analysis for the Fully Discrete Problems

In this section, we will formulate the Crank-Nicolson based fully discrete approximation to the model problem (2.1.1). We will show that for the fully discrete scheme the discrete energy does not increase with time and also derive the optimal order error estimate in $L^\infty(L^2)$ norm.

Let us write $\vartheta = u_t$, where ϑ is an auxiliary unknown. Then, our model equation (2.1.1) can be split into a first-order system of equations in t as

$$\begin{cases} u_t - \vartheta = 0 \text{ in } \Omega \times (0, T], \\ \vartheta_t + \kappa\vartheta - \nabla \cdot (\sigma \nabla u) = f \text{ in } \Omega \times (0, T]. \end{cases} \tag{2.4.1}$$

We break the temporal interval $[0,T]$ into equispaced sub-intervals $[t_{n-1},t_n]$ with time step $\tau = t_n - t_{n-1}$, where $n = 1,2,\cdots,N$. Consider the sequence $\{\mathcal{U}^n\}_{n=0}^N$ such that $\mathcal{U}^n \approx u_h(\cdot,t_n), 0 \le n \le N$. For any $v \in W_h^m$, we define the following notations:

$$\partial_\tau v^n = \frac{v^{n+1}-v^n}{\tau} \quad \& \quad v^{n+\frac{1}{2}} = \frac{v^{n+1}+v^n}{2}, \quad n = 0,1,\cdots,N-1.$$

We seek a suitable p such that

$$\|\mathcal{U}^n - u(\cdot,t_n)\| \le C_1 h^{m+1} + C_2 \tau^p.$$

Here, p is called the order of the time scheme.

Now, employing Crank-Nicolson fully discrete scheme to both the equations in (2.4.1), we obtain the fully discretized problem defined by: Find $\mathcal{U}^n, \vartheta^n \in W_h^m$ such that for $n = 1,2,\cdots,N-1$

$$\begin{cases} \partial_\tau \mathcal{U}^n = \vartheta^{n+\frac{1}{2}}, \\ m_h(\partial_\tau \vartheta^n, w) + s_h(\vartheta^{n+\frac{1}{2}}, w) + a_h(\mathcal{U}^{n+\frac{1}{2}}, w) = (f_h^{n+\frac{1}{2}}, w) \ \forall\ w \in W_h^m, \\ \mathcal{U}^0 = R_h u_0, \vartheta^0 = R_h v_0. \end{cases} \tag{2.4.2}$$

We have the following lemma regarding the existence of a unique solution $\mathcal{U}^n$ to the fully discrete problem.

Lemma 2.4.1. *There exist a unique sequence $\{\mathcal{U}^n\}_{n=0}^N$ which satisfies the problem (2.4.2).*

Proof. From (2.4.2), for $n \ge 0$, ϑ^{n+1} satisfies

$$\begin{aligned} &m_h(\vartheta^{n+1},w) + \left(\frac{\tau}{2}\right) s_h(\vartheta^{n+1},w) + \left(\frac{\tau^2}{4}\right) a_h(\vartheta^{n+1},w) \\ &= m_h(\vartheta^n,w) - \left(\frac{\tau}{2}\right) s_h(\vartheta^n,w) - \left(\frac{\tau^2}{4}\right) a_h(\vartheta^n,w) - \tau\, a_h(\mathcal{U}^n,w) + \tau\, (f_h^{n+\frac{1}{2}},w)\ \forall w \in W_h^m. \end{aligned}$$

This can be written as

$$c_h(\vartheta^{n+1},w) = l^n(w)\ \forall w \in W_h^m,$$

where c_h is the bilinear form

$$c_h(v,w) = m_h(v,w) + \left(\frac{\tau}{2}\right) s_h(v,w) + \left(\frac{\tau^2}{4}\right) a_h(v,w)\ \forall v,w \in W_h^m$$

and l^n is the linear operator

$$l^n(w) = m_h(\vartheta^n, w) - \left(\frac{\tau}{2}\right) s_h(\vartheta^n, w) - \left(\frac{\tau^2}{4}\right) a_h(\vartheta^n, w) - \tau\, a_h(\mathcal{U}^n, w) + \tau\, (f_h^{n+\frac{1}{2}}, w)\ \forall w \in W_h^m.$$

Clearly, c_h is positive definite as the bilinear forms m_h, s_h and a_h are positive definite. Also, the operator l^n is continuous. Hence, ϑ^{n+1} exists uniquely, which along with the first part of (2.4.2) implies that there exist unique $\mathcal{U}^{n+1}$, $n = 0, 1, \cdots, N-1$. □

Let us define the following notations:

$$\bar{\partial}_{tt}\mathcal{U}^n = \frac{\mathcal{U}^{n+1} - 2\mathcal{U}^n + \mathcal{U}^{n-1}}{\tau^2}, \quad \bar{\partial}_t\mathcal{U}^n = \frac{\mathcal{U}^{n+1} - \mathcal{U}^{n-1}}{2\tau}.$$

The fully discrete approximation (2.4.2) can also be written by

$$m_h(\bar{\partial}_{tt}\mathcal{U}^n, w) + s_h(\partial_\tau\mathcal{U}^n, w) + a_h(\mathcal{U}^{n+\frac{1}{2}}, w) = (f^{n+\frac{1}{2}}, w)\ \forall\ w \in W_h^m. \tag{2.4.3}$$

We have the following result regarding the discrete energy for the fully discrete scheme (2.4.3).

Theorem 2.4.1. *The discrete energy*

$$E_h^{n+\frac{1}{2}} = \frac{1}{2}\left[m_h(\partial_\tau\mathcal{U}^n, \partial_\tau\mathcal{U}^n) + \frac{\tau}{2}s_h(\partial_\tau\mathcal{U}^n, \partial_\tau\mathcal{U}^n) + a_h(\mathcal{U}^{n+\frac{1}{2}}, \mathcal{U}^{n+\frac{1}{2}})\right].$$

does not increase with time.

Proof. In the absence of forcing function, equation (2.4.3) becomes

$$m_h(\bar{\partial}_{tt}\mathcal{U}^n, w) + s_h(\partial_\tau\mathcal{U}^n, w) + a_h(\mathcal{U}^{n+\frac{1}{2}}, w) = 0. \tag{2.4.4}$$

It is easy to see that

$$\partial_\tau\mathcal{U}^n = \frac{\tau}{2}\bar{\partial}_{tt}\mathcal{U}^n + \bar{\partial}_t\mathcal{U}^n.$$

Thus from (2.4.4), we get

$$m_h(\bar{\partial}_{tt}\mathcal{U}^n, w) + \frac{\tau}{2}s_h(\bar{\partial}_{tt}\mathcal{U}^n, w) + s_h(\bar{\partial}_t\mathcal{U}^n, w) + a_h(\mathcal{U}^{n+\frac{1}{2}}, w) = 0.$$

Now, substituting $w = \bar{\partial}_t\mathcal{U}^n$, we obtain

$$m_h(\bar{\partial}_{tt}\mathcal{U}^n, \bar{\partial}_t\mathcal{U}^n) + \frac{\tau}{2}s_h(\bar{\partial}_{tt}\mathcal{U}^n, \bar{\partial}_t\mathcal{U}^n) + s_h(\bar{\partial}_t\mathcal{U}^n, \bar{\partial}_t\mathcal{U}^n) + a_h(\mathcal{U}^{n+\frac{1}{2}}, \bar{\partial}_t\mathcal{U}^n) = 0. \tag{2.4.5}$$

The first term in the above equation can be written as

$$m_h(\bar{\partial}_{tt}\mathcal{U}^n, \bar{\partial}_t\mathcal{U}^n) = \frac{1}{2\tau}\left[m_h(\partial_\tau\mathcal{U}^n, \partial_\tau\mathcal{U}^n) - m_h(\partial_\tau\mathcal{U}^{n-1}, \partial_\tau\mathcal{U}^{n-1})\right].$$

Similarly,

$$s_h(\bar{\partial}_{tt}\mathcal{U}^n, \bar{\partial}_t\mathcal{U}^n) = \frac{1}{2\tau}\left[s_h(\partial_\tau\mathcal{U}^n, \partial_\tau\mathcal{U}^n) - s_h(\partial_\tau\mathcal{U}^{n-1}, \partial_\tau\mathcal{U}^{n-1})\right].$$

Then (2.4.5) can be written as

$$\begin{aligned}&\frac{1}{2\tau}\left[m_h(\partial_\tau\mathcal{U}^n, \partial_\tau\mathcal{U}^n) - m_h(\partial_\tau\mathcal{U}^{n-1}, \partial_\tau\mathcal{U}^{n-1})\right]\\ &+ \frac{1}{4}\left[s_h(\partial_\tau\mathcal{U}^n, \partial_\tau\mathcal{U}^n) - s_h(\partial_\tau\mathcal{U}^{n-1}, \partial_\tau\mathcal{U}^{n-1})\right] + s_h(\bar{\partial}_t\mathcal{U}^n, \bar{\partial}_t\mathcal{U}^n) + a_h(\mathcal{U}^{n+\frac{1}{2}}, \bar{\partial}_t\mathcal{U}^n) = 0.\end{aligned} \tag{2.4.6}$$

Again, since $\bar{\partial}_t\mathcal{U}^n = (\mathcal{U}^{n+\frac{1}{2}} - \mathcal{U}^{n-\frac{1}{2}})/\tau$, we have

$$\begin{aligned}a_h(\mathcal{U}^{n+\frac{1}{2}} + \mathcal{U}^{n-\frac{1}{2}}, \bar{\partial}_t\mathcal{U}^n) &= \frac{1}{\tau}a_h(\mathcal{U}^{n+\frac{1}{2}} + \mathcal{U}^{n-\frac{1}{2}}, \mathcal{U}^{n+\frac{1}{2}} - \mathcal{U}^{n-\frac{1}{2}})\\ &= \frac{1}{\tau}\left[a_h(\mathcal{U}^{n+\frac{1}{2}}, \mathcal{U}^{n+\frac{1}{2}}) - a_h(\mathcal{U}^{n-\frac{1}{2}}, \mathcal{U}^{n-\frac{1}{2}})\right].\end{aligned} \tag{2.4.7}$$

Now, from (2.4.7) and (2.4.6), we can easily derive

$$\frac{1}{\tau}\left(E_h^{n+\frac{1}{2}} - E_h^{n-\frac{1}{2}}\right) + s_h(\bar{\partial}_t\mathcal{U}^n, \bar{\partial}_t\mathcal{U}^n) + \frac{\tau}{2}a_h(\bar{\partial}_t\mathcal{U}^n, \bar{\partial}_t\mathcal{U}^n) = 0.$$

This shows that the discrete energy does not increase with time. □

The following approximation result can be derived using Taylor's series and standard arguments. Since there is no technicality, we left out the details of the proof.

Lemma 2.4.2. *For $v \in H^3(0,T;L^2(\Omega))$, we have*

$$\|\partial_\tau v^n - v_t^{n+\frac{1}{2}}\|^2 \le C\tau^3\int_{t_n}^{t_{n+1}}\|v_{ttt}(t)\|^2 dt.$$

Towards estimating the error $e_h^n := \mathcal{U}^n - u^n$, we define the auxiliary functions $\xi^n := u_h^n - \mathcal{U}^n$, and $\eta^n = u_{ht}^n - \vartheta^n$ for $n = 1, 2, \cdots, N$. Then for the term ξ^n, we have the following estimate.

Lemma 2.4.3. *Let u_h^n and $\mathcal{U}^n$ be the solutions of (2.2.3) and (2.4.2), respectively. Then, we have*

$$\max_{0\le n\le N}\|\xi^n\|^2 \le C\tau^4\left(\int_0^T\|u_{htttt}(t)\|^2 dt + \int_0^T\|u_{httt}(t)\|^2 dt\right).$$

Proof. From (2.2.3), substituting the value of t by $t_{n+\frac{1}{2}}$, we get

$$m_h(\partial_\tau u_{ht}^n, w) + s_h(u_{ht}^{n+\frac{1}{2}}, w) + a_h(u_h^{n+\frac{1}{2}}, w) = (f_h^{n+\frac{1}{2}}, w) + m_h(\psi^n, w) \tag{2.4.8}$$

for all $w \in W_h^m$, where $\psi^n = \partial_\tau u_{ht}^n - u_{htt}^{n+\frac{1}{2}}$. Now, from (2.4.2) and (2.4.8), for any $w \in W_h^m$ it follows that

$$m_h(\partial_\tau \eta^n, w) + s_h(\eta^{n+\frac{1}{2}}, w) + a_h(\xi^{n+\frac{1}{2}}, w) = m_h(\psi^n, w),\ 1 \le n \le N-1. \tag{2.4.9}$$

It can be easily observed using first part of (2.4.2) that for $1 \le n \le N-1$

$$\partial_\tau \xi^n = \eta^{n+\frac{1}{2}} + \partial_\tau u_h^n - u_{ht}^{n+\frac{1}{2}} = \eta^{n+\frac{1}{2}} + \sigma^n, \tag{2.4.10}$$

where $\sigma^n = \partial_\tau u_h^n - u_{ht}^{n+\frac{1}{2}}$. We can notice that

$$\xi^n = \tau \sum_{m=0}^{n-1} \partial_\tau \xi^m \text{ and } \eta^n = \tau \sum_{m=0}^{n-1} \partial_\tau \eta^m.$$

Hence, from (2.4.10), it follows that

$$\begin{aligned} \partial_\tau \xi^n &= \frac{\tau}{2}\left[\sum_{m=0}^{n} \partial_\tau \eta^m + \sum_{m=0}^{n-1} \partial_\tau \eta^m\right] + \sigma^n, \\ \xi^{n+\frac{1}{2}} &= \frac{\tau}{2}\left[\sum_{m=0}^{n} \eta^{m+\frac{1}{2}} + \sum_{m=0}^{n-1} \eta^{m+\frac{1}{2}}\right] + \frac{\tau}{2}\left[\sum_{m=0}^{n} \sigma^m + \sum_{m=0}^{n-1} \sigma^m\right]. \end{aligned} \tag{2.4.11}$$

Next, we introduce a sequence $\{\alpha^n\}_{n=0}^N$ as

$$\alpha^0 = 0;\quad \alpha^n = \tau \sum_{m=0}^{n-1} \xi^{m+\frac{1}{2}}, n = 1, 2, \cdots, N.$$

The fact $\xi^0 = u_h^0 - \mathcal{U}^0 = 0$ gives

$$\alpha^{\frac{1}{2}} = \frac{\tau}{4}\xi^1 \text{ and } \alpha^{n+\frac{1}{2}} = \frac{\tau}{2}\left[\sum_{m=0}^{n} \xi^{m+\frac{1}{2}} + \sum_{m=0}^{n-1} \xi^{m+\frac{1}{2}}\right], n = 1, 2, \cdots, N-1. \tag{2.4.12}$$

Also, since $\eta^0 = u_{ht}^0 - \vartheta^0 = 0$, from (2.4.10), it follows that

$$\eta^1 = \frac{2}{\tau}\xi^1 - 2\sigma^0. \tag{2.4.13}$$

Hence, using the above identity (2.4.13) in (2.4.9) for $n = 0$, we obtain

$$\left(\frac{2}{\tau^2}\right) m_h(\xi^1, w)+\left(\frac{1}{\tau}\right) s_h(\xi^1, w)+\left(\frac{1}{2}\right) a_h(\xi^1, w) = m_h(\psi^0, w)+\left(\frac{2}{\tau}\right) m_h(\sigma^0, w)+s_h(\sigma^0, w),$$

for all $w \in W_h^m$. We now make the choice $w = \xi^1 = \frac{2}{\tau}\alpha^1$, to obtain

$$\left(\frac{2}{\tau^2}\right)m_h(\xi^1, \xi^1)+\left(\frac{1}{\tau}\right)s_h(\xi^1, \xi^1)+\left(\frac{2}{\tau^2}\right) a_h(\alpha^1, \alpha^1) = m_h(\psi^0, \xi^1)+\left(\frac{2}{\tau}\right)m_h(\sigma^0, \xi^1)+s_h(\sigma^0, \xi^1).$$

By using continuity and coercivity of m_h, s_h, a_h and the fact that $s_h(\xi^1, \xi^1) \geq 0$, the above equation can also be written as

$$\|\xi^1\|^2 + \|\nabla\alpha^1\|^2 \leq C\left(\frac{\tau^2}{2}\|\psi^0\|\|\xi^1\| + \tau\|\sigma^0\|\|\xi^1\| + \frac{\tau^2}{2}\|\sigma^0\|\|\xi^1\|\right).$$

Now, using Young's inequality, for suitable $\epsilon > 0$, we obtain

$$\|\xi^1\|^2 + \|\nabla\alpha^1\|^2 \leq C\left(\frac{\tau^4}{4}\|\psi^0\|^2 + \tau^2\|\sigma^0\|^2 + \epsilon\|\xi^1\|^2\right) \leq C\left(\frac{\tau^4}{4}\|\psi^0\|^2 + \tau^2\|\sigma^0\|^2\right). \quad (2.4.14)$$

Again, from (2.4.11) and (2.4.12), for any $w \in W_h^m$ and $1 \leq n \leq N-1$, we have

$$\begin{aligned}
&m_h(\partial_\tau\xi^n, w) + s_h(\xi^{n+\frac{1}{2}}, w) + a_h(\alpha^{n+\frac{1}{2}}, w)\\
=&\frac{\tau}{2}m_h\left(\partial_\tau\eta^n + 2\sum_{m=0}^{n-1}\partial_\tau\eta^m, w\right) + m_h(\sigma^n, w) + \frac{\tau}{2}s_h\left(\eta^{n+\frac{1}{2}} + 2\sum_{m=0}^{n-1}\eta^{m+\frac{1}{2}}, w\right)\\
&+\frac{\tau}{2}s_h\left(\sigma^n + 2\sum_{m=0}^{n-1}\sigma^m, w\right) + \frac{\tau}{2}a_h\left(\xi^{n+\frac{1}{2}} + 2\sum_{m=0}^{n-1}\xi^{m+\frac{1}{2}}, w\right). \quad (2.4.15)
\end{aligned}$$

Let us define

$$\mathcal{E}_1^n := \frac{\tau}{2}\psi^n + \tau\sum_{m=0}^{n-1}\psi^m + \sigma^n, \quad \mathcal{E}_2^n := \frac{\tau}{2}\sigma^n + \tau\sum_{m=0}^{n-1}\sigma^m.$$

Then using (2.4.9), equation (2.4.15) becomes, for any $w \in W_h^m$

$$m_h(\partial_\tau\xi^n, w) + s_h(\xi^{n+\frac{1}{2}}, w) + a_h(\alpha^{n+\frac{1}{2}}, w) = m_h(\mathcal{E}_1^n, w) + s_h(\mathcal{E}_2^n, w).$$

Now, make the choice $w = \xi^{n+\frac{1}{2}} = \partial_\tau\alpha^n$ to have

$$\begin{aligned}
&m_h(\xi^{n+1}, \xi^{n+1}) - m_h(\xi^n, \xi^n) + 2\tau s_h(\xi^{n+\frac{1}{2}}, \xi^{n+\frac{1}{2}}) + a_h(\alpha^{n+1}, \alpha^{n+1}) - a_h(\alpha^n, \alpha^n)\\
&= 2\tau m_h(\mathcal{E}_1^n, \xi^{n+\frac{1}{2}}) + 2\tau s_h(\mathcal{E}_2^n, \xi^{n+\frac{1}{2}}).
\end{aligned}$$

Since $s_h(\xi^{n+\frac{1}{2}}, \xi^{n+\frac{1}{2}}) \geq 0$, using continuity and coercivity property of m_h, s_h and a_h, we obtain

$$\|\xi^{n+1}\|^2 - \|\xi^n\|^2 + \|\nabla\alpha^{n+1}\|^2 - \|\nabla\alpha^n\|^2 \leq C\tau\left(\|\mathcal{E}_1^n\| + \|\mathcal{E}_2^n\|\right)\|\xi^{n+\frac{1}{2}}\|.$$

Applying Young's inequality and for $2 \leq l \leq N$, taking sum from $n = 1$ to $n = l-1$ on the right hand side, we find

$$\begin{aligned}\|\xi^l\|^2 + \|\nabla\alpha^l\|^2 &\leq C\bigg(\|\xi^1\|^2 + \|\nabla\alpha^1\|^2 + \tau\sum_{n=1}^{l-1}\left(\|\mathcal{E}_1^n\|^2 + \|\mathcal{E}_2^n\|^2\right) + \tau\epsilon\sum_{n=1}^{l-1}\|\xi^{n+\frac{1}{2}}\|^2\bigg)\\ &\leq C\bigg(\|\xi^1\|^2 + \|\nabla\alpha^1\|^2 + \tau\sum_{n=1}^{l-1}\left(\|\mathcal{E}_1^n\|^2 + \|\mathcal{E}_2^n\|^2\right) + \epsilon\max_{2\leq n\leq N}\|\xi^n\|^2\bigg).\end{aligned}$$

Since $\|\nabla\alpha^l\|^2 \geq 0$, suitable choice of $\epsilon > 0$ gives

$$\max_{2\leq n\leq N}\|\xi^n\|^2 \leq C\bigg(\|\xi^1\|^2 + \|\nabla\alpha^1\|^2 + \tau\sum_{n=1}^{l-1}\left(\|\mathcal{E}_1^n\|^2 + \|\mathcal{E}_2^n\|^2\right)\bigg).$$

Hence, from (2.4.14), the above equation is reduced to

$$\max_{1\leq n\leq N}\|\xi^n\|^2 \leq C\bigg(\tau^4\|\psi^0\|^2 + \tau^2\|\sigma^0\|^2 + \tau\sum_{n=1}^{l-1}\left(\|\mathcal{E}_1^n\|^2 + \|\mathcal{E}_2^n\|^2\right)\bigg). \tag{2.4.16}$$

Now for the estimate of $\mathcal{E}_1^n$, using triangle inequality, we have

$$\begin{aligned}\|\mathcal{E}_1^n\|^2 &\leq C\bigg(\frac{\tau^2}{4}\|\psi^n\|^2 + \tau^2\Big\|\sum_{m=0}^{n-1}\psi^m\Big\|^2 + \|\sigma^n\|^2\bigg)\\ &\leq C\bigg(\frac{\tau^2}{4}\|\psi^n\|^2 + \tau^2 N\sum_{m=0}^{n-1}\|\psi^m\|^2 + \|\sigma^n\|^2\bigg)\\ &\leq C\bigg(\frac{\tau^2}{4}\|\psi^n\|^2 + \tau T\sum_{m=0}^{n-1}\|\psi^m\|^2 + \|\sigma^n\|^2\bigg).\end{aligned}$$

Then, we use Lemma 2.4.2 to obtain

$$\|\mathcal{E}_1^n\|^2 \leq C\bigg(\tau^5\int_{t_n}^{t_{n+1}}\|u_{htttt}(t)\|^2dt + \tau^4\int_0^T\|u_{htttt}(t)\|^2dt + \tau^3\int_{t_n}^{t_{n+1}}\|u_{httt}(t)\|^2dt\bigg). \tag{2.4.17}$$

Similarly, for $\mathcal{E}_2^n$, we have

$$\|\mathcal{E}_2^n\|^2 \leq C\bigg(\tau^5 \int_{t_n}^{t_{n+1}} \|u_{httt}(t)\|^2 dt + \tau^4 \int_0^T \|u_{httt}(t)\|^2 dt\bigg). \tag{2.4.18}$$

Finally, using the above equation (2.4.17)-(2.4.18) in (2.4.16), it follows that

$$\max_{1\leq n\leq N} \|\xi^n\|^2 \leq C\tau^4\bigg(\int_0^T \|u_{htttt}(t)\|^2 dt + \int_0^T \|u_{httt}(t)\|^2 dt\bigg).$$

□

Now, using Lemma 2.4.3, the following L^2 norm error estimate is obtained.

Theorem 2.4.2. *Let u^n and $\mathcal{U}^n$ solution of (2.1.1) and (2.4.2), respectively. Assume that $u_0 \in H^{m+1}(\Omega) \cap H^4(\Omega)$, $v_0 \in H^{m+1}(\Omega) \cap H^3(\Omega)$, $u_t \in L^1(0,T;H^{m+1}(\Omega))$ and $f \in L^1(0,T;H^{m+1}(\Omega)) \cap H^3(0,T;H^1(\Omega))$, then for all $t \in (0,T]$, we have*

$$\max_{1\leq n\leq N} \|\mathcal{U}^n - u^n\| \leq C_1(u_0,u_t,f)h^{m+1} + C_2(u_0,v_0,f)\tau^2.$$

where

$$C_1(u_0,u_t,f) := C(|u_0|_{m+1} + |v_0|_{m+1} + \|u_t\|_{L^1(H^{m+1})} + \|f\|_{L^1(H^{m+1})})$$

and

$$C_2(u_0,v_0,f) := \tilde{C}\big(\|u_0\|_4 + \|v_0\|_3 + \|f\|_{H^3(H^1)}\big).$$

Proof. We divide the error as

$$\mathcal{U}^n - u^n := -\xi^n + u_h^n - u^n.$$

Now by triangle inequality, Lemma 2.4.3 and Theorem 2.3.2, we get

$$\begin{aligned}\max_{1\leq n\leq N} \|\mathcal{U}^n - u^n\| \leq & Ch^{m+1}(|u_0|_{m+1} + |v_0|_{m+1} + \|u_t\|_{L^1(H^{m+1})} + \|f\|_{L^1(H^{m+1})}) \\ & + \tilde{C}\tau^2\bigg(\int_0^T \|u_{htttt}(t)\|^2 dt + \int_0^T \|u_{httt}(t)\|^2 dt\bigg)^{\frac{1}{2}}.\end{aligned}$$

Finally, from Lemma 2.3.2, we get

$$\begin{aligned}\max_{1\leq n\leq N} \|\mathcal{U}^n - u^n\| \leq & Ch^{m+1}\big(|u_0|_{m+1} + |v_0|_{m+1} + \|u_t\|_{L^1(H^{m+1})} + \|f\|_{L^1(H^{m+1})}\big) \\ & + \tilde{C}\tau^2\big(\|u_0\|_4 + \|v_0\|_3 + \|f\|_{H^3(H^1)}\big).\end{aligned}$$

□

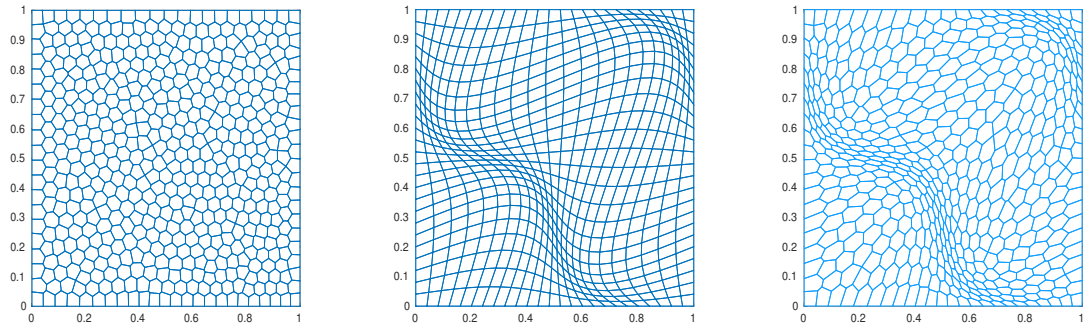

Figure 2.5.1: Sample meshes: $\mathcal{V}_h$(left), $\mathcal{S}_h$(center) and $\mathcal{P}_h$(right) with 512 elements.

2.5 Numerical Results

Here, we illustrate some numerical examples to test the practical performance of the given method. To show the flexibility of the method with respect to mesh discretization, we have considered different types of polygonal meshes such as Voronoi ($\mathcal{V}_h$), distorted square ($\mathcal{S}_h$) and distorted polygon ($\mathcal{P}_h$). The adopted polygonal meshes are shown in Figure 2.5.1. In Example 2.5.1, we have discussed convergence of proposed algorithm for a smooth solution in a convex domain with all three types of meshes. Next, we have considered a low regular solution in a convex domain in Example 2.5.2. Further, in Example 2.5.3 and Example 2.5.4, we have tested our algorithm for smooth solutions in L-shaped domain and circular domain, respectively. Finally, we have discussed a singularly perturbed problem with boundary layers in Example 2.5.5.

We evaluated the rate of convergence for the fully discrete approximation with respect to L^2 norm and H^1 semi-norm. More precisely, we calculate the following errors

$$\|u - u_h\| := \sqrt{\sum_{E\in\mathcal{T}_h} \|u - \Pi^0_{m,E} u_h\|^2_E},$$

$$|u - u_h|_1 := \sqrt{\sum_{E\in\mathcal{T}_h} |u - \Pi^\nabla_{m,E} u_h|^2_{1,E}}.$$

The experimental order of convergence (EOC) is computed using the formula

$$\text{EOC(i)} = \frac{\log(e(h_{i+1})/e(h_i))}{\log(h_{i+1}/h_i)}, \quad i = 1, 2, 3,$$

where h_i is the mesh size and $e(h_i)$ is the corresponding error.

For the temporal discretization, we chose the time step $\tau = O(h^{\frac{m+1}{2}})$ for $m = 1, 2, 3$ to ensure the order of convergence $O(h^{m+1} + \tau^2) = O(h^{m+1})$ in L^2 norm and $O(h^m + \tau^2) = O(h^m)$ in H^1 semi-norm. In Example 2.5.1-2.5.4, we have considered the model problem (2.1.1)-(2.1.2) with the coefficients $\sigma = \kappa = 1$, and source function f, initial data $\{u_0, v_0\}$ are chosen according to the choice of exact solution. The spatial domain Ω is considered to be $(0, 1) \times (0, 1)$ or else specified and time interval is set to be $[0, 1]$.

Example 2.5.1. (Smooth solution with convex domain) We consider the following smooth function as the exact solution

$$u(x, y, t) = t^2 \sin(\pi x) \sin(\pi y).$$

We have implemented the virtual element algorithm with all the three kind of mesh discretizations $\mathcal{V}_h$, $\mathcal{S}_h$ and $\mathcal{P}_h$ and the polynomial order of the method is consider to be $m = 1, 2, 3$.

Table 2.5.1 presents the numerical errors and experimental order of convergence (EOC) in both L^2 norm and H^1 semi-norm at the final time $T = 1$ for the Voronoi mesh $(\mathcal{V}_h)$. Exact and approximate solutions at final time are presented in Figure 2.5.2. Figure 2.5.3 clearly demonstrates the optimal order of convergence in L^2 norm and H^1 semi-norm.

In Table 2.5.2, we present the numerical errors and EOC in L^2 norm and H^1 semi-norm at the final time $T = 1$ for the mesh distorted square mesh $(\mathcal{S}_h)$. The exact solution and approximate solution at final time are illustrated in Figure 2.5.4. Further, the log-log plots are presented in Figure 2.5.5.

Table 2.5.3 depicts the numerical errors and EOC in L^2 norm and H^1 semi-norm at the final time $T = 1$ for distorted polygon mesh $(\mathcal{P}_h)$. The exact solution and approximate solution at $T = 1$ are illustrated in Figure 2.5.6. It is clear from Figure 2.5.7 that we have achieved optimal order of convergence.

The above observations confirm the theoretical prediction for optimal convergence as proved in Theorem 2.4.2.

Example 2.5.2. (Low regular solution) We consider the model problem for which the exact solution possesses a corner singularity in spatial direction. We set the exact solution as

$$u(x, y, t) = t^2 \sin t \; x(1 - x)y(1 - y)(x^2 + y^2)^{-1+\frac{k}{2}},$$

Table 2.5.1: L^2 and H^1 errors at $T = 1$ for the mesh $\mathcal{V}_h$ in Example 2.5.1

order	h	$\|u - u_h\|$	EOC	$\|u - u_h\|_1$	EOC
$m = 1$	0.1768	$3.29994e-02$	-	$7.72205e-02$	-
	0.1250	$1.49357e-02$	2.2865	$4.35894e-02$	1.6494
	0.0884	$7.14353e-03$	2.1282	$2.70620e-02$	1.3755
	0.0625	$3.50934e-03$	2.0508	$1.78692e-02$	1.1975
	0.0442	$1.71607e-03$	2.0636	$1.21311e-02$	1.1172
$m = 2$	0.1768	$1.16529e-03$	-	$9.26114e-03$	-
	0.1250	$4.46865e-04$	2.7645	$4.18753e-03$	2.2893
	0.0884	$1.51924e-04$	3.1131	$1.80323e-03$	2.4312
	0.0625	$5.37903e-05$	2.9957	$7.03635e-04$	2.7152
	0.0442	$1.88133e-05$	3.0304	$3.68326e-04$	1.8672
$m = 3$	0.1768	$4.46966e-04$	-	$5.77494e-03$	-
	0.1250	$1.05990e-04$	4.1509	$2.16169e-03$	2.8342
	0.0884	$2.63877e-05$	4.0122	$7.73879e-04$	2.9641
	0.0625	$6.36444e-06$	4.1033	$2.74277e-04$	2.9928
	0.0442	$1.54509e-06$	4.0836	$1.00159e-04$	2.9059

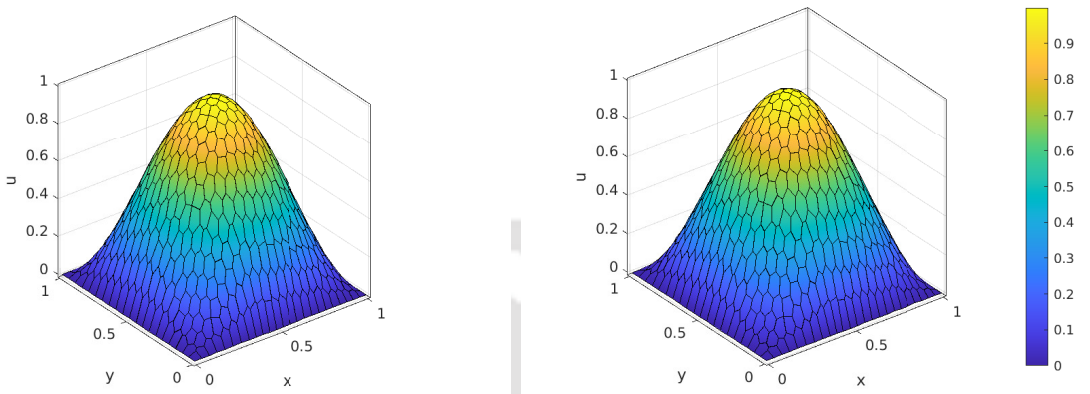

Figure 2.5.2: Approximate solution for $m = 3$ (left) with Voronoi mesh ($h = 0.0442$) and exact solution (right) at $t = 1$ in Example 2.5.1.

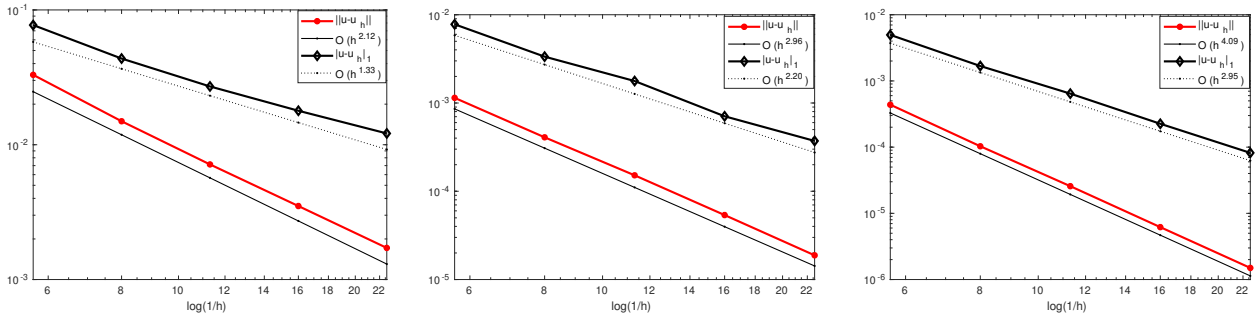

Figure 2.5.3: Log-log plots of the errors versus h at $t = 1$ for $m = 1$ (left), $m = 2$ (center) and $m = 3$ (right) for the Voronoi mesh in Example 2.5.1.

Table 2.5.2: L^2 and H^1 errors at $T = 1$ for the mesh $\mathcal{S}_h$ in Example 2.5.1

order	h	$\|u - u_h\|$	EOC	$\|u - u_h\|_1$	EOC
	1/5	$6.60504e-02$	-	$2.12355e-01$	-
$m = 1$	1/10	$1.70176e-02$	1.9565	$5.41042e-02$	1.9727
	1/15	$7.53787e-03$	2.0083	$2.34078e-02$	2.0664
	1/20	$4.22734e-03$	2.0104	$1.29691e-02$	2.0526
	1/25	$2.70095e-03$	2.0075	$8.23578e-03$	2.0349
	1/5	$3.31787e-03$	-	$3.84747e-02$	-
$m = 2$	1/10	$4.35366e-04$	2.9300	$5.96027e-03$	2.6905
	1/15	$1.29070e-04$	2.9986	$1.78788e-03$	2.9696
	1/20	$5.45437e-05$	2.9941	$7.56017e-04$	2.9919
	1/25	$2.79591e-05$	2.9948	$3.87541e-04$	2.9947
	1/5	$1.53670e-03$	-	$1.64671e-02$	-
$m = 3$	1/10	$1.28510e-04$	3.5799	$2.18415e-03$	2.9144
	1/15	$2.72297e-05$	3.8270	$6.43028e-04$	3.0158
	1/20	$8.84249e-06$	3.9097	$2.69618e-04$	3.0213
	1/25	$3.66703e-06$	3.9445	$1.37534e-04$	3.0166

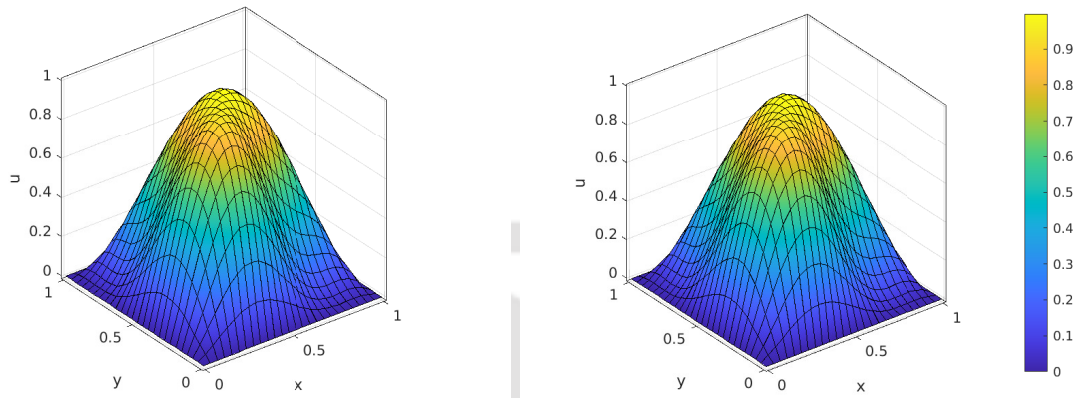

Figure 2.5.4: Approximate solution for $m = 3$ with distorted square mesh ($h = 1/25$) (left) and exact solution (right) at $t = 1$ in Example 2.5.1.

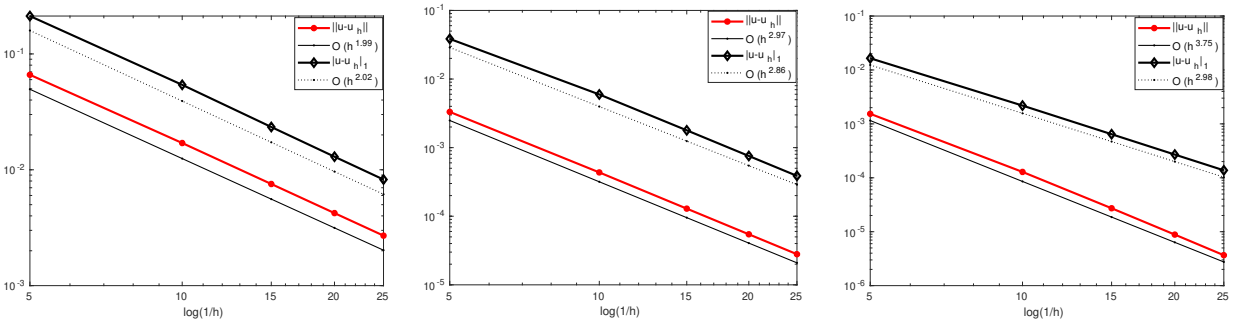

Figure 2.5.5: Log-log plots of the errors versus h at $t = 1$ for $m = 1$ (left), $m = 2$ (center) and $m = 3$ (right) for the distorted square mesh in Example 2.5.1.

Table 2.5.3: L^2 and H^1 errors at $T = 1$ for the mesh $\mathcal{P}_h$ in Example 2.5.1

order	h	$\|u - u_h\|$	EOC	$\|u - u_h\|_1$	EOC
$m = 1$	0.1768	$5.07343e-02$	-	$1.83324e-01$	-
	0.1250	$2.23318e-02$	2.3668	$9.34209e-02$	1.9444
	0.0884	$1.17906e-02$	1.8430	$5.63744e-02$	1.4575
	0.0625	$5.82943e-03$	2.0323	$2.95997e-02$	1.8588
	0.0442	$2.85423e-03$	2.0599	$1.98230e-02$	1.1565
$m = 2$	0.1768	$2.59901e-03$	-	$2.65365e-02$	-
	0.1250	$9.56562e-04$	2.8830	$1.26273e-02$	2.1420
	0.0884	$3.43951e-04$	2.9515	$5.55455e-03$	2.3697
	0.0625	$1.21152e-04$	3.0106	$2.95941e-03$	1.8166
	0.0442	$4.38861e-05$	2.9292	$1.54433e-03$	1.8761
$m = 3$	0.1768	$1.10888e-03$	-	$1.32793e-02$	-
	0.1250	$2.59202e-04$	4.1923	$4.38927e-03$	3.1930
	0.0884	$7.36591e-05$	3.6305	$1.59724e-03$	2.9170
	0.0625	$1.90696e-05$	3.8990	$5.80208e-04$	2.9217
	0.0442	$4.76837e-06$	3.9983	$2.13047e-04$	2.8900

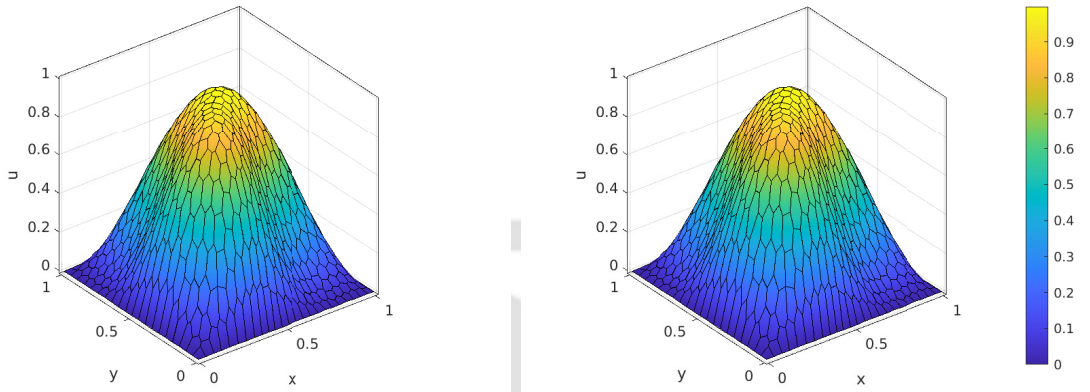

Figure 2.5.6: Approximate solution for $m = 3$ with distorted polygon mesh ($h = 0.0442$) (left) and exact solution (right) at $t = 1$ in Example 2.5.1.

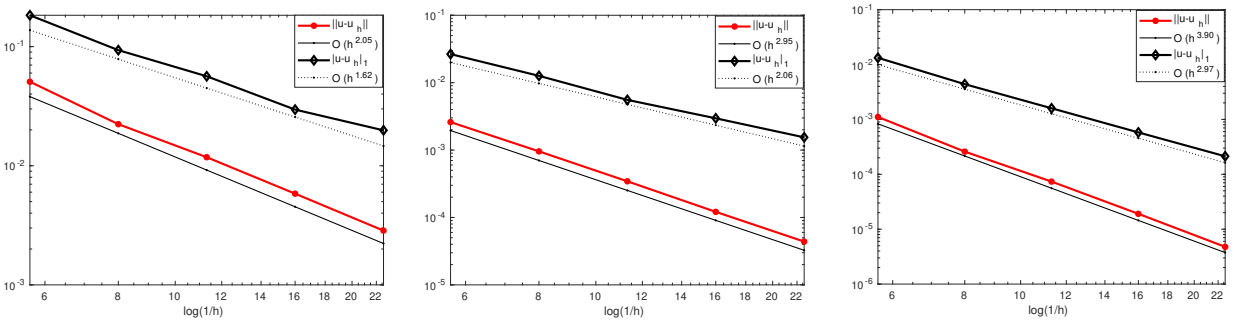

Figure 2.5.7: Log-log plots of the errors versus h at $t = 1$ for $m = 1$ (left), $m = 2$ (center) and $m = 3$ (right) for the distorted polygon mesh in Example 2.5.1.

Table 2.5.4: EOC in L^2 norm and H^1 semi-norm at $T = 1$ in Example 2.5.2

l	k	$m = 1$		$m = 2$	
		L^2-order	H^1-order	L^2-order	H^1-order
0	1	1.82	0.87	1.95	0.95
1	1/2	1.46	0.49	1.37	0.46
2	1/4	0.23	0.27	1.19	0.22
3	1/8	1.11	0.15	1.19	0.11
4	1/16	1.05	0.09	1.09	0.11
5	1/32	1.03	0.05	1.03	0.01

where $k \in (0, 1]$. It is easy to observe that u has a singularity at the corner point $(0, 0)$ and $u \in C^\infty(0, T; H^{1+k-\delta}(\Omega))$, but $u \notin C^\infty(0, T; H^{1+k}(\Omega))$, for some positive number δ. We choose Voronoi mesh $(\mathcal{V}_h)$ for the spatial discretization and compute the EOC in respective norms by setting $k = (1/2)^l$, $l = 0, 1, 2, 3, 4, 5$.

From the Table 2.5.4, we can easily observe that the numerical order of convergence at the final time $T = 1$ remains to be $O(h^{1+k})$ in L^2 norm and $O(h^k)$ in H^1 semi-norm for linear as well as higher-order methods, which is due to the low regularity of the exact solution. Figure 2.5.8 presents the contour plot of the exact and approximate solution for $k = 1/2$ at $t = 1$.

Example 2.5.3. (Smooth solution with non-convex domain) Consider a L-shaped domain $\Omega = (0, 1) \times (0, 1) \setminus [1/2, 1) \times [1/2, 1)$ with Voronoi mesh $(\mathcal{V}_h)$ discretization. The L-shaped domain with 512 Voronoi elements is shown in Figure 2.5.9. We set the exact solution as

$$u(x, y, t) = t^2 \sin t \sin(2\pi x) \sin(2\pi y).$$

In Table 2.5.5, we show the numerical errors and EOC in L^2 norm and H^1 semi-norm at the final time $T = 1$ for linear approximation. Figure 2.5.10 presents the contour plot of the exact and approximate solutions at $T = 1$. The log-log plot is presented in Figure 2.5.11.

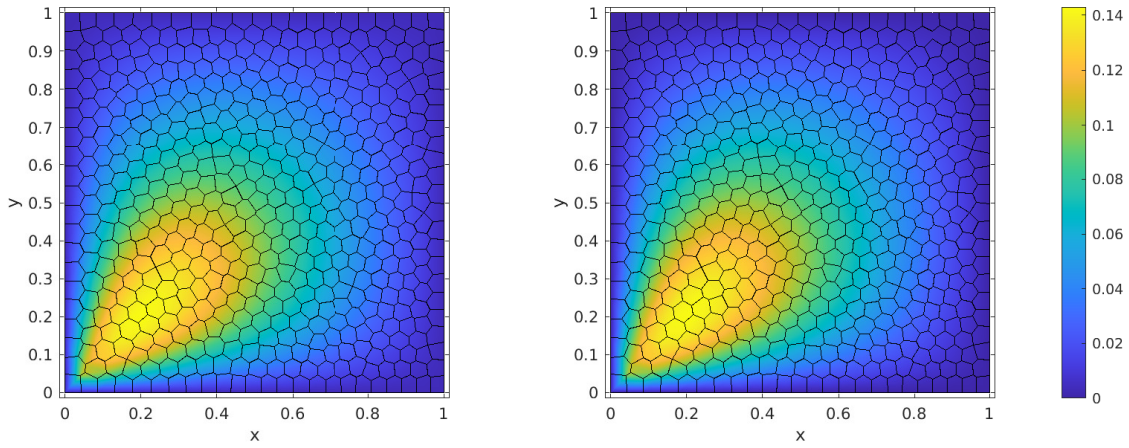

Figure 2.5.8: Approximate solution (left) for $m = 2$ ($h = 0.0442$) and exact solution (right) at $t = 1$ with $k = 0.5$ in Example 2.5.2.

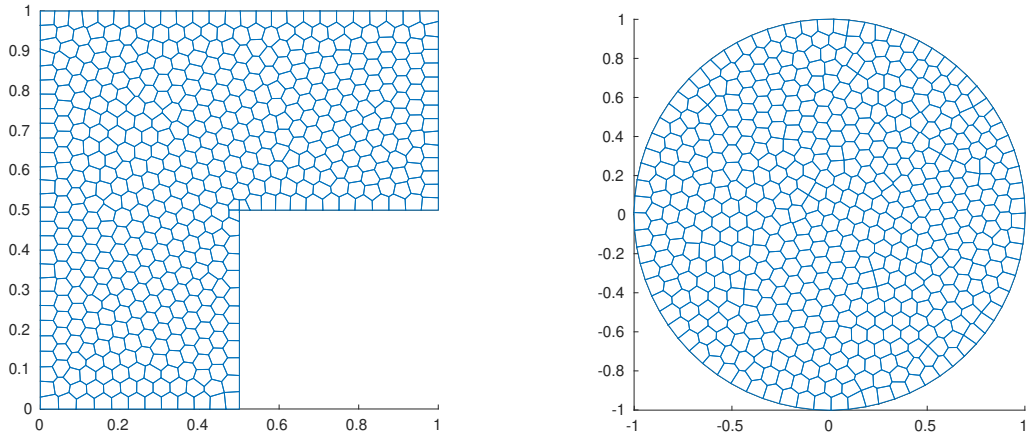

Figure 2.5.9: L-shaped (left) and Circular (right) domain with 512 Voronoi elements.

Table 2.5.5: L^2 and H^1 errors at $T = 1$ in Example 2.5.3

h	$\|u - u_h\|$	EOC	$\|u - u_h\|_1$	EOC
0.1690	$7.56436e-02$	-	$2.92561e-01$	-
0.1222	$3.52973e-02$	2.3477	$1.43332e-01$	2.1976
0.0874	$1.61814e-02$	2.3264	$6.90200e-02$	2.1798
0.0621	$7.98003e-03$	2.0742	$3.68324e-02$	1.8427
0.0441	$3.92766e-03$	2.0627	$2.45672e-02$	1.1784

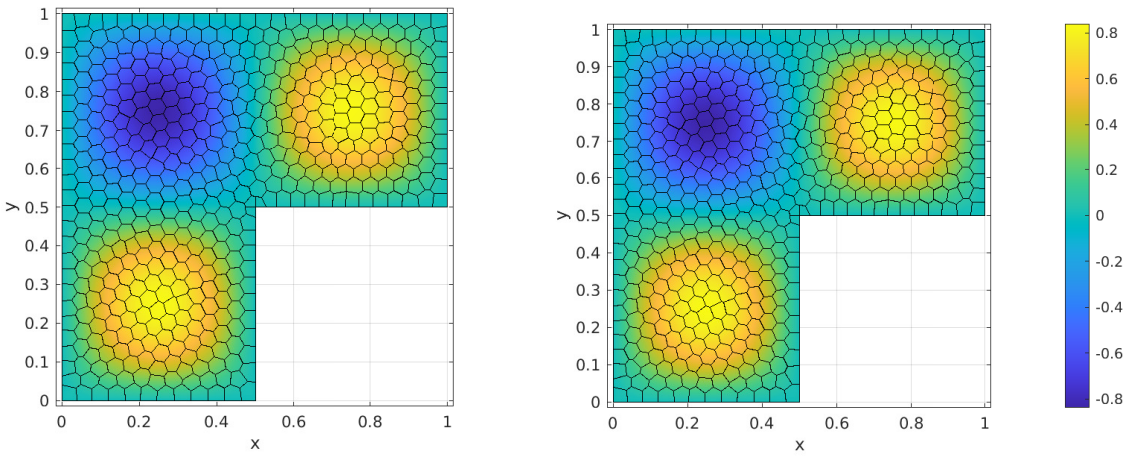

Figure 2.5.10: Approximate solution (left) and exact solution (right) at $t = 1$ in Example 2.5.3.

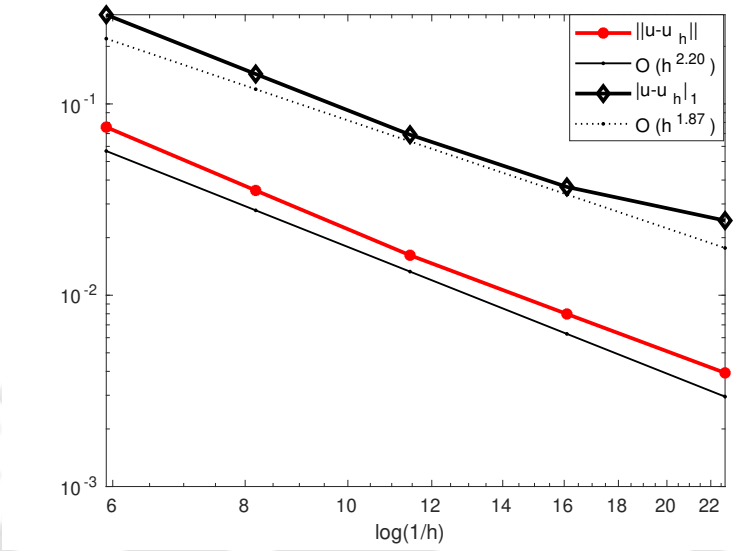

Figure 2.5.11: Log-log plot of the errors versus h at $t = 1$ in Example 2.5.4.

Example 2.5.4. (Smooth solution with circular domain) Consider a circular domain Ω with center at $(0, 0)$ and radius 1 with Voronoi mesh $(\mathcal{V}_h)$ discretization. The circular domain with 512 Voronoi elements is shown in Figure 2.5.9. We choose the exact solution

$$u(x, y, t) = t^2 \sin t(1 - x^2 - y^2) \sin(\pi x) \sin(\pi y).$$

Table 2.5.6 shows the numerical errors and EOC in L^2 norm and H^1 semi-norm at the final time $T = 1$ for linear and quadratic approximation. The contour plots of the exact and approximate solutions at $T = 1$ are presented in Figure 2.5.12. Figure 2.5.13 presents the log-log plots.

Example 2.5.5. (Singularly perturbed problem with boundary layers) We consider following singularly perturbed weakly damped wave equation

$$u_{tt} + u_t - \epsilon \Delta u = f(x, y, t), \text{ for } (x, y, t) \in \Omega \times (0, T], \tag{2.5.1}$$

where ϵ is the perturbation parameter. We set the exact solution as

$$u(x, y, t) = 10^{-4} t^2 \sin t \ \omega(x)\omega(y),$$

where $\omega(p) = r_1 + r_2 p + \exp(-\frac{1-p}{\epsilon})$, $r_1 = \exp(-1/\epsilon)$, $r_2 = -1 - r_1$.

Table 2.5.6: L^2 and H^1 errors at $T = 1$ in Example 2.5.4

Order	h	$\|u - u_h\|$	EOC	$\|u - u_h\|_1$	EOC
	0.1768	$1.46506e-01$	-	$4.65785e-01$	-
$m = 1$	0.1250	$6.64965e-02$	2.2792	$1.82503e-01$	2.7035
	0.0884	$3.10081e-02$	2.2013	$8.17590e-02$	2.3169
	0.0625	$1.48670e-02$	2.1211	$4.30456e-02$	1.8510
	0.0442	$7.29290e-03$	2.0551	$2.85357e-02$	1.1862
	0.1768	$1.27325e-02$	-	$2.88080e-01$	-
$m = 2$	0.1250	$4.50406e-03$	2.9984	$1.55206e-01$	1.7846
	0.0884	$1.53323e-03$	3.1093	$7.70855e-02$	2.0193
	0.0625	$5.54304e-04$	2.9356	$3.99548e-02$	1.8962
	0.0442	$1.91716e-04$	3.0634	$1.92289e-02$	2.1102

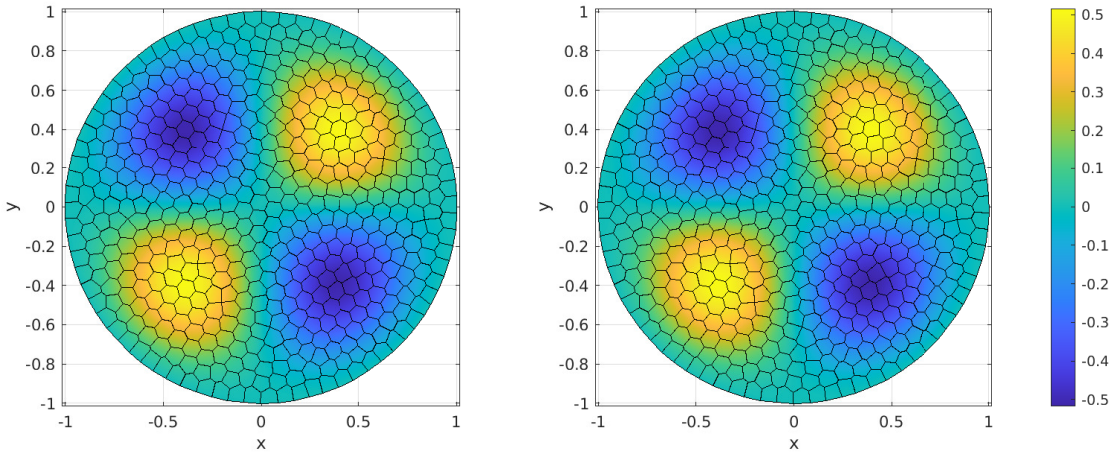

Figure 2.5.12: Approximate solution for $m = 2$ with $h = 0.0442$ (left) and exact solution (right) at $t = 1$ in Example 2.5.4.

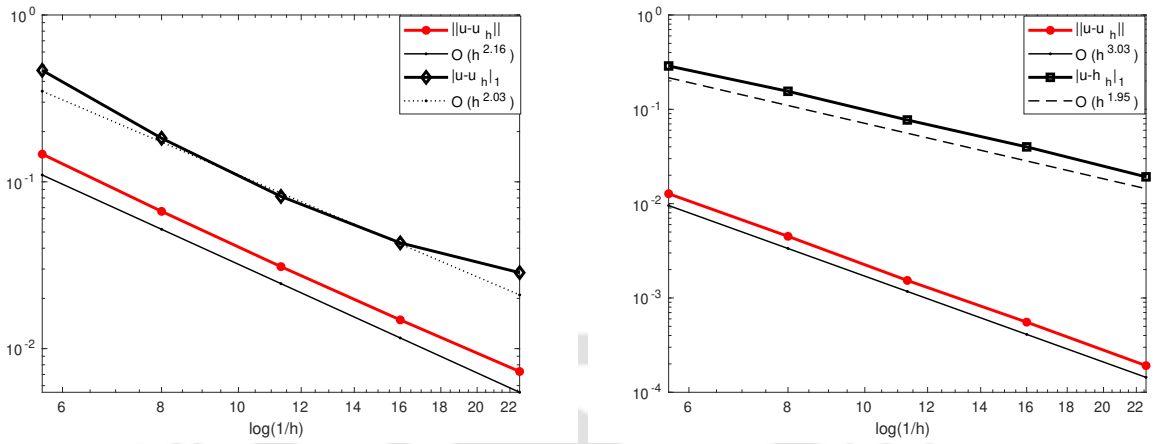

Figure 2.5.13: Log-log plots of the errors versus h at $t = 1$ for $m = 1$ (left) and $m = 2$ (right) in Example 2.5.4.

The chosen problem has two boundary layers along $x = 1$ and $y = 1$. We choose the Voronoi mesh $(\mathcal{V}_h)$ for the spatial discretization. In Table 2.5.7, we show the numerical errors and EOC in L^2 norm and H^1 semi-norm at the final time $T = 1$ for $\epsilon = 10^{-10}$ with linear virtual element approximation.

When standard FDMs or standard Galerkin FEMs are used on uniform meshes, non-physical and spurious oscillations occur unless meshes are taken sufficiently fine, which is useless for practical purposes. To suppress most non-physical oscillations while maintaining accuracy, the method adds an additional stabilization term in the upwind direction.

Table 2.5.7: L^2 and H^1 errors at $T = 1$ in Example 2.5.5

h	$\|u - u_h\|$	EOC	$\|u - u_h\|_1$	EOC
0.0884	$1.25615e-04$	–	$3.62801e-03$	–
0.0625	$4.57767e-05$	2.9126	$1.56670e-03$	2.4229
0.0510	$3.05630e-05$	1.9927	$1.15076e-03$	1.5219
0.0442	$2.34793e-05$	1.8331	$1.01911e-03$	0.8447
0.0312	$1.30867e-05$	1.6866	$7.85759e-04$	0.7503

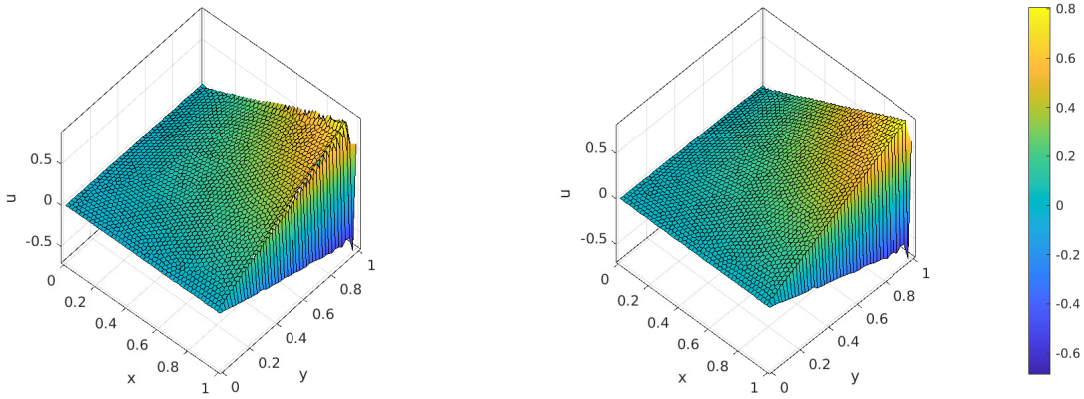

Figure 2.5.14: Approximate solution (left) and exact solution (right) at $t = 1$ in Example 2.5.5.

As demonstrated in existing literature that the standard discretization methods, such as conforming FEMs can be used on layer-adapted meshes, but some minor oscillations still show up in the discrete solution (cf. [111]). Here, we have demonstrated the boundary layer behaviour of VEM solution for the equation (2.5.1) with $\epsilon = 10^{-10}$ and exact solution $u(x, y, t) = t^2 \sin t\ \omega(x)\omega(y)$. The surface plots of the approximate solution and exact solution at final time with $m = 1$ and $h = 0.0221$ are shown in Figure 2.5.14. From Figure 2.5.14, for $\epsilon = 10^{-10} \lll h$, we observe that the numerical solutions do not exhibit unnatural oscillations near the boundary layers $x = 1$ and $y = 1$.

2.6 Conclusion

In this chapter, we have proposed a virtual element method for weakly damped wave equations. We have used polygonal meshes for the spatial discretization and obtained optimal order of convergence, i.e., $O(h^{m+1})$ in L^2 norm and $O(h^m)$ in H^1 semi-norm, where m is the polynomial degree of the method, and h is the mesh size. For the temporal discretization, we have employed the second-order Crank-Nicolson scheme and shown that the discrete energy doesn't grow with time. We have illustrated some numerical experiments with polynomial degree $m = 1, 2, 3$ and shown that the experimental order of convergence agrees with the theoretical results. The use of different types of polygonal meshes for spatial discretization shows the flexibility of the method with respect to mesh discretization.

3

Virtual Element Methods for Pulsed Electric Field Model Problems on Polygonal Meshes

In this chapter, we develop the virtual element method for pulsed electric field model problems on polygonal meshes. We have presented the spatially semi-discrete approximation and derive optimal order error estimates in L^2 norm and H^1 norm for the spatially discrete approximation. We have also developed the fully discrete approximation based on Crank-Nicolson temporal discretization and derived the convergence analysis. Finally, we illustrate some numerical experiments to confirm our theoretical findings.

3.1 Introduction

Let $\Omega \subset \mathbb{R}^2$ be a convex polygonal domain with boundary $\partial\Omega$ occupied by the concerned physical media having conductivity $\sigma = \sigma(x)$ and permittivity $\epsilon = \epsilon(x)$. We consider following pulsed electric field model for biological media [9, 107, 133]

$$-\nabla \cdot (\sigma(x)\nabla u(x,t) + \epsilon(x)\nabla u_t(x,t)) = f(x,t) \text{ in } \Omega \times (0,T] \tag{3.1.1}$$

with initial and boundary conditions

$$u(x,0) = u_0 \text{ in } \Omega; \quad u(x,t) = 0 \quad \text{on } \partial\Omega \times (0,T], \tag{3.1.2}$$

where u and f are the voltage potential and electric pulse of the model, respectively. Further, u_0 is the initial voltage and $T < \infty$ is the finite terminal observation time and u_t

Results of this Chapter are published in [102]

denotes the weak derivative of u with respect to time variable. We assume that there exists two positive constants $\underline{M}$ and $\overline{M}$ such that $\underline{M} \leq \epsilon(x),\ \sigma(x) \leq \overline{M}$ a. e. in Ω.

Equation (3.1.1) is numerically interesting as it does not belong to the well-studied classes of time-dependent equations and has applications in a variety of fields including but not limited to biotechnology, food sciences, medicines and electromagnetism. Ammari et al. studied the finite element methods for the model problem (3.1.1)-(3.1.2) on a physical media with heterogeneous conductivity and permittivity, and homogeneous jump conditions [9]. For the fully discrete approximation backward Euler temporal discretization has been employed and optimal convergence order in both $L^2(H^1)$ and $L^2(L^2)$ norms have been obtained. Further, Deka et al. extended the analysis of Ammari et al. and achieved optimal a priori error estimates in $L^\infty(H^1)$ and $L^\infty(L^2)$ norm for both homogeneous and non-homogeneous jump for the derivative ([55], [51]). A weak Galerkin FEM for the model with non-homogeneous jump conditions is developed in [52].

The main purpose of the current work is to analyze the VEM for the pulsed electric field model problem (3.1.1). Optimal error estimates are derived for both semi-discrete and fully discrete schemes in L^2 and H^1 norms. The fully discrete scheme can be reinterpreted as the Crank-Nicolson discretization of the reformulation of the governing equation in the first-order system, as in Baker [13]. Further, in support of our theoretical findings some numerical examples are presented with different meshes.

The rest of the content of this chapter is divided as follows: We present the construction of the virtual element semi-discrete problem in Section 3.2. Next, while Section 3.3 deals with the semi-discrete error analysis, Section 3.4 discusses fully discrete approximation and its convergence. Section 3.5 focuses on numerical examples. Finally, we conclude the work in Section 3.6

3.2 Semi-discrete Virtual Element Approximation

This section deals with construction of semi-discrete virtual element approximation for the model problem (3.1.1)-(3.1.2).

Following the standard way, we obtain the variational problem corresponding to the model problem (3.1.1)-(3.1.2) as : Find $u \in L^2(0,T;H_0^1(\Omega)) \cap H^1(0,T;L^2(\Omega))$ such that for all $v \in H_0^1(\Omega)$ and for a.e. $t \in (0,T]$

$$a_1(u,v) + a_2(u_t,v) = (f,v) \ \ \& \ \ u(0) = u_0, \tag{3.2.1}$$

where

$$a_1(u,v) = \int_\Omega \sigma(x)\nabla u \cdot \nabla v dx, \quad a_2(u,v) = \int_\Omega \epsilon(x)\nabla u \cdot \nabla v dx \quad \forall u, v \in H_0^1(\Omega). \tag{3.2.2}$$

We recall the virtual element framework discussed in Chapter 1, Section 1.4. We split the bilinear forms $a_i(\cdot,\cdot)$, $i = 1, 2$, into their local counterparts as

$$a_i(u,v) := \sum_{E\in\mathcal{T}_h} a_i^E(u,v) \ \forall \ u, v \in H_0^1(\Omega), \quad i = 1, 2.$$

Now, we define the following discrete bilinear forms on the local virtual space $W_h^m(E)$:

$$a_{1,h}^E(v,w) := \left(\sigma\boldsymbol{\Pi}_{m-1,E}^0\nabla v, \boldsymbol{\Pi}_{m-1,E}^0\nabla w\right)_E + S_\sigma^E\left((I-\Pi_{m,E}^\nabla)v, (I-\Pi_{m,E}^\nabla)w\right) \quad \&$$
$$a_{2,h}^E(v,w) := \left(\epsilon\boldsymbol{\Pi}_{m-1,E}^0\nabla v, \boldsymbol{\Pi}_{m-1,E}^0\nabla w\right)_E + S_\epsilon^E\left((I-\Pi_{m,E}^\nabla)v, (I-\Pi_{m,E}^\nabla)w\right),$$

where

$$S_\sigma^E(v,w) = \beta_\sigma^E \sum_{r=1}^{N^E} dof_r(v) dof_r(w) \quad \&$$
$$S_\epsilon^E(v,w) = \beta_\epsilon^E \sum_{r=1}^{N^E} dof_r(v) dof_r(w)$$

with $\beta_\sigma^E = P_E^a(\sigma)$, $\beta_\epsilon^E = P_E^a(\epsilon)$ and $N^E = \dim W_h^m(E)$.

The global bilinear forms on the global discrete space W_h^m are obtained by assembling the local counterpart as follows:

$$a_{i,h}(v,w) := \sum_{E\in\mathcal{T}_h} a_{i,h}^E(v,w), \quad \forall v, w \in W_h^m.$$

The global bilinear forms $a_{i,h}$, $i = 1, 2$ satisfies the following continuity and coercivity properties: For $v, w \in W_h^m$

$$a_{1,h}(v,w) \le (1+\beta_\sigma)\overline{M}|v|_1|w|_1 \ \& \ a_{2,h}(v,w) \le (1+\beta_\epsilon)\overline{M}|v|_1|w|_1$$

and $w \in W_h^m$

$$a_{1,h}(w,w) \ge \min\{1,\alpha_\sigma\}\underline{M}|w|_1^2 \ \& \ a_{2,h}(w,w) \ge \min\{1,\alpha_\epsilon\}\underline{M}|w|_1^2,$$

where α_σ, α_ϵ, β_σ, β_ϵ are some positive constants. The proof can be done by following the Lemma 1.4.5.

We will need the modified elliptic projection operators $R_h^i : H_0^1(\Omega) \to W_h^m$, $i = 1, 2$ defined by

$$a_{i,h}(R_h^i u, w) = a_i(u, w) \ \ \forall w \in W_h^m. \tag{3.2.3}$$

The operators R_h^i, $i = 1, 2$ satisfy the following approximation properties (Lemma 1.5.1).

Lemma 3.2.1. *Let R_h^i, $i = 1, 2$, be defined by (3.2.3). Then, for any $u \in H^{m+1}(\Omega)$, there exist a generic constant C independent of the mesh parameter h (but depends on the coefficients σ, ϵ) such that*

$$|R_h^i u - u|_1 \leq Ch^m |u|_{m+1}$$

and if Ω is a convex domain

$$\|R_h^i u - u\| \leq Ch^{m+1} |u|_{m+1}.$$

Now, the continuous time virtual element approximation to (3.2.1) is stated as follows: Find $u_h \in L^2(0, T; W_h^m) \cap H^1(0, T; W_h^m)$ such that for all $w_h \in W_h^m$ and for a.e. $t \in (0, T]$

$$\begin{cases} a_{1,h}(u_h(t), w_h) + a_{2,h}(u_{ht}(t), w_h) = (f_h(t), w_h), \\ u_h(0) = R_h^2 u_0, \end{cases} \tag{3.2.4}$$

where f_h is the discrete form of the source function f as defined in (1.4.14).

3.3 Error Analysis for the Semi-discrete Problems

This section is dedicated to the derivation of error estimates related to the semi-discrete approximation (3.2.4) in both L^2 and H^1 semi-norm. Before proceeding to the error estimates, we present the following results regarding the stability of the semi-discrete solution u_h with respect to the initial data and the source function.

Lemma 3.3.1. *Let u_h be the solution of (3.2.4), $u_0 \in H_0^1(\Omega)$ and $f \in H^k(L^2(\Omega))$, $k = 1, 2, 3$. Then we have*

$$|D_t^k u_h(0)|_1 \leq C\big(|u_0|_1 + \|f\|_{H^k(L^2)}\big),$$

where $D_t^k = \dfrac{\partial^k}{\partial t^k}$.

Proof. We take $t \to 0^+$ in (3.2.4) to get

$$a_{2,h}(u_{ht}(0), w_h) = -a_{1,h}(R_h^2 u_0, w_h) + (f_h(0), w_h). \tag{3.3.1}$$

From Lemma 1.4.6 and Lemma 1.2.1, we obtain

$$(f_h(0), w_h) \leq C\|f\|_{H^1(L^2)}\|w_h\|. \tag{3.3.2}$$

Now substituting $w_h = u_{ht}(0)$, using the coercivity of $a_{2,h}$, continuity of $a_{1,h}$ and the estimate (3.3.2), equation (3.3.1) yields

$$|u_{ht}(0)|_1 \leq C(|u_0|_1 + \|f\|_{H^1(L^2)}). \tag{3.3.3}$$

This proves the result for $k = 1$. Now, for $k = 2$, differentiating (3.2.4) with respect to t and then proceeding in a similar way, we get

$$|u_{htt}(0)|_1 \leq C(|u_{ht}(0)|_1 + \|f_t\|_{H^1(L^2)}).$$

Using (3.3.3), we obtain

$$|u_{htt}(0)|_1 \leq C(|u_0|_1 + \|f\|_{H^2(L^2)}).$$

Similarly, we can show that

$$|u_{httt}(0)|_1 \leq C(|u_0|_1 + \|f\|_{H^3(L^2)}).$$

This complete the rest of the proof. □

Lemma 3.3.2. *Let u_h be the solution of (3.2.4), $u_0 \in H_0^1(\Omega)$ and $f \in H^k(L^2(\Omega))$, $k = 0, 1, 2, 3$. Then we have*

$$|D_t^k u_h(t)|_1^2 + \|D_t^k u_h\|_{L^2(H^1)}^2 \leq C\big(|u_0|_1^2 + \|f\|_{H^k(L^2)}^2\big).$$

Proof. Substituting $w_h = u_h$ in (3.2.4), we obtain

$$a_{1,h}(u_h(t), u_h(t)) + \frac{1}{2}\frac{d}{dt}a_{2,h}(u_h(t), u_h(t)) = (f_h(t), u_h(t)).$$

Taking integration from 0 to t, the coercivity and continuity of $a_{1,h}$ and $a_{2,h}$ implies

$$\int_0^t |u_h(s)|_1^2 ds + |u_h(t)|_1^2 \leq C\Big(|u_h(0)|_1^2 + \int_0^t \|f_h(s)\|^2 |u_h(s)|_1^2 ds\Big).$$

Further, using H^1-stability of R_h^1 and Young's inequality in the above equation, we have

$$|u_h(t)|_1^2 + \|u_h\|_{L^2(H^1)}^2 \leq C\big(|u_0|_1^2 + \|f\|_{L^2(L^2)}^2\big).$$

This proves for $k = 0$. For the case $k = 1$, differentiating (3.2.4) with respect to t and then choosing $v_h = u_{ht}$, we obtain

$$a_{1,h}(u_{ht}(t), u_{ht}(t)) + \frac{1}{2}\frac{d}{dt}a_{2,h}(u_{ht}(t), u_{ht}(t)) = (f_{ht}(t), u_{ht}(t)).$$

Now, integration from 0 to t yields

$$\int_0^t |u_{ht}(s)|_1^2 ds + |u_{ht}(t)|_1^2 \leq C\Big(|u_{ht}(0)|_1^2 + \int_0^t \|f_{ht}(s)\|^2 |u_{ht}(s)|_1^2 ds\Big).$$

Further, applying Young's inequality and Lemma 3.3.1 in the above equation, we get

$$|u_{ht}(t)|_1^2 + \|u_{ht}\|_{L^2(H^1)}^2 \leq C\big(|u_0|_1^2 + \|f\|_{H^1(L^2)}^2\big). \tag{3.3.4}$$

Using, similar argument as in (3.3.4), we can show the result for $k = 2$ and $k = 3$. This completes the rest of the proof. □

We will now present the error estimates for the semi-discrete approximation. We have the following result for the optimal order error estimate in H^1 norm.

Theorem 3.3.1. *Assume that $u \in H^1(0,T;H^{m+1}(\Omega))$, $f \in L^2(0,T;H^m(\Omega))$ and $u_0 \in H^{m+1}(\Omega)$. Then for all $t \in (0,T]$, we have*

$$|u_h(t) - u(t)|_1 \leq Ch^m(|u_0|_{m+1} + \|u\|_{H^1(H^{m+1})} + \|f\|_{L^2(H^m)}).$$

Proof. Let us split the error $e_h(t) = u_h(t) - u(t)$ as

$$e_h(t) = (u_h(t) - R_h^2 u(t)) + (R_h^2 u(t) - u(t)) =: \phi(t) + \psi(t). \tag{3.3.5}$$

Applying Lemma 3.2.1, the following bounds for $\psi(t)$ is obtained as

$$|\psi(t)|_1 \leq Ch^m |u(t)|_{m+1} \leq Ch^m(|u_0|_{m+1} + \|u_t\|_{L^1(H^{m+1})}). \tag{3.3.6}$$

Therefore, we need to estimate the bound for the term $\phi(t)$ only. From (3.2.4), using the definitions the projection operators R_h^i, $i = 1, 2$, and the fact that the time derivative

commutes with R_h^i's, we have the following error equation for $\phi(t)$: For all $w_h \in W_h^m$ and for all $t \in (0, T]$

$$\begin{aligned}
&a_{1,h}(\phi(t), w_h) + a_{2,h}(\phi_t(t), w_h) \\
&= a_{1,h}(u_h(t), w_h) + a_{2,h}(u_{ht}(t), w_h) - \left[a_{1,h}(R_h^2 u(t), w_h) + a_{2,h}(R_h^2 u_t(t), w_h)\right] \\
&= (f_h(t) - f(t), w_h) + a_1(u(t), w_h) + a_2(u_t(t), w_h) \\
&\quad - \left[a_{1,h}(R_h^1 u(t), w_h) + a_{2,h}(R_h^2 u_t(t), w_h) + a_{1,h}(R_h^2 u(t) - R_h^1 u(t), w_h)\right] \\
&= (f_h(t) - f(t), w_h) + a_{1,h}(R_h^1 u(t) - R_h^2 u(t), w_h) \\
&=: T_1 + T_2. \qquad (3.3.7)
\end{aligned}$$

For the term T_1, from Lemma 1.4.6, we have

$$T_1 = (f_h(t) - f(t), w_h) \le Ch^m |f(t)|_m \|w_h\|. \qquad (3.3.8)$$

Again, for the term T_2, using the continuity of $a_{1,h}$ and approximation properties of R_h^1 and R_h^2, we obtain

$$\begin{aligned}
T_2 &= a_{1,h}(R_h^1 u(t) - R_h^2 u(t), w_h) \\
&= a_{1,h}(R_h^1 u(t) - u(t), w_h) - a_{1,h}(R_h^2 u(t) - u(t), w_h) \\
&\le (1 + \beta_\sigma)\overline{M}(|R_h^2 u(t) - u(t)|_1 + |R_h^1 u(t) - u(t)|_1)|w_h|_1 \\
&\le Ch^m |u(t)|_{m+1} |w_h|_1. \qquad (3.3.9)
\end{aligned}$$

Now, substituting the estimates for T_1 and T_2 from (3.3.8) and (3.3.9) and putting $w_h = \phi(t)$ in the error equation (3.3.7), we obtain

$$a_{1,h}(\phi(t), \phi(t)) + a_{2,h}(\phi_t(t), \phi(t)) \le Ch^m(|u(t)|_{m+1} + |f(t)|_m)|\phi(t)|_1.$$

Due to the symmetry property of $a_{2,h}$ the above equation can be written as

$$a_{1,h}(\phi(t), \phi(t)) + \frac{1}{2}\frac{d}{dt}a_{2,h}(\phi(t), \phi(t)) \le Ch^m(|u(t)|_{m+1} + |f(t)|_m)|\phi(t)|_1.$$

Integrating from 0 to t, and using the coercivity of $a_{1,h}$ and $a_{2,h}$, we get

$$\int_0^t |\phi(s)|_1^2 \, ds + |\phi(t)|_1^2 \le C \int_0^t h^m(|u(s)|_{m+1} + |f(s)|_m)|\phi(s)|_1 \, ds + |\phi(0)|_1^2. \qquad (3.3.10)$$

Since, $\phi(0) = u_h(0) - R_h^2 u(0) = 0$, using Young's inequality in (3.3.10), we obtain

$$\int_0^t |\phi(s)|_1^2 \, ds + |\phi(t)|_1^2 \leq C(\delta) h^{2m} (\|u\|^2_{L^2(H^{m+1})} + \|f\|^2_{L^2(H^m)}) + C_\delta \int_0^t |\phi(s)|_1^2 \, ds.$$

For suitable $\delta > 0$, neglecting the term $\int_0^t |\phi(s)|_1^2 \, ds$, we have

$$|\phi(t)|_1 \leq C h^m (\|u\|_{L^2(H^{m+1})} + \|f\|_{L^2(H^m)}). \tag{3.3.11}$$

Finally, plugging (3.3.6) and (3.3.11) in (3.3.5), we get

$$|u_h(t) - u(t)|_1 \leq C h^m (|u_0|_{m+1} + \|u\|_{H^1(H^{m+1})} + \|f\|_{L^2(H^m)}).$$

□

For the error estimate in L^2 norm, we will use a dual problem. Consider the following problem: Find $w \in H^1(\mathcal{J}; H_0^1(\Omega) \cap H^2(\Omega))$ such that

$$a_1(w(t), v) - a_2(w_t(t), v) = (\phi(t), v) \quad \forall v \in H_0^1(\Omega) \tag{3.3.12}$$

and $w(\tau) = 0$ for some $\tau \in \mathcal{J}$. We assume that there exists a unique solution $w \in H^1(\mathcal{J}; H_0^1(\Omega) \cap H^2(\Omega))$ satisfying (cf. [9])

$$\|w\|_{H^1(H^2)} \leq C \|\phi\|_{L^2(L^2)}. \tag{3.3.13}$$

Now, substituting $v = \phi_t(t)$ in (3.3.12) and then integrating from 0 to τ, we get

$$\frac{1}{2}(\|\phi(\tau)\|^2 - \|\phi(0)\|^2) = \int_0^\tau (a_1(w(t), \phi_t(t)) - a_2(w_t(t), \phi_t(t))) \, dt. \tag{3.3.14}$$

Since $w(\tau) = 0$ and $\phi(0) = 0$, we observe that

$$\begin{aligned} \int_0^\tau a_1(w(t), \phi_t(t)) \, dt &= -\int_0^\tau a_1(w_t(t), \phi(t)) \, dt + a_1(w(\tau), \phi(\tau)) - a_1(w(0), \phi(0)) \\ &= -\int_0^\tau a_1(w_t(t), \phi(t)) \, dt. \end{aligned} \tag{3.3.15}$$

Now, using the above equation (3.3.15) in (3.3.14), we obtain

$$\frac{1}{2}\|\phi(\tau)\|^2 = -\int_0^\tau (a_1(w_t(t), \phi(t)) + a_2(w_t(t), \phi_t(t))) \, dt.$$

Using the definition of R_h^1 and R_h^2, we have

$$\begin{aligned}\frac{1}{2}\|\phi(\tau)\|^2 &= -\int_0^\tau \left(a_{1,h}(R_h^1 w_t(t),\phi(t)) + a_{2,h}(R_h^2 w_t(t),\phi_t(t))\right)\ dt\\ &= -\int_0^\tau \left(a_{1,h}(R_h^2 w_t(t),\phi(t)) + a_{2,h}(R_h^2 w_t(t),\phi_t(t))\right) dt\\ &\quad + \int_0^\tau a_{1,h}(R_h^2 w_t(t) - R_h^1 w_t(t),\phi(t))\ dt.\end{aligned}$$

Now, from the error equation (3.3.7), we get

$$\begin{aligned}\frac{1}{2}\|\phi(\tau)\|^2 &= -\int_0^\tau \left(a_{1,h}(R_h^1 u(t) - R_h^2 u(t), R_h^2 w_t(t)) + (f_h(t) - f(t), R_h^2 w_t(t))\right)\ dt\\ &\quad + \int_0^\tau a_{1,h}(R_h^2 w_t(t) - R_h^1 w_t(t),\phi(t))\ dt. \qquad (3.3.16)\end{aligned}$$

We can easily observe that

$$\begin{aligned}&\int_0^\tau a_{1,h}(R_h^1 u(t) - R_h^2 u(t), R_h^2 w_t(t))\ dt\\ &= \int_0^\tau a_1(R_h^1 u(t) - R_h^2 u(t), w_t(t))\ dt + \int_0^\tau a_{1,h}(R_h^1 u(t) - R_h^2 u(t), R_h^2 w_t(t) - R_h^1 w_t(t))\ dt\\ &= \int_0^\tau \int_\Omega \left(R_h^1 u(t) - R_h^2 u(t)\right)\nabla.(\sigma(x)\nabla w_t(t))\ dxdt\\ &\quad + \int_0^\tau a_{1,h}(R_h^1 u(t) - R_h^2 u(t), R_h^2 w_t(t) - R_h^1 w_t(t))\ dt.\end{aligned}$$

Now rewriting (3.3.16), and using the continuity of the bilinear forms $a_{1,h}$ and $a_{2,h}$, we obtain

$$\begin{aligned}\|\phi(\tau)\|^2 \le C\Big[&\int_0^\tau \|R_h^1 u(t) - R_h^2 u(t)\||w_t(t)|_2\ dt + \int_0^\tau \|f_h(t) - f(t)\|\|R_h^2 w_t(t)\|\ dt\\ &+ \int_0^\tau |R_h^1 w_t(t) - R_h^2 w_t(t)|_1 \left(|R_h^1 u(t) - R_h^2 u(t)|_1 + |\phi(t)|_1\right)\ dt\Big].\end{aligned}$$

Using the approximation properties of R_h^1 and R_h^2, Lemma 1.4.6 and (3.3.11), we get

$$\|\phi(\tau)\|^2 \le C\int_0^\tau h^{m+1}\left(|u(t)|_{m+1} + |f(t)|_{m+1} + \|u\|_{L^2(H^{m+1})} + \|f\|_{L^2(H^m)}\right)|w_t(t)|_2\ dt.$$

Applying Young's inequality in the above equation, we have

$$\begin{aligned}\|\phi(\tau)\|^2 \le C(\delta)h^{2(m+1)}&\int_0^\tau \left(|u(t)|_{m+1} + |f(t)|_{m+1} + \|u\|_{L^2(H^{m+1})} + \|f\|_{L^2(H^m)}\right)^2 dt\\ &+ C_\delta\|w\|^2_{H^1(H^2)}, \qquad (3.3.17)\end{aligned}$$

for some $\delta > 0$. Now, from the a priori estimate (3.3.13), we have

$$\|\phi(\tau)\|^2 \leq C(\delta, T)\ h^{2(m+1)} \left(\|u\|^2_{L^2(H^{m+1})} + \|f\|^2_{L^2(H^{m+1})} \right) + C_\delta \|\phi\|^2_{L^2(L^2)}. \tag{3.3.18}$$

Now, we select τ such that $\|\phi(\tau)\| = \max_{t\in\mathcal{J}} \|\phi(t)\|$ and hence $\|\phi\|^2_{L^2(L^2)} \leq T\|\phi(\tau)\|^2$. Thus, for suitable $\delta > 0$, from the estimate (3.3.18), we obtain

$$\|\phi(\tau)\| \leq Ch^{m+1} \left(\|u\|_{L^2(H^{m+1})} + \|f\|_{L^2(H^{m+1})} \right). \tag{3.3.19}$$

Finally, with the above estimate (3.3.19), the L^2 norm error estimate for the semi-discrete approximation can be given by following theorem.

Theorem 3.3.2. *Assume that $u \in H^1(0,T;H^{m+1}(\Omega))$, $f \in L^2(0,T;H^{m+1}(\Omega))$ and $u_0 \in H^{m+1}(\Omega)$. Then for all $t \in (0,T]$, we have*

$$\|u_h(t) - u(t)\| \leq Ch^{m+1}(|u_0|_{m+1} + \|u\|_{H^1(H^{m+1})} + \|f\|_{L^2(H^{m+1})}).$$

Proof. As in (3.3.5), we split the error into two parts as

$$u_h(t) - u(t) =: \phi(t) + \psi(t). \tag{3.3.20}$$

Applying Lemma 3.2.1, we have the following bounds for $\psi(t)$

$$\|\psi(t)\| \leq Ch^{m+1}|u(t)|_{m+1} \leq Ch^{m+1}(|u_0|_{m+1} + \|u_t\|_{L^1(H^{m+1})}). \tag{3.3.21}$$

Now, from (3.3.19), we have

$$\|\phi(t)\| \leq \|\phi(\tau)\| \leq Ch^{m+1} \left(\|u\|_{L^2(H^{m+1})} + \|f\|_{L^2(H^{m+1})} \right). \tag{3.3.22}$$

Thus, applying triangle inequality and using the estimates (3.3.21) and (3.3.22), equation (3.3.20) yields

$$\|u_h(t) - u(t)\| \leq Ch^{m+1}(|u_0|_{m+1} + \|u\|_{H^1(H^{m+1})} + \|f\|_{L^2(H^{m+1})}).$$

□

3.4 Error Analysis for the Fully Discrete Problems

This section deals with the formulation of a fully discrete scheme to approximate the solution to the model problem (3.1.1). We consider the Crank-Nicolson based temporal discrete scheme and will establish both H^1 and L^2 norm error estimate for the fully discrete virtual element approximation.

We recall the discretization of the time domain $[0, T]$ and notations from Chapter 2, Section 2.4. Now, employing Crank-Nicolson scheme to the equation (3.2.4), we obtain the fully discretized problem defined by: Find $\mathcal{U}^n \in W_h^m$ such that for $n = 1, 2, \cdots, N-1$

$$\begin{cases} a_{1,h}(\mathcal{U}^{n+\frac{1}{2}}, w) + a_{2,h}(\partial_\tau \mathcal{U}^n, w) = (f_h^{n+\frac{1}{2}}, w) \ \forall \ w \in W_h^m, \\ \mathcal{U}^0 = R_h^2 u_0. \end{cases} \tag{3.4.1}$$

The existence and uniqueness follows immediately from the Lax–Milgram theorem. In the later discussion, we will require the following approximation result. It can be proved using the Taylor's series and standard arguments.

Lemma 3.4.1. *For any $v \in H^3(0, T; L^2(\Omega))$, we have*

$$|\partial_\tau v^n - v_t^{n+\frac{1}{2}}|_1 \leq C\tau \int_{t_n}^{t_{n+1}} |v_{ttt}(t)|_1 dt.$$

Towards estimating the error $e_h^n := \mathcal{U}^n - u^n$, we split the error as

$$e_h^n := \theta^n + \rho^n,$$

where $\theta^n = \mathcal{U}^n - u_h^n$ and $\rho^n = u_h^n - u^n$ for $n = 1, 2, \cdots, N$. For the term θ^n, we have the following result.

Lemma 3.4.2. *Let u_h^n and $\mathcal{U}^n$ solution of (3.2.4) and (3.4.1) at time $t = t_n$ respectively. Then, we have*

$$|\theta^n|_1 \leq C\tau^2 \int_0^T |u_{httt}(t)|_1 dt,$$
$$\|\theta^n\| \leq C\tau^2 \int_0^T |u_{httt}(t)|_1 dt.$$

Proof. From (3.2.4), substituting the value of t by t_l and t_{l+1} and then adding, we get

$$a_{1,h}(u_h^{l+\frac{1}{2}}, w) + a_{2,h}(\partial_\tau u_h^l, w) = (f_h^{l+\frac{1}{2}}, w) + a_{2,h}(\partial_\tau u_h^l - u_{ht}^{l+\frac{1}{2}}, w) \tag{3.4.2}$$

for all $w \in W_h^m$. Now, subtracting (3.4.2) from (3.4.1) and then substituting $w = \theta^{l+\frac{1}{2}}$, we obtain

$$a_{1,h}(\theta^{l+\frac{1}{2}}, \theta^{l+\frac{1}{2}}) + a_{2,h}(\partial_\tau \theta^l, \theta^{l+\frac{1}{2}}) = -a_{2,h}(\partial_\tau u_h^l - u_{ht}^{l+\frac{1}{2}}, \theta^{l+\frac{1}{2}}),\ 1 \le l \le N-1.$$

On solving, we get for $1 \le l \le N-1$

$$a_{1,h}(\theta^{l+\frac{1}{2}}, \theta^{l+\frac{1}{2}}) + \frac{1}{2\tau}\left(a_{2,h}(\theta^{l+1}, \theta^{l+1}) - a_{2,h}(\theta^l, \theta^l)\right) = -a_{2,h}(\partial_\tau u_h^l - u_{ht}^{l+\frac{1}{2}}, \theta^{l+\frac{1}{2}}).$$

Now, using the coercivity and continuity of the bilinear forms $a_{i,h}$, $i = 1, 2$ and neglecting positive term on left hand side, we obtain

$$|\theta^{l+1}|_1 - |\theta^l|_1 \le C\tau |\partial_\tau u_h^l - u_{ht}^{l+\frac{1}{2}}|_1. \tag{3.4.3}$$

Taking sum from $l = 0$ to $n-1$ with $2 \le n \le N$ and using $\theta^0 = 0$, we find

$$|\theta^n|_1 \le C\tau \sum_{l=0}^{n-1} |\partial_\tau u_h^l - u_{ht}^{l+\frac{1}{2}}|_1.$$

Again, substituting $l = 0$ in (3.4.3), we obtain

$$|\theta^1|_1 \le C\tau |\partial_\tau u_h^0 - u_{ht}^{\frac{1}{2}}|_1. \tag{3.4.4}$$

Combining (3.4.3) and (3.4.4), we get

$$\max_{1\le n\le N} |\theta^n|_1 \le C\tau \sum_{n=0}^{N} |\partial_\tau u_h^l - u_{ht}^{l+\frac{1}{2}}|_1.$$

Finally, using Lemma 3.4.1, we have

$$\max_{1\le n\le N} |\theta^n|_1 \le C\tau^2 \int_0^T |u_{httt}(t)|_1 dt.$$

Again, by Poincaŕe's inequality, we obtain

$$\|\theta^n\| \le C|\theta^n|_1 \le C\tau^2 \int_0^T |u_{httt}(t)|_1 dt.$$

□

Now, Lemma 3.4.2 along with Theorem 3.3.1 and Theorem 3.3.2 gives us the following estimates for the fully discrete approximation.

Theorem 3.4.1. *Let u^n and $\mathcal{U}^n$ solution of (3.1.1) and (3.4.1) at time $t = t_n$, respectively. Assume that $u_0 \in H^{m+1}(\Omega)$, $u \in H^1(0,T;H^{m+1}(\Omega))$ and $f \in L^2(0,T;H^{m+1}(\Omega)) \cap H^3(0,T;L^2(\Omega))$, then for all $t \in (0,T]$ we have*

$$\max_{1\le n\le N} |\mathcal{U}^n - u^n|_1 \le Ch^m\big(|u_0|_{m+1} + \|u\|_{H^1(H^{m+1})} + \|f\|_{L^2(H^m)}\big) + \tilde{C}\tau^2\big(|u_0|_1 + \|f\|_{H^3(L^2)}\big),$$

$$\max_{1\le n\le N} \|\mathcal{U}^n - u^n\| \le Ch^{m+1}\big(|u_0|_{m+1} + \|u\|_{H^1(H^{m+1})} + \|f\|_{L^2(H^{m+1})}\big) + \tilde{C}\tau^2\big(|u_0|_1 + \|f\|_{H^3(L^2)}\big).$$

Proof. From Theorem 3.3.1 and Theorem 3.3.2, at $t = t_n$, we have

$$|\rho^n|_1 = |u_h^n - u^n|_1 \le Ch^m(|u_0|_{m+1} + \|u\|_{H^1(H^{m+1})} + \|f\|_{L^2(H^m)}),$$
$$\|\rho^n\| = \|u_h^n - u^n\| \le Ch^{m+1}(|u_0|_{m+1} + \|u\|_{H^1(H^{m+1})} + \|f\|_{L^2(H^{m+1})}).$$

Again from Lemma 3.3.2 and Lemma 3.4.2, we get

$$\max_{1\le n\le N} (\|\theta^n\| + |\theta^n|_1) \le C\tau^2 \int_0^T |u_{httt}(t)|_1 dt \le C\tau^2 T\left(|u_0|_1 + \|f\|_{H^3(L^2)}\right).$$

Finally, applying triangle inequality to $e_h^n := \theta^n + \rho^n$, we get the result. □

3.5 Numerical Results

In this section, we illustrate numerical examples to test the practical performance of the proposed method. In all the examples, we consider the spatial domain $\Omega = (0,1) \times (0,1)$ and the time interval $\mathcal{J} = [0,1]$. We have implemented the second-order Crank-Nicolson scheme as the time scheme for the fully discrete problem. To illustrate the flexibility of the method with respect to mesh discretization, different types of polygonal meshes are considered such as square ($\mathcal{Q}_h$), non-uniform quadrilaterals ($\mathcal{N}_h$) and Voronoi ($\mathcal{V}_h$) meshes. The adopted polygonal meshes are shown in Figure 3.5.1.

In all the examples, we have considered the model problem (2.1.1)-(2.1.2) and the source function f, initial data $\{u_0, v_0\}$ are chosen according to the choice of exact solution. In Example 3.5.1, we have discussed the convergence of proposed algorithm for scalar coefficients in a convex domain with all three types of meshes. We also compared the CPU time for FEM and VEM with different polygonal meshes and shown the cost-efficiency of the proposed method. Further, we have tested our algorithm for matrix coefficients in Example 3.5.2.

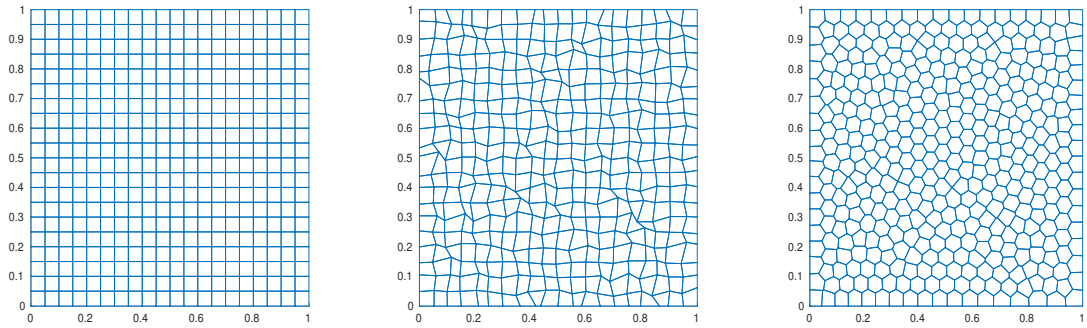

Figure 3.5.1: Sample meshes: $\mathcal{Q}_h$(left), $\mathcal{N}_h$(center) and $\mathcal{V}_h$(right) with 400 elements.

Example 3.5.1. (Constant coefficients) We select the exact solution to be

$$u(x, y, t) = \sin(t)\sin(\pi x)\sin(\pi y)$$

and the coefficients $\sigma = \epsilon = I$ in the model problem (3.1.1)-(3.1.2).

We have implemented linear VEM with the three types of meshes $\mathcal{Q}_h$, $\mathcal{N}_h$ and $\mathcal{V}_h$ and different time steps τ. The numerical errors and convergence rates both in L^2 norm and H^1 semi-norm at the final time $T = 1$ with $\tau = 10^{-4}$ are shown in Table 3.5.1. Here, we notice from Figure 3.5.2 that for all the meshes, we have achieved the expected order of convergence, i.e. second order for the L^2 norm and first order for the H^1 semi-norm.

Next, we applied the standard FEM with the triangular meshes and different time steps τ for the given model problem. Table 3.5.2 shows the CPU time for FEM and VEM with different types of meshes for different values of τ. This reflects that even for complex meshes like non uniform quadrilateral meshes or voronoi meshes, VEM is more cost-efficient than the standard FEM.

Example 3.5.2. (Matrix coefficients) We select the exact solution to the model problem (3.1.1)-(3.1.2) as

$$u(x, y, t) = \sin(t)\sin(\pi x)\sin(\pi y)$$

with coefficients

$$\sigma = \begin{bmatrix} 4 & 2 \\ 2 & 3 \end{bmatrix} \text{ and } \epsilon = \begin{bmatrix} 2 & 1 \\ 1 & 3 \end{bmatrix}.$$

We have implemented linear VEM with the meshes $\mathcal{N}_h$ and $\mathcal{V}_h$ with time step $\tau = 10^{-4}$. Table 3.5.3 shows the numerical errors and convergence rates both in L^2 norm and H^1

Table 3.5.1: L^2 and H^1 errors at $T = 1$ with $\tau = 10^{-4}$ in Example 3.5.1

mesh	h	$\|e_h\|$	EOC	$\|e_h\|_1$	EOC
$\mathcal{Q}_h$	1/5	$7.3392e-03$	-	$3.2770e-02$	-
	1/10	$1.7505e-03$	2.0679	$1.5632e-02$	1.0679
	1/20	$4.3373e-04$	2.0129	$7.7195e-03$	1.0179
	1/40	$1.0821e-04$	2.0030	$3.8476e-03$	1.0045
$\mathcal{N}_h$	0.3484	$7.8302e-03$	-	$4.3209e-02$	-
	0.2033	$2.4730e-03$	2.1393	$2.4150e-02$	1.0798
	0.1083	$6.3862e-04$	2.1496	$1.2094e-02$	1.0981
	0.0554	$1.5721e-04$	2.0951	$5.1260e-03$	1.2830
$\mathcal{V}_h$	0.3171	$1.0128e-02$	-	$5.6697e-02$	-
	0.1531	$2.6253e-03$	1.8549	$2.4589e-02$	1.1477
	0.0812	$6.7738e-04$	2.1364	$1.1856e-02$	1.1503
	0.0416	$1.9109e-04$	1.8936	$6.2519e-03$	0.9575

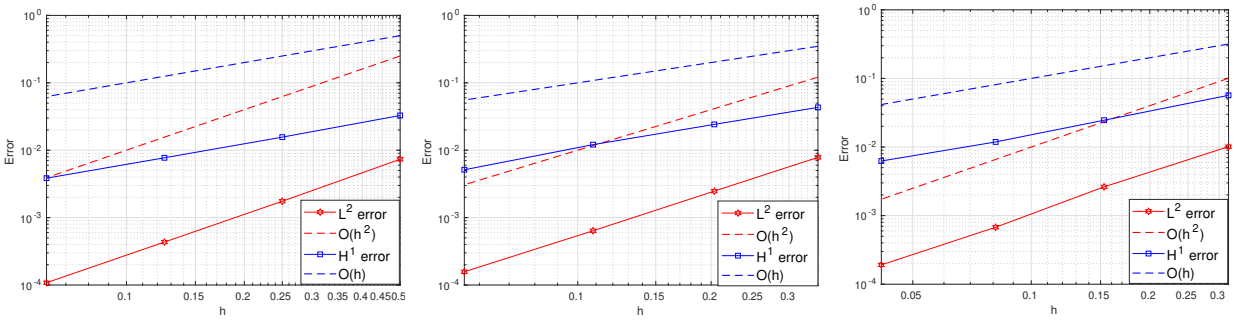

Figure 3.5.2: Log-log plots of the L^2 and H^1 errors versus h at $t = 1$ for $\mathcal{S}_h$ (left), $\mathcal{N}_h$ (center) and $\mathcal{V}_h$ (right) in Example 3.5.2.

Table 3.5.2: CPU time for FEM and VEM in seconds in Example 3.5.1

τ	FEM	VEM		
		$\mathcal{Q}_h$	$\mathcal{N}_h$	$\mathcal{V}_h$
h	7.293	0.975	-	-
10^{-2}	9.052	1.477	1.793	3.543
10^{-3}	75.627	9.726	12.739	27.934
10^{-4}	899.504	92.967	126.389	276.405

semi-norm at the final time $T = 1$. Figure 3.5.5 reflects that, we have achieved optimal order of convergence in both L^2 norm and H^1 semi-norm. The surface plot of approximate solution and contour plot of error at $T = 1$ are depicted in Figure 3.5.3-3.5.4.

3.6 Conclusion

In this work, we have developed a virtual element framework for the pulsed electric field model problem. We have obtained optimal order of convergence i.e. $O(h^{m+1}+\tau^2)$ in $L^\infty(L^2)$ norm and $O(h^m + \tau^2)$ in $L^\infty(H^1)$ norm. The agreement of the theoretical findings with the numerical results for different types of polygonal discretizations reflects the flexibility of the method with respect to shape of mesh polygons. It also shown that even for complex meshes, VEM is more cost-efficient than the standard FEM. We believe that this work can be used to develop virtual element methods for various problems that includes the strong damping.

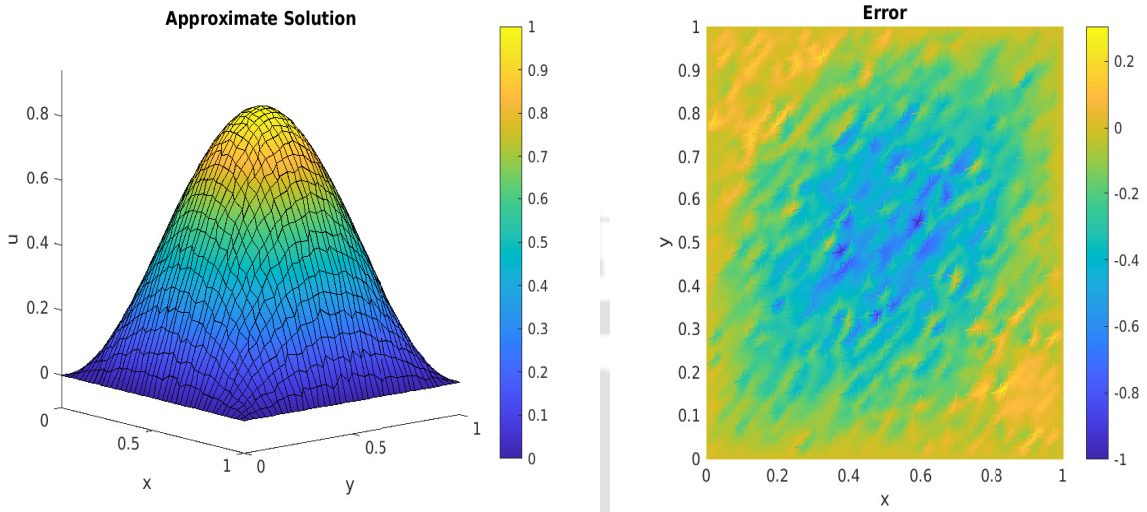

Figure 3.5.3: Approximate solution (left), and error plot (right) at $t = 1$ with $\tau = 10^{-4}$ and $h = 0.3796$ in Example 3.5.2.

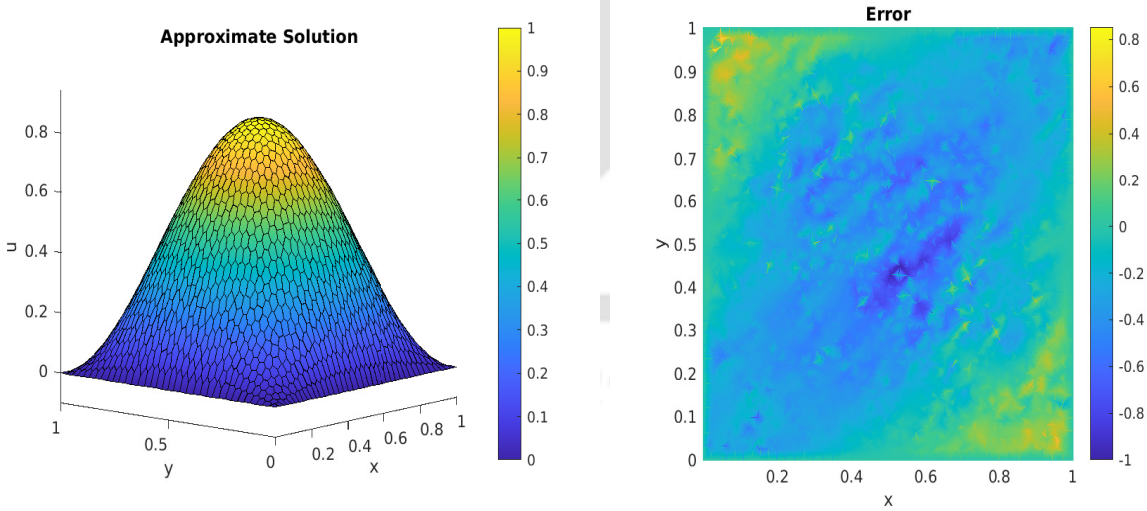

Figure 3.5.4: Approximate solution (left), and error plot (right) at $t = 1$ with $\tau = 10^{-4}$ and $h = 0.0416$ in Example 3.5.2.

Table 3.5.3: L^2 and H^1 errors at $T = 1$ with $\tau = 10^{-4}$ in Example 3.5.2

	h	$\|e_h\|$	EOC	$\|e_h\|_1$	EOC
$\mathcal{N}_h$	0.3372	$8.3355e-03$	-	$9.3259e-02$	-
	0.1708	$2.7728e-03$	1.6196	$4.3066e-02$	1.1369
	0.7952	$6.7135e-04$	1.8532	$1.9855e-02$	1.0117
	0.3796	$1.6496e-04$	1.9014	$7.8666e-03$	1.2542
$\mathcal{V}_h$	0.3171	$1.2558e-02$	-	$1.2991e-01$	-
	0.1531	$3.8006e-03$	1.6415	$5.9711e-02$	1.0676
	0.0812	$9.9992e-04$	2.1055	$2.6513e-02$	1.2802
	0.0416	$2.6240e-04$	2.0003	$1.3542e-02$	1.0045

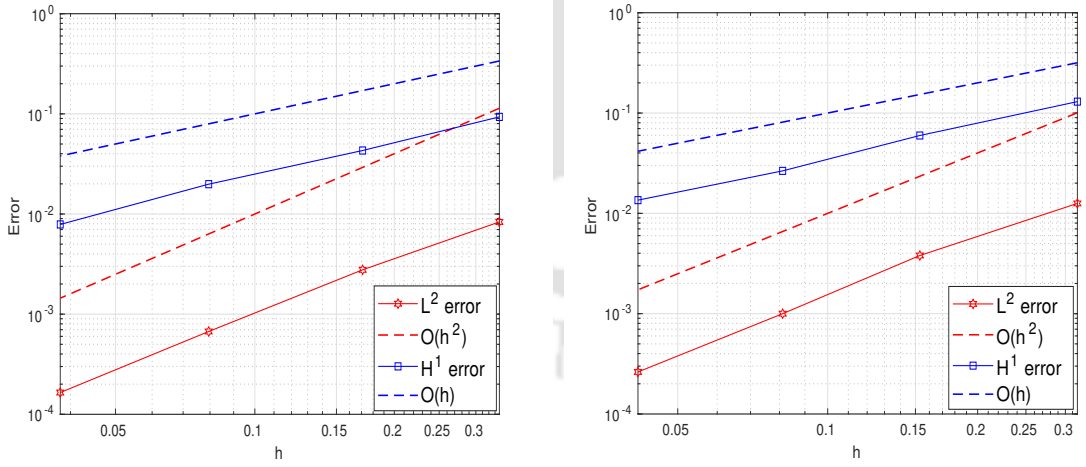

Figure 3.5.5: Log-log plots of the L^2 and H^1 errors versus h at $t = 1$ for $\mathcal{N}_h$ (left) and $\mathcal{V}_h$ (right) in Example 3.5.2.

4

Optimal Convergence Analysis of the VEM for Second-order Sobolev Equations

We develop a virtual element method for second-order Sobolev equations on polygonal meshes. We propose both semi-discrete and fully discrete schemes to numerically solve the linear Sobolev equations. For the time discretization, we have used implicit second-order Newmark scheme. Optimal convergence rates in both the L^2 norm and the H^1 semi-norm are established using a new non-standard projection operator. Numerical experiments are illustrated to confirm our theoretical findings.

4.1 Introduction

Our goal of the current work is to develop a virtual element method for second-order Sobolev equations with variable coefficients. We consider the following problem as our model problem

$$u_t(x,t) - \nabla \cdot (\sigma(x)\nabla u(x,t) + \epsilon(x)\nabla u_t(x,t)) = f(x,t) \text{ in } \Omega \times (0,T] \tag{4.1.1}$$

with ICs and BCs

$$u(x,0) = u_0 \text{ in } \Omega, \quad u(x,t) = 0 \quad \text{on } \partial\Omega \times (0,T], \tag{4.1.2}$$

where $\Omega \subset \mathbb{R}^2$ is a polygonal domain with smooth boundary $\partial\Omega$ and $T < \infty$. Here, f denotes the source function, $\epsilon(x)$ and $\sigma(x)$ are the damping coefficient and the diffusion coefficient, respectively. Further, we assume that there exists two positive constants $\underline{M}$ and $\overline{M}$ such that $\underline{M} \leq \epsilon(x),\ \sigma(x) \leq \overline{M}$ a. e. in Ω.

In recent years, many numerical methods have been studied extensively to solve the Sobolev equation via finite elements such as conforming FEMs [56, 96], mixed FEMs [97, 116], the weak Galerkin FEMs [60, 62], the local Discontinuous Galerkin (DG) methods [61] and the penalty DG method (PDG) [1]. But, in case of polygonal or polyhedral meshes employing FEM becomes very difficult task due to the complexity in basis construction and it demands higher computational cost to evaluate the integrals using Gauss quadrature.

Recently, Zhang et al. developed a virtual method for the Sobolev equations with constant coefficients [138] and Xu et al. gave a conforming virtual element method for Sobolev equations with non-homogeneous boundary condition [135]. Error analysis in [138] has been carried out using an elliptic projection operator for constant coefficients. Then the convergence results in [138] have been extended for variable coefficients by Xu et al. [135] assuming $\sigma = \epsilon$. However, in the case of variable coefficients with $\sigma \neq \epsilon$, we will have two different bilinear forms: one for $\nabla \cdot (\sigma \nabla u)$ and another for $\nabla \cdot (\epsilon \nabla u_t)$. It is observed that although the standard elliptic projection leads to an optimal error estimate in the energy norm, it is difficult to achieve an optimal convergence rate in L^2 norm. This is due to the fact that the elliptic projection operator can only takes care either $\nabla \cdot (\sigma \nabla u)$ or $\nabla \cdot (\epsilon \nabla u_t)$ in the error analysis (see, Remark 4.3.1). The derivation of the a priori error bound in L^2 norm heavily depends on the approximation properties (cf. Lemmas 4.3.4-4.3.5) of a newly introduced non-standard projection operator.

In this study, we develop a VEM for the second-order Sobolev equations (4.1.1). The virtual semi-discrete approximation of the model problem is constructed using three approximated bilinear forms. The fully discrete scheme is obtained by employing the Crank-Nicolson discretization. In fact the time discretization method is the well-known Newmark method for wave equation when we adopt the particular choice for the parameters in the Newmark scheme (cf. [67]), which has been used extensively in applications. We present rigorous error analysis for the semi-discrete scheme as well as fully discrete scheme and derive optimal convergence estimates. Further, in support of theoretical findings numerical examples are presented with different types of meshes and different polynomial degrees.

The remainder of the content is divided as follows. We present the construction of the virtual element semi-discrete problem in Section 4.2. Next, while Section 4.3 deals with the semi-discrete error analysis, Section 4.4 discusses fully discrete approximation and its convergence. Numerical examples and the conclusion are presented in Section 4.5 and Section 4.6, respectively.

4.2 Semi-discrete Virtual Element Approximation

In this section, we construct the semi-discrete virtual element approximation to the model problem (4.1.1)-(4.1.2).

Following the standard way, we easily obtain the variational problem corresponding to the model problem (4.1.1)-(4.1.2) as : Find $u \in L^2(0,T;H_0^1(\Omega)) \cap H^1(0,T;H^1(\Omega))$ such that for all $v \in H_0^1(\Omega)$ and for a.e. $t \in (0,T]$

$$\begin{cases} (u_t, v) + a_1(u,v) + a_2(u_t,v) = (f,v), \\ u(0) = u_0, \end{cases} \tag{4.2.1}$$

where $a_1(u,v)$ and $a_2(u,v)$ are bilinear forms on $H_0^1(\Omega)$ defined as in (3.2.2).

We recall the virtual element framework discussed in Chapter 1, Section 1.4. The bilinear forms $a_i(\cdot,\cdot)$, $i = 1,2$ can be splited into their local counterparts in the following manner

$$a_i(u,v) := \sum_{E\in\mathcal{T}_h} a_i^E(u,v) \ \forall\ u,v \in H_0^1(\Omega), \quad i = 1,2.$$

Then the discrete bilinear forms on the local virtual element space $W_h^m(E)$ can be defined as:

$$\begin{aligned} a_{1,h}^E(v,w) &:= \left(\sigma \boldsymbol{\Pi}_{m-1,E}^0 \nabla v, \boldsymbol{\Pi}_{m-1,E}^0 \nabla w\right)_E + S_\sigma^E\left((I-\Pi_{m,E}^\nabla)v, (I-\Pi_{m,E}^\nabla)w\right), \\ a_{2,h}^E(v,w) &:= \left(\epsilon \boldsymbol{\Pi}_{m-1,E}^0 \nabla v, \boldsymbol{\Pi}_{m-1,E}^0 \nabla w\right)_E + S_\epsilon^E\left((I-\Pi_{m,E}^\nabla)v, (I-\Pi_{m,E}^\nabla)w\right), \\ m_h^E(v,w) &:= (\Pi_{m,E}^0 v, \Pi_{m,E}^0 w)_E + S_0^E\left((I-\Pi_{m,E}^0)v, (I-\Pi_{m,E}^0)w\right) \end{aligned} \tag{4.2.2}$$

where

$$\begin{aligned} S_\sigma^E(v,w) &= \beta_\sigma^E \sum_{r=1}^{N^E} dof_r(v) dof_r(w), \\ S_\epsilon^E(v,w) &= \beta_\epsilon^E \sum_{r=1}^{N^E} dof_r(v) dof_r(w) \quad \& \\ S_0^E(v,w) &= |E| \sum_{r=1}^{N^E} dof_r(v) dof_r(w) \end{aligned}$$

with $\beta_\sigma^E = P_E^a(\sigma)$, $\beta_\epsilon^E = P_E^a(\epsilon)$ and $N^E = \dim W_h^m(E)$.

Now the global bilinear forms on the global discrete space W_h^m can be obtained by assembling the local counterpart as:

$$a_{i,h}(v,w) := \sum_{E\in\mathcal{T}_h} a_{i,h}^E(v,w),\ i=1,2\ \&\ \ m_h(v,w) := \sum_{E\in\mathcal{T}_h} m_h^E(v,w) \quad \forall v,w \in W_h^m.$$

The global bilinear forms $a_{i,h}$, $i=1,2$ and m_h satisfies the following continuity and coercivity properties (Lemma 1.4.5): For $v,w \in W_h^m$

$$\begin{aligned} a_{1,h}(v,w) &\le (1+\beta_\sigma)\overline{M}|v|_1|w|_1, \\ a_{2,h}(v,w) &\le (1+\beta_\epsilon)\overline{M}|v|_1|w|_1\ \&\\ m_h(v,w) &\le (1+\beta_0)\|v\|\|w\| \end{aligned}$$

and $w \in W_h^m$

$$\begin{aligned} a_{1,h}(w,w) &\ge \min\{1,\alpha_\sigma\}\underline{M}|w|_1^2, \\ a_{2,h}(w,w) &\ge \min\{1,\alpha_\epsilon\}\underline{M}|w|_1^2\ \&\\ m_h(w,w) &\ge \min\{1,\alpha_0\}\|w\|^2, \end{aligned}$$

where α_σ, α_ϵ, α_0, β_σ, β_ϵ, β_0 are some positive constants.

We have the following semi-discrete virtual element approximation to (4.2.1): Find $u_h \in C^1(0,T;W_h^m)$ such that

$$\begin{cases} m_h(u_{ht},w_h) + a_{1,h}(u_h,w_h) + a_{2,h}(u_{ht},w_h) = (f_h,w_h) \quad \forall w_h \in W_h^m, \\ u_h(0) = R_h^2 u_0, \end{cases} \tag{4.2.3}$$

where f_h is the discrete form of the source function f as define in (1.4.14). Here, R_h^i, $i=1,2$ are the modified elliptic projection operators as defined in (3.2.3). In addition, we also need the L^2 projection operator L_h defined in (1.5.11).

4.3 Error Analysis for the Semi-discrete Problems

This section is dedicated to the derivation of error estimates related to the semi-discrete approximation (4.2.3) in both L^2 and H^1 semi-norm.

Before proceeding to the error analysis, we present following result regarding the stability of the semi-discrete solution u_h with respect to the initial data and the source function.

Lemma 4.3.1. *Suppose $u_0 \in H_0^1(\Omega)$ and $f \in H^k(L^2(\Omega))$, $k = 1, 2, 3$. Then, we have*

$$\|D_t^k u_h(0)\|_1 \leq C\big(|u_0|_1 + \|f\|_{H^k(L^2)}\big),$$

where $D_t^k = \dfrac{\partial^k}{\partial t^k}$.

Proof. Taking $t \to 0^+$ in (4.2.3) and then using definition of the elliptic projection operator R_h^1, we get

$$\begin{aligned} m_h(u_{ht}(0), w_h) + a_{2,h}(u_{ht}(0), w_h) &= -a_{1,h}(u_h(0), w_h) + (f_h(0), w_h) \\ &= -a_{1,h}(R_h^2 u_0, w_h) + (f_h(0), w_h). \end{aligned} \tag{4.3.1}$$

For the first term in (4.3.1), using the continuity property of $a_{1,h}$ and H^1-stability of R_h^2, we have

$$-a_{1,h}(R_h^2 u_0, w_h) \leq C|u_0|_1|w_h|_1. \tag{4.3.2}$$

From Lemma 1.4.6 and Lemma 1.2.1, we obtain

$$(f_h(0), w_h) \leq C\|f\|_{H^1(L^2)}\|w_h\|. \tag{4.3.3}$$

Now, substituting $w_h = u_{ht}(0)$ in (4.3.1), using the coercivity of m_h and $a_{2,h}$, and the estimates (4.3.3), (4.3.2) yields

$$\|u_{ht}(0)\|_1 \leq C(|u_0|_1 + \|f\|_{H^1(L^2)}). \tag{4.3.4}$$

This proves the result for $k = 1$. Now, for the case $k = 2$, differentiating (4.2.3) with respect to t and then proceeding in a similar way, we get

$$\|u_{htt}(0)\|_1 \leq C(|u_{ht}(0)|_1 + \|f_t\|_{H^1(L^2)}).$$

Using (4.3.4), we obtain

$$\|u_{htt}(0)\|_1 \leq C(|u_0|_1 + \|f\|_{H^2(L^2)}).$$

Similarly, we can show that

$$\|u_{httt}(0)\|_1 \leq C(|u_0|_1 + \|f\|_{H^3(L^2)}).$$

□

Lemma 4.3.2. *Let $u_0 \in H_0^1(\Omega)$ and $f \in H^k(L^2(\Omega))$, $k = 0, 1, 2, 3$. Then, we have*

$$\|D_t^k u_h\|_1^2 + \|D_t^k u_h\|_{L^2(H^1)}^2 \leq C\big(\|u_0\|_1^2 + \|f\|_{H^k(L^2)}^2\big).$$

Proof. Substituting $w_h = u_h$ in (4.2.3), we obtain

$$\frac{1}{2}\frac{d}{dt}m_h(u_h, u_h) + a_{1,h}(u_h, u_h) + \frac{1}{2}\frac{d}{dt}a_{2,h}(u_h, u_h) = (f_h, u_h).$$

Now, integrating from 0 to t, the coercivity and continuity properties of m_h, $a_{1,h}$ and $a_{2,h}$ imply

$$\|u_h(t)\|_1^2 + \int_0^t |u_h(s)|_1^2 ds \leq C\Big(\|u_h(0)\|_1^2 + \int_0^t \|f_h(s)\|\|u_h(s)\| ds\Big).$$

Further, using H^1 and L^2-stability of R_h^2 and Young's inequality in the above equation, we have

$$\|u_h\|_1^2 + \|u_h\|_{L^2(H^1)}^2 \leq C\big(\|u_0\|_1^2 + \|f\|_{L^2(L^2)}^2\big).$$

This proves for $k = 0$. Now, for $k = 1$, differentiating (4.2.3) with respect to t and then substituting $w_h = u_{ht}$, we obtain

$$\frac{1}{2}\frac{d}{dt}m_h(u_{ht}, u_{ht}) + a_{1,h}(u_{ht}, u_{ht}) + \frac{1}{2}\frac{d}{dt}a_{2,h}(u_{ht}, u_{ht}) = (f_{ht}, u_{ht}).$$

Following similar way as the previous case, we have

$$\|u_{ht}\|_1^2 + \|u_{ht}\|_{L^2(H^1)}^2 \leq C\big(\|u_0\|_1^2 + \|f\|_{L^2(L^2)}^2\big).$$

For the cases when $k = 2, 3$, proceeding in a similar manner, we obtain the results. □

Next, we derive the following convergence result in H^1 semi-norm for the semi-discrete approximation (4.2.3).

Theorem 4.3.1. *Assume that $u \in H^1(0, T; H^{m+1}(\Omega))$, $f \in L^2(0, T; H^m(\Omega))$ and $u_0 \in H^{m+1}(\Omega)$. Then for all $t \in (0, T]$, we have*

$$|u_h(t) - u(t)|_1 \leq Ch^m(|u_0|_{m+1} + \|u\|_{H^1(H^{m+1})} + \|f\|_{L^2(H^m)}).$$

Proof. Let us split the error $e_h(t) = u_h(t) - u(t)$ as

$$e_h(t) =: \phi(t) + \psi(t), \tag{4.3.5}$$

where $\phi(t) =: u_h(t) - R_h^2 u(t)$ and $\psi(t) =: R_h^2 u(t) - u(t)$. Applying Lemma 3.2.1, we have the following bounds for $\psi(t)$

$$|\psi(t)|_1 \leq Ch^m |u(t)|_{m+1} \leq Ch^m (|u_0|_{m+1} + \|u_t\|_{L^1(H^{m+1})}). \tag{4.3.6}$$

Therefore, we need to bound the term $\phi(t)$ only. From (4.2.3), using the definitions of the projection operators R_h^i, $i = 1, 2$ and L_h, we have the following error equation for $\phi(t)$. For all $w_h \in W_h^m$ and for all $t \in (0, T]$, we obtain

$$\begin{aligned}
&m_h(\phi_t(t), w_h) + a_{1,h}(\phi(t), w_h) + a_{2,h}(\phi_t(t), w_h) \\
&= m_h(u_{ht}(t), w_h) + a_{1,h}(u_h(t), w_h) + a_{2,h}(u_{ht}(t), w_h) \\
&\quad - \left[m_h(R_h^2 u_t(t), w_h) + a_{1,h}(R_h^2 u(t), w_h) + a_{2,h}(R_h^2 u_t(t), w_h)\right] \\
&= (f_h(t) - f(t), w_h) + (u_t(t), w_h) + a_1(u(t), w_h) + a_2(u_t(t), w_h) \\
&\quad - \left[m_h(R_h^2 u_t(t), w_h) + a_{1,h}(R_h^1 u(t), w_h) + a_{2,h}(R_h^2 u_t(t), w_h) + a_{1,h}(R_h^2 u(t) - R_h^1 u(t), w_h)\right] \\
&= (f_h(t) - f(t), w_h) + a_{1,h}(R_h^1 u(t) - R_h^2 u(t), w_h) + m_h(L_h u_t(t) - R_h^2 u_t(t), w_h) \\
&=: T_1 + T_2 + T_3.
\end{aligned} \tag{4.3.7}$$

For the term T_1, from Lemma 1.4.6, we have

$$T_1 = (f_h(t) - f(t), w_h) \leq Ch^m |f(t)|_m \|w_h\|. \tag{4.3.8}$$

Next, using the continuity of $a_{1,h}$ and approximation properties of R_h^1 and R_h^2, we obtain

$$\begin{aligned}
T_2 &= a_{1,h}(R_h^1 u(t) - R_h^2 u(t), w_h) \\
&= a_{1,h}(R_h^1 u(t) - u(t), w_h) - a_{1,h}(R_h^2 u(t) - u(t), w_h) \\
&\leq (1 + \beta_\sigma)\overline{M}(|R_h^2 u(t) - u(t)|_1 + |R_h^1 u(t) - u(t)|_1)|w_h|_1 \\
&\leq Ch^m |u(t)|_{m+1} |w_h|_1.
\end{aligned} \tag{4.3.9}$$

Also, for the term T_3, using the continuity of m_h and approximation properties of L_h and R_h^2, we have

$$\begin{aligned}
m_h(L_h u_t(t) - R_h^2 u_t(t), w_h) &= m_h(L_h u_t(t) - u_t(t), w_h) + m_h(u_t(t) - R_h^2 u_t(t), w_h) \\
&\leq (1 + \beta_0)\left(\|L_h u_t(t) - u_t(t)\| + \|u_t(t) - R_h^2 u_t(t)\|\right)\|w_h\| \\
&\leq Ch^m |u_t(t)|_m \|w_h\|.
\end{aligned} \tag{4.3.10}$$

Now, combine the estimates (4.3.8)-(4.3.10) with the identity (4.3.7) and set $w_h = \phi(t)$ to obtain

$$\begin{aligned} &m_h(\phi_t(t), \phi(t)) + a_{1,h}(\phi(t), \phi(t)) + a_{2,h}(\phi_t(t), \phi(t)) \\ &\leq Ch^m(|u(t)|_{m+1} + |u_t(t)|_m + |f(t)|_m)|\phi(t)|_1, \end{aligned}$$

which yields

$$\begin{aligned} &\frac{1}{2}\frac{d}{dt}m_h(\phi(t), \phi(t)) + a_{1,h}(\phi(t), \phi(t)) + \frac{1}{2}\frac{d}{dt}a_{2,h}(\phi(t), \phi(t)) \\ &\leq Ch^m(|u(t)|_{m+1} + |u_t(t)|_m + |f(t)|_m)|\phi(t)|_1. \end{aligned}$$

Integrating above estimate over $[0, t]$ and then using the coercivity of bilinear maps m_h, $a_{1,h}$ and $a_{2,h}$, we get

$$\begin{aligned} &\|\phi(t)\|^2 + \int_0^t |\phi(s)|_1^2 \, ds + |\phi(t)|_1^2 \\ &\leq C\int_0^t h^m(|u(s)|_{m+1} + |u_t(s)|_m + |f(s)|_m)|\phi(s)|_1 \, ds + \|\phi(0)\|^2 + |\phi(0)|_1^2. \end{aligned} \tag{4.3.11}$$

Since, $\phi(0) = 0$, employing Young's inequality in (4.3.11), we obtain

$$\|\phi(t)\|^2 + \int_0^t |\phi(s)|_1^2 \, ds + |\phi(t)|_1^2 \leq Ch^{2m}(\|u\|^2_{L^2(H^{m+1})} + \|u_t\|^2_{L^2(H^m)} + \|f\|^2_{L^2(H^m)}).$$

Neglecting the terms $\|\phi(t)\|^2$ and $\int_0^t |\phi(s)|_1^2 \, ds$, we arrive at

$$|\phi(t)|_1 \leq Ch^m(\|u\|_{H^1(H^{m+1})} + \|f\|_{L^2(H^m)}). \tag{4.3.12}$$

Finally, plugging (4.3.6) and (4.3.12) in (4.3.5) leads to the desire result. □

For the L^2 norm error estimate, we define the following non-standard projection operator: For $v \in H^1(0, T; \mathcal{X})$, where $\mathcal{X} = H_0^1(\Omega) \cap H^2(\Omega)$, define $\mathcal{E}_h : \mathcal{X} \to W_h^m$ by

$$a_{1,h}(\mathcal{E}_h v, w_h) + a_{2,h}((\mathcal{E}_h v)_t, w_h) = (f_v, w_h) \ \ \forall w_h \in W_h^m \tag{4.3.13}$$

with $(\mathcal{E}_h v)(0) = R_h^2 v(0) \in W_h^m$ and

$$f_v = -\nabla \cdot (\sigma \nabla v + \epsilon \nabla v_t). \tag{4.3.14}$$

From (4.1.1) and (4.3.14), we note that

$$f = f_u + u_t. \tag{4.3.15}$$

We have the following result regarding the well-posedness of the non-standard projection operator $\mathcal{E}_h$.

Lemma 4.3.3. *For $v \in \mathcal{X}$ there exists a unique solution $v_h \in W_h^m$ to the problem*

$$\begin{cases} a_{1,h}(v_h, w) + a_{2,h}(v_{ht}, w) = (f_v, w) \ \ \forall w \in W_h^m, \\ v_h(0) = R_h^2 v(0). \end{cases} \tag{4.3.16}$$

Proof. Let $\{\phi_i\}_{i=1}^{N_h}$ be the basis functions of the finite-dimensional space W_h^m. Then, we can express $v_h \in W_h^m$ as

$$v_h = \sum_{i=1}^{N_h} c_i(t)\phi_i,$$

where $c_i : (0, T] \to \mathbb{R}$ are coefficient functions. We denote by $C^0 = [c_1(0), \ldots, c_{N_h}(0)]^T$ the components of the given initial approximations $v_h(0)$. Then the problem (4.3.16) can be written as: Find $C(t) = [c_1(t), \ldots, c_{N_h}(t)]^T$, $t \in (0, T]$ such that

$$\begin{cases} AC(t) + BC'(t) = F(t), \\ C(0) = C^0, \end{cases} \tag{4.3.17}$$

where $A = [A_{i,j}]$ and $B = [B_{i,j}]$ are $N_h \times N_h$ matrix with $A_{i,j} = a_{1,h}(\phi_i, \phi_j)$ and $B_{i,j} = a_{2,h}(\phi_i, \phi_j)$, $i, j = 1, 2, \ldots, N_h$ and $F = [F_1, \ldots, F_{N_h}]^T$ with $F_j = (f_v, \phi_j)$, $j = 1, 2, \ldots, N_h$.

Due to the coercivity and continuity of the bilinear forms $a_{1,h}(\cdot, \cdot)$ and $a_{2,h}(\cdot, \cdot)$, it is easy to show that the matrices A and B are well-defined and invertible. Also, the right hand side matrix F is well-defined since

$$|(f_v, \phi_j)| \le \|f_v\|\|\phi_j\| \le \| - \nabla \cdot (\sigma_1 \nabla v + \sigma_2 \nabla v_t)\|\|\phi_j\| \le \overline{M}\|v\|_{H^1(H^2)}\|\phi_j\|.$$

Hence, the matrix equation (4.3.17) can be written as

$$C'(t) + B^{-1}AC(t) = B^{-1}F(t) \tag{4.3.18}$$

with initial condition $C(0) = C^0$. Now, from the standard theory of ODE, we can show that the IVP (4.3.18) has a unique solution. Consequently, there exists a unique v_h in W_h^m satisfying (4.3.16). □

Now, we need to find the bounds for the projection error $\mathcal{E}_h u - u$ in both L^2 and H^1 semi-norm. To do this, it is enough to derive the bounds for $\zeta_u := \mathcal{E}_h u - R_h^2 u$.

Lemma 4.3.4. *For $u \in L^2(0,T;H^{m+1}(\Omega))$, we have*

$$|\zeta_u(t)|_1 \leq Ch^m \|u\|_{L^2(H^{m+1})},$$
$$\|\zeta_u(t)\| \leq Ch^{m+1} \|u\|_{L^2(H^{m+1})}.$$

Proof. Using the definitions of the projection operators R_h^i $(i = 1,\ 2)$ and (4.3.13), we have the following error relation for $\zeta_u(t)$. For any $w_h \in W_h^m$, we have

$$\begin{aligned} &a_{1,h}(\zeta_u(t), w_h) + a_{2,h}(\zeta_{ut}(t), w_h) \\ &= a_{1,h}(\mathcal{E}_h u(t), w_h) + a_{2,h}(\mathcal{E}_h u_t(t), w_h) - \left[a_{1,h}(R_h^2 u(t), w_h) + a_{2,h}(R_h^2 u_t(t), w_h)\right] \\ &= a_{1,h}(R_h^1 u(t) - R_h^2 u(t), w_h). \end{aligned} \tag{4.3.19}$$

Now, using the continuity of $a_{1,h}$ and approximation properties of R_h^1 and R_h^2, we obtain

$$\begin{aligned} a_{1,h}(\zeta_u(t), w_h) + a_{2,h}(\zeta_{ut}(t), w_h) &= a_{1,h}(R_h^1 u(t) - R_h^2 u(t), w_h) \\ &= a_{1,h}(R_h^1 u(t) - u(t), w_h) - a_{1,h}(R_h^2 u(t) - u(t), w_h) \\ &\leq (1+\beta_\sigma)\overline{M}(|R_h^2 u(t) - u(t)|_1 + |R_h^1 u(t) - u(t)|_1)|w_h|_1 \\ &\leq Ch^m |u(t)|_{m+1}|w_h|_1. \end{aligned} \tag{4.3.20}$$

Then, set $w_h = \zeta_u(t)$ in the above equation (4.3.20) to have

$$a_{1,h}(\zeta_u(t), \zeta_u(t)) + a_{2,h}(\zeta_{ut}(t), \zeta_u(t)) \leq Ch^m |u(t)|_{m+1}|\zeta_u(t)|_1.$$

As an immediate consequence of above estimate, we obtain

$$\int_0^t |\zeta_u(s)|_1^2 \, ds + |\zeta_u(t)|_1^2 \leq C\left(\int_0^t h^m |u(s)|_{m+1}|\zeta_u(s)|_1 \, ds + |\zeta_u(0)|_1^2\right). \tag{4.3.21}$$

For any $\delta > 0$, apply Young's inequality in (4.3.21) to have

$$\int_0^t |\zeta_u(s)|_1^2 \, ds + |\zeta_u(t)|_1^2 \leq C(\delta)h^{2m}\|u\|^2_{L^2(H^{m+1})} + C_\delta \int_0^t |\zeta_u(s)|_1^2 \, ds.$$

Here, we have used the fact that $\zeta_u(0) = \mathcal{E}_h u(0) - R_h^2 u(0) = 0$. Now, for suitable $\delta > 0$, neglecting the term $\int_0^t |\zeta_u(s)|_1^2 \, ds$, we arrive at

$$|\zeta_u(t)|_1 \leq Ch^m \|u\|_{L^2(H^{m+1})}. \tag{4.3.22}$$

For the L^2 norm estimate, we choose the following dual problem: Find $w \in H^1(\mathcal{J}; \mathcal{X})$ satisfying

$$a_1(w(t), v) - a_2(w_t(t), v) = (\zeta_u(t), v) \quad \forall v \in H_0^1(\Omega) \tag{4.3.23}$$

and $w(\tau) = 0$ for some $\tau \in \mathcal{J}$. Then, there exists a unique solution $w \in H^1(\mathcal{J}; \mathcal{X})$ such that (cf. [9])

$$\|w\|_{H^1(H^2)} \leq C \|\zeta_u\|_{L^2(L^2)}. \tag{4.3.24}$$

Substituting $v = \zeta_{ut}(t)$ in (4.3.23), we get

$$\frac{1}{2} \frac{d}{dt} \|\zeta_u(t)\|^2 = a_1(w(t), \zeta_{ut}(t)) - a_2(w_t(t), \zeta_{ut}(t)).$$

Integration from 0 to τ yields

$$\frac{1}{2}(\|\zeta_u(\tau)\|^2 - \|\zeta_u(0)\|^2) = \int_0^\tau (a_1(w(t), \zeta_{ut}(t)) - a_2(w_t(t), \zeta_{ut}(t)))dt. \tag{4.3.25}$$

Since $w(\tau) = 0$ and $\zeta_u(0) = 0$, we observe that

$$\begin{aligned} \int_0^\tau a_1(w(t), \zeta_{ut}(t))dt &= -\int_0^\tau a_1(w_t(t), \zeta_u(t))dt + a_1(w(\tau), \zeta_u(\tau)) - a_1(w(0), \zeta_u(0)) \\ &= -\int_0^\tau a_1(w_t(t), \zeta_u(t))dt. \end{aligned} \tag{4.3.26}$$

Then, combine (4.3.25)-(4.3.26) to obtain

$$\frac{1}{2}\|\zeta_u(\tau)\|^2 = -\int_0^\tau (a_1(w_t(t), \zeta_u(t)) + a_2(w_t(t), \zeta_{ut}(t))) \, dt.$$

Using the definitions of projection operators R_h^1 and R_h^2, we have

$$\begin{aligned} \frac{1}{2}\|\zeta_u(\tau)\|^2 &= -\int_0^\tau \left(a_{1,h}(R_h^1 w_t(t), \zeta_u(t)) + a_{2,h}(R_h^2 w_t(t), \zeta_{ut}(t))\right) dt \\ &= -\int_0^\tau \left(a_{1,h}(R_h^2 w_t(t), \zeta_u(t)) + a_{2,h}(R_h^2 w_t(t), \zeta_{ut}(t))\right) dt \\ &\quad + \int_0^\tau a_{1,h}(R_h^2 w_t(t) - R_h^1 w_t(t), \zeta_u(t))dt. \end{aligned}$$

Now, from the error equation (4.3.19), we get

$$\frac{1}{2}\|\zeta_u(\tau)\|^2 = -\int_0^\tau a_{1,h}(R_h^1u(t)-R_h^2u(t),R_h^2w_t(t))dt+\int_0^\tau a_{1,h}(R_h^2w_t(t)-R_h^1w_t(t),\zeta_u(t))dt.$$

It is easy to observe that

$$\begin{aligned}
&\int_0^\tau a_{1,h}(R_h^1u(t)-R_h^2u(t),R_h^2w_t(t))dt\\
=&\int_0^\tau a_1(R_h^1u(t)-R_h^2u(t),w_t(t))dt+\int_0^\tau a_{1,h}(R_h^1u(t)-R_h^2u(t),R_h^2w_t(t)-R_h^1w_t(t))dt\\
=&\int_0^\tau\int_\Omega \left(R_h^1u(t)-R_h^2u(t)\right)\nabla.\left(\sigma(x)\nabla w_t(t)\right)dxdt\\
&+\int_0^\tau a_{1,h}(R_h^1u(t)-R_h^2u(t),R_h^2w_t(t)-R_h^1w_t(t))dt,
\end{aligned}$$

which together with continuity properties of the bilinear forms $a_{1,h}$ and $a_{2,h}$ leads to

$$\begin{aligned}
\|\zeta_u(\tau)\|^2 \leq& C\Big[\int_0^\tau \|R_h^1u(t)-R_h^2u(t)\||w_t(t)|_2dt\\
&+\int_0^\tau |R_h^1w_t(t)-R_h^2w_t(t)|_1\left(|R_h^1u(t)-R_h^2u(t)|_1+|\zeta_u(t)|_1\right)dt\Big].
\end{aligned}$$

Using the approximation properties of projection operators R_h^1 and R_h^2, and (4.3.22), we obtain

$$\|\zeta_u(\tau)\|^2 \leq C\int_0^\tau h^{m+1}\left(|u(t)|_{m+1}+\|u\|_{L^2(H^{m+1})}\right)|w_t(t)|_2dt.$$

Employing Young's inequality in the above equation, we get

$$\|\zeta_u(\tau)\|^2 \leq C(\delta)h^{2(m+1)}\int_0^\tau \left(|u(t)|_{m+1}+\|u\|_{L^2(H^{m+1})}\right)^2dt+C_\delta\|w\|^2_{H^1(H^2)},$$

for some $\delta>0$. Further, from the a priori estimate (4.3.24), we have

$$\|\zeta_u(\tau)\|^2 \leq C(\delta,T)\ h^{2(m+1)}\|u\|^2_{L^2(H^{m+1})}+C_\delta\|\zeta_u\|^2_{L^2(L^2)}. \tag{4.3.27}$$

Now, we select τ such that $\|\zeta_u(\tau)\| = \max_{t\in\mathcal{J}}\|\zeta_u(t)\|$ and hence $\|\zeta_u\|^2_{L^2(L^2)} \leq T\|\zeta_u(\tau)\|^2$. Thus, for suitable $\delta>0$, from the estimate (4.3.27), we obtain

$$\|\zeta_u(t)\| \leq \|\zeta_u(\tau)\| \leq Ch^{m+1}\|u\|_{L^2(H^{m+1})}.$$

This completes the proof. □

Similarly, with the modified dual problem: Find $w \in H^1(\mathcal{J}; \mathcal{X})$ such that

$$a_1(w(t), v) - a_2(w_t(t), v) = (\zeta_{ut}(t), v) \quad \forall v \in H_0^1(\Omega)$$

and $w(\tau) = 0$ for some $\tau \in \mathcal{J}$, we get the following estimate.

Lemma 4.3.5. *For $u \in L^2(0, T; H^{m+1}(\Omega))$, we have*

$$\|\zeta_{ut}(t)\|_{L^2(L^2)} \leq Ch^{m+1}\|u\|_{L^2(H^{m+1})}.$$

Now, we will present the main result of this section. The semi-discrete approximation (4.2.3) has the following error estimate in L^2 norm.

Theorem 4.3.2. *Assume that $u \in H^1(0, T; H^{m+1}(\Omega))$, $f \in L^2(0, T; H^{m+1}(\Omega))$ and $u_0 \in H^{m+1}(\Omega)$. Then for all $t \in (0, T]$, we have*

$$\|u_h(t) - u(t)\| \leq Ch^{m+1}\left(|u_0|_{m+1} + \|u\|_{H^1(H^{m+1})} + \|f\|_{L^2(H^{m+1})}\right).$$

Proof. We split the error term $e_h = u_h - u$ into two standard components θ and ρ using the following relation

$$e_h(t) =: \theta(t) + \rho(t), \tag{4.3.28}$$

where $\theta = u_h - \mathcal{E}_h u$ and $\rho = \mathcal{E}_h u - u$. From Lemma 4.3.4 and approximation property of R_h^2, we have the following bounds for $\rho(t)$:

$$\|\rho(t)\| \leq \|\zeta_u(t)\| + \|R_h^2 u(t) - u(t)\| \leq Ch^{m+1}(|u_0|_{m+1} + \|u\|_{H^1(H^{m+1})}). \tag{4.3.29}$$

Using the definition of projection operator $\mathcal{E}_h$ and L_h, and equation (4.3.15), we arrive at the following important identity: For all $w_h \in W_h^m$

$$\begin{aligned}
&m_h(\theta_t(t), w_h) + a_{1,h}(\theta(t), w_h) + a_{2,h}(\theta_t(t), w_h) \\
&= m_h(u_{ht}(t), w_h) + a_{1,h}(u_h(t), w_h) + a_{2,h}(u_{ht}(t), w_h) \\
&\quad - [m_h((\mathcal{E}_h u(t))_t, w_h) + a_{1,h}(\mathcal{E}_h u(t), w_h) + a_{2,h}((\mathcal{E}_h u(t))_t, w_h)] \\
&= (f_h(t) - f_u(t), w_h) - m_h((\mathcal{E}_h u(t))_t, w_h) \\
&= (f_h(t) - f(t), w_h) + (u_t(t), w_h) - m_h((\mathcal{E}_h u(t))_t, w_h) \\
&= (f_h(t) - f(t), w_h) + m_h(L_h u_t(t) - (\mathcal{E}_h u(t))_t, w_h) \\
&=: I_1 + I_2.
\end{aligned} \tag{4.3.30}$$

For the term I_1, from Lemma 1.4.6, we have

$$(f_h(t) - f(t), w_h) \leq \|f_h(t) - f(t)\|\|w_h\| \leq Ch^{m+1}|f(t)|_{m+1}\|w_h\|. \tag{4.3.31}$$

Desired bound for the term I_2 follows from the following estimate:

$$\begin{aligned} m_h(L_h u_t(t) - (\mathcal{E}_h u(t))_t, w_h) &\leq (1+\beta_0)\|L_h u_t(t) - (\mathcal{E}_h u(t))_t\|\|w_h\| \\ &\leq (1+\beta_0)\left(\|L_h u_t(t) - u_t(t)\| + \|(\mathcal{E}_h u(t))_t - u_t(t)\|\right)\|w_h\| \\ &\leq C\left(h^{m+1}|u_t(t)|_{m+1} + \|\rho_t(t)\|\right)\|w_h\|. \end{aligned} \tag{4.3.32}$$

Plugging (4.3.31)-(4.3.32) in (4.3.30), and substituting $w_h = \theta(t)$, we obtain

$$\begin{aligned} &\frac{1}{2}\frac{d}{dt}m_h(\theta(t),\theta(t)) + a_{1,h}(\theta(t),\theta(t)) + \frac{1}{2}\frac{d}{dt}a_{2,h}(\theta(t),\theta(t)) \\ &\leq C\left[h^{m+1}\left(|u_t(t)|_{m+1} + |f(t)|_{m+1}\right) + \|\rho_t(t)\|\right]\|\theta(t)\|. \end{aligned}$$

Now, using coercivity properties of m_h and $a_{i,h}$, $i = 1, 2$, we have

$$\frac{1}{2}\frac{d}{dt}\|\theta(t)\|^2 + |\theta(t)|_1^2 + \frac{1}{2}\frac{d}{dt}|\theta(t)|_1^2 \leq C\left[h^{m+1}\left(|u_t(t)|_{m+1} + |f(t)|_{m+1}\right) + \|\rho_t(t)\|\right]\|\theta(t)\|.$$

Integrating over $[0, t]$, and then using the fact $\theta(0) = 0$ and Young's inequality, we get

$$\begin{aligned} &\|\theta(t)\|^2 + \int_0^t |\theta(s)|_1^2\, ds + |\theta(t)|_1^2 \\ &\leq C(\delta)\int_0^t \left[h^{2(m+1)}\left(|u_t(s)|_{m+1} + |f(s)|_{m+1}\right)^2 + \|\rho_t(t)\|^2\right]\, ds + C_\delta \int_0^t \|\theta(s)\|^2\, ds. \end{aligned}$$

Now for suitable $\delta > 0$, applying Gronwall's inequality and neglecting the terms $\int_0^t |\theta(s)|_1^2\, ds$ and $|\theta(t)|_1^2$, we obtain

$$\|\theta(t)\|^2 \leq C\left[h^{2(m+1)}\left(\|u_t\|^2_{L^2(H^{m+1})} + \|f\|^2_{L^2(H^{m+1})}\right) + \|\rho_t(t)\|^2_{L^2(L^2)}\right]. \tag{4.3.33}$$

Again, from Lemma 4.3.5 and triangle inequality, we have

$$\|\rho_t(t)\|_{L^2(L^2)} \leq \|\zeta_{ut}(t)\|_{L^2(L^2)} + \|R_h^2 u(t) - u(t)\|_{L^2(L^2)} \leq Ch^{m+1}\|u\|_{L^2(H^{m+1})}.$$

Hence, equation (4.3.33) becomes

$$\|\theta(t)\| \leq Ch^{m+1}\left(\|u\|_{H^1(H^{m+1})} + \|f\|_{L^2(H^{m+1})}\right). \tag{4.3.34}$$

Finally, from the estimates in (4.3.29) and (4.3.34) along with (4.3.28), we get the theorem.

□

Remark 4.3.1. The non-standard projection operator $\mathcal{E}_h : \mathcal{X} \to W_h^m$ is motivated by the finite element approximation for the following pulsed electric model (cf. [9])

$$-\nabla \cdot \left(\sigma \nabla \tilde{u} + \epsilon \nabla \tilde{u}_t\right) = f,$$

$\tilde{u}$ is the electric voltage, and σ and ϵ are the conductivity and permittivity, respectively. For the L^2 norm estimate, we have used $\mathcal{E}_h$ as an intermediate operator and which simplifies the error analysis. Suppose, we split the error term $e_h = u_h - u$ into two components $\tilde{\theta}$ and $\tilde{\rho}$ using following relation

$$e_h(t) =: \tilde{\theta}(t) + \tilde{\rho}(t),$$

where $\tilde{\theta} = u_h - R_h u(t)$ and $\tilde{\rho} = R_h u(t) - u$ with $R_h = R_h^1$ or $R_h = R_h^2$. Then, for $R_h = R_h^1$ and $\sigma \neq \epsilon$, identity (4.3.30) reduces to

$$\begin{aligned}
&m_h(\tilde{\theta}_t(t), w_h) + a_{1,h}(\tilde{\theta}(t), w_h) + a_{2,h}(\tilde{\theta}_t(t), w_h) \\
&= m_h(u_{ht}(t), w_h) + a_{1,h}(u_h(t), w_h) + a_{2,h}(u_{ht}(t), w_h) \\
&- \left[m_h((R_h^1 u(t))_t, w_h) + a_{1,h}(R_h^1 u(t), w_h) + a_{2,h}((R_h^1 u(t))_t, w_h)\right] \\
&= (f_h(t), w_h) - \left[m_h((R_h^1 u(t))_t, w_h) + a_1(u(t), w_h) + a_{2,h}((R_h^1 u(t))_t, w_h)\right] \\
&= (f_h(t) - f(t), w_h) + (u_t(t), w_h) - m_h((R_h^1 u(t))_t, w_h) + a_2(u_t(t), w_h) - a_{2,h}((R_h^1 u(t))_t, w_h) \\
&= (f_h(t) - f(t), w_h) + m_h((L_h u(t))_t - (R_h^1 u(t))_t, w_h) + a_{2,h}((R_h^2 u(t))_t - (R_h^1 u(t))_t, w_h).
\end{aligned}$$

It is important to note that the term $a_{2,h}((R_h^2 u(t))_t - (R_h^1 u(t))_t, w_h)$ contains the elliptic type bilinear form $a_{2,h}$. Due to presence of $a_{2,h}$, it is not possible to recover the optimal order of convergence, i.e., $O(h^{m+1})$ for the L^2 norm estimate of $\tilde{\theta}$. Because, we cannot shift the spatial derivative from $R_h^1 u(t) - R_h^2 u(t)$ to w_h in a standard way. To overcome this difficulty, we have introduced the non-standard projection operator $\mathcal{E}_h$ to deal with this term.

4.4 Error Analysis for the Fully Discrete Problems

In this section, we will formulate the Crank-Nicolson scheme (implicit second-order Newmark scheme) based fully discrete approximation to the model problem (4.1.1)-(4.1.2) and derive the optimal order error estimate in both $L^\infty(L^2)$ and $L^\infty(H^1)$ norm.

We recall the discretization of the time domain $[0,T]$ and notations from Chapter 2, Section 2.4. Now, employing Crank-Nicolson fully discrete scheme to the equations in (4.2.3), we obtain the fully discretized problem defined as : For $n = 1, 2, \cdots, N-1$, find $\mathcal{U}^n \in W_h^m$ such that

$$\begin{cases} m_h(\partial_\tau \mathcal{U}^n, w) + a_{1,h}(\mathcal{U}^{n+\frac{1}{2}}, w) + a_{2,h}(\partial_\tau \mathcal{U}^n, w) = (f_h^{n+\frac{1}{2}}, w) \ \forall \ w \in W_h^m, \\ \mathcal{U}^0 = R_h^2 u_0. \end{cases} \tag{4.4.1}$$

Regarding the existence of a unique solution $\mathcal{U}^n$ to the fully discrete problem, we have the following lemma.

Lemma 4.4.1. *There exist a unique sequence $\{\mathcal{U}^n\}_{n=0}^N$ which satisfies the problem (4.4.1).*

Proof. From (4.4.1), for $n \geq 0$, $\mathcal{U}^{n+1}$ satisfies

$$\begin{aligned} &m_h(\mathcal{U}^{n+1}, w) + \left(\frac{\tau}{2}\right) a_{1,h}(\mathcal{U}^{n+1}, w) + a_{2,h}(\mathcal{U}^{n+1}, w) \\ &= m_h(\mathcal{U}^n, w) - \left(\frac{\tau}{2}\right) a_{1,h}(\mathcal{U}^n, w) + a_{2,h}(\mathcal{U}^n, w) + \tau\, (f_h^{n+\frac{1}{2}}, w) \ \forall w \in W_h^m. \end{aligned}$$

Since, the bilinear forms m_h and $a_{i,h}$, $i = 1, 2$ are positive definite, $\mathcal{U}^{n+1}$, $n = 0, 1, \cdots, N-1$ exists uniquely. □

The following approximation result can be derived, which will be required later.

Lemma 4.4.2. *For a Banach space $\mathbb{B}$ and for $v \in H^3(0,T;\mathbb{B})$, we have*

$$\|\partial_\tau v^n - v_t^{n+\frac{1}{2}}\|_{\mathbb{B}}^2 \leq C\tau^3 \int_{t_n}^{t_{n+1}} \|v_{ttt}(t)\|_{\mathbb{B}}^2 dt.$$

Towards estimating the error $e_h^n := \mathcal{U}^n - u^n$, we define the auxiliary functions $\xi^n = \mathcal{U}^n - u_h^n$ and $\rho^n = u_h^n - u^n$ for $n = 1, 2, \cdots, N$.

Lemma 4.4.3. *For the term $\xi^n = \mathcal{U}^n - u_h^n$, we have the following estimate*

$$\max_{1\leq n\leq N} (\|\xi^n\| + |\xi^n|_1) \leq C\tau^2 \left(\int_0^T \|u_{httt}(t)\| dt + \int_0^T |u_{htt}(t)|_1 dt \right).$$

Proof. From (4.2.3), for $t = t_{l+\frac{1}{2}}$, we get

$$m_h(\partial_\tau u_h^l, w) + a_{1,h}(u_h^{l+\frac{1}{2}}, w) + a_{2,h}(\partial_\tau u_h^l, w) = (f_h^{l+\frac{1}{2}}, w) + m_h(\vartheta^l, w) + a_{2,h}(\vartheta^l, w) \tag{4.4.2}$$

for all $w \in W_h^m$, where $\vartheta^l = \partial_\tau u_h^l - u_{ht}^{l+\frac{1}{2}}$. Now, from (4.4.1) and (4.4.2), for any $w \in W_h^m$, it follows that

$$m_h(\partial_\tau \xi^l, w) + a_{1,h}(\xi^{l+\frac{1}{2}}, w) + a_{2,h}(\partial_\tau \xi^l, w) = -m_h(\vartheta^l, w) - a_{2,h}(\vartheta^l, w),\ 1 \le l \le N-1.$$

We choose $w = \xi^{l+\frac{1}{2}}$ in the above equation to obtain

$$\frac{1}{2\tau}\left(m_h(\xi^{l+1}, \xi^{l+1}) - m_h(\xi^l, \xi^l)\right) + a_{1,h}(\xi^{l+\frac{1}{2}}, \xi^{l+\frac{1}{2}}) + \frac{1}{2\tau}\left(a_{2,h}(\xi^{l+1}, \xi^{l+1}) - a_{2,h}(\xi^l, \xi^l)\right)$$
$$= -m_h(\vartheta^l, \xi^{l+\frac{1}{2}}) - a_{2,h}(\vartheta^l, \xi^{l+\frac{1}{2}}),\ 1 \le l \le N-1.$$

Using the coercivity and continuity of the bilinear forms m_h and $a_{i,h}$, $i = 1, 2$, we arrive at

$$\|\xi^{l+1}\|^2 - \|\xi^l\|^2 + 2\tau|\xi^{l+\frac{1}{2}}|_1^2 + |\xi^{l+1}|_1^2 - |\xi^l|_1^2 \le C\tau\left(\|\vartheta^l\|^2\|\xi^{l+\frac{1}{2}}\|^2 + |\vartheta^l|_1^2|\xi^{l+\frac{1}{2}}|_1^2\right).$$

Now, applying Young's inequality, we get

$$\|\xi^{l+1}\|^2 - \|\xi^l\|^2 + |\xi^{l+1}|_1^2 - |\xi^l|_1^2 \le C(\delta)\tau\left(\|\vartheta^l\|^2 + |\vartheta^l|_1^2\right), \tag{4.4.3}$$

for some suitable $\delta > 0$. Here, we have used the Poincaré's inequality

$$\|\xi^{l+\frac{1}{2}}\| \le C|\xi^{l+\frac{1}{2}}|_1.$$

Summing from $l = 0$ to $l = n-1$ with $2 \le n \le N$ and since $\xi^0 = 0$, we find

$$\|\xi^n\|^2 + |\xi^n|_1^2 \le C\tau\sum_{l=0}^{n-1}\left(\|\vartheta^l\|^2 + |\vartheta^l|_1^2\right). \tag{4.4.4}$$

Substituting $l = 0$ in (4.4.3), we obtain

$$\|\xi^1\|^2 + |\xi^1|_1^2 \le C\tau\left(\|\vartheta^0\|^2 + |\vartheta^0|_1^2\right). \tag{4.4.5}$$

Now, combining (4.4.4) and (4.4.5), we get

$$\max_{1\le n\le N}\left(\|\xi^n\|^2 + |\xi^n|_1^2\right) \le C\tau\sum_{n=0}^{N-1}\left(\|\vartheta^n\|^2 + |\vartheta^n|_1^2\right).$$

Finally, using Lemma 4.4.2, we have

$$\max_{1\le n\le N}\left(\|\xi^n\|^2 + |\xi^n|_1^2\right) \le C\tau^4\left(\int_0^T \|u_{httt}(t)\|^2 dt + \int_0^T |u_{httt}(t)|_1^2 dt\right).$$

□

Now, by Theorems 4.3.1-4.3.2, Lemma 4.3.2 and Lemma 4.4.3, we derive the following error estimate in $L^\infty(L^2)$ and $L^\infty(H^1)$ norm.

Theorem 4.4.1. *Let u^n and $\mathcal{U}^n$ solution of (4.1.1) and (4.4.1) at time $t = t_n$, respectively. Assume that $u \in H^1(0,T;H^{m+1}(\Omega))$ and $f \in L^2(0,T;H^{m+1}(\Omega)) \cap H^3(0,T;L^2(\Omega))$, then for all $t \in (0,T]$, we have*

$$\max_{1\le n\le N} \|\mathcal{U}^n - u^n\| \le Ch^{m+1}\left(|u_0|_{m+1} + \|u\|_{H^1(H^{m+1})} + \|f\|_{L^2(H^{m+1})}\right) + \tilde{C}\tau^2\left(|u_0|_1 + \|f\|_{H^3(L^2)}\right),$$

$$\max_{1\le n\le N} |\mathcal{U}^n - u^n|_1 \le Ch^{m}\left(|u_0|_{m+1} + \|u\|_{H^1(H^{m+1})} + \|f\|_{L^2(H^{m})}\right) + \tilde{C}\tau^2\left(|u_0|_1 + \|f\|_{H^3(L^2)}\right).$$

4.5 Numerical Results

This section includes some numerical experiments conducted to test the practical performance of the proposed algorithm. To show the method is flexible to handle any polygonal discretization, several forms of polygonal meshes, including Voronoi ($\mathcal{V}_h$), distorted square ($\mathcal{S}_h$) and distorted polygon ($\mathcal{P}_h$) have been taken into consideration. In Example 4.5.1, we implement the proposed virtual element algorithm with all three types of meshes by considering a smooth solution to test the optimal convergence. Again, in Example 4.5.2, we show that the discrete bilinear forms in (4.5.1) produce sub-optimal convergence. Next, we have considered a low regular solution in a convex domain in Example 4.5.3. Further, in Example 4.5.4 and Example 4.5.5, we have tested our algorithm for smooth solutions in L-shaped domain and circular domain, respectively. Finally, we have discussed a numerical example with high-contrast coefficients in Example 4.5.6.

In all the examples, we have consider the model problem (4.1.1)-(4.1.2) and source function f, initial data u_0 are chosen according to the choice of exact solution. The time interval set to be $[0,1]$ and the spatial domain Ω is considered to be $(0,1)\times(0,1)$ or else specified.

Example 4.5.1. (Smooth solution with convex domain) We set the exact solution to the model problem (4.1.1)-(4.1.2) as

$$u(x,y,t) = t\sin(\pi x)\sin(\pi y)$$

and coefficients $\sigma = x + y + 1$ and $\epsilon = x^2 + y^2 + 1$. We have implemented the VEM algorithm with all the three kind of mesh discretizations $\mathcal{V}_h$, $\mathcal{S}_h$ and $\mathcal{P}_h$ and polynomial order $m = 1, 2, 3$.

Table 4.5.1: L^2 and H^1 errors at $T = 1$ for the mesh $\mathcal{V}_h$ in Example 4.5.1

order	h	$\|u - u_h\|$	EOC	$\|u - u_h\|_1$	EOC
$m = 1$	0.1768	$3.08240e-02$	-	$7.75091e-02$	-
	0.1250	$1.57508e-02$	1.9373	$4.37357e-02$	1.6511
	0.0884	$7.55517e-03$	2.1198	$2.91824e-02$	1.1674
	0.0625	$3.75129e-03$	2.0202	$1.84470e-02$	1.3234
	0.0442	$1.84871e-03$	2.0417	$1.25079e-02$	1.1211
$m = 2$	0.1768	$1.80177e-02$	-	$8.82435e-02$	-
	0.1250	$6.56264e-03$	2.9141	$4.64632e-02$	1.8508
	0.0884	$2.43029e-03$	2.8663	$1.92991e-02$	2.5351
	0.0625	$8.60933e-04$	2.9943	$8.02536e-03$	2.5318
	0.0442	$2.99273e-04$	3.0489	$3.94643e-03$	2.0480
$m = 3$	0.1768	$3.74984e-04$	-	$4.86042e-03$	-
	0.1250	$9.38621e-05$	3.9964	$1.68819e-03$	3.0512
	0.0884	$2.24492e-05$	4.1278	$6.15544e-04$	2.9111
	0.0625	$5.44045e-06$	4.0897	$2.16750e-04$	3.0117
	0.0442	$1.32813e-06$	4.0687	$7.75599e-05$	2.9653

Table 4.5.1 presents the numerical errors and EOC in both L^2 norm and H^1 semi-norm at $T = 1$ for the mesh $\mathcal{V}_h$. Exact and approximate solutions at $T = 1$ are shown in Figure 4.5.1. Figure 4.5.2 depicts the log-log plots.

In Table 4.5.2, we present the numerical errors and EOC for the mesh $\mathcal{S}_h$. The exact solution and approximate solution are illustrated in Figure 4.5.3. Further, the log-log plots are presented in Figure 4.5.4.

Table 4.5.3 depicts the numerical errors and EOC for the mesh $\mathcal{P}_h$. The exact solution and approximate solution are illustrated in Figure 4.5.5. Figure 4.5.6 shows the log-log plots. The above observations confirm that we have achieved optimal order of convergence as per the theoretical prediction as proved in Theorem 4.4.1.

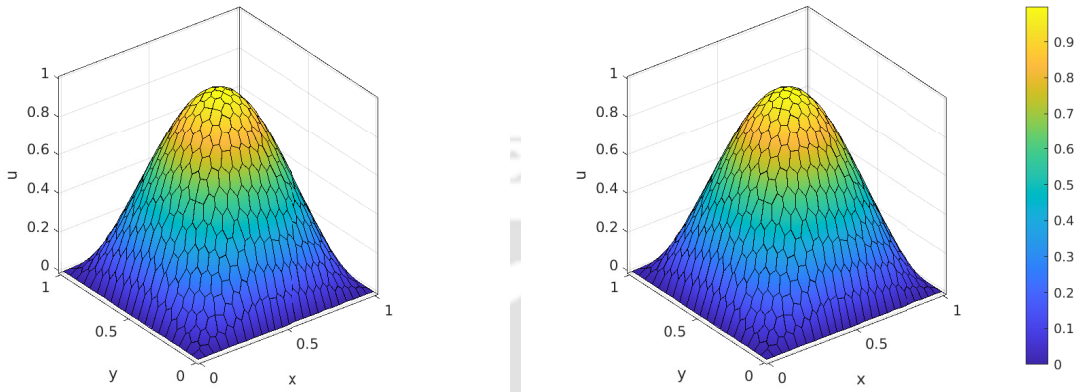

Figure 4.5.1: Approximate solution for $m = 3$ (left) with Voronoi mesh ($h = 0.0442$) and exact solution (right) at $t = 1$ in Example 4.5.1.

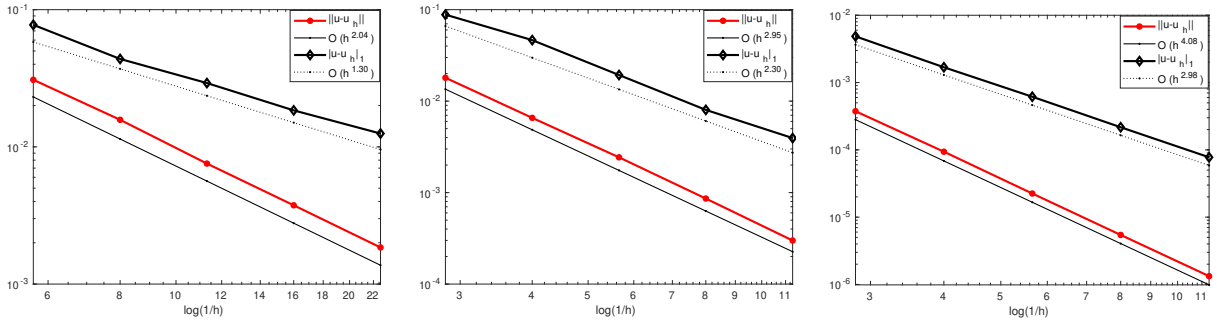

Figure 4.5.2: Log-log plots of the errors versus h at $t = 1$ for $m = 1$ (left), $m = 2$ (center) and $m = 3$ (right) for Voronoi mesh in Example 4.5.1.

Table 4.5.2: L^2 and H^1 errors at $T = 1$ for the mesh $\mathcal{S}_h$ in Example 4.5.1

order	h	$\|u - u_h\|$	EOC	$\|u - u_h\|_1$	EOC
	1/5	$5.42362e-02$	-	$1.63733e-01$	-
$m = 1$	1/10	$1.59321e-02$	1.7673	$4.86620e-02$	1.7505
	1/15	$7.34057e-03$	1.9112	$2.23908e-02$	1.9145
	1/20	$4.18403e-03$	1.9540	$1.27409e-02$	1.9599
	1/25	$2.69477e-03$	1.9716	$8.19693e-03$	1.9766
	1/5	$3.14003e-03$	-	$2.75012e-02$	-
$m = 2$	1/10	$4.37026e-04$	2.8450	$5.65103e-03$	2.2829
	1/15	$1.30381e-04$	2.9831	$1.93969e-03$	2.6372
	1/20	$5.49857e-05$	3.0012	$8.71653e-04$	2.7805
	1/25	$2.81271e-05$	3.0041	$4.61239e-04$	2.8523
	1/5	$1.51538e-03$	-	$1.51247e-02$	-
$m = 3$	1/10	$1.30091e-04$	3.5421	$2.06263e-03$	2.8744
	1/15	$2.75497e-05$	3.8283	$6.11223e-04$	2.9997
	1/20	$8.93906e-06$	3.9125	$2.57241e-04$	3.0083
	1/25	$3.70496e-06$	3.9470	$1.31501e-04$	3.0070

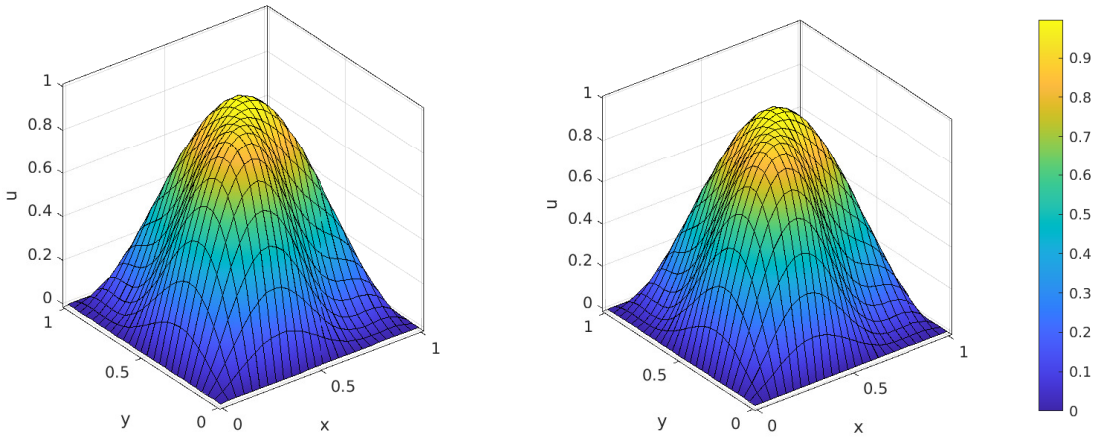

Figure 4.5.3: Approximate solution for $m = 3$ with distorted square mesh ($h = 1/25$) (left) and exact solution (right) at $t = 1$ in Example 4.5.1.

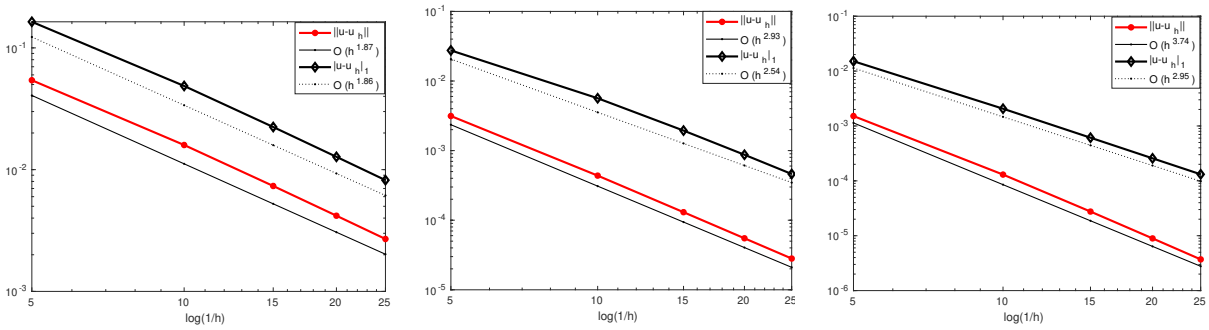

Figure 4.5.4: Log-log plots of the errors versus h at $t = 1$ for $m = 1$ (left), $m = 2$ (center) and $m = 3$ (right) for distorted square mesh in Example 4.5.1.

Table 4.5.3: L^2 and H^1 errors at $T = 1$ for the mesh $\mathcal{P}_h$ in Example 4.5.1

order	h	$\|u - u_h\|$	EOC	$\|u - u_h\|_1$	EOC
$m = 1$	0.1768	$4.42154e-02$	-	$1.62012e-01$	-
	0.1250	$2.04910e-02$	2.2191	$8.90899e-02$	1.7255
	0.0884	$1.12866e-02$	1.7208	$5.50352e-02$	1.3898
	0.0625	$5.65985e-03$	1.9915	$2.89688e-02$	1.8517
	0.0442	$2.81779e-03$	2.0124	$2.01445e-02$	1.0482
$m = 2$	0.1768	$2.55365e-03$	-	$2.48531e-02$	-
	0.1250	$9.55207e-04$	2.8373	$1.17839e-02$	2.1513
	0.0884	$3.46966e-04$	2.9220	$5.98151e-03$	1.9565
	0.0625	$1.21800e-04$	3.0206	$3.14527e-03$	1.8546
	0.0442	$4.41005e-05$	2.9313	$1.76831e-03$	1.6616
$m = 3$	0.1768	$1.04565e-03$	-	$1.16950e-02$	-
	0.1250	$2.55598e-04$	4.0649	$4.08281e-03$	3.0365
	0.0884	$7.50386e-05$	3.5363	$1.57336e-03$	2.7514
	0.0625	$1.94974e-05$	3.8887	$5.67805e-04$	2.9408
	0.0442	$4.84741e-06$	4.0160	$2.03518e-04$	2.9605

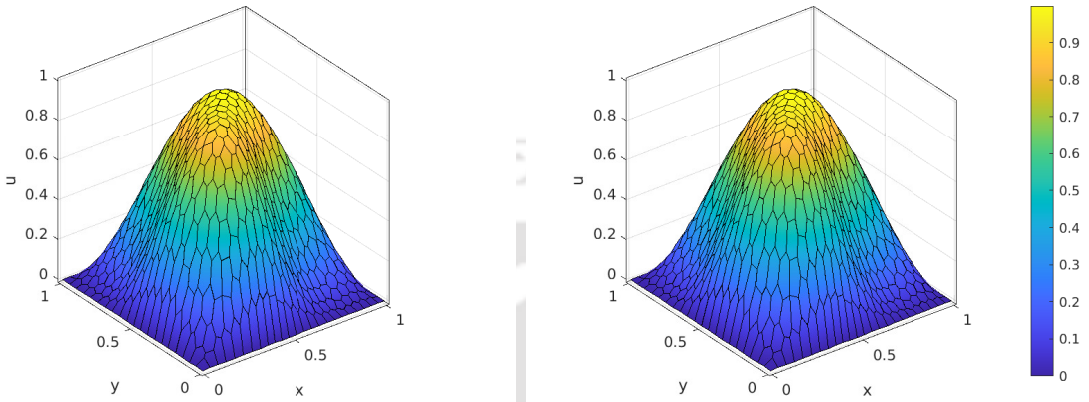

Figure 4.5.5: Approximate solution for $m = 3$ with distorted polygon mesh ($h = 0.0442$) (left) and exact solution (right) at $t = 1$ in Example 4.5.1.

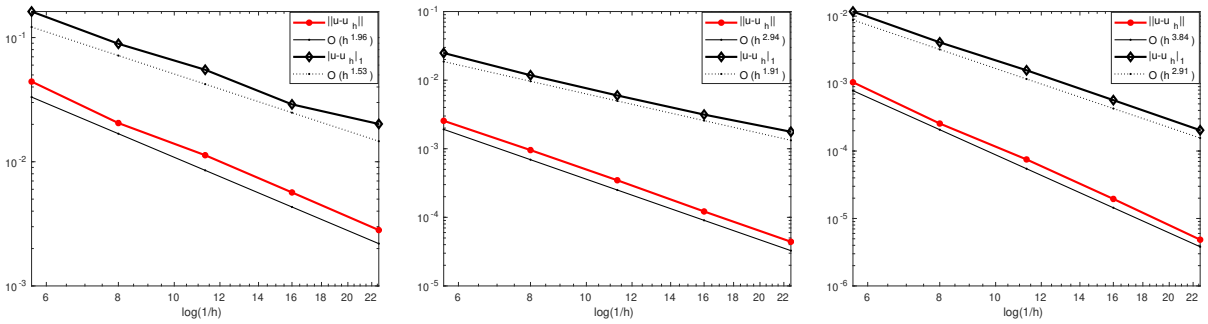

Figure 4.5.6: Log-log plots of the errors versus h at $t = 1$ for $m = 1$ (left), $m = 2$ (center) and $m = 3$ (right) for distorted polygon mesh in Example 4.5.1.

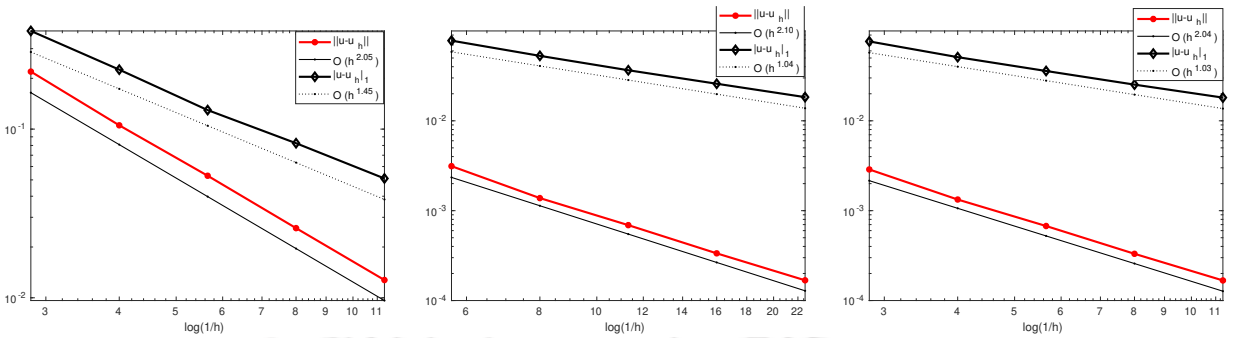

Figure 4.5.7: Log-log plots of the errors versus h at $t = 1$ for $m = 1$ (left), $m = 2$ (center) and $m = 3$ (right) in Example 4.5.2.

Example 4.5.2. (Sub-optimal convergence)

Remark 4.5.1. *In the case of constant-coefficient the following discrete bilinear form a_h is usually considered in order to approximate the original bilinear form (see. [16]):*

$$a_h^E(v,w) := \left(\nabla\Pi^\nabla_{m,E}v, \nabla\Pi^\nabla_{m,E}w\right)_E + \left((I-\Pi^\nabla_{m,E})v, (I-\Pi^\nabla_{m,E})w\right)_E,$$

for $v, w \in W_h^m(E)$. For variable coefficients, a natural extension of the above choice would suggest considering the discrete bilinear forms $a_{i,h}$, $i = 1, 2$ as

$$\begin{aligned} a_{1,h}^E(v,w) &:= \left(\sigma\nabla\Pi^\nabla_{m,E}v, \nabla\Pi^\nabla_{m,E}w\right)_E + S_1^E\left((I-\Pi^\nabla_{m,E})v, (I-\Pi^\nabla_{m,E})w\right), \\ a_{2,h}^E(v,w) &:= \left(\epsilon\nabla\Pi^\nabla_{m,E}v, \nabla\Pi^\nabla_{m,E}w\right)_E + S_2^E\left((I-\Pi^\nabla_{m,E})v, (I-\Pi^\nabla_{m,E})w\right) \end{aligned} \tag{4.5.1}$$

for $v, w \in W_h^m(E)$. For $m = 1$, this choice coincides with (4.2.2). However, for $m \geq 2$ it fails to deliver optimal order of convergence.

In this example, we use the discrete bilinear forms given by (4.5.1) in place of (4.2.2) for the computation. We consider all the inputs as in Example 4.5.1.

We display the errors and convergence orders for $m = 1, 2, 3$ in Table 4.5.4 for the Voronoi mesh $(\mathcal{V}_h)$. Figure 4.5.7 presents the log-log plots at $T = 1$. We can observe from the Table 4.5.4 that for $m = 1$, the order of accuracy is preserved, but for $m = 2$ and $m = 3$, there is a loss in the convergence order in both the L^2 norm and the H^1 semi-norms as predicted in the above remark.

Table 4.5.4: L^2 and H^1 errors and convergence orders for Example 4.5.2

order	h	$\|u-u_h\|$	EOC	$\|u-u_h\|_1$	EOC
	0.1768	$2.19271e-01$	-	$3.81965e-01$	-
$m=1$	0.1250	$1.05323e-01$	2.1158	$2.25164e-01$	1.5249
	0.0884	$5.29038e-02$	1.9868	$1.29639e-01$	1.5929
	0.0625	$2.58778e-02$	2.0633	$8.24794e-02$	1.3048
	0.0442	$2.58778e-02$	2.0442	$5.09768e-02$	1.3884
	0.1768	$3.12799e-03$	-	$7.79999e-02$	-
$m=2$	0.1250	$1.38022e-03$	2.3607	$5.28180e-02$	1.1249
	0.0884	$6.90224e-04$	1.9995	$3.65327e-02$	1.0637
	0.0625	$3.35167e-04$	2.0844	$2.58502e-02$	0.9980
	0.0442	$1.67947e-04$	1.9937	$1.83382e-02$	0.9907
	0.1768	$2.87517e-03$	-	$7.64253e-02$	-
$m=3$	0.1250	$1.33055e-03$	2.2233	$5.10892e-02$	1.1621
	0.0884	$6.75045e-04$	1.9579	$3.58453e-02$	1.0225
	0.0625	$3.31262e-04$	2.0540	$2.52706e-02$	1.0087
	0.0442	$1.67341e-04$	1.9704	$1.81192e-02$	0.9599

Table 4.5.5: EOC in L^2 norm and H^1 semi-norm at $T = 1$ in Example 4.5.3

l	k	$m = 1$		$m = 2$	
		L^2-order	H^1-order	L^2-order	H^1-order
0	1	1.88	0.94	1.88	0.96
1	1/2	1.60	0.56	1.59	0.54
2	1/4	1.38	0.32	1.32	0.30
3	1/8	1.24	0.20	1.19	0.17
4	1/16	1.15	0.14	1.14	0.11
5	1/32	1.09	0.10	1.15	0.08

Example 4.5.3. (Low regular solution) We consider the model problem (4.1.1)-(4.1.2) on a two-dimensional domain, for which the exact solution possesses a corner singularity in spatial direction. We set the exact solution as

$$u(x, y, t) = t \sin t \; x(1 - x)y(1 - y)(x^2 + y^2)^{-1+\frac{k}{2}},$$

where $k \in (0, 1]$ and the coefficients $\sigma = \epsilon = 1$. It is easy to see that u has a singularity at the corner point $(0, 0)$ and $u \in C^\infty(0, T; H^{1+k-\delta}(\Omega))$ but $u \notin C^\infty(0, T; H^{1+k}(\Omega))$, for some positive number δ. We choose the Voronoi mesh $(\mathcal{V}_h)$ for the spatial discretization and compute the EOC in respective norms by setting $k = (1/2)^l$, $l = 0, 1, 2, 3, 4, 5$.

From Table 4.5.5, we can easily observe that the numerical order of convergence at the final time $T = 1$ remains to be $O(h^{1+k})$ in L^2 norm and $O(h^k)$ in H^1 semi-norm for linear as well as higher order methods, which is due to the low regularity of the exact solution. Figure 4.5.8 presents the contour plot of the exact and approximate solution for $k = 1/2$ at $t = 1$.

Example 4.5.4. (Smooth solution with non-convex domain) For this numerical experiment, we consider a L-shaped domain $\Omega = (0, 1) \times (0, 1) \setminus [1/2, 1) \times [1/2, 1)$. We choose the Voronoi mesh $(\mathcal{V}_h)$ for the spatial discretization. We set the exact solution to the model problem (4.1.1)-(4.1.2) as

$$u = t \sin t \sin(2\pi x) \sin(2\pi y)$$

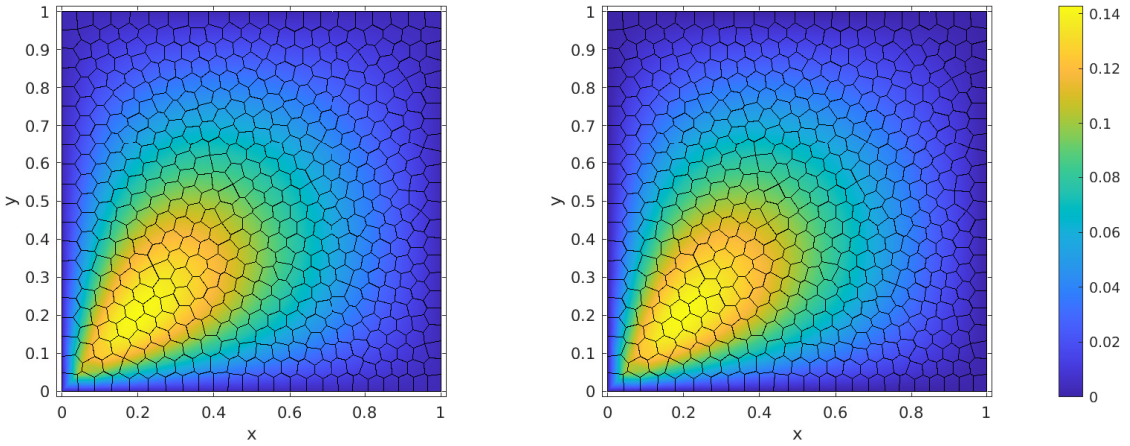

Figure 4.5.8: Approximate solution (left) for $m = 2$ ($h = 0.0442$) and exact solution (right) at $t = 1$ with $k = 0.5$ in Example 4.5.3.

and the coefficients $\sigma = \epsilon = 1$.

In Table 4.5.6, we show the numerical errors and EOC in L^2 norm and H^1 semi-norm at the final time $T = 1$ for linear and quadratic approximations. Figure 4.5.9 presents the contour plot of the exact and approximate solutions at $T = 1$. The order of accuracy obtained to be $O(h^{m+1})$ in L^2 norm and $O(h^m)$ in H^1 semi-norm. The log-log plots are presented in Figure 4.5.10.

Example 4.5.5. (Smooth solution with circular domain) In this example, we consider a circular domain Ω with center at $(0, 0)$ and radius 1. We choose Voronoi mesh $(\mathcal{V}_h)$ for the spatial discretization. We choose the exact solution to the model problem (4.1.1)-(4.1.2) to be

$$u = t \sin t(1 - x^2 - y^2) \sin(\pi x) \sin(\pi y)$$

and the coefficients $\sigma = \epsilon = 1$.

In Table 4.5.7, we show the numerical errors and EOC in L^2 norm and H^1 semi-norm at the final time $T = 1$ for linear and quadratic approximations. Figure 4.5.11 presents the contour plot of the exact and approximate solutions at $T = 1$. The order of accuracy obtained to be $O(h^{m+1})$ in L^2 norm and $O(h^m)$ in H^1 semi-norm. The log-log plots are presented in Figure 4.5.12.

Table 4.5.6: L^2 and H^1 errors at $T = 1$ in Example 4.5.4

	h	$\|u - u_h\|$	EOC	$\|u - u_h\|_1$	EOC
	0.1690	$7.18839e-02$	-	$2.60757e-01$	-
$m = 1$	0.1222	$3.49862e-02$	2.2179	$1.42172e-01$	1.8682
	0.0874	$1.63971e-02$	2.2605	$7.20476e-02$	2.0275
	0.0621	$8.20723e-03$	2.0307	$3.85717e-02$	1.8333
	0.0441	$4.09242e-03$	2.0248	$2.54238e-02$	1.2129
	0.1690	$4.06743e-03$	-	$4.54247e-02$	-
$m = 2$	0.1222	$1.60966e-03$	2.8551	$1.86356e-02$	2.7443
	0.0874	$5.51263e-04$	3.1963	$8.08752e-03$	2.4899
	0.0621	$1.97476e-04$	3.0122	$3.40738e-03$	2.5362
	0.0441	$6.93784e-05$	3.0437	$1.43303e-03$	2.5203

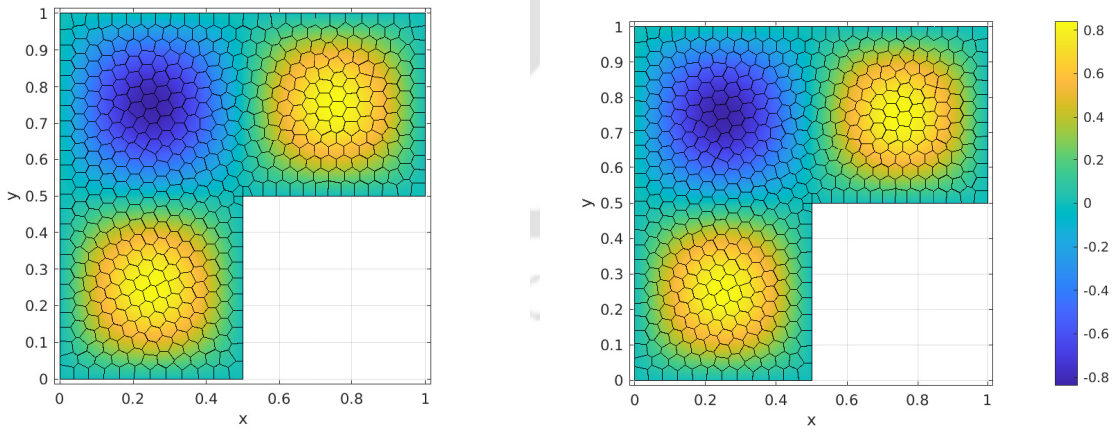

Figure 4.5.9: Approximate solution (left) for $m = 2$ ($h = 0.0441$) and exact solution (right) at $t = 1$ in Example 4.5.4.

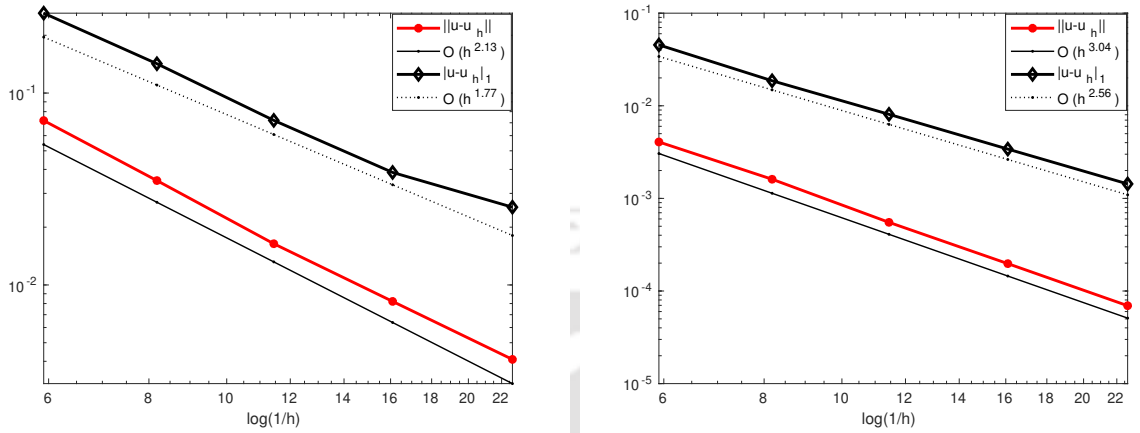

Figure 4.5.10: Log-log plots of the errors versus h at $t = 1$ for $m = 1$ (left) and $m = 2$ (right) in Example 4.5.4.

Table 4.5.7: L^2 and H^1 errors at $T = 1$ in Example 4.5.5

	h	$\|u - u_h\|$	EOC	$\|\|u - u_h\|\|$	EOC
$m = 1$	0.1768	$1.46506e-01$	-	$4.65785e-01$	-
	0.1250	$6.64965e-02$	2.2792	$1.82503e-01$	2.7035
	0.0884	$3.10081e-02$	2.2013	$8.17590e-02$	2.3169
	0.0625	$1.48670e-02$	2.1211	$4.30456e-02$	1.8510
	0.0442	$7.29290e-03$	2.0551	$2.85357e-02$	1.1862
$m = 2$	0.1768	$1.23339e-02$	-	$4.56535e-02$	-
	0.1250	$4.41018e-03$	2.9674	$2.36235e-02$	1.9010
	0.0884	$1.56553e-03$	2.9884	$1.26268e-02$	1.8075
	0.0625	$5.98096e-04$	2.7764	$6.09017e-03$	2.1039
	0.0442	$2.15650e-04$	2.9434	$2.97930e-03$	2.0630

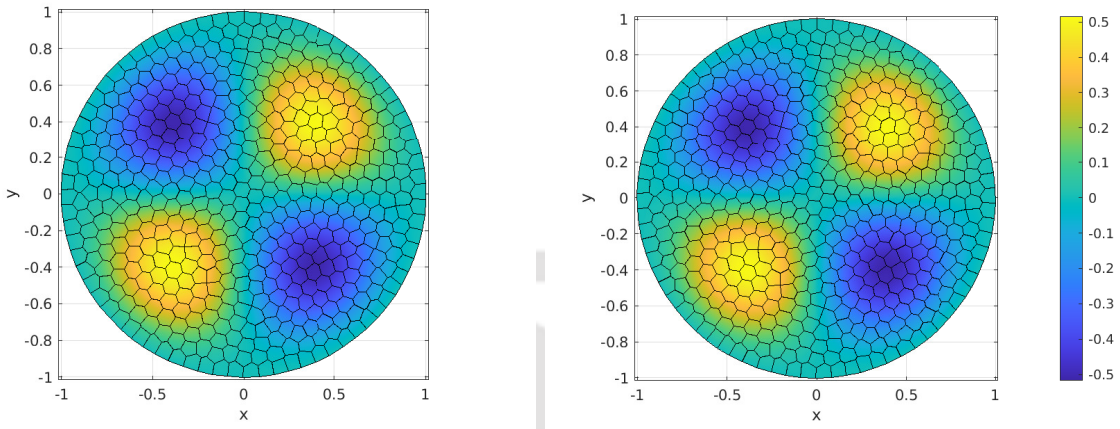

Figure 4.5.11: Approximate solution (left) for $m = 2$ ($h = 0.0442$) and exact solution (right) at $t = 1$ in Example 4.5.5.

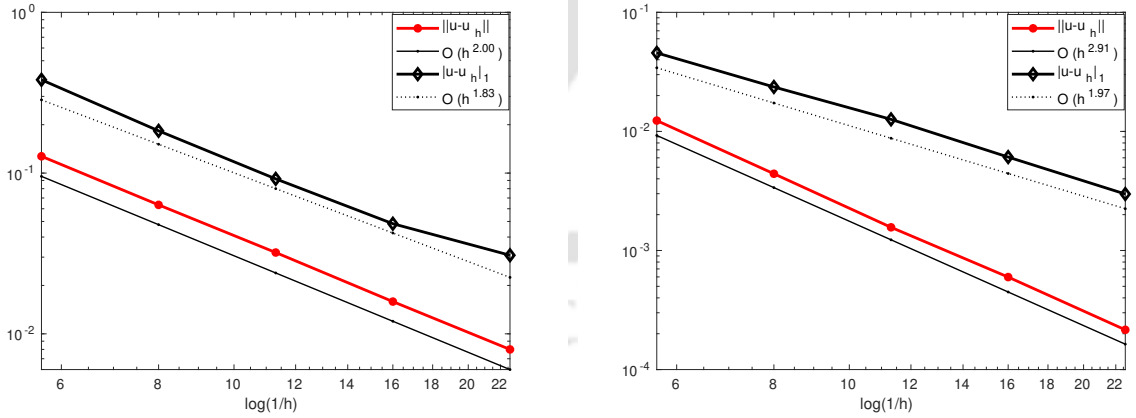

Figure 4.5.12: Log-log plots of the errors versus h at $t = 1$ for $m = 1$ (left) and $m = 2$ (right) in Example 4.5.5.

Example 4.5.6. (Heat transport in metallic films) We consider the following problem from [54]

$$\gamma u_{tt} + \beta u_t + \delta u - \nabla \cdot (\sigma \nabla u + \epsilon \nabla u_t) = f \text{ in } \Omega \times [0,1],$$

where $\Omega = (-1,1) \times (-1,1)$. This problem arises commonly in the study of heat transport in metallic films during ultrafast laser heating [104, 127]. With $\gamma = \delta = 0$, we get the following Sobolev equation:

$$\beta u_t - \nabla \cdot (\sigma \nabla u + \epsilon \nabla u_t) = f \text{ in } \Omega \times [0,1].$$

We select the exact solution to be

$$u = t \exp(-t) \sin(\pi x) \sin(\pi y).$$

The physical coefficients β, σ and ϵ are chosen as [126]

$$(\beta, \sigma, \epsilon) = \left(\frac{C_E^2}{\alpha_E}, \alpha_e, C_E^2 \right) = \left(1.2 \times 10^{12}, 1.2 \times 10^{-4}, 1.44 \times 10^{8} \right),$$

where C_E represents the equivalent thermal wave speed, where as α_e and α_E stand for electron and equivalent thermal diffusivity, respectively of the material.

In Table 4.5.8, we show the numerical errors and EOC in L^2 norm and H^1 semi-norm at the final time $T = 1$ for $m = 1, 2$. Figure 4.5.13 presents the contour plot of the exact and approximate solutions at $T = 1$. The order of accuracy obtained to be $O(h^{m+1})$ in L^2 norm and $O(h^m)$ in H^1 semi-norm. The log-log plots is presented in Figure 4.5.14.

4.6 Conclusion

In this chapter, we have proposed a virtual element method for second-order Sobolev equations with variable coefficients. We have obtained optimal order of convergence, i.e., $O(h^m)$ in H^1 semi-norm and $O(h^{m+1})$ in L^2 norm, where m is the polynomial degree of the method, and h is the mesh size. A new non-standard projection operator is used to derive the optimal convergence estimate in L^2 norm. For the temporal discretization, we have employed the second-order Crank-Nicolson scheme and derived the optimal convergence estimates for the fully discrete scheme. We have illustrated some numerical experiments with polynomial degree $m = 1, 2, 3$ and shown that the experimental order of convergence agrees with the theoretical results. The use of different types of polygonal meshes for spatial discretization shows the flexibility of the method with respect to mesh discretization.

Table 4.5.8: L^2 and H^1 errors at $T = 1$ in Example 4.5.6

	h	$\|u - u_h\|$	EOC	$\|\|u - u_h\|\|$	EOC
$m = 1$	0.3536	$1.73257e-01$	-	$5.60085e-01$	-
	0.2500	$5.90302e-02$	3.1068	$2.13977e-01$	2.7764
	0.1768	$2.14328e-02$	2.9233	$8.51907e-02$	2.6574
	0.1250	$8.12301e-03$	2.7995	$3.98674e-02$	2.1910
	0.0884	$3.31517e-03$	2.5859	$2.36739e-02$	1.5038
$m = 2$	0.3536	$1.92957e-02$	-	$3.73776e-01$	-
	0.2500	$5.60325e-03$	3.5679	$1.77208e-01$	2.1535
	0.1768	$1.84692e-03$	3.2023	$8.25805e-02$	2.2031
	0.1250	$5.61565e-04$	3.4352	$3.25714e-02$	2.6844
	0.0884	$1.66199e-04$	3.5131	$1.17394e-02$	2.9445

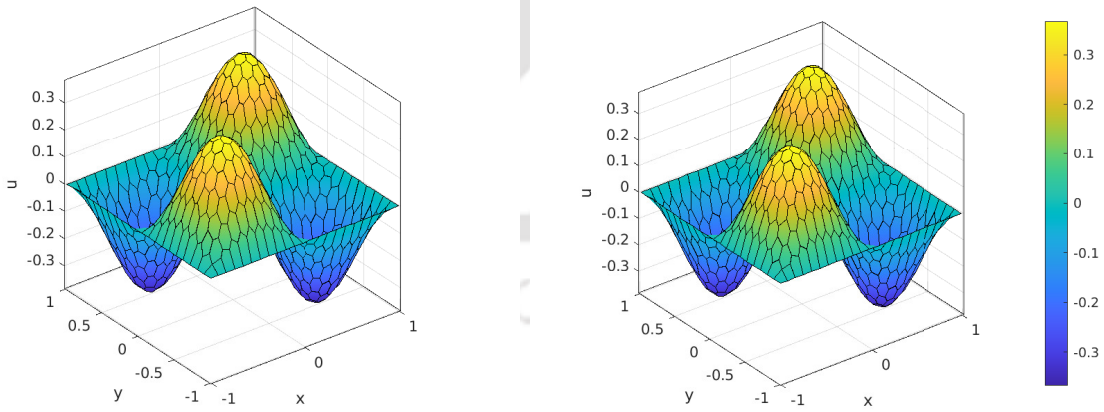

Figure 4.5.13: Approximate solution (left) for $m = 2$ ($h = 0.0884$) and exact solution (right) at $t = 1$ in Example 4.5.6.

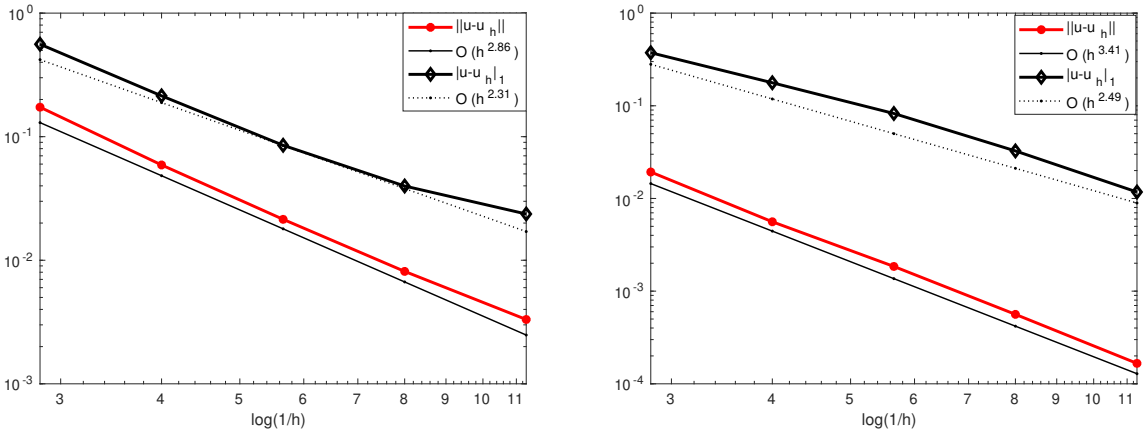

Figure 4.5.14: Log-log plots of the errors versus h at $t = 1$ for $m = 1$ (left) and $m = 2$ (right) in Example 4.5.6.

5

VEMs for Viscoelastic Wave Equations

We develop a virtual element method for viscoelastic wave equations on polygonal meshes. We propose both semi-discrete and fully discrete schemes to numerically solve the linear viscoelastic wave. For the time discretization, we have used implicit second-order Newmark scheme. Optimal convergence rates in both the L^2 norm and the H^1 semi-norm are established using a new non-standard projection operator. Numerical experiments are illustrated to confirm our theoretical findings.

5.1 Introduction

Our goal of the current work is to develop the virtual element method for hyperbolic type equations with strong damping. We consider the following problem as our model problem

$$u_{tt}(x,t) - \nabla \cdot (\sigma(x)\nabla u(x,t) + \epsilon(x)\nabla u_t(x,t)) = f(x,t) \text{ in } \Omega \times (0,T] \tag{5.1.1}$$

with ICs and BCs

$$u(x,0) = u_0 \;\; \& \;\; u_t(x,0) = v_0 \;\text{ in } \Omega; \;\; u(x,t) = 0 \quad \text{on } \partial\Omega \times (0,T], \tag{5.1.2}$$

where $\Omega \subset \mathbb{R}^2$ is a polygonal domain with smooth boundary $\partial\Omega$ and $T < \infty$ is the finite terminal observation time. Here $\sigma, \epsilon \in L^\infty(\Omega)$ are the diffusion coefficient and the damping coefficient, respectively such that

$$\underline{M} \leq \sigma(x), \epsilon(x) \leq \overline{M} \quad \forall x \in \bar{\Omega}$$

for some positive constants $\underline{M}$ and $\overline{M}$.

Many numerical methods have been developed to solve the equation (5.1.1) mostly using finite difference method or classical finite element methods [84, 85, 122, 134, 137]. But, in case of polygonal or polyhedral meshes employing FEM becomes very difficult task due to the complexity in basis construction and it demands higher computational cost to evaluate the integrals using Gauss quadrature. To avoid above difficulties associated with numerical approximation of the model problem, we will propose a newly introduced numerical method known as the virtual element method (VEM), which will be simple to implement and also cost-efficient.

In this chapter, we develop a novel VEM for the viscoelastic wave equation (5.1.1). The virtual semi-discrete approximation of the model problem is constructed using three approximated bilinear forms. The fully discrete scheme is obtained by first reformulating the governing equation into a system of first-order equations and then employing the Crank-Nicolson discretization. In fact time discretization method is the well-known Newmark method for wave equation when we adopt the particular choice for the parameters in the Newmark scheme (cf. [67]), which has been used extensively in applications. We present rigorous error analysis for the semi-discrete scheme as well as fully discrete scheme and derive optimal convergence estimates. Further, in support of theoretical findings numerical examples are presented with different types of meshes and different polynomial degrees.

The remainder of the content is divided as follows. We present the semi-discrete virtual element approximation in Section 5.2. Next, while Section 5.3 deals with the semi-discrete error analysis, Section 5.4 discusses fully discrete approximation and its convergence. Numerical examples and the conclusion are presented in Section 5.5 and Section 5.6, respectively.

5.2 Semi-discrete Virtual Element Approximation

This section deals with construction of semi-discrete virtual element approximation for the model problem (5.1.1)-(5.1.2).

Following the standard way, we easily obtain the variational formulation corresponding to the model problem (5.1.1)-(5.1.2) as: Find $u \in L^2(0,T;H_0^1(\Omega)) \cap H^1(0,T;H^1(\Omega)) \cap H^2(0,T;L^2(\Omega))$ such that for all $v \in H_0^1(\Omega)$ and for a.e. $t \in (0,T]$

$$\begin{cases} (u_{tt},v) + a_1(u,v) + a_2(u_t,v) = (f,v) \ \ \forall v \in H_0^1(\Omega), \\ u(0) = u_0, \ u_t(0) = v_0 \end{cases} \tag{5.2.1}$$

where $a_1(u,v)$ and $a_2(u,v)$ are bilinear forms on $H_0^1(\Omega)$ defined as in (3.2.2).

We recall the virtual element framework discussed in Chapter 1, Section 1.4. Let $\{\mathcal{T}_h\}$ be a partition of the domain Ω into elements (arbitrary polygons) E. The bilinear forms $a_i(\cdot,\cdot)$, $i=1,2$ can be splited into their local counterparts in the following manner

$$a_i(u,v) := \sum_{E\in\mathcal{T}_h} a_i^E(u,v) \;\forall\; u,v \in H_0^1(\Omega), \quad i=1,2.$$

Then the discrete bilinear forms on the local virtual element space $W_h^m(E)$ can be defined as:

$$\begin{aligned}
a_{1,h}^E(v,w) &:= \left(\sigma\mathbf{\Pi}_{m-1,E}^0\nabla v, \mathbf{\Pi}_{m-1,E}^0\nabla w\right)_E + S_\sigma^E\left((I-\Pi_{m,E}^\nabla)v,(I-\Pi_{m,E}^\nabla)w\right),\\
a_{2,h}^E(v,w) &:= \left(\epsilon\mathbf{\Pi}_{m-1,E}^0\nabla v, \mathbf{\Pi}_{m-1,E}^0\nabla w\right)_E + S_\epsilon^E\left((I-\Pi_{m,E}^\nabla)v,(I-\Pi_{m,E}^\nabla)w\right) \quad \&\\
m_h^E(v,w) &:= (\Pi_{m,E}^0 v, \Pi_{m,E}^0 w)_E + S_0^E\left((I-\Pi_{m,E}^0)v,(I-\Pi_{m,E}^0)w\right),
\end{aligned}$$

where

$$\begin{aligned}
S_\sigma^E(v,w) &= \beta_\sigma^E \sum_{r=1}^{N^E} dof_r(v)dof_r(w),\\
S_\epsilon^E(v,w) &= \beta_\epsilon^E \sum_{r=1}^{N^E} dof_r(v)dof_r(w) \quad \&\\
S_0^E(v,w) &= |E| \sum_{r=1}^{N^E} dof_r(v)dof_r(w)
\end{aligned}$$

with $\beta_\sigma^E = P_E^a(\sigma)$, $\beta_\epsilon^E = P_E^a(\epsilon)$ and $N^E = \dim W_h^m(E)$.

Now the global bilinear forms on the global discrete space W_h^m can be obtained by assembling the local counterpart as:

$$a_{i,h}(v,w) := \sum_{E\in\mathcal{T}_h} a_{i,h}^E(v,w), \;\; i=1,2 \;\; \& \;\; m_h(v,w) := \sum_{E\in\mathcal{T}_h} m_h^E(v,w) \quad \forall v,w \in W_h^m.$$

The global bilinear forms $a_{i,h}$, $i=1,2$ and m_h satisfies the following continuity and coercivity properties (Lemma 1.4.5): For $v,w \in W_h^m$

$$\begin{aligned}
a_{1,h}(v,w) &\le (1+\beta_\sigma)\overline{M}|v|_1|w|_1,\\
a_{2,h}(v,w) &\le (1+\beta_\epsilon)\overline{M}|v|_1|w|_1 \;\&\\
m_h(v,w) &\le (1+\beta_0)\|v\|\|w\|
\end{aligned}$$

and $w \in W_h^m$

$$a_{1,h}(w,w) \geq \min\{1,\alpha_\sigma\}\underline{M}|w|_1^2,$$
$$a_{2,h}(w,w) \geq \min\{1,\alpha_\epsilon\}\underline{M}|w|_1^2 \ \&$$
$$m_h(w,w) \geq \min\{1,\alpha_0\}\|w\|^2,$$

where α_σ, α_ϵ, α_0, β_σ, β_ϵ, β_0 are some positive constants.

We have the following semi-discrete virtual element approximation to (5.2.1): Find $u_h \in C^2(0,T;W_h^m)$ such that

$$\begin{cases} m_h(u_{htt},w_h) + a_{1,h}(u_h,w_h) + a_{2,h}(u_{ht},w_h) = (f_h,w_h) \quad \forall w_h \in W_h^m, \\ u_h(0) = R_h^2 u_0, \ u_{ht}(0) = R_h^2 v_0, \end{cases} \tag{5.2.2}$$

where f_h is the discrete form of the source function f as define in (1.4.14). Here, R_h^i, $i = 1,2$ are the modified elliptic projection operators as defined in (3.2.3). In addition, we also need the L^2 projection operator L_h defined in (1.5.11).

5.3 Error Analysis for the Semi-discrete Problems

This section is dedicated to the convergence analysis of semi-discrete approximation (5.2.2). Optimal convergence rates in both the H^1 semi-norm and the L^2 are established on polygonal meshes.

Before proceeding to the error analysis, we present the following result regarding the stability of the semi-discrete solution u_h with respect to the initial data and the source function.

Lemma 5.3.1. *Let $u_0, v_0 \in H_0^1(\Omega) \cap H^{2k-2}(\Omega)$ and $f \in H^{k-1}(H^{2k-4}(\Omega))$, $k = 2,3,4$. Then, we have*

$$\|D_t^k u_h(0)\| \leq C\big(|u_0|_{2k-2} + |v_0|_{2k-2} + \|f\|_{H^{k-1}(H^{2k-4})}\big),$$
$$|D_t^{k-1} u_h(0)|_1 \leq C\big(|u_0|_{2k-3} + |v_0|_{2k-3} + \|f\|_{H^{k-2}(H^{2k-5})}\big),$$

where $D_t^k = \dfrac{\partial^k}{\partial t^k}$.

Proof. Taking $t \to 0^+$ in (5.2.2), we obtain

$$m_h(u_{htt}(0),w) = a_{1,h}(R_h^1 u_0 - R_h^2 u_0, w) - a_1(u_0,w) - a_2(v_0,w) + (f_h(0),w). \tag{5.3.1}$$

Here, we have used the relation

$$a_{i,h}(R_h^2 v, w) = a_i(v, w)\ \forall w \in W_h^m,\ i = 1, 2.$$

For the first term in (5.3.1), using continuity property of $a_{1,h}$ and approximation properties of projection operators R_h^i, $i = 1, 2$, we have

$$a_{1,h}(R_h^1 u_0 - R_h^2 u_0, w) \leq C|u_0|_2 \|w\|. \tag{5.3.2}$$

Again, we have

$$(f_h(0), w) \leq C\|f\|_{H^1(L^2)}\|w\|. \tag{5.3.3}$$

Here, we have used Lemma 1.4.6 and Lemma 1.2.1. Now, we substitute $w = u_{htt}(0)$, and combine the estimates (5.3.2) and (5.3.3) in (5.3.1) to have

$$\|u_{htt}(0)\| \leq C(|u_0|_2 + |v_0|_2 + \|f\|_{H^1(L^2)}).$$

H^1-stability of the projection operator R_h^2 gives

$$|u_{ht}(0)|_1 = |R_h^2 v_0|_1 \leq C|v_0|_1.$$

This proves for $k = 2$. For the case $k = 3$, subtracting (5.2.1) from (5.2.2) and setting $t \to 0^+$ in the resulting equation, we get

$$m_h(u_{htt}(0) - R_h^2 u_{tt}(0), w) = a_{1,h}(R_h^2 u_0 - R_h^1 u_0, w) + (f_h(0) - f(0), w). \tag{5.3.4}$$

Choosing $w = u_{htt}(0) - R_h^2 u_{tt}(0)$ in the above equation (5.3.4), we have the following estimate. For $s \geq 0$

$$\|u_{htt}(0) - R_h^2 u_{tt}(0)\| \leq Ch^s \left(|u_0|_{s+2} + \|f\|_{H^1(H^s)}\right). \tag{5.3.5}$$

Again, the above estimate (5.3.5), together with inverse inequality yields

$$|u_{htt}(0) - R_h^2 u_{tt}(0)|_1 \leq Ch^{-1}\|u_{htt}(0) - R_h^2 u_{tt}(0)\| \leq Ch^{s-1}\left(|u_0|_{s+2} + \|f\|_{H^1(H^s)}\right). \tag{5.3.6}$$

For $s = 1$ in (5.3.6), we get

$$|u_{htt}(0)|_1 \leq C\left(|u_0|_3 + \|f\|_{H^1(H^1)}\right) + |R_h^2 u_{tt}(0)|_1 \leq C\left(|u_0|_3 + \|f\|_{H^1(H^1)} + |u_{tt}(0)|_1\right). \tag{5.3.7}$$

From (5.1.1), as $t \to 0^+$ we have

$$|u_{tt}(0)|_1 = |\nabla \cdot (\sigma \nabla u(0) + \epsilon \nabla u_t(0)) + f(0)|_1 \leq C \left(|u_0|_3 + |v_0|_3 + \|f\|_{H^1(H^1)}\right). \tag{5.3.8}$$

Now, plugging (5.3.8) in (5.3.7), we obtain

$$|u_{htt}(0)|_1 \leq C \left(|u_0|_3 + |v_0|_3 + \|f\|_{H^1(H^1)}\right).$$

Differentiate (5.2.2) with respect to t and then take $t \to 0^+$ to have

$$\begin{aligned} m_h(u_{httt}(0), w) =& (f_{ht}(0), w) - a_{1,h}(R_h^2 v_0 - R_h^1 v_0, w) - a_{2,h}(u_{htt}(0) - R_h^2 u_{tt}(0), w) \\ & - a_1(v_0, w) - a_2(u_{tt}(0), w). \end{aligned} \tag{5.3.9}$$

Using the same argument as (5.3.2), we have

$$a_{1,h}(R_h^2 v_0 - R_h^1 v_0, w) \leq C|v_0|_2 \|w\|. \tag{5.3.10}$$

Also, using (5.3.6) with $s = 2$, we get

$$a_{2,h}(u_{htt}(0) - R_h^2 u_{tt}(0), w) \leq C|u_{htt}(0) - R_h^2 u_{tt}(0)|_1 |w|_1 \leq C \left(|u_0|_4 + \|f\|_{H^1(H^2)}\right) \|w\|. \tag{5.3.11}$$

Again, we can easily obtain that

$$(f_{ht}(0), w) \leq \|f\|_{H^2(L^2)} \|w\| \tag{5.3.12}$$

and

$$|u_{tt}(0)|_2 = |\nabla \cdot (\sigma \nabla u(0) + \epsilon \nabla u_t(0)) + f(0)|_2 \leq C \left(|u_0|_4 + |v_0|_4 + \|f\|_{H^1(H^2)}\right). \tag{5.3.13}$$

Substituting the above estimates (5.3.10)-(5.3.13) in (5.3.9) and choosing $w = u_{httt}(0)$, we obtain

$$\|u_{httt}(0)\| \leq C \left(|u_0|_4 + |v_0|_4 + \|f\|_{H^2(H^2)}\right).$$

For the case when $k = 4$, proceeding in a similar way we get

$$|u_{httt}(0)|_1 \leq C \left(|u_0|_5 + |v_0|_5 + \|f\|_{H^2(H^3)}\right) \quad \&$$

$$\|u_{htttt}(0)\| \leq C \left(|u_0|_6 + |v_0|_6 + \|f\|_{H^3(H^4)}\right).$$

□

Lemma 5.3.2. *Let $u_0, v_0 \in H_0^1(\Omega) \cap H^{2k-2}(\Omega)$ and $f \in H^{k-1}(H^{2k-4}(\Omega))$, $k = 3, 4$. Then, we have*

$$\|D_t^k u_h(t)\|^2 + \int_0^t |D_t^k u_h(t)|_1^2 dt \leq C\big(|u_0|_{2k-2}^2 + |v_0|_{2k-2}^2 + \|f\|_{H^{k-1}(H^{2k-4})}^2\big).$$

Proof. We differentiate (5.2.2) twice with respect to t then substitute $w = u_{htt}(t)$, to have

$$\frac{1}{2}\frac{d}{dt} m_h(u_{htt}(t), u_{htt}(t)) + \frac{1}{2}\frac{d}{dt} a_{1,h}(u_{htt}(t), u_{htt}(t)) + a_{2,h}(u_{htt}(t), u_{htt}(t)) = (f_{htt}(t), u_{htt}(t)).$$

Integrating the above equation over $[0, t]$, and then using Young's inequality and coercivity properties of the bilinear forms, we obtain

$$\|u_{htt}(t)\|^2 + \int_0^t |u_{htt}(t)|_1^2 dt \leq C\Big(\|u_{htt}(0)\|^2 + |u_{htt}(0)|_1^2 + \int_0^t \|f_{htt}(t)\|^2 dt\Big).$$

Further, using Lemma 5.3.1 in the above equation, we have

$$\|u_{htt}(t)\|^2 + \int_0^t |u_{htt}(t)|_1^2 dt \leq C(|u_0|_4^2 + |v_0|_4^2 + \|f\|_{H^2(H^2)}^2).$$

This proves for $k = 3$. Analogously, for $k = 4$ we can show

$$\|u_{htttt}(t)\|^2 + \int_0^t |u_{htttt}(t)|_1^2 dt \leq C(|u_0|_6^2 + |v_0|_6^2 + \|f\|_{H^3(H^4)}^2).$$

□

Next, we derive following convergence result in H^1 semi-norm for the semi-discrete approximation (5.2.2).

Theorem 5.3.1. *Assume that $u \in H^2(0, T; H^{m+1}(\Omega))$, $f \in L^2(0, T; H^m(\Omega))$ and $u_0 \in H^{m+1}(\Omega)$. Then for all $t \in (0, T]$, we have*

$$|u_h(t) - u(t)|_1 \leq Ch^m(|u_0|_{m+1} + \|u\|_{H^2(H^{m+1})} + \|f\|_{L^2(H^m)}).$$

Proof. Let us split the error $e_h(t) = u_h(t) - u(t)$ as

$$e_h(t) = \phi(t) + \psi(t), \tag{5.3.14}$$

where $\phi(t) =: u_h(t) - R_h^2 u(t)$ and $\psi(t) =: R_h^2 u(t) - u(t)$.

Now, due to Lemma 3.2.1, we have the following bound for $\psi(t)$

$$|\psi(t)|_1 \leq Ch^m |u(t)|_{m+1} \leq Ch^m(|u_0|_{m+1} + \|u_t\|_{L^1(H^{m+1})}). \tag{5.3.15}$$

Therefore, we need to bound the term $\phi(t)$ only. From (5.2.2), using the definitions of projection operators R_h^i $(i = 1,\ 2)$ and L_h, we have the following error equation for $\phi(t)$. For all $w_h \in W_h^m$ and for all $t \in (0, T]$, we obtain

$$
\begin{aligned}
&m_h(\phi_{tt}(t), w_h) + a_{1,h}(\phi(t), w_h) + a_{2,h}(\phi_t(t), w_h)\\
&= m_h(u_{htt}(t), w_h) + a_{1,h}(u_h(t), w_h) + a_{2,h}(u_{ht}(t), w_h)\\
&\quad - \left[m_h(R_h^2 u_{tt}(t), w_h) + a_{1,h}(R_h^2 u(t), w_h) + a_{2,h}(R_h^2 u_t(t), w_h)\right]\\
&= (f_h(t) - f(t), w_h) + (u_{tt}(t), w_h) + a_1(u(t), w_h) + a_2(u_t(t), w_h)\\
&\quad - \left[m_h(R_h^2 u_{tt}(t), w_h) + a_{1,h}(R_h^1 u(t), w_h) + a_{2,h}(R_h^2 u_t(t), w_h) + a_{1,h}(R_h^2 u(t) - R_h^1 u(t), w_h)\right]\\
&= (f_h(t) - f(t), w_h) + a_{1,h}(R_h^1 u(t) - R_h^2 u(t), w_h) + m_h(L_h u_{tt}(t) - R_h^2 u_{tt}(t), w_h)\\
&=: T_1 + T_2 + T_3. \qquad (5.3.16)
\end{aligned}
$$

For the term T_1, from Lemma 1.4.6, we have

$$T_1 = (f_h(t) - f(t), w_h) \le Ch^m |f(t)|_m \|w_h\|. \qquad (5.3.17)$$

Next, using the continuity of $a_{1,h}$ and approximation properties of R_h^1 and R_h^2, we obtain

$$
\begin{aligned}
T_2 &= a_{1,h}(R_h^1 u(t) - R_h^2 u(t), w_h)\\
&= a_{1,h}(R_h^1 u(t) - u(t), w_h) - a_{1,h}(R_h^2 u(t) - u(t), w_h)\\
&\le (1 + \beta_\sigma)\overline{M}(|R_h^2 u(t) - u(t)|_1 + |R_h^1 u(t) - u(t)|_1)|w_h|_1\\
&\le Ch^m |u(t)|_{m+1} |w_h|_1. \qquad (5.3.18)
\end{aligned}
$$

Also, for the term T_3, using the continuity of m_h and approximation properties of L_h and R_h^2, we have

$$
\begin{aligned}
m_h(L_h u_{tt}(t) - R_h^2 u_{tt}(t), w_h) &= m_h(L_h u_{tt}(t) - u_{tt}(t), w_h) + m_h(u_{tt}(t) - R_h^2 u_{tt}(t), w_h)\\
&\le (1 + \beta_0)\left(\|L_h u_{tt}(t) - u_{tt}(t)\| + \|u_{tt}(t) - R_h^2 u_{tt}(t)\|\right)\|w_h\|\\
&\le Ch^m |u_{tt}(t)|_m \|w_h\|. \qquad (5.3.19)
\end{aligned}
$$

Now, combine the estimates (5.3.17)-(5.3.19) with the identity (5.3.16) and set $w_h = \phi_t(t)$ to obtain

$$\begin{aligned} &m_h(\phi_{tt}(t), \phi_t(t)) + a_{1,h}(\phi(t), \phi_t(t)) + a_{2,h}(\phi_t(t), \phi_t(t)) \\ &\leq Ch^m(|u(t)|_{m+1} + |u_{tt}(t)|_m + |f(t)|_m)|\phi_t(t)|_1, \end{aligned}$$

which yields

$$\begin{aligned} &\frac{1}{2}\frac{d}{dt}m_h(\phi_t(t), \phi_t(t)) + \frac{1}{2}\frac{d}{dt}a_{1,h}(\phi(t), \phi(t)) + a_{2,h}(\phi_t(t), \phi_t(t)) \\ &\leq Ch^m(|u(t)|_{m+1} + |u_{tt}(t)|_m + |f(t)|_m)|\phi_t(t)|_1. \end{aligned}$$

Integrating above estimate over $[0, t]$ and using the coercivity of the bilinear maps m_h, $a_{i,h}$, $i = 1, 2$, we obtain

$$\begin{aligned} &\|\phi_t(t)\|^2 + |\phi(t)|_1^2 + \int_0^t |\phi_t(s)|_1^2 \, ds \\ &\leq C\int_0^t h^m(|u(s)|_{m+1} + |u_{tt}(s)|_m + |f(s)|_m)|\phi_t(s)|_1 \, ds + \|\phi_t(0)\|^2 + |\phi(0)|_1^2. \end{aligned} \tag{5.3.20}$$

Since $\phi(0) = 0 = \phi_t(0)$, employing Young's inequality in (5.3.20) results in

$$\|\phi_t(t)\|^2 + |\phi(t)|_1^2 + \int_0^t |\phi_t(s)|_1^2 \, ds \leq Ch^{2m}(\|u\|^2_{L^2(H^{m+1})} + \|u_{tt}\|^2_{L^2(H^m)} + \|f\|^2_{L^2(H^m)}).$$

Neglecting the terms $\|\phi_t(t)\|^2$ and $\int_0^t |\phi_t(s)|_1^2 \, ds$, we arrive at

$$|\phi(t)|_1 \leq Ch^m(\|u\|_{H^2(H^{m+1})} + \|f\|_{L^2(H^m)}). \tag{5.3.21}$$

Finally, plugging (5.3.15) and (5.3.21) in (5.3.14) leads to the desire result. □

For the L^2 norm error estimate, we will use the non-standard projection operator $\mathcal{E}_h$ defined in equation (4.3.13). From (5.1.1) and (4.3.13), we note that

$$f = f_u + u_{tt}. \tag{5.3.22}$$

Now, we will present the main result of this section. The semi-discrete approximation (5.2.2) has the following error estimate in L^2 norm.

Theorem 5.3.2. *Assume that* $f \in L^1(0,T;H^{m+1}(\Omega))$, $u \in H^1(0,T;H^{m+1}(\Omega))$ *and* $u_0, v_0 \in H^{m+1}(\Omega)$. *Then for all* $t \in (0,T]$, *we have*

$$\|u_h(t) - u(t)\| \leq Ch^{m+1}\left(|u_0|_{m+1} + |v_0|_{m+1} + \|u\|_{H^1(H^{m+1})} + \|f\|_{L^1(H^{m+1})}\right).$$

Proof. We split the error term $e_h = u_h - u$ into two standard components θ and ρ using the following relation

$$e_h(t) =: \theta(t) + \rho(t), \tag{5.3.23}$$

where $\theta = u_h - \mathcal{E}_h u$ and $\rho = \mathcal{E}_h u - u$. From Lemma 4.3.4 and approximation property of R_h^2, we have the following bounds for $\rho(t)$:

$$\|\rho(t)\| \leq \|\zeta_u(t)\| + \|R_h^2 u(t) - u(t)\| \leq Ch^{m+1}(|u_0|_{m+1} + \|u\|_{H^1(H^{m+1})}). \tag{5.3.24}$$

Using the definitions of projection operators $\mathcal{E}_h$ and L_h, and equation (5.3.22), we arrive at the following important identity: For all $w_h \in W_h^m$

$$\begin{aligned}
&m_h(\theta_{tt}(t), w_h) + a_{1,h}(\theta(t), w_h) + a_{2,h}(\theta_t(t), w_h)\\
&= m_h(u_{htt}(t), w_h) + a_{1,h}(u_h(t), w_h) + a_{2,h}(u_{ht}(t), w_h)\\
&- [m_h((\mathcal{E}_h u(t))_{tt}, w_h) + a_{1,h}(\mathcal{E}_h u(t), w_h) + a_{2,h}((\mathcal{E}_h u(t))_t, w_h)]\\
&= (f_h(t) - f_u(t), w_h) - m_h((\mathcal{E}_h u(t))_{tt}, w_h)\\
&= (f_h(t) - f(t), w_h) + (u_{tt}(t), w_h) - m_h((\mathcal{E}_h u(t))_{tt}, w_h)\\
&= (f_h(t) - f(t), w_h) + m_h(L_h u_{tt}(t) - (\mathcal{E}_h u(t))_{tt}, w_h).
\end{aligned}$$

Now, setting $\eta = L_h u - \mathcal{E}_h u$ and rearranging the above equation, we obtain

$$\begin{aligned}
&\frac{d}{dt} m_h(\theta_t(t), w_h) - m_h(\theta_t(t), w_{ht}) + a_{1,h}(\theta(t), w_h) + a_{2,h}(\theta_t(t), w_h)\\
&= (f_h(t) - f(t), w_h) + m_h(\eta_{tt}(t), w_h)\\
&= (f_h(t) - f(t), w_h) + \frac{d}{dt} m_h(\eta_t(t), w_h) - m_h(\eta_t(t), w_{ht}).
\end{aligned} \tag{5.3.25}$$

Next, for some $\varsigma \in [0,T]$, we define

$$\widehat{\theta}(\cdot, t) = \int_t^{\varsigma} \theta(\cdot, s) ds, \quad 0 \leq t \leq T.$$

Then, clearly $\widehat{\theta}(\cdot,\varsigma)=0$ and $\widehat{\theta}_t(\cdot,t)=-\theta(\cdot,t)$, $0\le t\le T$. Substitute $w_h=\widehat{\theta}(t)\in W_h^m$ in (5.3.25) to have

$$\begin{aligned}&\frac{d}{dt}m_h(\theta_t(t),\widehat{\theta}(t))+m_h(\theta_t(t),\theta(t))+a_{1,h}(\theta(t),\widehat{\theta}(t))+a_{2,h}(\theta_t(t),\widehat{\theta}(t))\\&=(f_h(t)-f(t),\widehat{\theta}(t))+\frac{d}{dt}m_h(\eta_t(t),\widehat{\theta}(t))+m_h(\eta_t(t),\theta(t)).\end{aligned}$$

Since $\eta_t(t)-\theta_t(t)=L_hu_t(t)-u_{ht}(t)$, the above equation reduces to

$$\begin{aligned}&\frac{1}{2}\frac{d}{dt}m_h(\theta(t),\theta(t))-\frac{1}{2}\frac{d}{dt}a_{1,h}(\widehat{\theta}(t),\widehat{\theta}(t))+\frac{d}{dt}a_{2,h}(\theta(t),\widehat{\theta}(t))+a_{2,h}(\theta(t),\theta(t))\\&=(f_h(t)-f(t),\widehat{\theta}(t))+\frac{d}{dt}m_h(L_hu_t(t)-u_{ht}(t),\widehat{\theta}(t))+m_h(\eta_t(t),\theta(t)).\end{aligned}$$

Integrating above equation from 0 to ς, and then using the facts $\theta(0)=0=\theta_t(0)$ and $\widehat{\theta}(\varsigma)=0$, we obtain

$$\begin{aligned}&\frac{1}{2}m_h(\theta(\varsigma),\theta(\varsigma))+\frac{1}{2}a_{1,h}(\widehat{\theta}(0),\widehat{\theta}(0))+\int_0^{\varsigma}a_{2,h}(\theta(t),\theta(t))dt\\&=\int_0^{\varsigma}(f_h(t)-f(t),\widehat{\theta}(t))dt+m_h(u_{ht}(0)-L_hu_t(0),\widehat{\theta}(0))+\int_0^{\varsigma}m_h(\eta_t(t),\theta(t))dt\\&=:I_1+I_2+I_3.\end{aligned}\tag{5.3.26}$$

Since $\theta(t)$ is continuous in t, we set ς in such a way that

$$\|\theta(\varsigma)\|=\sup_{0\le t\le T}\|\theta(t)\|,\tag{5.3.27}$$

which yields $\|\widehat{\theta}(t)\|\le C\|\theta(\varsigma)\|$ for all $t\in(0,T]$.

Next, we try to bound each of the term appeared in the right side of (5.3.26). For the term I_1, from Lemma 1.4.6, we have

$$(f_h(t)-f(t),\widehat{\theta}(t))\le\|f_h(t)-f(t)\|\|\widehat{\theta}(t)\|\le Ch^{m+1}|f(t)|_{m+1}\|\widehat{\theta}(t)\|,$$

which together with (5.3.27) yields

$$\int_0^{\varsigma}(f_h(t)-f(t),\widehat{\theta}(t))dt\le Ch^{m+1}\int_0^{\varsigma}|f(t)|_{m+1}\|\widehat{\theta}(t)\|dt\le Ch^{m+1}\|\theta(\varsigma)\|\|f\|_{L^1(H^{m+1})}.\tag{5.3.28}$$

Desired bound for the term I_2 follows from the following estimate

$$\begin{aligned} m_h(u_{ht}(0) - L_h u_t(0), \widehat{\theta}(0)) \leq & (1+\beta_0)\|u_{ht}(0) - L_h u_t(0)\|\|\widehat{\theta}(0)\| \\ \leq & C\|R_h^2 v_0 - L_h v_0\|\|\theta(\varsigma)\| \\ \leq & Ch^{m+1}|v_0|_{m+1}\|\theta(\varsigma)\|. \end{aligned} \tag{5.3.29}$$

Then for the term I_3, Lemma 4.3.5 leads to

$$\begin{aligned} \int_0^\varsigma m_h(\eta_t(t), \theta(t))dt \leq & C\int_0^\varsigma \|\eta_t(t)\|\|\theta(t)\|dt \\ \leq & C\|\theta(\varsigma)\| \int_0^\varsigma \left(\|L_h u_t(t) - u_t(t)\| + \|(\mathcal{E}_h u)_t(t) - u_t(t)\|\right) dt \\ \leq & C\|\theta(\varsigma)\| \left(h^{m+1}\int_0^\varsigma |u_t(t)|_{m+1}dt + \|(\mathcal{E}_h u)_t(t) - u_t(t)\|_{L^2(L^2)} \right) \\ \leq & Ch^{m+1}\|\theta(\varsigma)\| \left(|u_0|_{m+1} + \|u\|_{H^1(H^{m+1})} \right). \end{aligned} \tag{5.3.30}$$

Plugging the estimates (5.3.28)-(5.3.30) in (5.3.26), and using coercivity property of m_h and $a_{i,h}(i = 1,\ 2)$, we obtain

$$\begin{aligned} & \|\theta(\varsigma)\|^2 + |\widehat{\theta}(0)|_1^2 + \int_0^\varsigma |\theta(t)|_1^2 dt \\ & \leq Ch^{m+1}\left(|u_0|_{m+1} + |v_0|_{m+1} + \|u\|_{H^1(H^{m+1})} + \|f\|_{L^1(H^{m+1})} \right) \|\theta(\varsigma)\|, \end{aligned}$$

which yields

$$\|\theta(\varsigma)\| \leq Ch^{m+1}\left(|u_0|_{m+1} + |v_0|_{m+1} + \|u\|_{H^1(H^{m+1})} + \|f\|_{L^1(H^{m+1})} \right).$$

Hence,

$$\|\theta(t)\| \leq \|\theta(\varsigma)\| \leq Ch^{m+1}\left(|u_0|_{m+1} + |v_0|_{m+1} + \|u\|_{H^1(H^{m+1})} + \|f\|_{L^1(H^{m+1})} \right). \tag{5.3.31}$$

Finally, from the estimates in (5.3.24) and (5.3.31) along with (5.3.23), we get the theorem.

□

5.4 Error Analysis for the Fully Discrete Problems

In this section, we will formulate the Crank-Nicolson scheme (implicit second-order Newmark scheme) based fully discrete approximation to the model problem (5.1.1)-(5.1.2) and

derive the optimal order error estimate in $L^\infty(L^2)$ norm. For the error analysis, we closely follow the technique used in Baker [13] with a modification to include the damping term.

Let us write $\vartheta = u_t$, where ϑ is an auxiliary unknown. Then, our model equation (5.1.1) can be rewritten as the following system of first order equations in t.

$$\begin{cases} u_t - \vartheta = 0 \text{ in } \Omega \times (0,T], \\ \vartheta_t - \nabla \cdot (\sigma(x)\nabla u + \epsilon(x)\nabla \vartheta) = f \text{ in } \Omega \times (0,T]. \end{cases} \tag{5.4.1}$$

Now, employing Crank-Nicolson fully discrete scheme to both the equations in (5.4.1), we obtain the fully discretized problem defined as: For $n = 1, 2, \cdots, N-1$, find $\mathcal{U}^n, \vartheta^n \in W_h^m$ such that

$$\begin{cases} \partial_\tau \mathcal{U}^n = \vartheta^{n+\frac{1}{2}}, \\ m_h(\partial_\tau \vartheta^n, w) + a_{1,h}(\mathcal{U}^{n+\frac{1}{2}}, w) + a_{2,h}(\vartheta^{n+\frac{1}{2}}, w) = (f_h^{n+\frac{1}{2}}, w) \ \forall\ w \in W_h^m, \\ \mathcal{U}^0 = R_h^2 u_0, \vartheta^0 = R_h^2 v_0. \end{cases} \tag{5.4.2}$$

Regarding the existence of unique solution $\mathcal{U}^n$ to the fully discrete problem, we have the following lemma.

Lemma 5.4.1. *There exists a unique sequence $\{\mathcal{U}^n\}_{n=0}^N$ which satisfies the problem (5.4.2).*

Proof. From (5.4.2), for $n \geq 0$, ϑ^{n+1} satisfies

$$\begin{aligned} &m_h(\vartheta^{n+1}, w) + \left(\frac{\tau^2}{4}\right) a_{1,h}(\vartheta^{n+1}, w) + \left(\frac{\tau}{2}\right) a_{2,h}(\vartheta^{n+1}, w) \\ &= m_h(\vartheta^n, w) - \left(\frac{\tau^2}{4}\right) a_{1,h}(\vartheta^n, w) - \tau a_{1,h}(\mathcal{U}^n, w) - \left(\frac{\tau}{2}\right) a_{2,h}(\vartheta^n, w) + \tau(f_h^{n+\frac{1}{2}}, w) \ \forall w \in W_h^m. \end{aligned}$$

Since, the bilinear forms m_h and $a_{i,h}$, $i = 1, 2$ are positive definite, ϑ^{n+1} exists uniquely and hence from the first part of (5.4.2), there exists unique $\mathcal{U}^{n+1}$, $n = 0, 1, \cdots, N-1$. □

Towards estimating the error $e_h^n := u^n - \mathcal{U}^n$, we define the auxiliary functions $\xi^n := u_h^n - \mathcal{U}^n$ and $\eta^n = u_{ht}^n - \vartheta^n$ for $n = 1, 2, \cdots, N$.

Lemma 5.4.2. *Let u_h^n and $\mathcal{U}^n$ solution of (5.2.2) and (5.4.2) at time $t = t_n$, respectively. Then, we have*

$$\max_{0 \leq n \leq N} \|\xi^n\|^2 \leq C\tau^4 \left(\int_0^T \|u_{htttt}(t)\|^2 dt + \int_0^T \|u_{httt}(t)\|^2 dt + \int_0^T |u_{htttt}(t)|_1^2 dt + \int_0^T |u_{httt}(t)|_1^2 dt \right).$$

Proof. From (5.2.2), for $t = t_{n+\frac{1}{2}}$, we get

$$m_h(\partial_\tau u_{ht}^n, w) + a_{1,h}(u_h^{n+\frac{1}{2}}, w) + a_{2,h}(u_{ht}^{n+\frac{1}{2}}, w) = (f_h^{n+\frac{1}{2}}, w) + m_h(\psi^n, w) \tag{5.4.3}$$

for all $w \in W_h^m$, where $\psi^n = \partial_\tau u_{ht}^n - u_{htt}^{n+\frac{1}{2}}$. Now, from (5.4.2) and (5.4.3), for any $w \in W_h^m$, it follows that

$$m_h(\partial_\tau \eta^n, w) + a_{1,h}(\xi^{n+\frac{1}{2}}, w) + a_{2,h}(\eta^{n+\frac{1}{2}}, w) = m_h(\psi^n, w), \ 1 \le n \le N-1. \tag{5.4.4}$$

It can be easily observed using first part of (5.4.2) that

$$\partial_\tau \xi^n = \eta^{n+\frac{1}{2}} + \partial_\tau u_h^n - u_{ht}^{n+\frac{1}{2}} = \eta^{n+\frac{1}{2}} + \sigma^n, \tag{5.4.5}$$

where $\sigma^n = \partial_\tau u_h^n - u_{ht}^{n+\frac{1}{2}}$, $1 \le n \le N-1$. Again, note that

$$\xi^n = \tau \sum_{m=0}^{n-1} \partial_\tau \xi^m \text{ and } \eta^n = \tau \sum_{m=0}^{n-1} \partial_\tau \eta^m.$$

Hence, from (5.4.5), we obtain

$$\begin{aligned} \partial_\tau \xi^n &= \frac{\tau}{2}\left[\sum_{m=0}^{n} \partial_\tau \eta^m + \sum_{m=0}^{n-1} \partial_\tau \eta^m\right] + \sigma^n, \\ \xi^{n+\frac{1}{2}} &= \frac{\tau}{2}\left[\sum_{m=0}^{n} \eta^{m+\frac{1}{2}} + \sum_{m=0}^{n-1} \eta^{m+\frac{1}{2}}\right] + \frac{\tau}{2}\left[\sum_{m=0}^{n} \sigma^m + \sum_{m=0}^{n-1} \sigma^m\right]. \end{aligned} \tag{5.4.6}$$

Next, we introduce a sequence $\{\alpha^n\}_{n=0}^N$ as

$$\alpha^0 = 0, \ \alpha^n = \tau \sum_{m=0}^{n-1} \xi^{m+\frac{1}{2}}, \ n = 1, 2, \cdots, N.$$

Then, using the fact that $\xi^0 = u_h^0 - \mathcal{U}^0 = 0$, we observe that

$$\alpha^{\frac{1}{2}} = \frac{\tau}{4}\xi^1 \text{ and } \alpha^{n+\frac{1}{2}} = \frac{\tau}{2}\left[\sum_{m=0}^{n} \xi^{m+\frac{1}{2}} + \sum_{m=0}^{n-1} \xi^{m+\frac{1}{2}}\right], \ n = 1, 2, \cdots, N-1. \tag{5.4.7}$$

Using $\eta^0 = u_{ht}^0 - \vartheta^0 = 0$, from (5.4.5), it follows that

$$\eta^1 = \frac{2}{\tau}\xi^1 - 2\sigma^0. \tag{5.4.8}$$

Hence, for $n = 0$, above identity (5.4.8) together with (5.4.4) leads to

$$\left(\frac{2}{\tau^2}\right) m_h(\xi^1, w)+\frac{1}{2}a_{1,h}(\xi^1, w)+\left(\frac{1}{\tau}\right) a_{2,h}(\xi^1, w) = m_h(\psi^0, w)+\left(\frac{2}{\tau}\right)m_h(\sigma^0, w)+a_{2,h}(\sigma^0, w),$$

for all $w \in W_h^m$. We now make the choice $w = \xi^1 = \frac{2}{\tau}\alpha^1$ to obtain

$$\begin{aligned}&\left(\frac{2}{\tau^2}\right) m_h(\xi^1, \xi^1) + \left(\frac{2}{\tau^2}\right) a_{1,h}(\alpha^1, \alpha^1) + \left(\frac{1}{\tau}\right) a_{2,h}(\xi^1, \xi^1)\\ &= m_h(\psi^0, \xi^1) + \left(\frac{2}{\tau}\right) m_h(\sigma^0, \xi^1) + a_{2,h}(\sigma^0, \xi^1).\end{aligned}$$

Using the continuity and coercivity properties of m_h, $a_{1,h}$ and $a_{2,h}$, and then employing Young's inequality, the above equation yield

$$\begin{aligned}\|\xi^1\|^2 + |\alpha^1|_1^2 + \tau|\xi^1|_1^2 &\le C\left(\frac{\tau^2}{2}\|\psi^0\|\|\xi^1\| + \tau\|\sigma^0\|\|\xi^1\| + \frac{\tau^2}{2}|\sigma^0|_1|\xi^1|_1\right)\\ &\le C\left(\frac{\tau^4}{8\delta}\|\psi^0\|^2 + \frac{\tau^2}{2\delta}\|\sigma^0\|^2 + \frac{\tau^4}{8\delta}|\sigma^0|_1^2 + \delta\|\xi^1\|^2 + \frac{\delta}{2}|\xi^1|_1^2\right).\end{aligned}$$

Then, for suitable $\delta > 0$ using and the fact $|\xi^1|_1^2 \ge 0$, we obtain

$$\|\xi^1\|^2 + |\alpha^1|_1^2 \le C\left(\tau^4\|\psi^0\|^2 + \tau^2\|\sigma^0\|^2 + \tau^4|\sigma^0|_1^2\right). \tag{5.4.9}$$

Again, from (5.4.6) and (5.4.7), for any $w \in W_h^m$, and $1 \le n \le N-1$, we have

$$\begin{aligned}&m_h(\partial_\tau\xi^n, w) + a_{1,h}(\alpha^{n+\frac{1}{2}}, w) + a_{2,h}(\xi^{n+\frac{1}{2}}, w)\\ &= \frac{\tau}{2}m_h\left(\partial_\tau\eta^n + 2\sum_{m=0}^{n-1}\partial_\tau\eta^m, w\right) + m_h(\sigma^n, w) + \frac{\tau}{2}a_{1,h}\left(\xi^{n+\frac{1}{2}} + 2\sum_{m=0}^{n-1}\xi^{m+\frac{1}{2}}, w\right)\\ &\quad + \frac{\tau}{2}a_{2,h}\left(\eta^{n+\frac{1}{2}} + 2\sum_{m=0}^{n-1}\eta^{m+\frac{1}{2}}, w\right) + \frac{\tau}{2}a_{2,h}\left(\sigma^n + 2\sum_{m=0}^{n-1}\sigma^m, w\right).\end{aligned} \tag{5.4.10}$$

For our convenience, we define

$$\mathcal{E}_1^n := \frac{\tau}{2}\psi^n + \tau\sum_{m=0}^{n-1}\psi^m + \sigma^n \;\;\&\;\; \mathcal{E}_2^n := \frac{\tau}{2}\sigma^n + \tau\sum_{m=0}^{n-1}\sigma^m.$$

Using (5.4.4), for any $w \in W_h^m$, equation (5.4.10) becomes

$$m_h(\partial_\tau\xi^n, w) + a_{1,h}(\alpha^{n+\frac{1}{2}}, w) + a_{2,h}(\xi^{n+\frac{1}{2}}, w) = m_h(\mathcal{E}_1^n, w) + a_{2,h}(\mathcal{E}_2^n, w).$$

In particular, for $w = \xi^{n+\frac{1}{2}} = \partial_\tau \alpha^n$, we obtain

$$m_h(\xi^{n+1},\xi^{n+1}) - m_h(\xi^n,\xi^n) + 2\tau a_{2,h}(\xi^{n+\frac{1}{2}},\xi^{n+\frac{1}{2}}) + a_{1,h}(\alpha^{n+1},\alpha^{n+1}) - a_{1,h}(\alpha^n,\alpha^n)$$
$$= 2\tau m_h(\mathcal{E}_1^n,\xi^{n+\frac{1}{2}}) + 2\tau a_{2,h}(\mathcal{E}_2^n,\xi^{n+\frac{1}{2}}).$$

Using the continuity and coercivity properties of m_h, $a_{1,h}$ and $a_{2,h}$, and then employing Young's inequality, we get

$$\begin{aligned}
&\|\xi^{n+1}\|^2 - \|\xi^n\|^2 + \tau|\xi^{n+\frac{1}{2}}|_1^2 + |\alpha^{n+1}|_1^2 - |\alpha^n|_1^2 \\
&\leq C\tau\left(\|\mathcal{E}_1^n\|\|\xi^{n+\frac{1}{2}}\| + |\mathcal{E}_2^n|_1|\xi^{n+\frac{1}{2}}|_1\right) \\
&\leq C\tau\left(\frac{1}{2\delta_1}\|\mathcal{E}_1^n\|^2 + \frac{\delta_1}{2}\|\xi^{n+\frac{1}{2}}\|^2 + \frac{1}{2\delta_2}|\mathcal{E}_2^n|_1^2 + \frac{\delta_2}{2}|\xi^{n+\frac{1}{2}}|_1^2\right).
\end{aligned}$$

Now, setting suitable $\delta_2 > 0$ and then neglecting $|\xi^{n+\frac{1}{2}}|_1^2 > 0$, we get

$$\|\xi^{n+1}\|^2 - \|\xi^n\|^2 + |\alpha^{n+1}|_1^2 - |\alpha^n|_1^2 \leq C\tau\left(\|\mathcal{E}_1^n\|^2 + |\mathcal{E}_2^n|_1^2 + \hat{\delta}_1\|\xi^{n+\frac{1}{2}}\|^2\right).$$

For $2 \leq l \leq N$, taking sum from $n = 1$ to $n = l-1$, we arrive at

$$\begin{aligned}
\|\xi^l\|^2 + |\alpha^l|_1^2 &\leq \|\xi^1\|^2 + |\alpha^1|_1^2 + C\tau\left(\sum_{n=1}^{l-1}\left(\|\mathcal{E}_1^n\|^2 + |\mathcal{E}_2^n|_1^2\right) + \hat{\delta}_1\sum_{n=1}^{l-1}\|\xi^{n+\frac{1}{2}}\|^2\right) \\
&\leq \|\xi^1\|^2 + |\alpha^1|_1^2 + C\left(\tau\sum_{n=1}^{l-1}\left(\|\mathcal{E}_1^n\|^2 + |\mathcal{E}_2^n|_1^2\right) + \hat{\delta}_1\max_{2\leq n\leq N}\|\xi^n\|^2\right).
\end{aligned}$$

Since $|\alpha^l|_1^2 \geq 0$, a suitable $\hat{\delta}_1$ yields

$$\max_{2\leq n\leq N}\|\xi^n\|^2 \leq C\left(\|\xi^1\|^2 + |\alpha^1|_1^2 + \tau\sum_{n=1}^{l-1}\left(\|\mathcal{E}_1^n\|^2 + |\mathcal{E}_2^n|_1^2\right)\right).$$

Hence, from (5.4.9), the above equation is reduced to

$$\max_{1\leq n\leq N}\|\xi^n\|^2 \leq C\left(\tau^4\|\psi^0\|^2 + \tau^2\|\sigma^0\|^2 + \tau^4|\sigma^0|_1^2 + \tau\sum_{n=1}^{l-1}\left(\|\mathcal{E}_1^n\|^2 + |\mathcal{E}_2^n|_1^2\right)\right). \tag{5.4.11}$$

Now, we need to derive the estimates for both $\mathcal{E}_1^n$ and $\mathcal{E}_2^n$. For the term $\mathcal{E}_1^n$, using triangle

inequality, we have

$$\begin{aligned}\|\mathcal{E}_1^n\|^2 &\leq C\bigg(\frac{\tau^2}{4}\|\psi^n\|^2+\tau^2\Big\|\sum_{m=0}^{n-1}\psi^m\Big\|^2+\|\sigma^n\|^2\bigg)\\ &\leq C\bigg(\tau^2\|\psi^n\|^2+\tau^2N\sum_{m=0}^{n-1}\|\psi^m\|^2+\|\sigma^n\|^2\bigg)\\ &\leq C\bigg(\tau^2\|\psi^n\|^2+\tau T\sum_{m=0}^{n-1}\|\psi^m\|^2+\|\sigma^n\|^2\bigg).\end{aligned}$$

Then, we use Lemma 4.3.2 to obtain

$$\|\mathcal{E}_1^n\|^2 \leq C\bigg(\tau^5\int_{t_n}^{t_{n+1}}\|u_{htttt}(t)\|^2dt+\tau^4\int_0^T\|u_{htttt}(t)\|^2dt+\tau^3\int_{t_n}^{t_{n+1}}\|u_{htt t}(t)\|^2dt\bigg). \tag{5.4.12}$$

Proceeding in a similar manner, we have the following estimate for the term $\mathcal{E}_2^n$

$$|\mathcal{E}_2^n|_1^2 \leq C\bigg(\tau^5\int_{t_n}^{t_{n+1}}|u_{htt t}(t)|_1^2dt+\tau^4\int_0^T|u_{htt t}(t)|_1^2dt\bigg). \tag{5.4.13}$$

Finally, using the above estimates (5.4.12)-(5.4.13) in (5.4.11), it follows that

$$\max_{1\leq n\leq N}\|\xi^n\|^2 \leq C\tau^4\bigg(\int_0^T\|u_{htttt}(t)\|^2dt+\int_0^T\|u_{htt t}(t)\|^2dt+\int_0^T|u_{htttt}(t)|_1^2dt+\int_0^T|u_{htt t}(t)|_1^2dt\bigg).$$

This completes the derivation of the desired estimate. □

Now, we are in a position to discuss the main result of this section.

Theorem 5.4.1. *Let u^n and $\mathcal{U}^n$ solution of (5.1.1) and (5.4.2) at time $t=t_n$, respectively. Assume that $u_0, v_0 \in H^{m+1}(\Omega)\cap H^6(\Omega)$, $u \in H^1(0,T;H^{m+1}(\Omega))$ and $f \in L^1(0,T;H^{m+1}(\Omega))\cap H^3(0,T;H^4(\Omega))$, then for all $t\in(0,T]$, we have*

$$\begin{aligned}\max_{1\leq n\leq N}\|u^n-\mathcal{U}^n\| \leq& Ch^{m+1}\left(|u_0|_{m+1}+|v_0|_{m+1}+\|u\|_{H^1(H^{m+1})}+\|f\|_{L^1(H^{m+1})}\right)\\ &+\tilde{C}\tau^2\left(|u_0|_6+|v_0|_6+\|f\|_{H^3(H^4)}\right).\end{aligned}$$

Proof. We divide the error as

$$u^n-\mathcal{U}^n := u^n-u_h^n+\xi^n.$$

Now, by triangle inequality, Lemma 5.4.2 and Theorem 5.3.2, we have

$$\begin{aligned}
&\max_{1\le n\le N} \|u^n - \mathcal{U}^n\| \\
&\le Ch^{m+1}\left(|u_0|_{m+1} + |v_0|_{m+1} + \|u\|_{H^1(H^{m+1})} + \|f\|_{L^1(H^{m+1})}\right) \\
&+ \tilde{C}\tau^2\left(\int_0^T \|u_{htttt}(t)\|^2 dt + \int_0^T \|u_{httt}(t)\|^2 dt + \int_0^T |u_{htttt}(t)|_1^2 dt + \int_0^T |u_{httt}(t)|_1^2 dt\right)^{\frac{1}{2}}.
\end{aligned}$$

Finally, from Lemma 5.3.2, we obtain

$$\begin{aligned}
\max_{1\le n\le N} \|\mathcal{U}^n - u^n\| \le& Ch^{m+1}\left(|u_0|_{m+1} + |v_0|_{m+1} + \|u\|_{H^1(H^{m+1})} + \|f\|_{L^1(H^{m+1})}\right) \\
&+ \tilde{C}\tau^2\left(|u_0|_6 + |v_0|_6 + \|f\|_{H^3(H^4)}\right).
\end{aligned}$$

□

5.5 Numerical Results

This section includes some numerical experiments conducted to test the practical performance of the proposed algorithm. To show the method is flexible to handle any polygonal discretization, several forms of polygonal meshes, including Voronoi ($\mathcal{V}_h$), distorted square ($\mathcal{S}_h$) and distorted polygon ($\mathcal{P}_h$) have been taken into consideration. In Example 5.5.1, we implement the proposed virtual element algorithm with all three types of meshes by considering a smooth solution to test the optimal convergence. Next, we have considered a low regular solution in a convex domain in Example 5.5.2. Further, in Example 5.5.3 and Example 5.5.4, we have tested our algorithm for smooth solutions in L-shaped domain and circular domain, respectively. Finally, we have discussed a numerical example with high-contrast coefficients in Example 5.5.5.

In all the examples, we have consider the model problem (5.1.1)-(5.1.2) and source function f, initial data $\{u_0, v_0\}$ are chosen according to the choice of exact solution. The time interval set to be $[0, 1]$ and the spatial domain Ω is considered to be $(0, 1) \times (0, 1)$ or else specified.

Example 5.5.1. (Smooth solution with convex domain) We set the exact solution to the model problem (5.1.1)-(5.1.2) as

$$u(x, y, t) = t^2 \sin(\pi x) \sin(\pi y)$$

Table 5.5.1: L^2 and H^1 errors at $T = 1$ for the mesh $\mathcal{V}_h$ in Example 5.5.1

order	h	$\|u - u_h\|$	EOC	$\|u - u_h\|_1$	EOC
$m = 1$	0.1768	$2.61748e-02$	-	$9.70000e-02$	-
	0.1250	$1.25773e-02$	2.1147	$4.94816e-02$	1.9422
	0.0884	$6.30157e-03$	1.9941	$3.73415e-02$	0.8122
	0.0625	$3.17611e-03$	1.9769	$2.48356e-02$	1.1767
	0.0442	$1.58552e-03$	2.0046	$1.73213e-02$	1.0397
$m = 2$	0.1768	$1.15631e-03$	-	$1.06699e-02$	-
	0.1250	$4.11688e-04$	2.9798	$4.90870e-03$	2.2403
	0.0884	$1.51656e-04$	2.8768	$2.65949e-03$	1.7684
	0.0625	$5.38738e-05$	2.9909	$1.20649e-03$	2.2807
	0.0442	$1.88562e-05$	3.0291	$6.09103e-04$	1.9721
$m = 3$	0.1768	$3.82548e-04$	-	$4.71982e-03$	-
	0.1250	$8.95659e-05$	4.1892	$1.61077e-03$	3.1020
	0.0884	$1.51901e-04$	4.0435	$6.16064e-04$	2.7732
	0.0625	$5.35002e-06$	4.0871	$2.17125e-04$	3.0091
	0.0442	$1.30602e-06$	4.0687	$7.77034e-05$	2.9649

and coefficients $\sigma = x + y + 1$ and $\epsilon = x^2 + y^2 + 1$. We have implemented the VEM algorithm with all the three kind of mesh discretizations $\mathcal{V}_h$, $\mathcal{S}_h$ and $\mathcal{P}_h$ and polynomial order $m = 1, 2, 3$.

Table 5.5.1 presents the numerical errors and experimental order of convergence (EOC) in both L^2 norm and H^1 semi-norm at the final time $T = 1$ for the Voronoi mesh $(\mathcal{V}_h)$. Exact and approximate solutions at final time are presented in Figure 5.5.1. Figure 5.5.2 shows the log-log plots.

In Table 5.5.2, we present the numerical errors and EOC for the distorted square mesh $(\mathcal{S}_h)$. The exact solution and approximate solution are illustrated in Figure 5.5.3. Further, the log-log plots are presented in Figure 5.5.4.

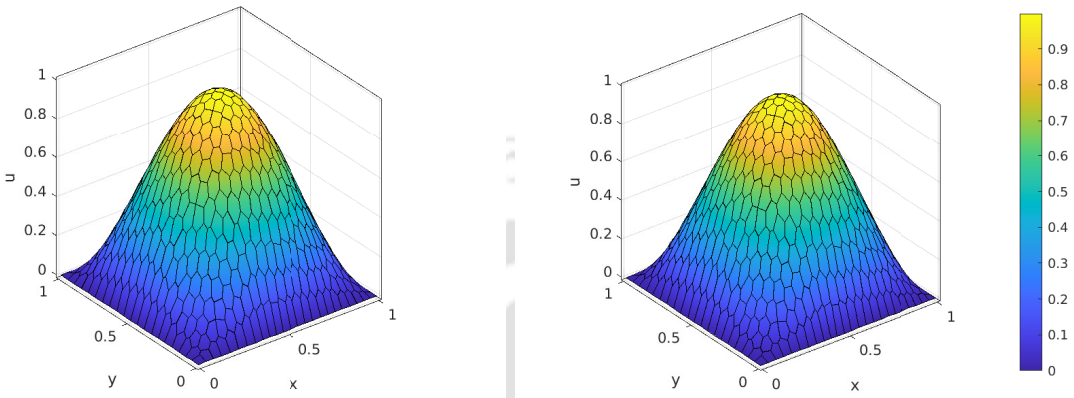

Figure 5.5.1: Approximate solution for $m = 3$ (left) with Voronoi mesh ($h = 0.0442$) and exact solution (right) at $t = 1$ in Example 5.5.1.

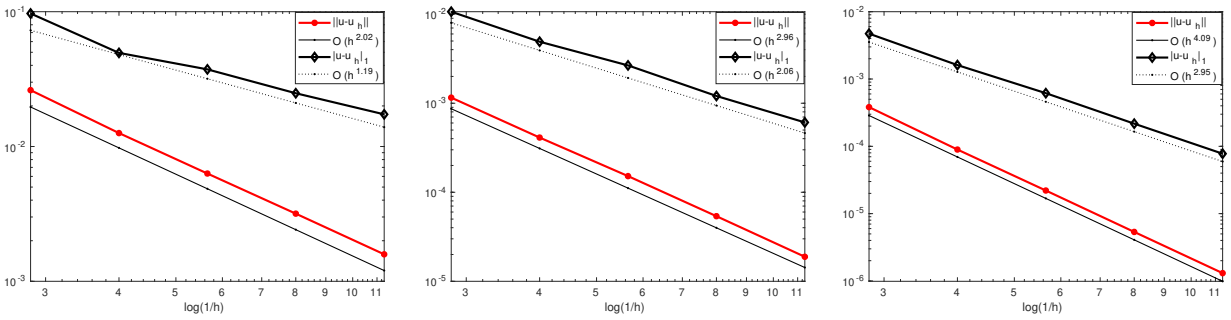

Figure 5.5.2: Log-log plots of the errors versus h at time $t = 1$ for $m = 1$ (left), $m = 2$ (center) and $m = 3$ (right) for Voronoi mesh in Example 5.5.1.

Table 5.5.2: L^2 and H^1 errors at $T = 1$ for the mesh $\mathcal{S}_h$ in Example 5.5.1

order	h	$\|u - u_h\|$	EOC	$\|u - u_h\|_1$	EOC
	1/5	$4.67166e-02$	-	$1.65063e-01$	-
$m = 1$	1/10	$1.31993e-02$	1.8235	$4.84775e-02$	1.7676
	1/15	$6.01407e-03$	1.9387	$2.20540e-02$	1.9425
	1/20	$3.41316e-03$	1.9691	$1.25085e-02$	1.9712
	1/25	$2.19373e-03$	1.9809	$8.03640e-03$	1.9827
	1/5	$3.16781e-03$	-	$2.88455e-02$	-
$m = 2$	1/10	$4.37745e-04$	2.8553	$5.78713e-03$	2.3174
	1/15	$1.30419e-04$	2.9864	$1.97029e-03$	2.6573
	1/20	$5.49871e-05$	3.0021	$8.82478e-04$	2.7920
	1/25	$2.81262e-05$	3.0043	$4.66187e-04$	2.8598
	1/5	$1.50179e-03$	-	$1.51458e-02$	-
$m = 3$	1/10	$1.28654e-04$	3.5451	$2.06526e-03$	2.8745
	1/15	$2.72339e-05$	3.8293	$6.12509e-04$	2.9977
	1/20	$8.83515e-06$	3.9131	$2.57918e-04$	3.0065
	1/25	$3.66159e-06$	3.9474	$1.31889e-04$	3.0056

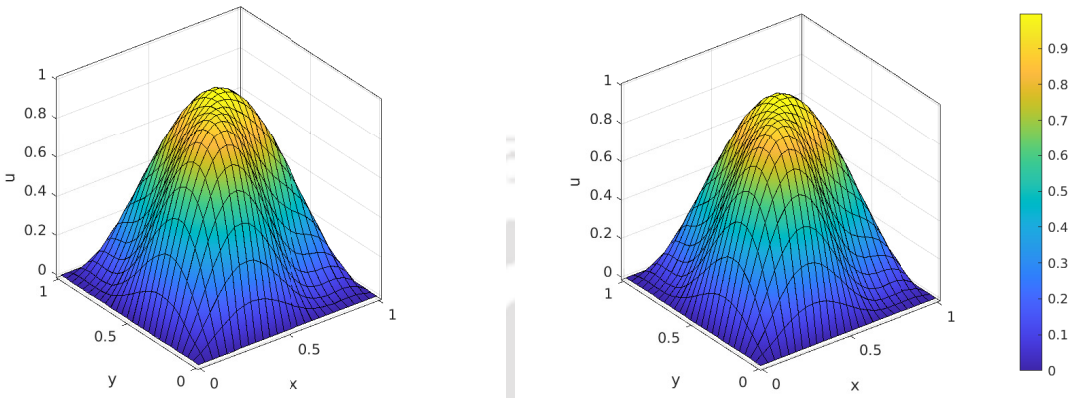

Figure 5.5.3: Approximate solution for $m = 3$ with distorted square mesh ($h = 1/25$) (left) and exact solution (right) at $t = 1$ in Example 5.5.1.

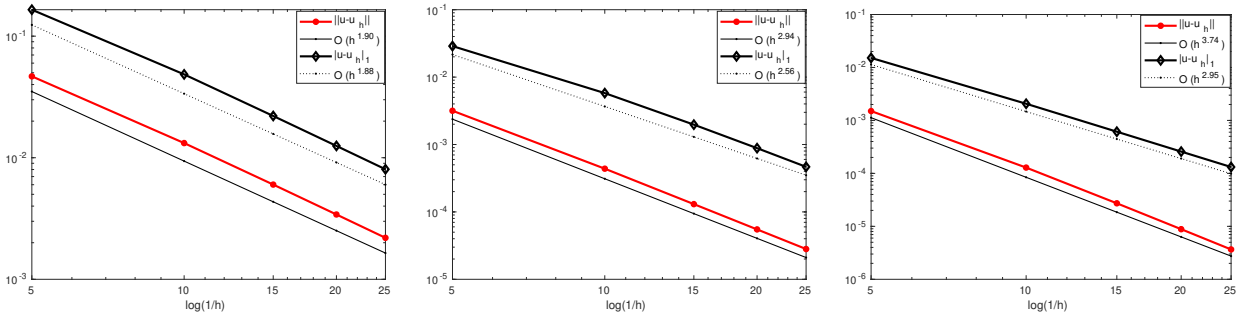

Figure 5.5.4: Log-log plots of the errors versus h at time $t = 1$ for $m = 1$ (left), $m = 2$ (center) and $m = 3$ (right) for distorted square mesh in Example 5.5.1.

Table 5.5.3: L^2 and H^1 errors at $T = 1$ for the mesh $\mathcal{P}_h$ in Example 5.5.1

order	h	$\|u - u_h\|$	EOC	$\|u - u_h\|_1$	EOC
$m = 1$	0.1768	$3.83448e-02e$	-	$1.87811e-01$	-
	0.1250	$3.83448e-02$	2.2321	$1.19431e-01$	1.3062
	0.0884	$9.54295e-03$	1.7809	$6.50830e-02$	1.7516
	0.0625	$4.79751e-03$	1.9843	$3.48073e-02$	1.8058
	0.0442	$2.38308e-03$	2.0189	$2.53114e-02$	0.9192
$m = 2$	0.1768	$2.56280e-03$	-	$2.51635e-02$	-
	0.1250	$9.56241e-04$	2.8446	$1.19214e-02$	2.1556
	0.0884	$3.47052e-04$	2.9244	$6.03260e-03$	1.9654
	0.0625	$1.21800e-04$	3.0213	$3.17480e-03$	1.8522
	0.0442	$4.40927e-05$	2.9318	$1.77272e-03$	1.6814
$m = 3$	0.1768	$1.03409e-03$	-	$1.17179e-02$	-
	0.1250	$2.52917e-04$	4.0633	$4.07680e-03$	3.0464
	0.0884	$7.40454e-05$	3.5444	$1.56346e-03$	2.7654
	0.0625	$1.92577e-05$	3.8859	$5.65798e-04$	2.9328
	0.0442	$4.78150e-06$	4.0198	$2.02913e-04$	2.9589

Table 5.5.3 depicts the numerical errors and EOC for distorted polygon mesh ($\mathcal{P}_h$). The exact solution and approximate solution are illustrated in Figure 5.5.5. The log-log plots are displayed in Figure 5.5.6.

The above observations confirm that we have achieved optimal order of convergence as per the theoretical prediction as proved in Theorem 4.4.1.

Example 5.5.2. (Low regular solution) We consider the model problem (5.1.1)-(5.1.2) on a two-dimensional domain, for which the exact solution possesses a corner singularity in spatial direction. We set the exact solution as

$$u(x, y, t) = t^2 \sin t \, x(1 - x)y(1 - y)(x^2 + y^2)^{-1+\frac{k}{2}},$$

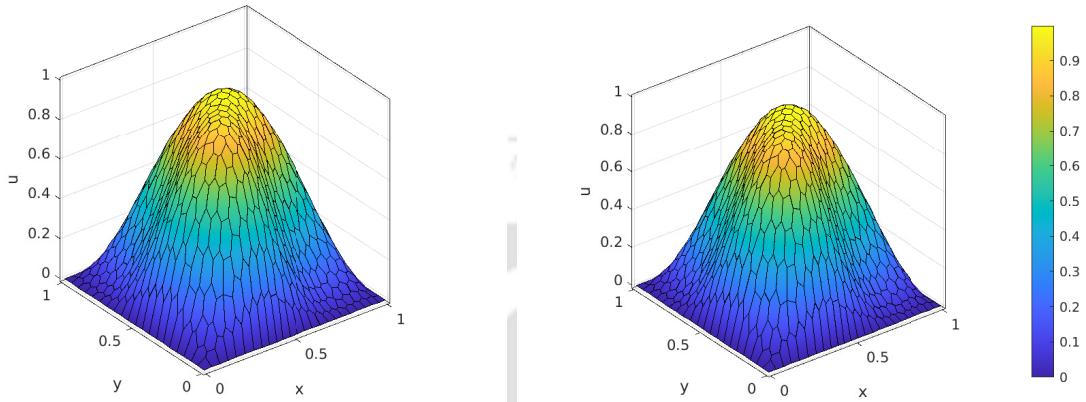

Figure 5.5.5: Approximate solution for $m = 3$ with distorted polygon mesh ($h = 0.0442$) (left) and exact solution (right) at $t = 1$ in Example 5.5.1.

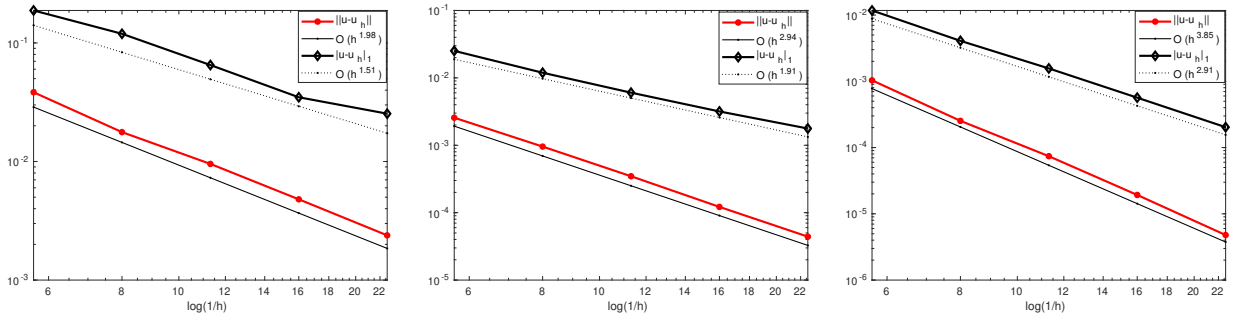

Figure 5.5.6: Log-log plots of the errors versus h at time $t = 1$ for $m = 1$ (left), $m = 2$ (center) and $m = 3$ (right) for distorted polygon mesh in Example 5.5.1.

Table 5.5.4: EOC in L^2 norm and H^1 semi-norm at $T = 1$ in Example 5.5.2

l	k	$m = 1$		$m = 2$	
		L^2-order	H^1-order	L^2-order	H^1-order
0	1	1.85	0.90	1.92	0.95
1	$\frac{1}{2}$	1.53	0.52	1.49	0.50
2	$\frac{1}{4}$	1.30	0.29	1.29	0.26
3	$\frac{1}{8}$	1.17	0.17	1.17	0.14
4	$\frac{1}{16}$	1.10	0.12	1.12	0.11
5	$\frac{1}{32}$	1.06	0.07	1.07	0.04

where $k \in (0, 1]$ and the coefficients $\sigma = \epsilon = 1$. It is easy to see that u has a singularity at the corner point $(0, 0)$ and $u \in C^\infty(0, T; H^{1+k-\delta}(\Omega))$ but $u \notin C^\infty(0, T; H^{1+k}(\Omega))$, for some positive number δ. We choose the Voronoi mesh $(\mathcal{V}_h)$ for the spatial discretization and compute the EOC in respective norms by setting $k = (1/2)^l$, $l = 0, 1, 2, 3, 4, 5$.

From Table 5.5.4, we can easily observe that the numerical order of convergence at the final time $T = 1$ remains to be $O(h^{1+k})$ in L^2 norm and $O(h^k)$ in H^1 semi-norm for linear as well as higher order methods, which is due to the low regularity of the exact solution. Figure 5.5.7 presents the contour plot of the exact and approximate solution for $k = 1/2$ at $t = 1$.

Example 5.5.3. (Smooth solution with non-convex domain) For this numerical experiment, we consider a L-shaped domain $\Omega = (0, 1) \times (0, 1) \setminus [1/2, 1) \times [1/2, 1)$. We choose the Voronoi mesh $(\mathcal{V}_h)$ for the spatial discretization. We set the exact solution to the model problem (5.1.1)-(5.1.2) as

$$u = t^2 \sin t \sin(2\pi x) \sin(2\pi y)$$

with coefficients $\sigma = \exp(x + y)$ and $\epsilon = \exp(x - y)$.

In Table 5.5.5, we show the numerical errors and EOC in L^2 norm and H^1 semi-norm at the final time $T = 1$ for linear and quadratic approximations. Figure 5.5.8 presents the contour plot of the exact and approximate solutions at $T = 1$. The order of accuracy

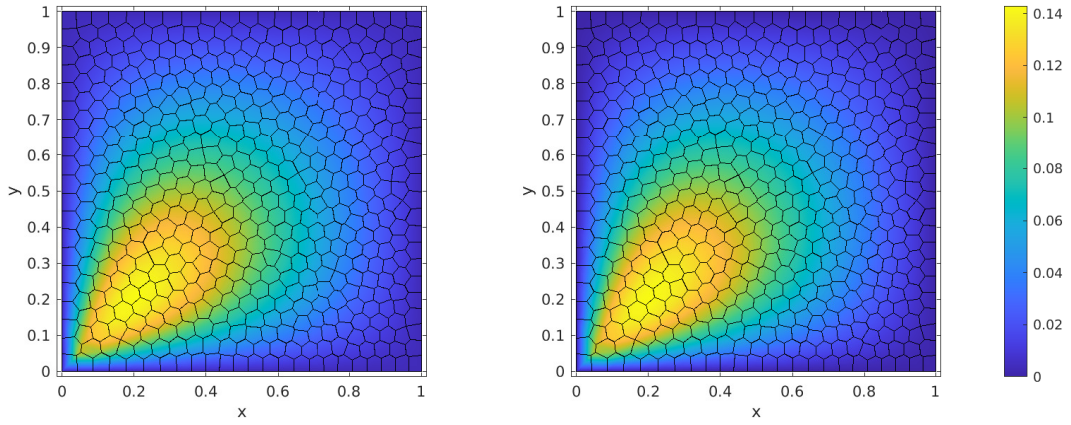

Figure 5.5.7: Approximate solution (left) for $m = 2$ ($h = 0.0442$) and exact solution (right) at $t = 1$ with $k = 0.5$ in Example 5.5.2.

obtained to be $O(h^{m+1})$ in L^2 norm and $O(h^m)$ in H^1 semi-norm. The log-log plots are presented in Figure 5.5.9.

Example 5.5.4. (Smooth solution with circular domain) In this example, we consider a circular domain Ω with center at $(0, 0)$ and radius 1. We choose Voronoi mesh $(\mathcal{V}_h)$ for the spatial discretization. We choose the exact solution to the model problem (5.1.1)-(5.1.2) to be

$$u = t^2 \sin t(1 - x^2 - y^2) \sin(\pi x) \sin(\pi y)$$

with coefficients $\sigma = \sin(x + y) + 3$ and $\epsilon = \cos(x + y) + 3$.

In Table 5.5.6, we show the numerical errors and EOC in L^2 norm and H^1 semi-norm at the final time $T = 1$ for linear and quadratic approximations. Figure 5.5.10 presents the contour plot of the exact and approximate solutions at $T = 1$. The order of accuracy obtained to be $O(h^{m+1})$ in L^2 norm and $O(h^m)$ in H^1 semi-norm. The log-log plots are presented in Figure 5.5.11.

Example 5.5.5. (Heat transport in metallic films) We consider the following problem from [54]

$$u_{tt} + \beta u_t + \delta u - \nabla \cdot (\sigma \nabla u + \epsilon \nabla u_t) = f \text{ in } \Omega \times [0, 1],$$

where $\Omega = (-1, 1) \times (-1, 1)$. This problem arises commonly in the study of heat transport in metallic films during ultrafast laser heating [104, 127]. Taking $\beta = \delta = 0$, we get the

Table 5.5.5: L^2 and H^1 errors at $T = 1$ in Example 5.5.3

order	h	$\|u - u_h\|$	EOC	$\|u - u_h\|_1$	EOC
	0.1690	$6.43252e-02$	-	$2.34265e-01$	-
$m = 1$	0.1222	$3.20003e-02$	2.1505	$1.39463e-01$	1.5975
	0.0874	$1.49289e-02$	2.2742	$8.41951e-02$	1.5053
	0.0621	$7.44547e-03$	2.0413	$4.31186e-02$	1.9635
	0.0441	$3.70905e-03$	2.0276	$3.03787e-02$	1.0190
	0.1690	$4.09895e-03$	-	$4.83320e-02$	-
$m = 2$	0.1222	$1.62075e-03$	2.8578	$2.10437e-02$	2.5610
	0.0874	$5.54743e-04$	3.1980	$9.69457e-03$	2.3118
	0.0621	$1.99082e-04$	3.0069	$4.64121e-03$	2.1613
	0.0441	$6.93271e-05$	3.0695	$1.88311e-03$	2.6248

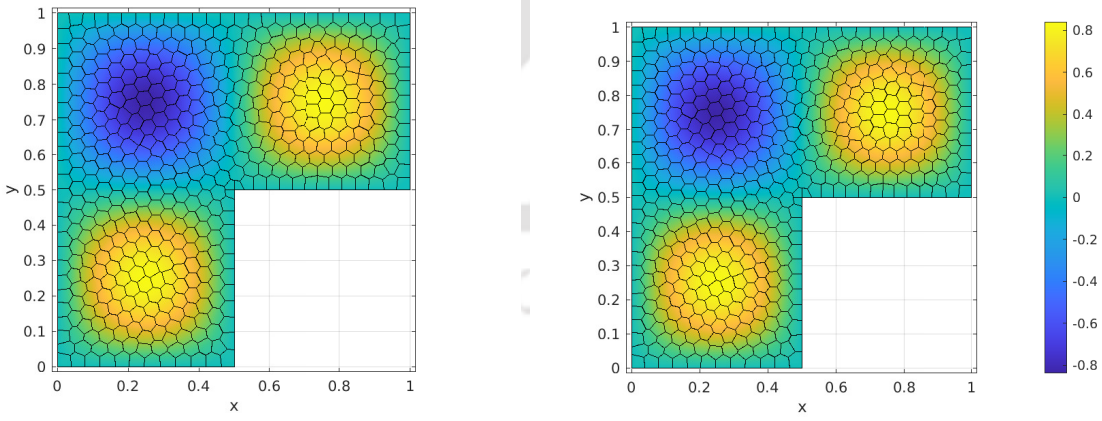

Figure 5.5.8: Approximate solution (left) for $m = 2$ ($h = 0.0441$) and exact solution (right) at $t = 1$ in Example 5.5.3.

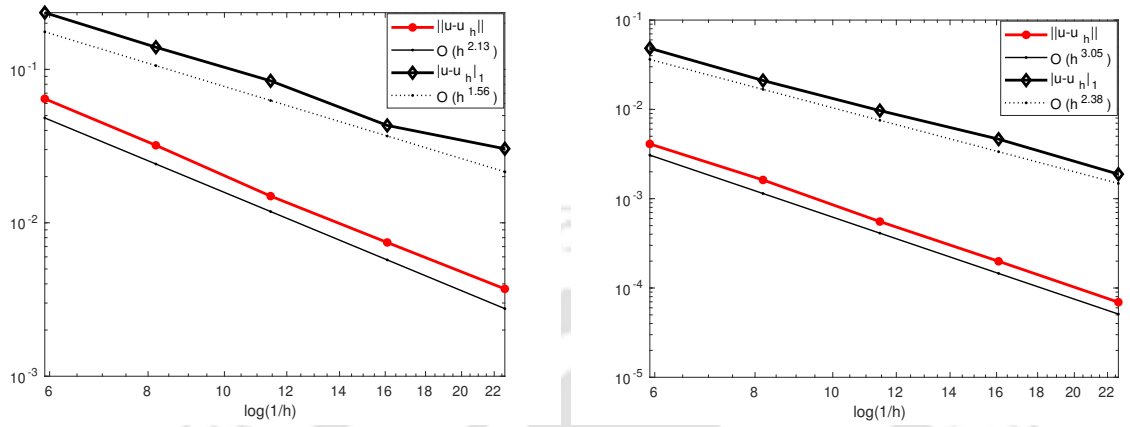

Figure 5.5.9: Log-log plots of the errors versus h at time $t = 1$ for $m = 1$ (left) and $m = 2$ (right) in Example 5.5.3.

Table 5.5.6: L^2 and H^1 errors at $T = 1$ in Example 5.5.4

	h	$\|u - u_h\|$	EOC	$\|u - u_h\|_1$	EOC
$m = 1$	0.1768	$1.04274e-01$	-	$6.05100e-01$	-
	0.1250	$5.12754e-02$	2.0481	$3.66079e-01$	1.4500
	0.0884	$2.56913e-02$	1.9940	$2.05113e-01$	1.6715
	0.0625	$1.24411e-02$	2.0923	$1.34633e-01$	1.2148
	0.0442	$6.39399e-03$	1.9206	$7.77335e-02$	1.5848
$m = 2$	0.1768	$1.22424e-02$	-	$4.89415e-02$	-
	0.1250	$4.43330e-03$	2.9309	$2.64050e-02$	1.7805
	0.0884	$1.62139e-03$	2.9023	$1.41753e-02$	1.7949
	0.0625	$6.39371e-04$	2.6850	$7.18102e-03$	1.9622
	0.0442	$2.35928e-04$	2.8766	$3.54101e-03$	2.0401

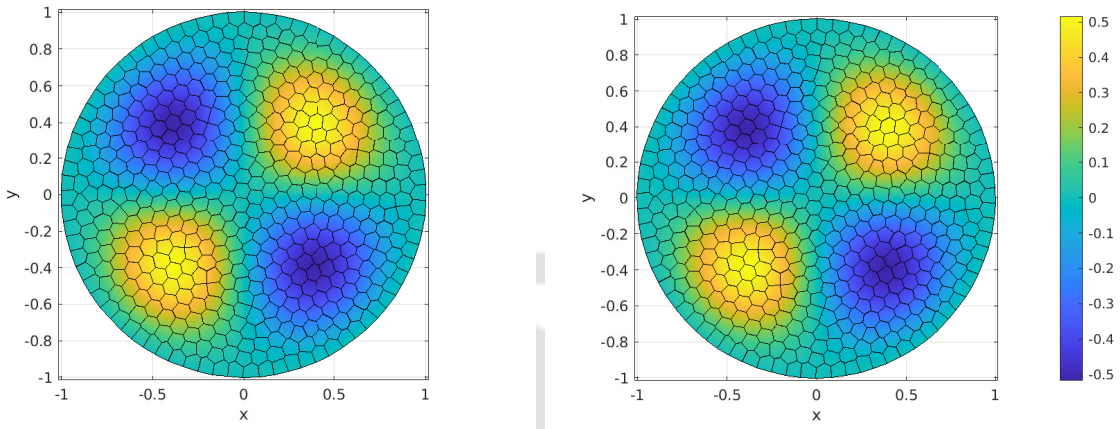

Figure 5.5.10: Approximate solution (left) for $m = 2$ ($h = 0.0442$) and exact solution (right) at $t = 1$ in Example 5.5.4.

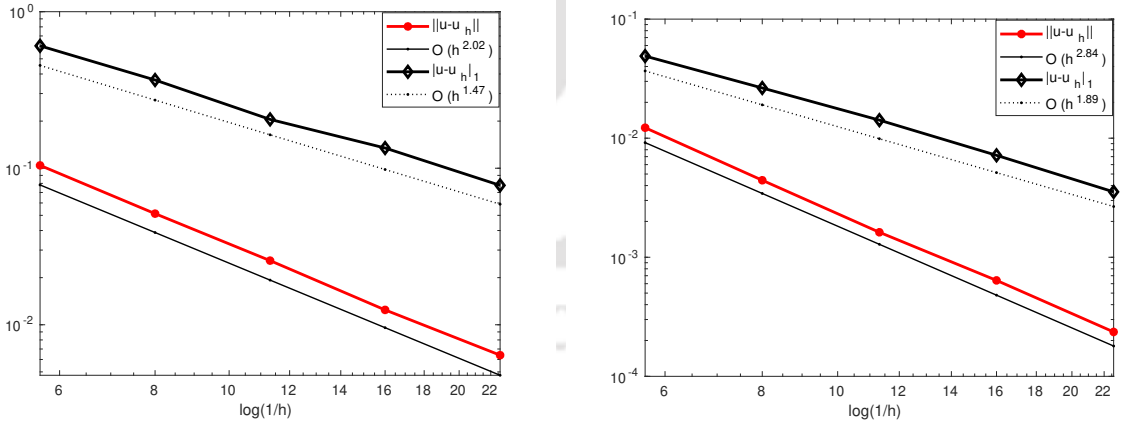

Figure 5.5.11: Log-log plots of the errors versus h at time $t = 1$ for $m = 1$ (left) and $m = 2$ (right) in Example 5.5.4.

Table 5.5.7: L^2 and H^1 errors at $T = 1$ in Example 5.5.5

	h	$\|u - u_h\|$	EOC	$\|u - u_h\|_1$	EOC
$m = 1$	0.3536	$9.26667e-02$	-	$1.82903e-01$	-
	0.2500	$4.45558e-02$	2.1129	$9.47960e-02$	1.8964
	0.1768	$2.24323e-02$	1.9801	$4.50057e-02$	2.1494
	0.1250	$1.10125e-02$	2.0529	$2.50633e-02$	1.6891
	0.0884	$5.40927e-03$	2.0513	$1.44628e-02$	1.5865
$m = 2$	0.3536	$6.51046e-03$	-	$2.76175e-02$	-
	0.2500	$2.38503e-03$	2.8975	$1.24913e-02$	2.2893
	0.1768	$8.86910e-04$	2.8543	$5.02222e-03$	2.6291
	0.1250	$3.15313e-04$	2.9840	$2.03924e-03$	2.6006
	0.0884	$1.09812e-04$	3.0435	$9.47558e-04$	2.2115

following viscoelastic wave equation.

$$u_{tt} - \nabla \cdot (\sigma \nabla u + \epsilon \nabla u_t) = f \text{ in } \Omega \times [0, 1].$$

We set the exact solution as

$$u = t^2 \exp(-t) \sin(\pi x) \sin(\pi y).$$

The physical coefficients σ and ϵ are chosen as [126]

$$(\sigma, \epsilon) = \left(\alpha_e, C_E^2\right) = \left(1.2 \times 10^{-4}, 1.44 \times 10^{8}\right),$$

where C_E represents the equivalent thermal wave speed and α_e stand for electron thermal diffusivity, respectively of the material. In Table 5.5.7, we show the numerical errors and EOC in L^2 norm and H^1 semi-norm at the final time $T = 1$ for $m = 1, 2$. Figure 5.5.12 presents the contour plot of the exact and approximate solutions at $T = 1$. The order of accuracy obtained to be $O(h^{m+1})$ in L^2 norm and $O(h^m)$ in H^1 semi-norm. The log-log plots are presented in Figure 5.5.13.

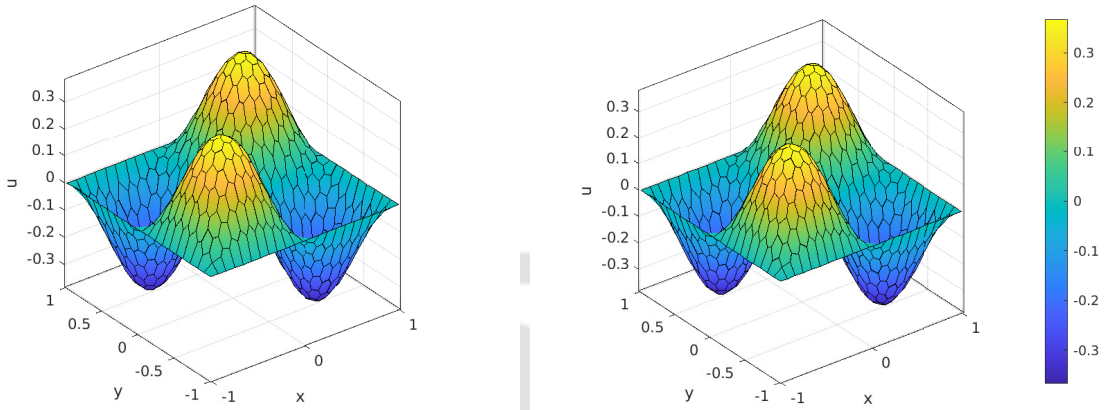

Figure 5.5.12: Approximate solution (left) for $m = 2$ ($h = 0.0884$) and exact solution (right) at $t = 1$ in Example 5.5.5.

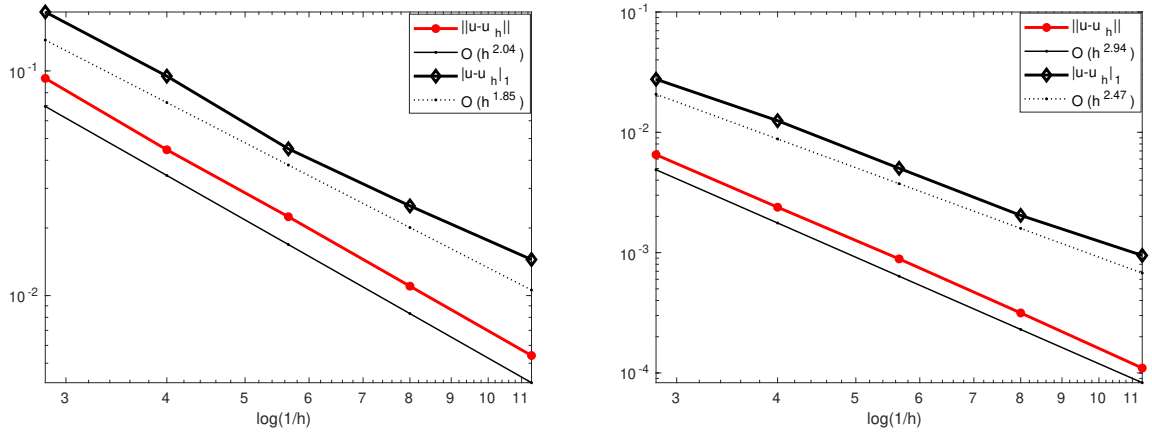

Figure 5.5.13: Log-log plots of the errors versus h at time $t = 1$ for $m = 1$ (left) and $m = 2$ (right) in Example 5.5.5.

5.6 Conclusion

In this chapter, we have proposed a virtual element method for viscoelastic wave equations with variable coefficients. We have obtained optimal order of convergence, i.e., $O(h^{m+1})$ in L^2 norm and $O(h^m)$ in H^1 semi-norm, where m is the polynomial degree of the method and h is the mesh size. A new non-standard projection operator is used to derive the optimal convergence estimate in L^2 norm. For the temporal discretization, we have employed the second-order Crank-Nicolson scheme and derived the optimal convergence estimates for the fully discrete scheme. We have illustrated some numerical experiments with polynomial degree $m = 1, 2, 3$ and shown that the experimental order of convergence agrees with the theoretical results. The use of different types of polygonal meshes for the spatial discretization shows the flexibility of the method with respect to mesh discretization.

6

Higher Order Time Stepping VEMs for Wave Equations

This chapter is devoted to high-order time stepping methods for the wave equation. A general Newmark scheme for temporal discretization is considered along with the virtual element discretization in space on polygonal meshes. Rigorous analysis has been done on the stability and convergence of the proposed method. Optimal convergence is obtained in spatial direction along with fourth-order convergence in time for some special cases. Numerical experiments are illustrated to confirm our theoretical findings.

6.1 Introduction

We consider the following wave equation as our model problem

$$u_{tt} - \nabla \cdot (\sigma(x)\nabla u) = f(x,t), \text{ for } (x,t) \in \Omega \times (0,T] \tag{6.1.1}$$

with ICs and BCs

$$u(x,0) = u_0 \ \ \& \ \ u_t(x,0) = v_0 \text{ for } x \in \Omega; \ \ u(x,t) = 0 \text{ for } (x,t) \in \partial\Omega \times (0,T], \tag{6.1.2}$$

where $\Omega \subset \mathbb{R}^2$ is a polygonal domain with smooth boundary $\partial\Omega$ and $T < \infty$. Here $\sigma(x) \in L^\infty(\Omega)$ is the diffusion coefficient such that for some positive constants $\underline{M}$ and $\overline{M}$

$$\underline{M} \leq \sigma(x) \leq \overline{M} \quad \forall x \in \bar{\Omega}.$$

It has always been an interesting topic among scientists and researchers to develop efficient and accurate numerical approximation for the wave equation. In the past years, many numerical methods has been developed for solving the wave equation using FDMs ([8, 36, 80, 117]), classical FEMs ([13, 14, 37, 53, 64, 88, 106, 112]), discontinuous Galerkin

methods ([69, 70, 78, 108]) and mixed FEMs ([39, 40, 65, 77]). In [128] Vacca developed a virtual element (VEM) approach for the wave equation (6.1.1) with constant coefficients on polygonal meshes. The work mainly focuses on the semi-discrete error analysis of proposed method while for the fully-discrete approximation both Newmark and Bathe method has been used. But the detail analysis of stability and convergence for the proposed methods are missing. Also, the methods are shown to be at most second-order accurate in the temporal discretization.

While using higher order methods for spatial discretization second-order temporal schemes are insufficient to produce a higher order method together. To preserve the accuracy provided by the spatial direction, we should use higher order time schemes. Such scheme can be obtained by the modified equation approach, where appropriate modification is done on the existing second-order schemes by looking at the truncation error [36, 37, 117].

In this chapter, we develop a fully discrete VEM associated with the wave equation (6.1.1) using general Newmark scheme. We present a full theoretical analysis for the semi-discrete error as well as fully discrete and derive optimal convergence estimates. We analyse the stability of the fully discrete scheme and show that the method conserves the discrete energy. Further, in support of theoretical findings, we presented some numerical examples with different two-level and three-level Newmark schemes.

The remainder of the content is divided as follows: We present the construction of the virtual semi-discrete approximation in Section 6.2 while the corresponding error analysis in Section 6.3. Next, Section 6.4 and 6.5 deal with the fully discrete approximation and its convergence analysis. Numerical examples and the conclusion are presented in Section 6.6 and Section 6.7, respectively.

6.2 Semi-discrete Virtual Element Approximation

This subsection deals with construction of virtual element framework for the model problem (6.1.1)-(6.1.2).

Following the standard way, we easily obtain the variational problem for the model problem (6.1.1)-(6.1.2) as : Find $u \in L^2(0,T;H_0^1(\Omega)) \cap H^2(0,T;L^2(\Omega))$ so that for a.e. $t \in (0,T]$

$$\begin{cases} (u_{tt}, v) + a(u,v) = (f,v), \quad \forall v \in H_0^1(\Omega), \\ u(0) = u_0 \ \ \& \ \ u_t(0) = v_0, \end{cases} \tag{6.2.1}$$

where $a(u,v) = (\sigma(x)\nabla u, \nabla v)\ \forall u, v \in H_0^1(\Omega)$.

The existence and uniqueness of a solution to the continuous problem follow from the coercivity and continuity of the bilinear form $a(\cdot,\cdot)$ on $H_0^1(\Omega)$. In the absence of forcing function f, the continuous energy is given by

$$E(t) = \frac{1}{2}\left[(u_t, u_t) + a(u,u)\right].$$

We recall that due to the symmetry and coercivity of the bilinear form $a(\cdot,\cdot)$, the continuous energy $E(t)$ conserves for all time.

We recall the virtual element framework discussed in Chapter 1, Section 1.4. The bilinear form can be splited into its local counterparts in the following manner

$$a(u,v) := \sum_{E\in\mathcal{T}_h} a^E(u,v)\ \forall\ u, v \in H_0^1(\Omega).$$

We introduce the following local discrete bilinear forms on the local virtual element space $W_h^m(E)$:

$$a_h^E(v,w) := \left(\sigma\boldsymbol{\Pi}^0_{m-1,E}\nabla v, \boldsymbol{\Pi}^0_{m-1,E}\nabla w\right)_E + S_\sigma^E\left((I-\Pi^\nabla_{m,E})v, (I-\Pi^\nabla_{m,E})w\right) \quad \&$$
$$m_h^E(v,w) := (\Pi^0_{m,E}v, \Pi^0_{m,E}w)_E + S_0^E\left((I-\Pi^0_{m,E})v, (I-\Pi^0_{m,E})w\right),$$

where

$$S_\sigma^E(v,w) = \beta_\sigma^E \sum_{r=1}^{N^E} dof_r(v) dof_r(w) \quad \&$$
$$S_0^E(v,w) = |E| \sum_{r=1}^{N^E} dof_r(v) dof_r(w)$$

with $\beta_\sigma^E = P_E^a(\sigma)$ and $N^E = \dim W_h^m(E)$.

The global bilinear forms on the global discrete space W_h^m can be obtained by assembling the local counterpart as:

$$a_h(v,w) := \sum_{E\in\mathcal{T}_h} a_h^E(v,w); \quad m_h(v,w) := \sum_{E\in\mathcal{T}_h} m_h^E(v,w) \ \ \forall v, w \in W_h^m.$$

Regarding the continuity and coercivity of the discrete bilinear forms, we have the following result (Lemma 1.4.5).

Lemma 6.2.1. *The bilinear forms a_h and m_h satisfies*

$$a_h(v,w) \leq (1+\beta_\sigma)\overline{M}|v|_1|w|_1 \quad \& \quad m_h(v,w) \leq (1+\beta_0)\|v\|\|w\| \quad \forall v,w \in W_h^m$$

and

$$a_h(w,w) \geq \min\{1,\alpha_\sigma\}\underline{M}|w|_1^2 \quad \& \quad m_h(w,w) \geq \min\{1,\alpha_0\}\|w\|^2 \quad \forall w \in W_h^m,$$

where $\alpha_\sigma, \beta_\sigma, \alpha_0, \beta_0$ are some positive constants.

Now, we have the following semi-discrete virtual element approximation to (6.2.1): Find $u_h \in L^2(0,T;W_h^m) \cap H^2(0,T;W_h^m)$ such that for a.e. $t \in (0,T]$

$$\begin{cases} m_h(u_{htt}, w_h) + a_h(u_h, w_h) = (f_h, w_h) \quad \forall w_h \in W_h^m, \\ u_h(0) = R_h u_0, \ u_{ht}(0) = R_h v_0 \end{cases} \tag{6.2.2}$$

where f_h is the discrete form of the source function f as define in (1.4.14). Here, $R_h : H_0^1(\Omega) \to W_h^m$ is the elliptic projection operator defined by

$$a_h(R_h u, w) = a(u,w) \ \ \forall w \in W_h^m. \tag{6.2.3}$$

In addition, we need the L^2 projection operator $L_h : L^2(\Omega) \to W_h^m$ given by

$$m_h(L_h u, w) = (u,w) \ \ \forall w \in W_h^m. \tag{6.2.4}$$

6.3 Error Analysis for the Semi-discrete Problems

This section is dedicated to the derivation of error estimates related to the semi-discrete approximation (6.2.2) both in L^2 and H^1 semi-norm.

We have the following result for the error estimate of the semi-discrete approximation (6.2.2) in H^1 semi-norm.

Theorem 6.3.1. *Assume that $u_0 \in H^{m+1}(\Omega)$ and $u_t, u_{tt}, f \in L^2(0,T;H^{m+1}(\Omega))$. Then for all $t \in (0,T]$, we have*

$$|u_h(t) - u(t)|_1 \leq Ch^m(|u_0|_{m+1} + \|u_t\|_{L^1(H^{m+1})}) + Ch^{m+1}(\|u_{tt}\|_{L^2(H^{m+1})} + \|f\|_{L^2(H^{m+1})}).$$

Proof. Let us divide the error $e_h(t) = u_h(t) - u(t)$ as

$$e_h(t) = \phi(t) + \psi(t), \tag{6.3.1}$$

where $\phi(t) =: u_h(t) - R_h u(t)$ and $\psi(t) =: R_h u(t) - u(t)$. We have the following bounds for $\psi(t)$ due to Lemma 2.2.1:

$$|\psi(t)|_1 \leq Ch^m |u(t)|_{m+1} \leq Ch^m (|u_0|_{m+1} + \|u_t\|_{L^1(H^{m+1})}). \tag{6.3.2}$$

Therefore, we only need to estimate the bound for the term $\phi(t)$. From (6.2.2) and using the definition of the projection operator R_h, we have the following error equation for $\phi(t)$: For all $w_h \in W_h^m$ and for all $t \in (0, T]$

$$\begin{aligned} m_h(\phi_{tt}(t), w_h) + a_h(\phi(t), w_h) &= (f_h(t), w_h) - m_h(R_h u_{tt}(t), w_h) - a_h(R_h u(t), w_h) \\ &= (f_h(t) - f(t), w_h) + (u_{tt}(t), w_h) - m_h(R_h u_{tt}(t), w_h) \\ &=: T_1 + T_2. \end{aligned} \tag{6.3.3}$$

For the term T_1, from Lemma 1.4.6, we have

$$T_1 = (f_h(t) - f(t), w_h) \leq Ch^{m+1} |f(t)|_{m+1} \|w_h\|. \tag{6.3.4}$$

Now for the term T_2, using the definition of projection operator L_h, continuity of m_h and approximation properties of L_h and R_h, we obtain

$$\begin{aligned} T_2 &= (u_{tt}(t), w_h) - m_h(R_h u_{tt}(t), w_h) \\ &= m_h(L_h u_{tt}(t) - R_h u_{tt}(t), w_h) \\ &\leq \beta_0 \|L_h u_{tt}(t) - R_h u_{tt}(t)\| \|w_h\| \\ &\leq Ch^{m+1} |u_{tt}(t)|_{m+1} \|w_h\|. \end{aligned} \tag{6.3.5}$$

Now, substituting the estimates for T_1 and T_2 from (6.3.4)-(6.3.5) and putting $w_h = \phi_t(t)$ in the error equation (6.3.3), we obtain

$$m_h(\phi_{tt}(t), \phi_t(t)) + a_h(\phi(t), \phi_t(t)) \leq Ch^{m+1} (|u_{tt}(t)|_{m+1} + |f(t)|_{m+1}) \|\phi_t(t)\|.$$

The above equation can be rewritten as

$$\frac{1}{2} \frac{d}{dt} m_h(\phi_t(t), \phi_t(t)) + \frac{1}{2} \frac{d}{dt} a_h(\phi(t), \phi(t)) \leq Ch^{m+1} (|u_{tt}(t)|_{m+1} + |f(t)|_{m+1}) \|\phi_t(t)\|.$$

Integrating from 0 to t and using the fact that $\phi(0) = \phi_t(0) = 0$, we get

$$m_h(\phi_t(t), \phi_t(t)) + a_h(\phi(t), \phi(t)) \leq \int_0^t Ch^{m+1}(|u_{tt}(s)|_{m+1} + |f(s)|_{m+1})\|\phi_t(s)\|ds. \quad (6.3.6)$$

Employing Young's inequality in (6.3.6) and neglecting $\|\phi_t(t)\|^2$ and $\|\phi_t(t)\|^2_{L^2(L^2)}$, we obtain

$$|\phi(t)|_1^2 \leq Ch^{2(m+1)}(\|u_{tt}\|^2_{L^2(H^{m+1})} + \|f\|^2_{L^2(H^{m+1})}). \quad (6.3.7)$$

Now plugging (6.3.2) and (6.3.7) in (6.3.1), we get the desired result. □

Now, we will present the main result of this section. The semi-discrete approximation (6.2.2) has the following error estimate in L^2 norm.

Theorem 6.3.2. *Assume that $u_0, v_0 \in H^{m+1}(\Omega)$ and $u_t, f \in L^1(0,T; H^{m+1}(\Omega))$. Then, we have*

$$\|u_h(t) - u(t)\| \leq Ch^{m+1}(|u_0|_{m+1} + |v_0|_{m+1} + \|u_t\|_{L^1(H^{m+1})} + \|f\|_{L^1(H^{m+1})}) \quad \forall t \in (0,T].$$

Proof. As in (6.3.1), let us split the error $e_h(t) = u_h(t) - u(t) =: \phi(t) + \psi(t)$. Applying Lemma 2.2.1, we have the following bounds for $\psi(t)$ in L^2 norm

$$\|\psi(t)\| \leq Ch^{m+1}|u(t)|_{m+1} \leq Ch^{m+1}(|u_0|_{m+1} + \|u_t\|_{L^1(H^{m+1})}). \quad (6.3.8)$$

Now, in order to obtain the bounds for the term $\phi(t)$, using the definition of projection operator L_h and then taking $\rho = L_h u - R_h u$ in the error equation (6.3.3), we have the following relation: For all $w_h \in W_h^m$ and for all $t \in (0,T]$

$$\begin{aligned}
&\frac{d}{dt}m_h(\phi_t(t), w_h) - m_h(\phi_t(t), w_{ht}) + a_h(\phi(t), w_h) \\
&= (f_h(t) - f(t), w_h) + \frac{d}{dt}(u_t(t), w_h) - (u_t(t), w_{ht}) - \frac{d}{dt}m_h(R_h u_t(t), w_h) + m_h(R_h u_t(t), w_{ht}) \\
&= (f_h(t) - f(t), w_h) + \frac{d}{dt}m_h(\rho_t(t), w_h) - m_h(\rho_t(t), w_{ht}). \quad (6.3.9)
\end{aligned}$$

Define,

$$\widehat{\phi}(\cdot, t) = \int_t^\zeta \phi(\cdot, s)ds, \quad 0 \leq t \leq T.$$

Then, clearly $\widehat{\phi}(\cdot, \zeta) = 0$ and $\widehat{\phi}_t(\cdot, t) = -\phi(\cdot, t)$, $0 \leq t \leq T$. Now, substituting $w_h = \widehat{\phi}(t) \in W_h^m$ in (6.3.9), we get

$$\begin{aligned}
&\frac{d}{dt}m_h(\phi_t(t), \widehat{\phi}(t)) + m_h(\phi_t(t), \phi(t)) + a_h(\phi(t), \widehat{\phi}(t)) \\
&= \left(f_h(t) - f(t), \widehat{\phi}(t)\right) + \frac{d}{dt}m_h(\rho_t(t), \widehat{\phi}(t)) + m_h(\rho_t(t), \phi(t))
\end{aligned}$$

which can be rewritten as

$$\begin{aligned}&\frac{1}{2}\frac{d}{dt}m_h(\phi(t),\phi(t)) - \frac{1}{2}\frac{d}{dt}a_h(\widehat{\phi}(t),\widehat{\phi}(t))\\&= \Big(f_h(t) - f(t), \widehat{\phi}(t)\Big) + \frac{d}{dt}m_h(\rho_t(t) - \phi_t(t), \widehat{\phi}(t)) + m_h(\rho_t(t), \phi(t)).\end{aligned}$$

Integrating 0 to ζ and using $\widehat{\phi}(\cdot,\zeta) = 0$, $\phi(0) = \phi_t(0) = 0$, we get

$$\begin{aligned}&\frac{1}{2}m_h(\phi(\zeta),\phi(\zeta)) + \frac{1}{2}a_h(\widehat{\phi}(0),\widehat{\phi}(0))\\&= \int_0^\zeta \Big(f_h(s) - f(s), \widehat{\phi}(s)\Big)\, ds - m_h(\rho_t(0), \widehat{\phi}(0)) + \int_0^\zeta m_h(\rho_t(s),\phi(s))ds\\&= I_1 + I_2 + I_3. \qquad (6.3.10)\end{aligned}$$

Since $\phi(t)$ is continuous in the variable t, we let

$$\|\phi(\zeta)\| = \sup_{0\le t\le T}\|\phi(t)\|.$$

Then, one can easily see that $\|\widehat{\phi}(t)\| \le C\|\phi(\zeta)\|$ for all $t \in (0,T]$. Hence, Lemma 1.4.6 implies

$$\begin{aligned}I_1 = \int_0^\zeta \Big(f_h(s) - f(s), \widehat{\phi}(s)\Big)\, ds &\le Ch^{m+1}\int_0^\zeta |f(s)|_{m+1}\|\widehat{\phi}(s)\|ds\\&\le Ch^{m+1}\|f\|_{L^1(H^{m+1})}\|\phi(\zeta)\|.\end{aligned}$$

Next, for I_2 using the continuity of the bilinear form m_h, we get

$$I_2 = m_h(\rho_t(0), \widehat{\phi}(0)) \le Ch^{m+1}|v_0|_{m+1}\|\phi(\zeta)\|.$$

Similarly,

$$I_3 = \int_0^\zeta m_h(\rho_t(s),\phi(s))ds \le Ch^{m+1}\|u_t\|_{L^1(H^{m+1})}\|\phi(\zeta)\|.$$

Using all the estimates in (6.3.10), we get

$$\|\phi(\zeta)\|^2 \le Ch^{m+1}(|v_0|_{m+1} + \|f\|_{L^1(H^{m+1})} + \|u_t\|_{L^1(H^{m+1})})\|\phi(\zeta)\|.$$

Hence

$$\|\phi(t)\| \le \|\phi(\zeta)\| \le Ch^{m+1}(|v_0|_{m+1} + \|f\|_{L^1(H^{m+1})} + \|u_t\|_{L^1(H^{m+1})}). \qquad (6.3.11)$$

Now, from (6.3.8) and (6.3.11), we get the theorem. □

6.4 Fully Discrete Virtual Element Approximation

In this section, we will formulate the fully discrete approximation to the model problem (6.1.1) using the general Newmark scheme. We will show that the scheme satisfies the energy conservation law for $\boldsymbol{\gamma} = \frac{1}{2}$. We also analyse the stability and convergence of the proposed scheme.

We recall the discretization of the time domain $[0, T]$ and notations from Chapter 2, Section 2.4. In addition, we define the following notations: For any $v \in W_h^m$

$$\bar{\partial}_{tt} v^n = \frac{v^{n+1} - 2v^n + v^{n-1}}{\tau^2} \quad \& \quad \bar{\partial}_t v^n = \frac{v^{n+1} - v^{n-1}}{2\tau}, \quad n = 0, 1, \cdots, N-1.$$

6.4.1 Three-level schemes

The discrete time virtual element approximation to the problem (6.1.1) based on Newmark scheme can be given by: Find a sequence $\mathcal{U}^n \in W_h^m$ such that for $n = 1, 2, \cdots, N-1$

$$m_h(\bar{\partial}_{tt}\mathcal{U}^n, w_h) + a_h(\mathcal{U}^{n,\boldsymbol{\theta},\boldsymbol{\gamma}}, w_h) = (f_h^{n,\boldsymbol{\theta},\boldsymbol{\gamma}}, w_h) \ \forall \ w_h \in W_h^m, \tag{6.4.1}$$

where

$$v^{n,\boldsymbol{\theta},\boldsymbol{\gamma}} = \boldsymbol{\theta} v^{n+1} + \left(\frac{1}{2} - 2\boldsymbol{\theta} + \boldsymbol{\gamma}\right) v^n + \left(\frac{1}{2} + \boldsymbol{\theta} - \boldsymbol{\gamma}\right) v^{n-1}$$

with $\boldsymbol{\gamma} \geq 0$ and $\boldsymbol{\theta} \in [0, 0.5]$ are arbitrary parameters.

For different choices of $\boldsymbol{\theta}$ and $\boldsymbol{\gamma}$ in (6.4.1), we get different classes of schemes. By Taylor series expansion, it is easy to show that the scheme (6.4.1) is second-order accurate for $\boldsymbol{\gamma} = \frac{1}{2}$ and only first-order accurate for $\boldsymbol{\gamma} \neq \frac{1}{2}$. For $\boldsymbol{\gamma} = \frac{1}{2}$, (6.4.1) reduces to

$$m_h(\bar{\partial}_{tt}\mathcal{U}^n, w_h) + a_h(\mathcal{U}^{n,\boldsymbol{\theta}}, w_h) = (f_h^{n,\boldsymbol{\theta}}, w_h) \ \forall \ w_h \in W_h^m, \tag{6.4.2}$$

where

$$v^{n,\boldsymbol{\theta}} = \boldsymbol{\theta} v^{n+1} + (1 - 2\boldsymbol{\theta})\, v^n + \boldsymbol{\theta} v^{n-1}.$$

Again, the scheme is explicit if $\boldsymbol{\theta} = 0$, and implicit if $\boldsymbol{\theta} \neq 0$. For example, when $\boldsymbol{\gamma} = \frac{1}{2}$ and $\boldsymbol{\theta} = 0$, (6.4.1) becomes the second-order explicit leapfrog scheme given by

$$m_h(\bar{\partial}_{tt}\mathcal{U}^n, w_h) + a_h(\mathcal{U}^n, w_h) = (f_h^n, w_h) \ \forall \ w_h \in W_h^m. \tag{6.4.3}$$

Similarly, choosing $\boldsymbol{\gamma} = \frac{3}{2}$ and $\boldsymbol{\theta} = 1$, we obtain the following first-order implicit scheme

$$m_h(\bar{\partial}_{tt}\mathcal{U}^n, w_h) + a_h(\mathcal{U}^{n+1}, w_h) = (f_h^{n+1}, w_h) \; \forall \; w_h \in W_h^m. \tag{6.4.4}$$

For the three-level scheme (6.4.1), we require suitable initial conditions $\mathcal{U}^0, \mathcal{U}^1 \in W_h^m$. We choose $\mathcal{U}_0 = R_h u_0$ and $\mathcal{U}^1$ as the solution of the following equation

$$m_h(\mathcal{U}^1 - \mathcal{U}^0, w_h) + \tau^2 \boldsymbol{\theta} a_h(\mathcal{U}^1 - \mathcal{U}^0, w_h) = \tau \; (v_0, w_h) + \frac{\tau^2}{2}(\bar{\mathcal{U}}^0, w_h) \tag{6.4.5}$$

for all $w_h \in W_h^m$, where

$$(\bar{\mathcal{U}}^0, w_h) = (f^0, w_h) - (u_0, w_h).$$

For the special case $\boldsymbol{\theta} = 1/12$, a higher-order approximation has to be considered. We choose $\mathcal{U}^1$ as follows

$$\begin{aligned} &m_h(\mathcal{U}^1 - \mathcal{U}^0, w_h) + \tau^2 \boldsymbol{\theta} a_h(\mathcal{U}^1 - \mathcal{U}^0, w_h) \\ &= \tau \; (v_0, w_h) + \frac{\tau^2}{2}(\bar{\mathcal{U}}^0, w_h) - \frac{\tau^3}{12} a(v_0, w_h) + \frac{\tau^3}{6}(f_t^0, w_h) + \frac{\tau^4}{24}(f_{tt}^0, w_h), \end{aligned} \tag{6.4.6}$$

for all $w_h \in W_h^m$. The fully discrete problem is now defined by (6.4.1) and (6.4.5) if $\boldsymbol{\theta} \neq 1/12$ and by (6.4.1) and (6.4.6) for $\boldsymbol{\theta} = 1/12$. We have the following lemma regarding the existence of a unique solution $\mathcal{U}^n$ to the fully discrete problem.

Lemma 6.4.1. *There exist a unique sequence $\{\mathcal{U}^n\}_{n=0}^N$ which satisfies the fully discrete problem given by (6.4.1)-(6.4.5) or (6.4.1)-(6.4.6).*

Proof. It can be clearly seen from (6.4.5) and (6.4.6) that $\mathcal{U}^0, \mathcal{U}^1 \in W_h^m$ are defined uniquely for any value of $\boldsymbol{\theta}$. From (6.4.1), for $n \geq 1$, $\mathcal{U}^{n+1}$ satisfies

$$\begin{aligned} m_h\left(\mathcal{U}^{n+1}, w_h\right) + \tau^2 \boldsymbol{\theta} \; a_h\left(\mathcal{U}^{n+1}, w_h\right) =& \tau^2 \left(f_h^{n,\boldsymbol{\theta},\boldsymbol{\gamma}}, w_h\right) + m_h\left(2\mathcal{U}^n - \mathcal{U}^{n-1}, w_h\right) \\ &- \tau^2 a_h\left(\left(\frac{1}{2} - 2\boldsymbol{\theta} + \boldsymbol{\gamma}\right)\mathcal{U}^n + \left(\frac{1}{2} + \boldsymbol{\theta} - \boldsymbol{\gamma}\right)\mathcal{U}^{n-1}, w_h\right) \end{aligned}$$

for all $w \in W_h^m$. This can be written as

$$c_h(\mathcal{U}^{n+1}, w_h) = l_h(w_h) \; \forall w_h \in W_h^m,$$

where c_h is the bilinear form

$$c_h(v, w) = m_h(v, w) + \tau^2 \boldsymbol{\theta} \; a_h(v, w) \; \forall v, w \in W_h^m$$

and l_h is the linear operator

$$\begin{aligned} l_h(w) =& \tau^2 \left(f_h^{n,\boldsymbol{\theta},\boldsymbol{\gamma}}, w \right) + m_h \left(2\mathcal{U}^n - \mathcal{U}^{n-1}, w \right) \\ & - \tau^2 a_h \left(\left(\frac{1}{2} - 2\boldsymbol{\theta} + \boldsymbol{\gamma} \right) \mathcal{U}^n + \left(\frac{1}{2} + \boldsymbol{\theta} - \boldsymbol{\gamma} \right) \mathcal{U}^{n-1}, w \right) \end{aligned}$$

for all $w \in W_h^m$. Clearly, c_h is positive definite as the bilinear forms m_h and a_h are positive definite. Also, the operator l_h is continuous. Hence, $\mathcal{U}^{n+1}$ for $n = 0, 1, \cdots, N-1$ exists uniquely. □

6.4.2 Two-level schemes

Let us write $\vartheta = u_t$, where ϑ is an auxiliary unknown. Then our model equation (6.1.1) can be split into the following system of first-order equations in t:

$$\begin{cases} u_t - \vartheta = 0 \text{ in } \Omega \times (0, T], \\ \vartheta_t - \nabla \cdot (\sigma(x) \nabla u) = f \text{ in } \Omega \times (0, T]. \end{cases} \tag{6.4.7}$$

We construct the discrete time virtual element approximation to the system (6.4.7) in the following way: Find $\mathcal{U}^n, \vartheta^n \in W_h^m$ such that for $n = 1, 2, \cdots, N-1$

$$\begin{cases} \partial_\tau \mathcal{U}^n - \vartheta^{n,\boldsymbol{\beta}} = 0, \\ m_h(\partial_\tau \vartheta^n, w_h) + a_h(\mathcal{U}^{n,\boldsymbol{\alpha}}, w_h) = (f_h^{n,\boldsymbol{\alpha}}, w_h) \ \forall \ w_h \in W_h^m, \end{cases} \tag{6.4.8}$$

where $0 \leq \boldsymbol{\alpha}, \boldsymbol{\beta} \leq 1$ are parameters and for any parameter δ

$$v^{n,\delta} = \delta v^{n+1} + (1 - \delta) v^n, \quad v \in W_h^m.$$

The expression (6.4.8) represents various temporal discretization on choosing suitable values for the parameters $\boldsymbol{\alpha}$ and $\boldsymbol{\beta}$. The scheme (6.4.8) is unconditionally stable for $\boldsymbol{\alpha}, \boldsymbol{\beta} \geq 1/2$. It represents the well-known Crank-Nicolson scheme for the choice $(\boldsymbol{\alpha}, \boldsymbol{\beta}) = (1/2, 1/2)$. This is an unconditionally stable implicit scheme and one need to solve a linear system of equations in order to obtain U^{n+1}, ϑ^{n+1} from U^n, ϑ^n for each n. From Taylor's series expansions, we can see that the scheme is of second-order accurate in time. The better accuracy rate and unconditional stability makes the Crank-Nicolson scheme interesting and

hence widely used for second-order hyperbolic problems with first-order system formulation [13].

For $(\boldsymbol{\alpha}, \boldsymbol{\beta}) = (0, 1)$, it coincides with the central scheme

$$m_h(\bar{\partial}_{tt} U^n, w_h) + a_h(\mathcal{U}^n, w_h) = (f_h^n, w_h) \quad \forall w_h \in W_h^m.$$

This is an explicit second-order scheme with no artificial viscosity. It performs very well for smooth exact solution. But for the case when the initial data u_0 has a jump discontinuity, severe spurious oscillation occurs.

With $(\boldsymbol{\alpha}, \boldsymbol{\beta})$=$(1, 1)$, we get a first-order accurate implicit scheme with better stability properties but with heavy artificial viscosity.

For the two-level scheme (6.4.8), we choose the initial values as

$$\mathcal{U}^0 = R_h u_0, \ \vartheta^0 = R_h v_0. \tag{6.4.9}$$

Regarding the existence of unique solution $\mathcal{U}^n$ to the fully discrete problem, we have the following lemma.

Lemma 6.4.2. *There exist a unique sequence $\{\mathcal{U}^n\}_{n=0}^N$ which satisfies the problem (6.4.8)-(6.4.9).*

Proof. It can be clearly seen from (6.4.9) that $\mathcal{U}^0, \vartheta^0 \in W_h^m$ are defined uniquely for any value of $\boldsymbol{\alpha}$ and $\boldsymbol{\beta}$. From (6.4.8), for $n \geq 0$, ϑ^{n+1} satisfies

$$\begin{aligned} &m_h(\vartheta^{n+1}, w_h) + \tau^2 \boldsymbol{\alpha}\boldsymbol{\beta}\, a_h(\vartheta^{n+1}, w_h) \\ &= m_h(\vartheta^n, w_h) - \tau^2 \boldsymbol{\alpha}(1-\boldsymbol{\beta})\, a_h(\vartheta^n, w_h) - \tau(1-2\boldsymbol{\alpha})\, a_h(\mathcal{U}^n, w_h) + \tau\, (f_h^{n+\boldsymbol{\alpha}}, w_h) \end{aligned}$$

for all $w_h \in W_h^m$. This can be written as

$$\mathbf{c}_h(\vartheta^{n+1}, w_h) = \mathbf{l}_h(w_h)\ \forall w_h \in W_h^m,$$

where $\mathbf{c}_h$ is the bilinear form

$$\mathbf{c}_h(v, w) = m_h(v, w) + \tau^2 \boldsymbol{\alpha}\boldsymbol{\beta}\, a_h(v, w)\ \forall v, w \in W_h^m$$

and $\mathbf{l}_h$ is the linear operator

$$\mathbf{l}_h(w) = m_h(\vartheta^n, w) - \tau^2 \boldsymbol{\alpha}(1-\boldsymbol{\beta})\, a_h(\vartheta^n, w) - \tau(1-2\boldsymbol{\alpha})\, a_h(\mathcal{U}^n, w) + \tau\, (f_h^{n+\boldsymbol{\alpha}}, w)\ \forall w \in W_h^m.$$

Clearly, $\mathbf{c}_h$ is positive definite as the bilinear forms m_h and a_h are positive definite and $\boldsymbol{\alpha}, \boldsymbol{\beta} \geq 0$. Also, the operator $\mathbf{l}_h$ is continuous. Hence, ϑ^{n+1} for $n = 0, 1, \cdots, N-1$ exists uniquely. Now, from the first part of (6.4.8), it is easy to see that there exist unique $\mathcal{U}^{n+1}$, $n = 0, 1, \cdots, N-1$. □

6.4.3 Stability analysis

We now analyse the stability of the fully discrete scheme (6.4.1) in the absence of forcing function. We have the following result regarding the discrete energy.

Theorem 6.4.1. *For the scheme (6.4.1) the discrete energy*

$$E_h^{n+\frac{1}{2}} = \frac{1}{2}\left[m_h(\partial_\tau \mathcal{U}^n, \partial_\tau \mathcal{U}^n) + \tau^2\left(\boldsymbol{\theta} - \frac{\boldsymbol{\gamma}}{2}\right) a_h(\partial_\tau \mathcal{U}^n, \partial_\tau \mathcal{U}^n) + a_h\left(\mathcal{U}^{n+\frac{1}{2}}, \mathcal{U}^{n+\frac{1}{2}}\right)\right],$$

does not increases with time and is conserved when $\boldsymbol{\gamma} = \frac{1}{2}$.

Proof. In the absence of forcing function, i.e., $f = 0$, the equation (6.4.1) becomes

$$m_h(\bar{\partial}_{tt}\mathcal{U}^n, w_h) + a_h(\mathcal{U}^{n,\boldsymbol{\theta},\boldsymbol{\gamma}}, w_h) = 0. \tag{6.4.10}$$

It is easy to see that

$$\begin{aligned}\mathcal{U}^{n,\boldsymbol{\theta},\boldsymbol{\gamma}} &= \tau^2\boldsymbol{\theta}\bar{\partial}_{tt}\mathcal{U}^n + \left(\frac{1}{2}+\boldsymbol{\gamma}\right)\mathcal{U}^n + \left(\frac{1}{2}-\boldsymbol{\gamma}\right)\mathcal{U}^{n-1} \\ &= \tau^2\left(\boldsymbol{\theta} - \frac{\boldsymbol{\gamma}}{2}\right)\bar{\partial}_{tt}\mathcal{U}^n + \boldsymbol{\gamma}\left(\mathcal{U}^{n+\frac{1}{2}} + \mathcal{U}^{n-\frac{1}{2}}\right) + (1-2\boldsymbol{\gamma})\mathcal{U}^{n-\frac{1}{2}}. \end{aligned} \tag{6.4.11}$$

Thus from (6.4.10), we get

$$\begin{aligned} m_h(\bar{\partial}_{tt}\mathcal{U}^n, w_h) + \tau^2\left(\boldsymbol{\theta} - \frac{\boldsymbol{\gamma}}{2}\right) a_h(\bar{\partial}_{tt}\mathcal{U}^n, w_h) + \boldsymbol{\gamma} a_h\left(\mathcal{U}^{n+\frac{1}{2}} + \mathcal{U}^{n-\frac{1}{2}}, w_h\right) \\ + (1-2\boldsymbol{\gamma}) a_h\left(\mathcal{U}^{n-\frac{1}{2}}, w_h\right) = 0. \end{aligned}$$

Now, substituting $w_h = \bar{\partial}_t \mathcal{U}^n$, we obtain

$$\begin{aligned} &m_h(\bar{\partial}_{tt}\mathcal{U}^n, \bar{\partial}_t\mathcal{U}^n) + \tau^2\left(\boldsymbol{\theta} - \frac{\boldsymbol{\gamma}}{2}\right) a_h(\bar{\partial}_{tt}\mathcal{U}^n, \bar{\partial}_t\mathcal{U}^n) \\ &+ \boldsymbol{\gamma} a_h\left(\mathcal{U}^{n+\frac{1}{2}} + \mathcal{U}^{n-\frac{1}{2}}, \bar{\partial}_t\mathcal{U}^n\right) + (1-2\boldsymbol{\gamma}) a_h\left(\mathcal{U}^{n-\frac{1}{2}}, \bar{\partial}_t\mathcal{U}^n\right) = 0. \end{aligned} \tag{6.4.12}$$

The first term in the above equation can be written as

$$m_h(\bar{\partial}_{tt}\mathcal{U}^n, \bar{\partial}_t\mathcal{U}^n) = \frac{1}{2\tau}\left[m_h(\partial_\tau\mathcal{U}^n, \partial_\tau\mathcal{U}^n) - m_h(\partial_\tau\mathcal{U}^{n-1}, \partial_\tau\mathcal{U}^{n-1})\right].$$

Similarly,

$$a_h(\bar{\partial}_{tt}\mathcal{U}^n, \bar{\partial}_t\mathcal{U}^n) = \frac{1}{2\tau}\left[a_h(\partial_\tau\mathcal{U}^n, \partial_\tau\mathcal{U}^n) - a_h(\partial_\tau\mathcal{U}^{n-1}, \partial_\tau\mathcal{U}^{n-1})\right].$$

Again, since $\bar{\partial}_t \mathcal{U}^n = (\mathcal{U}^{n+\frac{1}{2}} - \mathcal{U}^{n-\frac{1}{2}})/\tau$, we have

$$\begin{aligned} a_h(\mathcal{U}^{n+\frac{1}{2}} + \mathcal{U}^{n-\frac{1}{2}}, \bar{\partial}_t \mathcal{U}^n) &= \frac{1}{\tau} a_h(\mathcal{U}^{n+\frac{1}{2}} + \mathcal{U}^{n-\frac{1}{2}}, \mathcal{U}^{n+\frac{1}{2}} - \mathcal{U}^{n-\frac{1}{2}}) \\ &= \frac{1}{\tau}\left[a_h(\mathcal{U}^{n+\frac{1}{2}}, \mathcal{U}^{n+\frac{1}{2}}) - a_h(\mathcal{U}^{n-\frac{1}{2}}, \mathcal{U}^{n-\frac{1}{2}})\right]. \end{aligned}$$

Also, we have

$$a_h\left(\mathcal{U}^{n-\frac{1}{2}}, \mathcal{U}^{n+\frac{1}{2}} - \mathcal{U}^{n-\frac{1}{2}}\right) \leq \frac{1}{2}\left[a_h(\mathcal{U}^{n+\frac{1}{2}}, \mathcal{U}^{n+\frac{1}{2}}) - a_h(\mathcal{U}^{n-\frac{1}{2}}, \mathcal{U}^{n-\frac{1}{2}})\right].$$

Thus, for $\boldsymbol{\gamma} \geq \frac{1}{2}$

$$(1-2\boldsymbol{\gamma}) a_h\left(\mathcal{U}^{n-\frac{1}{2}}, \mathcal{U}^{n+\frac{1}{2}} - \mathcal{U}^{n-\frac{1}{2}}\right) \geq \frac{1-2\boldsymbol{\gamma}}{2}\left[a_h(\mathcal{U}^{n+\frac{1}{2}}, \mathcal{U}^{n+\frac{1}{2}}) - a_h(\mathcal{U}^{n-\frac{1}{2}}, \mathcal{U}^{n-\frac{1}{2}})\right]$$

as $1 - 2\boldsymbol{\gamma} \leq 0$. Then (6.4.12) can be written as

$$\begin{aligned} &\frac{1}{2\tau}\left[m_h(\partial_\tau \mathcal{U}^n, \partial_\tau \mathcal{U}^n) + m_h(\partial_\tau \mathcal{U}^{n-1}, \partial_\tau \mathcal{U}^{n-1})\right] \\ &+ \frac{\tau}{2}\left(\boldsymbol{\theta} - \frac{\boldsymbol{\gamma}}{2}\right)\left[a_h(\partial_\tau \mathcal{U}^n, \partial_\tau \mathcal{U}^n) + a_h(\partial_\tau \mathcal{U}^{n-1}, \partial_\tau \mathcal{U}^{n-1})\right] \\ &+ \frac{1}{2\tau}\left[a_h(\mathcal{U}^{n+\frac{1}{2}}, \mathcal{U}^{n+\frac{1}{2}}) - a_h(\mathcal{U}^{n-\frac{1}{2}}, \mathcal{U}^{n-\frac{1}{2}})\right] \leq 0. \end{aligned}$$

Now, from the definition of $E_h^{n+\frac{1}{2}}$, we can easily derive

$$\frac{1}{\tau}\left(E_h^{n+\frac{1}{2}} - E_h^{n-\frac{1}{2}}\right) \leq 0.$$

This shows that the discrete energy does not increase with time.

Again, for $\boldsymbol{\gamma} = \frac{1}{2}$, we can derive

$$\frac{1}{\tau}\left(E_h^{n+\frac{1}{2}} - E_h^{n-\frac{1}{2}}\right) = 0.$$

This imply that the discrete energy is conserved. □

Theorem 6.4.2. *The scheme (6.4.1) is stable if* $\boldsymbol{\gamma} \geq \frac{1}{2}$ *and*

$$\tau^2\left(\frac{\boldsymbol{\gamma}}{2} - \boldsymbol{\theta}\right) \sup_{w \in W_h^m} \frac{a_h(w,w)}{m_h(w,w)} \leq 1. \tag{6.4.13}$$

It is unconditionally stable for $2\boldsymbol{\theta} \geq \boldsymbol{\gamma} \geq \dfrac{1}{2}$.

Proof. The scheme (6.4.1) is stable if and only if the discrete energy $E_h^{n+\frac{1}{2}}$ is positive semi-definite. When $2\boldsymbol{\theta} \geq \boldsymbol{\gamma} \geq \frac{1}{2}$, $E_h^{n+\frac{1}{2}}$ is positive semi-definite since each term in $E_h^{n+\frac{1}{2}}$ is positive semi-definite. For the case when $\boldsymbol{\gamma} \geq \frac{1}{2}$ and $\boldsymbol{\theta} < \frac{\boldsymbol{\gamma}}{2}$, for $E_h^{n+\frac{1}{2}}$ to be positive semi-definite it is enough to require the bilinear form

$$c(v,w) := m_h(v,w) + \tau^2 \left(\boldsymbol{\theta} - \frac{\boldsymbol{\gamma}}{2}\right) a_h(v,w),$$

to be positive semi-definite, that is

$$m_h(w,w) + \tau^2 \left(\boldsymbol{\theta} - \frac{\boldsymbol{\gamma}}{2}\right) a_h(w,w) \geq 0, \ \forall w \in W_h^m.$$

Equivalently, the above condition can be expressed as

$$\tau^2 \left(\frac{\boldsymbol{\gamma}}{2} - \boldsymbol{\theta}\right) \frac{a_h(w,w)}{m_h(w,w)} \leq 1, \ \forall w \in W_h^m$$

or

$$\tau^2 \left(\frac{\boldsymbol{\gamma}}{2} - \boldsymbol{\theta}\right) \sup_{w \in W_h^m} \frac{a_h(w,w)}{m_h(w,w)} \leq 1.$$

□

Corollary 6.4.1. *The scheme (6.4.2) is stable if*

$$\tau^2 \left(\frac{1}{4} - \boldsymbol{\theta}\right) \sup_{w \in W_h^m} \frac{a_h(w,w)}{m_h(w,w)} \leq 1.$$

Consequently, the scheme (6.4.3) is stable if

$$\frac{\tau^2}{4} \sup_{w \in W_h^m} \frac{a_h(w,w)}{m_h(w,w)} \leq 1.$$

The scheme (6.4.4) is unconditionally stable.

6.4.4 Equivalence between the three-level and two level schemes

In this subsection, we will see that the two-level scheme (6.4.8) and the three-level scheme (6.4.2) are equivalent for some particular choice of parameters.

For the purpose of comparing the two-level scheme (6.4.8) and the three-level scheme (6.4.2), we need to eliminate ϑ^n and ϑ^{n+1} from (6.4.8). First, multiplying $\tau^2\boldsymbol{\beta}$ to the second

part of (6.4.8) and then adding with the first part, we obtain

$$\begin{aligned} &m_h(\mathcal{U}^{n+1}, w_h) + \tau^2\boldsymbol{\alpha}\boldsymbol{\beta}a_h(\mathcal{U}^{n+1}, w_h) \\ &= m_h(\mathcal{U}^n, w_h) - \tau^2\boldsymbol{\beta}(1-\boldsymbol{\alpha})a_h(\mathcal{U}^n, w_h) + \tau m_h(\vartheta^n, w_h) + (\boldsymbol{\beta} f_h^{n+\boldsymbol{\alpha}}, w_h). \end{aligned} \tag{6.4.14}$$

Again, multiplying $\tau(1-\boldsymbol{\beta})$ to the second part of (6.4.8) and then subtracting the first part from the resulting equation, we have

$$\begin{aligned} &m_h(\vartheta^{n+1}, w_h) \\ &= m_h\left(\frac{\mathcal{U}^{n+1}-\mathcal{U}^n}{\tau}, w_h\right) - \tau(1-\boldsymbol{\beta})a_h\left(\boldsymbol{\alpha}\mathcal{U}^{n+1} + (1-\boldsymbol{\alpha})\mathcal{U}^n, w_h\right) + \tau(1-\boldsymbol{\beta})(f_h^{n+\boldsymbol{\alpha}}, w_h). \end{aligned} \tag{6.4.15}$$

Now to eliminate ϑ^n from (6.4.14), substituting the value of $m_h(\vartheta^n, w_h)$ from (6.4.15) in (6.4.14), yields

$$\begin{aligned} &m_h(\bar{\partial}_{tt}\mathcal{U}^n, w_h) + a_h\left(\boldsymbol{\alpha}\boldsymbol{\beta}\mathcal{U}^{n+1} + (\boldsymbol{\alpha}+\boldsymbol{\beta}-2\boldsymbol{\alpha}\boldsymbol{\beta})\mathcal{U}^n + (1-\boldsymbol{\alpha})(1-\boldsymbol{\beta})\mathcal{U}^{n-1}, w_h\right) \\ &= \left(\boldsymbol{\beta} f_h^{n+\boldsymbol{\alpha}} + (1-\boldsymbol{\beta}) f_h^{n-1+\boldsymbol{\alpha}}, w_h\right), \end{aligned} \tag{6.4.16}$$

for all $w_h \in W_h^m$. The initial condition for the scheme (6.4.16) is given by $\mathcal{U}^0 = R_h u_0$, $\vartheta^0 = R_h v_0$ and

$$m_h\left(\frac{\mathcal{U}^1-\mathcal{U}^0}{\tau}, w_h\right) + \tau\boldsymbol{\alpha}\boldsymbol{\beta}a_h\left(\mathcal{U}^1-\mathcal{U}^0, w_h\right) + \tau\boldsymbol{\beta}a_h\left(\mathcal{U}^0, w_h\right) - m_h(\vartheta_0, w_h) = \tau\boldsymbol{\beta}(f_h^{\boldsymbol{\alpha}}, w_h).$$

Comparing (6.4.2) and (6.4.16), we can observe that both scheme are equivalent if

$$\boldsymbol{\alpha}\boldsymbol{\beta} = \boldsymbol{\theta} \text{ and } \boldsymbol{\alpha}+\boldsymbol{\beta} = 1.$$

Here, we must point out that this equivalence does not mean that (6.4.16) and (6.4.2) produce the same sequence of approximation solutions $\{\mathcal{U}^n\}_{n=0}^N$, as they may not have the same value for $\mathcal{U}^1$. Indeed, for (6.4.16), $\mathcal{U}^1$ is computed from the scheme itself, and it can be different from that chosen for (6.4.2). Thus, the condition $\boldsymbol{\alpha}+\boldsymbol{\beta} = 1$ (except when $\boldsymbol{\alpha} = \boldsymbol{\beta} = \frac{1}{2}$) does not imply that (6.4.16) is second-order accurate. Also, claiming that (6.4.16) becomes fourth-order accurate in time when $\boldsymbol{\alpha}+\boldsymbol{\beta} = 1$ and $\boldsymbol{\alpha}\boldsymbol{\beta} = \frac{1}{12}$ is not correct. Indeed, the temporal accuracy of the scheme cannot exceed two according to the first Dahlquist barrier [47].

To extract further properties, we rearrange (6.4.16) in the following form

$$m_h(\bar{\partial}_{tt}\mathcal{U}^n, w_h) + a_h\left(\boldsymbol{\alpha\beta}\mathcal{U}^{n+1} + (1-2\boldsymbol{\alpha\beta})\mathcal{U}^n + \boldsymbol{\alpha\beta}\mathcal{U}^{n-1}, w_h\right)$$
$$+ (\boldsymbol{\alpha}+\boldsymbol{\beta}-1)a_h\left(\mathcal{U}^n - \mathcal{U}^{n-1}, w_h\right) = \left(\boldsymbol{\beta} f_h^{n+\boldsymbol{\alpha}} + (1-\boldsymbol{\beta}) f_h^{n-1+\boldsymbol{\alpha}}, w_h\right). \tag{6.4.17}$$

Hence, the scheme can be seen as a natural first-order fully discrete approximation of the modified wave equation

$$u_{tt} - \tau(\boldsymbol{\alpha}+\boldsymbol{\beta}-1)\nabla\cdot(\sigma\nabla u_t) - \nabla\cdot(\sigma\nabla u) = f. \tag{6.4.18}$$

If $\boldsymbol{\alpha}+\boldsymbol{\beta} \geq 1$, then (6.4.18) represents a strongly damped wave equation. The term $\tau(\boldsymbol{\alpha}+\boldsymbol{\beta}-1)$ works as an artificial viscosity and the energy decreases strictly when it is non-zero. We remark that Euler Schemes and the Crank-Nicolson scheme do not introduce a dissipation error into the time integration as we have $\boldsymbol{\alpha}+\boldsymbol{\beta}=1$ in these cases.

We now rearrange (6.4.1) in the following form

$$m_h(\bar{\partial}_{tt}\mathcal{U}^n, w_h) + a_h(\mathcal{U}^{n,\boldsymbol{\theta}}, w_h) + \left(\boldsymbol{\gamma} - \frac{1}{2}\right) a_h(\mathcal{U}^n - \mathcal{U}^{n-1}, w_h) = (f_h^{n,\boldsymbol{\theta}}, w_h). \tag{6.4.19}$$

So, it appears as a first-order fully discrete approximation of the modified wave equation

$$u_{tt} - \tau\left(\boldsymbol{\gamma} - \frac{1}{2}\right)\nabla\cdot(\sigma\nabla u_t) - \nabla\cdot(\sigma\nabla u) = f. \tag{6.4.20}$$

which represents a strongly damped wave equation when $\boldsymbol{\gamma} \geq \frac{1}{2}$. Hence, taking $\boldsymbol{\gamma} \geq \frac{1}{2}$ introduces an algorithm damping into the time integration. For long time integration, it is then preferable to choose $\boldsymbol{\gamma} \geq \frac{1}{2}$. In this case, the scheme is first-order accurate and unconditionally stable provided that $\boldsymbol{\theta} \geq \frac{\gamma}{2}$ (see Theorem 6.4.1).

Finally, by examining the three-level schemes (6.4.19) and (6.4.17), we find that the two schemes (6.4.1) and (6.4.8) are equivalent when

$$\boldsymbol{\alpha\beta} = \boldsymbol{\theta} \text{ and } \boldsymbol{\alpha}+\boldsymbol{\beta} = \frac{1}{2} + \boldsymbol{\gamma}.$$

This system of two equations has a solution $(\boldsymbol{\alpha}, \boldsymbol{\beta})$ only if

$$0 \leq \boldsymbol{\theta} \leq \frac{1}{4}\left(\frac{1}{2} + \boldsymbol{\gamma}\right)^2.$$

Hence, we deduce that the Newmark scheme (6.4.1) is more flexible in choosing the algorithm parameters than (6.4.8), and has better stability properties. To see this, consider for

instance the special case where both schemes are equivalent to the three-level scheme (6.4.2). In this case, the choice $(\boldsymbol{\alpha}, \boldsymbol{\beta})=\left(\frac{1}{2}, \frac{1}{2}\right)$ is the only case for (6.4.8) to be unconditionally stable, whereas (6.4.1) is unconditionally stable for all $\boldsymbol{\theta} \geq \frac{1}{4}$.

6.5 Error Analysis for the Fully Discrete Problems

The following approximation result can be derived, which will be required later.

Lemma 6.5.1. *For $v \in H^4(0,T;L^2(\Omega))$, we have*

$$\|\bar{\partial}_{tt}v^n - v_{tt}^{n,\boldsymbol{\theta},\boldsymbol{\gamma}}\| \leq \left|\boldsymbol{\gamma}-\frac{1}{2}\right| \int_{t_{n-1}}^{t_n} \|D_t^3 v(s)\| ds + \left(\frac{1}{6}+\boldsymbol{\theta}\right)\tau \int_{t_{n-1}}^{t_{n+1}} \|D_t^4 v(s)\| ds,$$

where $D_t^k = \dfrac{\partial^k}{\partial t^k}$. Moreover, when $\boldsymbol{\theta} = \frac{1}{12}$, for $v \in H^6(0,T;L^2(\Omega))$, we have

$$\|\bar{\partial}_{tt}v^n - v_{tt}^{n,\boldsymbol{\theta},\boldsymbol{\gamma}}\| \leq \left|\boldsymbol{\gamma}-\frac{1}{2}\right| \int_{t_{n-1}}^{t_n} \|D_t^3 v(s)\| ds + \left(\frac{1}{5!}+\frac{1}{72}\right)\tau^3 \int_{t_{n-1}}^{t_{n+1}} \|D_t^6 v(s)\| ds.$$

Proof. We have the following identity

$$\bar{\partial}_{tt}v^n = v_{tt}^n + \frac{1}{6\tau^2}\int_{-\tau}^{\tau} (\tau-|s|)^3 D_t^4 v(\cdot, t^n+s) ds. \tag{6.5.1}$$

Again, using Taylor's expansion we can derive

$$v_{tt}^{n,\boldsymbol{\theta},\boldsymbol{\gamma}} = v_{tt}^n + \boldsymbol{\theta}\int_{-\tau}^{\tau}(\tau-|s|)D_t^4 v(\cdot,t^n+s)ds + \left(\boldsymbol{\gamma}-\frac{1}{2}\right)\int_{-\tau}^{0} D_t^3 v(\cdot,t^n+s)ds. \tag{6.5.2}$$

Subtracting (6.5.2) from (6.5.1), yields

$$\begin{aligned}\bar{\partial}_{tt}v^n - v_{tt}^{n,\boldsymbol{\theta},\boldsymbol{\gamma}} =& \frac{1}{6\tau^2}\int_{-\tau}^{\tau}(\tau-|s|)^3 D_t^4 v(\cdot,t^n+s)ds - \boldsymbol{\theta}\int_{-\tau}^{\tau}(\tau-|s|)D_t^4 v(\cdot,t^n+s)ds \\ &- \left(\boldsymbol{\gamma}-\frac{1}{2}\right)\int_0^{\tau} D_t^3 v(\cdot,t^n+s)ds.\end{aligned}$$

Using triangle inequality and since $\tau-|s| \leq \tau$, $s \in [\tau,\tau]$, we have

$$\begin{aligned}\|\bar{\partial}_{tt}v^n - v_{tt}^{n,\boldsymbol{\theta},\boldsymbol{\gamma}}\| &\leq \left(\frac{1}{6}+\boldsymbol{\theta}\right)\tau\int_{-\tau}^{\tau}\|D_t^4 v(t^n+s)\|ds + \left|\boldsymbol{\gamma}-\frac{1}{2}\right|\int_0^{\tau}\|D_t^3 v(t^n+s)\|ds \\ &\leq \left(\frac{1}{6}+\boldsymbol{\theta}\right)\tau\int_{t_{n-1}}^{t_n}\|D_t^4 v(s)\|ds + \left|\boldsymbol{\gamma}-\frac{1}{2}\right|\int_{t_{n-1}}^{t_n}\|D_t^3 v(s)\|ds.\end{aligned}$$

For $\boldsymbol{\theta} = \frac{1}{12}$, we need higher order Taylor's expansion. We have following refinement of (6.5.1) and (6.5.2)

$$\bar{\partial}_{tt} v^n = v^n_{tt} + \frac{\tau^2}{12} D_t^4 v^n + \frac{1}{5!\tau^2} \int_{-\tau}^{\tau} (\tau - |s|)^5 D_t^6 v(\cdot, t^n + s) ds$$

and

$$v^{n,\boldsymbol{\theta},\boldsymbol{\gamma}}_{tt} = v^n_{tt} + \frac{\tau^2}{12} D_t^4 v^n + \frac{1}{72} \int_{-\tau}^{\tau} (\tau - |s|)^3 D_t^6 v(\cdot, t^n + s) ds + \left(\boldsymbol{\gamma} - \frac{1}{2}\right) \int_{-\tau}^{0} D_t^3 v(\cdot, t^n + s) ds.$$

Now following similar steps as the previous case, we obtain

$$\|\bar{\partial}_{tt} v^n - v^{n,\boldsymbol{\theta},\boldsymbol{\gamma}}_{tt}\| \leq \left(\frac{1}{5!} + \frac{1}{72}\right) \tau^3 \int_{t_{n-1}}^{t_{n+1}} \|D_t^6 v(s)\| ds + \left|\boldsymbol{\gamma} - \frac{1}{2}\right| \int_{t_{n-1}}^{t_n} \|D_t^3 v(s)\| ds.$$

□

Towards estimating the error $e^n_h := \mathcal{U}^n - u^n$, we define the auxiliary functions $\xi^n := \mathcal{U}^n - R_h u^n$ for $n = 1, 2, \cdots, N$. We define a sequence ψ^n, $n \geq 0$ such that

$$(\psi^0, w_h) = \frac{1}{\tau^2} m_h(\xi^1 - \xi^0, w_h) + \boldsymbol{\theta}\, a_h(\xi^1 - \xi^0, w_h)$$

and for $n \geq 1$

$$(\psi^n, w_h) = (f^{n,\boldsymbol{\theta},\boldsymbol{\gamma}}_h - f^{n,\boldsymbol{\theta},\boldsymbol{\gamma}}, w_h) + (u^{n,\boldsymbol{\theta},\boldsymbol{\gamma}}_{tt}, w_h) - m_h(\bar{\partial}_{tt} R_h u^n, w_h)$$

for all $w_h \in W^m_h$. We set

$$\Psi^r = \tau \sum_{n=0}^{r} \psi^n.$$

Then, we have the following estimate for the term ξ^n.

Proposition 6.5.1. *It holds*

$$\max_{0 \leq n \leq N} \|\xi^n\| \leq C\tau \sum_{n=0}^{N-1} \|\Psi^n\|.$$

Proof. Considering (6.1.1) with $t = t^{n-1}$, $t = t^n$ and $t = t^{n+1}$, multiplying with $\boldsymbol{\theta}$, $\frac{1}{2} - 2\boldsymbol{\theta} + \boldsymbol{\gamma}$ and $\frac{1}{2} + \boldsymbol{\theta} - \boldsymbol{\gamma}$, respectively, and then adding, we obtain

$$(u^{n,\boldsymbol{\theta},\boldsymbol{\gamma}}_{tt}, w_h) + a_h(R_h u^{n,\boldsymbol{\theta},\boldsymbol{\gamma}}, w_h) = (f^{n,\boldsymbol{\theta},\boldsymbol{\gamma}}, w_h), \ \forall w_h \in W^m_h. \tag{6.5.3}$$

Here, we have used the definition of projection operator R_h. Now subtracting (6.5.3) from (6.4.1), for any $w_h \in W_h^m$ it follows that

$$m_h(\bar{\partial}_{tt}\xi^n, w_h) + a_h(\xi^{n,\boldsymbol{\theta},\boldsymbol{\gamma}}, w_h) = (\psi^n, w_h),\ 1 \le n \le N-1.$$

Using (6.4.11), the above equation can be rearranged as

$$m_h(\bar{\partial}_{tt}\xi^n, w_h) + \tau^2\left(\boldsymbol{\theta} - \frac{\boldsymbol{\gamma}}{2}\right) a_h(\bar{\partial}_{tt}\xi^n, w_h) + \boldsymbol{\gamma} a_h(\xi^{n+\frac{1}{2}}, w_h) + (1-\boldsymbol{\gamma}) a_h(\xi^{n-\frac{1}{2}}, w_h) = (\psi^n, w_h),$$

for $1 \le n \le N-1$. Now summing over $n = 1$ to $n = r$ and multiplying by τ, we obtain

$$\begin{aligned} &m_h\left(\frac{\xi^{r+1} - \xi^r}{\tau}, w_h\right) + \tau\left(\boldsymbol{\theta} - \frac{\boldsymbol{\gamma}}{2}\right) a_h(\xi^{r+1} - \xi^r, w_h) + \tau \sum_{n=1}^{r} a_h(\boldsymbol{\gamma}\xi^{n+\frac{1}{2}} + (1-\boldsymbol{\gamma})\xi^{n-\frac{1}{2}}, w_h) \\ &= \tau \sum_{n=1}^{r} (\psi^n, w_h) + m_h\left(\frac{\xi^1 - \xi^0}{\tau}, w_h\right) + \tau\left(\boldsymbol{\theta} - \frac{\boldsymbol{\gamma}}{2}\right) a_h(\xi^1 - \xi^0, w_h). \end{aligned} \tag{6.5.4}$$

Let us define

$$\alpha^0 = -\boldsymbol{\gamma}\xi^0,\ \alpha^r = -\boldsymbol{\gamma}\xi^0 + \sum_{n=1}^{r-1} \xi^{n+\frac{1}{2}}. \tag{6.5.5}$$

It can be easily derived that

$$\sum_{n=1}^{r}\left(\boldsymbol{\gamma}\xi^{n+\frac{1}{2}} + (1-\boldsymbol{\gamma})\xi^{n-\frac{1}{2}}\right) = \boldsymbol{\gamma}\alpha^{r+1} + (1-\boldsymbol{\gamma})\alpha^r - \frac{\boldsymbol{\gamma}}{2}(\xi^1 - \xi^0),\ \alpha^{r+1} - \alpha^r = \xi^{r+\frac{1}{2}}.$$

The expression (6.5.4) can be written as: for all $w_h \in W_h^m$ and $1 \le r \le N-1$

$$\begin{aligned} &m_h\left(\frac{\xi^{r+1} - \xi^r}{\tau}, w_h\right) + \tau\left(\boldsymbol{\theta} - \frac{\boldsymbol{\gamma}}{2}\right) a_h(\xi^{r+1} - \xi^r, w_h) + \frac{\tau}{2} a_h(\boldsymbol{\gamma}\alpha^{r+1} + (1-\boldsymbol{\gamma})\alpha^r, w_h) \\ &= (\Psi^r, w_h). \end{aligned}$$

Now by substituting $w_h = \xi^{r+1} + \xi^r$ and multiplying with τ, the previous equation yields

$$\begin{aligned} &m_h(\xi^{r+1}, \xi^{r+1}) - m_h(\xi^r, \xi^r) + \tau^2\left(\boldsymbol{\theta} - \frac{\boldsymbol{\gamma}}{2}\right)\left[a_h(\xi^{r+1}, \xi^{r+1}) - a_h(\xi^r, \xi^n)\right] \\ &+ 2\tau^2\left[\boldsymbol{\gamma} a_h(\alpha^{r+1} + \alpha^r, \alpha^{r+1} - \alpha^r) + (1 - 2\boldsymbol{\gamma}) a_h(\alpha^r, \alpha^{r+1} - \alpha^r)\right] = \tau(\Psi^r, \xi^{r+1} + \xi^r), \end{aligned} \tag{6.5.6}$$

for $1 \le r \le N-1$. Again, since $1-2\boldsymbol{\gamma} \le 0$ and $(x, x-y) \le \frac{1}{2}[(x,x)-(y,y)]$, we have

$$\frac{1-2\boldsymbol{\gamma}}{2}\left[a_h(\alpha^{r+1},\alpha^{r+1}) - a_h(\alpha^r,\alpha^r)\right] \le (1-2\boldsymbol{\gamma})a_h(\alpha^r,\alpha^{r+1}-\alpha^r).$$

Thus (6.5.6) can be written as

$$\begin{aligned} &m_h(\xi^{r+1},\xi^{r+1}) - m_h(\xi^r,\xi^r) + \tau^2\left(\boldsymbol{\theta}-\frac{\boldsymbol{\gamma}}{2}\right)\left[a_h(\xi^{r+1},\xi^{r+1}) - a_h(\xi^r,\xi^n)\right] \\ &+ \tau^2\left[a_h(\alpha^{r+1},\alpha^{r+1}) + a_h(\alpha^r,\alpha^r)\right] \le \tau(\Psi^r, \xi^{r+1}+\xi^r),\ 1 \le r \le N-1. \end{aligned}$$

Taking summation from $r=0$ to $r=n-1$, $1 \le n \le N$, we get

$$\begin{aligned} &m_h(\xi^n,\xi^n) - m_h(\xi^0,\xi^0) + \tau^2\left(\boldsymbol{\theta}-\frac{\boldsymbol{\gamma}}{2}\right)\left[a_h(\xi^n,\xi^n) - a_h(\xi^0,\xi^0)\right] + \tau^2\left[a_h(\alpha^n,\alpha^n) - a_h(\alpha^0,\alpha^0)\right] \\ &\le \tau\sum_{r=0}^{n-1}(\Psi^r, \xi^{r+1}+\xi^r). \end{aligned}$$

Using (6.5.5), above equation implies

$$\begin{aligned} &m_h(\xi^n,\xi^n) + \tau^2\left(\boldsymbol{\theta}-\frac{\boldsymbol{\gamma}}{2}\right)a_h(\xi^n,\xi^n) + \tau^2(\alpha^n,\alpha^n) \\ &\le \tau\sum_{r=0}^{n-1}(\Psi^r, \xi^{r+1}+\xi^r) + m_h(\xi^0,\xi^0) + \tau^2\left(\boldsymbol{\theta}+\boldsymbol{\gamma}^2-\frac{\boldsymbol{\gamma}}{2}\right)a_h(\xi^0,\xi^0). \end{aligned}$$

Ignoring positive terms on left hand side, we get

$$\begin{aligned} &m_h(\xi^n,\xi^n)\left(1+\tau^2\left(\boldsymbol{\theta}-\frac{\boldsymbol{\gamma}}{2}\right)\frac{a_h(\xi^n,\xi^n)}{m_h(\xi^n,\xi^n)}\right) \\ &\le \tau\sum_{r=0}^{n-1}(\Psi^r, \xi^{r+1}+\xi^r) + m_h(\xi^0,\xi^0) + \tau^2\left(\boldsymbol{\theta}+\boldsymbol{\gamma}^2-\frac{\boldsymbol{\gamma}}{2}\right)a_h(\xi^0,\xi^0). \end{aligned}$$

Now using the coercivity and continuity of m_h and a_h and the fact $\xi^0 = \mathcal{U}^0 - u_h^0 = 0$, we have

$$\bar{C}\|\xi^n\|^2 \le C\tau\sum_{r=0}^{n-1}(\Psi^r, \xi^{r+1}+\xi^r) \le C\tau\sum_{r=0}^{n-1}\|\Psi^r\|\,\|\xi^{r+1}+\xi^r\|,$$

where

$$\bar{C} = \left(1+\tau^2\left(\boldsymbol{\theta}-\frac{\boldsymbol{\gamma}}{2}\right)\frac{a_h(\xi^n,\xi^n)}{m_h(\xi^n,\xi^n)}\right).$$

From the stability condition (6.4.13), it is easy to verify that $\bar{C}$ is positive. Taking maximum over $n = 0$ to $n = N$, the above equation becomes

$$\max_{0\le n\le N} \|\xi^n\|^2 \le \frac{2C\tau}{\bar{C}} \max_{0\le n\le N} \|\xi^n\| \sum_{n=0}^{N-1} \|\Psi^n\|.$$

This gives us

$$\max_{0\le n\le N} \|\xi^n\| \le \frac{2C\tau}{\bar{C}} \sum_{n=0}^{N-1} \|\Psi^n\|.$$

□

In order to obtain the bound for the term $\Psi^n = \tau \sum_{r=0}^{n} \psi^r$, we need the bounds for ψ^0 and ψ^r, $r \ge 1$. For ψ^0, we have the following result.

Lemma 6.5.2. *We have for* $\boldsymbol{\theta} \ne \frac{1}{12}$

$$\tau\|\psi^0\| \le C\left[h^{m+1}\|u_t\|_{C(\bar{\mathcal{J}};H^{m+1}(\Omega))} + \tau^2\left(\|D_t^3 u\|_{C(\bar{\mathcal{J}};L^2(\Omega))} + \|f_t\|_{C(\bar{\mathcal{J}};L^2(\Omega))}\right)\right]$$

and for $\boldsymbol{\theta} = \frac{1}{12}$

$$\tau\|\psi^0\| \le C\left[h^{m+1}\|u_t\|_{C(\bar{\mathcal{J}};H^{m+1}(\Omega))} + \tau^4\left(\|D_t^5 u\|_{C(\bar{\mathcal{J}};L^2(\Omega))} + \|D_t^3 f\|_{C(\bar{\mathcal{J}};L^2(\Omega))}\right)\right].$$

Proof. From the definition of ψ^0, we can write

$$\begin{aligned}\tau^2(\psi^0, w_h) =& m_h(\xi^1 - \xi^0, w_h) + \tau^2\boldsymbol{\theta}\, a_h(\xi^1 - \xi^0, w_h)\\ =& m_h(\mathcal{U}^1 - \mathcal{U}^0, w_h) - (u^1 - u^0, w_h) + \tau^2\boldsymbol{\theta}\left[a_h(\mathcal{U}^1 - \mathcal{U}^0, w_h) - a(u^1 - u^0, w_h)\right]\\ &+ m_h((L_h - R_h)(u^1 - u^0), w_h). \end{aligned} \tag{6.5.7}$$

Taking $n = 0$ and $n = 1$ in equation (6.1.1), and then subtracting, we get

$$a(u^1 - u^0, w_h) = (f^1 - f^0, w_h) - (u_{tt}^1 - u_{tt}^0, w_h),\ \forall w_h \in W_h^m. \tag{6.5.8}$$

Again from Taylor's formula with integral remainder, we have

$$(u^1 - u^0, w_h) = \tau\,(v_0, w_h) + \frac{\tau^2}{2}\,(u_{tt}^0, w_h) + \frac{1}{2}\int_{t_0}^{t_1} (\tau - s)^2 (D_t^3 u(\cdot, s), w_h) ds,\ \forall w_h \in W_h^m. \tag{6.5.9}$$

Adding $\tau^2\boldsymbol{\theta}$ times (6.5.8) with (6.5.9), then subtracting from initial condition (6.4.5), results in

$$\begin{aligned}
&m_h(\mathcal{U}^1-\mathcal{U}^0,w_h)-(u^1-u^0,w_h)+\tau^2\boldsymbol{\theta}\left[a_h(\mathcal{U}^1-\mathcal{U}^0,w_h)-a(u^1-u^0,w_h)\right]\\
&=-\frac{1}{2}\int_{t^0}^{t^1}(\tau-s)^2(D_t^3u(\cdot,s),w_h)ds+\tau^2\boldsymbol{\theta}\,(u_{tt}^1-u_{tt}^0,w_h)-\tau^2\boldsymbol{\theta}\,(f^1-f^0,w_h),\ \forall w_h\in W_h^m.
\end{aligned}$$

Here, we have used the fact

$$(f^0,w_h)-a(u_0,w_h)=(u_{tt}^0,w_h).$$

Substituting the above estimate in (6.5.7), we obtain

$$\begin{aligned}
\tau^2(\psi^0,w_h)=&-\frac{1}{2}\int_{t_0}^{t_1}(\tau-s)^2(D_t^3u(\cdot,s),w_h)ds+\tau^2\boldsymbol{\theta}\,(u_{tt}^1-u_{tt}^0,w_h)\\
&-\tau^2\boldsymbol{\theta}\,(f^1-f^0,w_h)+m_h((L_h-R_h)(u^1-u^0),w_h)\\
=&I_1+I_2+I_3+I_4.
\end{aligned}\tag{6.5.10}$$

For the term I_1, we have following bound

$$\left|\frac{1}{2}\int_{t^0}^{t^1}(\tau-s)^2(D_t^3u(\cdot,s),w_h)ds\right|\le\frac{\tau^2}{2}\int_{t_0}^{t_1}|(D_t^3u(\cdot,s),w_h)|ds\le C\tau^3\|D_t^3u\|_{C(\bar{\mathcal{J}};L^2(\Omega))}\|w_h\|.\tag{6.5.11}$$

Similarly, I_2 and I_3 can be bounded as

$$\left|\tau^2\boldsymbol{\theta}\,(u_{tt}^1-u_{tt}^0,w_h)\right|\le\tau^2\boldsymbol{\theta}\int_{t_0}^{t_1}|(D_t^3u(\cdot,s),w_h)|ds\le C\tau^3\boldsymbol{\theta}\|D_t^3u\|_{C(\bar{\mathcal{J}};L^2(\Omega))}\|w_h\|\tag{6.5.12}$$

and

$$\left|\tau^2\boldsymbol{\theta}\,(f^1-f^0,w_h)\right|\le\tau^2\boldsymbol{\theta}\int_{t_0}^{t_1}|m_h(f_t(\cdot,s),w_h)|ds\le C\tau^3\boldsymbol{\theta}\|f_t\|_{C(\bar{\mathcal{J}};L^2(\Omega))}\|w_h\|,\tag{6.5.13}$$

respectively. For I_4, using Lemma 2.2.1, we have

$$\begin{aligned}
|m_h((L_h-R_h)(u^1-u^0),w_h)|&\le\int_{t_0}^{t_1}|(L_h-R_h)(u_t(\cdot,s),w_h)|ds\\
&\le C\tau h^{m+1}\|u_t\|_{C(\bar{\mathcal{J}};H^{m+1}(\Omega))}\|w_h\|.
\end{aligned}\tag{6.5.14}$$

Using the estimates (6.5.11)-(6.5.14) in (6.5.10) yields

$$\tau^2 \left|m_h(\psi^0, w_h)\right| \leq C \left[h^{m+1}\tau \|u_t\|_{C(\bar{\mathcal{J}};H^{m+1}(\Omega))} + \tau^3 \left(\|D_t^3 u\|_{C(\bar{\mathcal{J}};L^2(\Omega))} + \|f_t\|_{C(\bar{\mathcal{J}};L^2(\Omega))}\right)\right] \|w_h\|.$$

Hence, we obtain

$$\tau\|\psi^0\| \leq C \left[h^{m+1}\|u_t\|_{C(\bar{\mathcal{J}};H^{m+1}(\Omega))} + \tau^2 \left(\|D_t^3 u\|_{C(\bar{\mathcal{J}};L^2(\Omega))} + \|f_t\|_{C(\bar{\mathcal{J}};L^2(\Omega))}\right)\right].$$

For $\boldsymbol{\theta} = \frac{1}{12}$, we consider the higher order Taylor's formula with integral reminder to obtain

$$\begin{aligned}
&(u^1 - u^0, w_h)\\
&= \tau(v_0, w_h) + \frac{\tau^2}{2}(u_{tt}^0, w_h) + \frac{\tau^3}{6}(D_t^3 u^0, w_h) + \frac{\tau^4}{24}(D_t^4 u^0, w_h) + \frac{1}{24}\int_{t_0}^{t_1} (\tau - s)^4 (D_t^5 u(\cdot, s), w_h) ds
\end{aligned}$$

for all $w_h \in W_h^m$. Proceeding similarly as previous case with the initial condition (6.4.6), we obtain

$$\begin{aligned}
&m_h(\mathcal{U}^1 - \mathcal{U}^0, w_h) - (u^1 - u^0, w_h) + \tau^2\boldsymbol{\theta}\left[a_h(\mathcal{U}^1 - \mathcal{U}^0, w_h) - a(u^1 - u^0, w_h)\right]\\
&= -\frac{1}{24}\int_{t^0}^{t^1} (\tau - s)^4 (D_t^5 u(\cdot, s), w_h) ds + \frac{\tau^2}{24}\int_{t_0}^{t_1} (\tau - s)^2 (D_t^5 u(\cdot, s), w_h) ds\\
&\quad + \frac{\tau^2}{12}\left(\tau f_t^0 + \frac{\tau^2}{2} f_{tt}^0 - f^1 + f^0, w_h\right)
\end{aligned}$$

for all $w_h \in W_h^m$. Here, we have used the facts

$$(f_t^0, w_h) - a(v_0, w_h) = (D_t^3 u^0, w_h)$$

and

$$(u_{tt}^1 - u_{tt}^0, w_h) = \tau\,(D_t^3 u^0, w_h) + \frac{\tau^2}{2}\,(D_t^4 u^0, w_h) + \frac{1}{2}\int_{t_0}^{t_1} (\tau - s)^2 (D_t^5 u(\cdot, s), w_h) ds$$

for all $w_h \in W_h^m$. Substituting the above estimate in (6.5.7), we obtain

$$\begin{aligned}
\tau^2(\psi^0, w_h) =& -\frac{1}{24}\int_{t^0}^{t^1} (\tau - s)^4 (D_t^5 u(\cdot, s), w_h) ds + \frac{\tau^2}{24}\int_{t_0}^{t_1} (\tau - s)^2 (D_t^5 u(\cdot, s), w_h) ds\\
&+ \frac{\tau^2}{12}\left(\tau f_t^0 + \frac{\tau^2}{2} f_{tt}^0 - f^1 + f^0, w_h\right) + m_h((L_h - R_h)(u^1 - u^0), w_h)\\
=& J_1 + J_2 + J_3 + J_4. \qquad (6.5.15)
\end{aligned}$$

As in (6.5.11), we can derive

$$J_1, J_2 \leq \frac{\tau^5}{24}\|D_t^5 u\|_{C(\bar{\mathcal{J}};L^2(\Omega))}. \tag{6.5.16}$$

For J_3, using the Taylor's formula with integral reminder, we obtain

$$\begin{aligned} J_3 \leq \left|\frac{\tau^2}{12}(\tau f_t^0 + \frac{\tau^2}{2} f_{tt}^0 - f^1 + f^0, w_h)\right| &= \frac{\tau^2}{24}\left|\int_{t^0}^{t^1} (\tau - s)^2 (D_t^3 f(\cdot, s), w_h) ds\right| \\ &\leq \frac{\tau^5}{24}\|D_t^3 f\|_{C(\bar{\mathcal{J}};L^2(\Omega))}. \end{aligned} \tag{6.5.17}$$

Now, plugging the estimates (6.5.16)-(6.5.17) and (6.5.14) in (6.5.15) yields

$$\begin{aligned} &\tau^2 \left|m_h(\psi^0, w_h)\right| \\ &\leq C\left[h^{m+1}\tau\|u_t\|_{C(\bar{\mathcal{J}};H^{m+1}(\Omega))} + \tau^5\left(\|D_t^5 u\|_{C(\bar{\mathcal{J}};L^2(\Omega))} + \|D_t^3 f\|_{C(\bar{\mathcal{J}};L^2(\Omega))}\right)\right]\|w_h\|. \end{aligned}$$

Hence, we obtain

$$\tau\|\psi^0\| \leq C\left[h^{m+1}\|u_t\|_{C(\bar{\mathcal{J}};H^{m+1}(\Omega))} + \tau^4\left(\|D_t^5 u\|_{C(\bar{\mathcal{J}};L^2(\Omega))} + \|D_t^3 f\|_{C(\bar{\mathcal{J}};L^2(\Omega))}\right)\right].$$

□

Again, for $r \geq 1$, ψ^r satisfies the following estimate.

Lemma 6.5.3. *For $1 \leq r \leq N-1$, we have*

$$\begin{aligned} \|\psi^r\| \leq C\Bigg[&h^{m+1}\left(\|f\|_{H^1(\mathcal{J};H^{m+1}(\Omega))} + \frac{1}{\tau}\int_{t_{r-1}}^{t_{r+1}} |u_{tt}(s)|_{m+1} ds\right) \\ &+ \left|\boldsymbol{\gamma} - \frac{1}{2}\right|\int_{t_{r-1}}^{t_r} \|D_t^3 u(s)\| ds + \left(\frac{1}{6} + \boldsymbol{\theta}\right)\tau\int_{t_{r-1}}^{t_{r+1}} \|D_t^4 u(s)\| ds\Bigg] \end{aligned}$$

for $\boldsymbol{\theta} \neq \frac{1}{12}$ and

$$\begin{aligned} \|\psi^r\| \leq C\Bigg[&h^{m+1}\left(\|f\|_{H^1(\mathcal{J};H^{m+1}(\Omega))} + \frac{1}{\tau}\int_{t_{r-1}}^{t_{r+1}} |u_{tt}(s)|_{m+1} ds\right) \\ &+ \left|\boldsymbol{\gamma} - \frac{1}{2}\right|\int_{t_{r-1}}^{t_r} \|D_t^3 u(s)\| ds + \left(\frac{1}{5!} + \frac{1}{72}\right)\tau^3\int_{t_{r-1}}^{t_{r+1}} \|D_t^6 u(s)\| ds\Bigg] \end{aligned}$$

for $\boldsymbol{\theta} = \frac{1}{12}$.

Proof. We have

$$\begin{aligned}(\psi^r, w_h) &= (f_h^{r,\boldsymbol{\theta},\boldsymbol{\gamma}} - f^{r,\boldsymbol{\theta},\boldsymbol{\gamma}}, w_h) + m_h(\bar{\partial}_{tt} R_h u^r, w_h) - (u_{tt}^{r,\boldsymbol{\theta},\boldsymbol{\gamma}}, w_h) \\ &= (f_h^{r,\boldsymbol{\theta},\boldsymbol{\gamma}} - f^{r,\boldsymbol{\theta},\boldsymbol{\gamma}}, w_h) + m_h(\bar{\partial}_{tt} R_h u^r - \bar{\partial}_{tt} L_h u^r, w_h) + (\bar{\partial}_{tt} u^r - u_{tt}^{r,\boldsymbol{\theta},\boldsymbol{\gamma}}, w_h) \\ &= T_1 + T_2 + T_3.\end{aligned}$$

For T_1, using Lemma 1.4.6 and Lemma 1.2.1, we have

$$T_1 = (f_h^{r,\boldsymbol{\theta},\boldsymbol{\gamma}} - f^{r,\boldsymbol{\theta},\boldsymbol{\gamma}}, w_h) \leq Ch^{m+1} |f^{r,\boldsymbol{\theta},\boldsymbol{\gamma}}|_{m+1} \|w_h\| \leq Ch^{m+1} \|f\|_{H^1(\mathcal{J};H^{m+1}(\Omega))} \|w_h\|.$$

Similarly for T_2, from Lemma 2.2.1, we obtain

$$\begin{aligned}T_2 = m_h(\bar{\partial}_{tt} R_h u^r - \bar{\partial}_{tt} L_h u^r, w_h) &\leq Ch^{m+1} |\bar{\partial}_{tt} u^r|_{m+1} \|w_h\| \\ &\leq C \frac{h^{m+1}}{\tau} \int_{t_{r-1}}^{t_{r+1}} |u_{tt}(s)|_{m+1} ds \, \|w_h\|.\end{aligned}$$

Since,

$$\bar{\partial}_{tt} u^r = \frac{1}{\tau^2} \int_{-\tau}^{\tau} (\tau - |s|) u_{tt}(\cdot, t^r + s) ds.$$

From Lemma 6.5.1, we have

$$\begin{aligned}T_3 &\leq \|\bar{\partial}_{tt} u^r - u_{tt}^{r,\boldsymbol{\theta},\boldsymbol{\gamma}}\| \|w_h\| \\ &\leq \left(\left| \boldsymbol{\gamma} - \frac{1}{2} \right| \int_{t_{r-1}}^{t_r} \|D_t^3 u(s)\| ds + \left(\frac{1}{6} + \boldsymbol{\theta} \right) \tau \int_{t_{r-1}}^{t_{r+1}} \|D_t^4 u(s)\| ds \right) \|w_h\|\end{aligned}$$

for $\boldsymbol{\theta} \neq \frac{1}{12}$ and for $\boldsymbol{\theta} = \frac{1}{12}$

$$T_3 \leq \left(\left| \boldsymbol{\gamma} - \frac{1}{2} \right| \int_{t_{r-1}}^{t_r} \|D_t^3 u(s)\| ds + \left(\frac{1}{5!} + \frac{1}{72} \right) \tau^3 \int_{t_{r-1}}^{t_{r+1}} \|D_t^6 u(s)\| ds \right) \|w_h\|.$$

Now, combining the estimates for T_1, T_2 and T_3, yields the desired estimate. □

Plugging the estimates from Lemma 6.5.2 and Lemma 6.5.3 in proposition 6.5.1, the following bound can be obtained for the term ξ^n.

Lemma 6.5.4.

$$\begin{aligned}\max_{0 \leq n \leq N} \|\xi^n\| \leq & Ch^{m+1} \left(\|u_t\|_{C(\bar{\mathcal{J}};H^{m+1}(\Omega))} + \|f\|_{H^1(\mathcal{J};H^{m+1}(\Omega))} + \|u_{tt}\|_{L^1(\mathcal{J};H^{m+1}(\Omega))} \right) \\ & + C\tau \left| \boldsymbol{\gamma} - \frac{1}{2} \right| \|D_t^3 u\|_{L^1(\mathcal{J};L^2(\Omega))} \\ & + C\tau^2 \left(\|D_t^3 u\|_{C(\bar{\mathcal{J}};L^2(\Omega))} + \|f_t\|_{C(\bar{\mathcal{J}};L^2(\Omega))} + \|D_t^4 u(t)\|_{L^1(\mathcal{J};L^2(\Omega))} \right)\end{aligned}$$

for $\boldsymbol{\theta} \neq \frac{1}{12}$ *and*

$$\begin{aligned}\max_{0\leq n\leq N}\|\xi^n\| \leq & Ch^{m+1}\left(\|u_t\|_{C(\bar{\mathcal{J}};H^{m+1}(\Omega))}+\|f\|_{H^1(\mathcal{J};H^{m+1}(\Omega))}+\|u_{tt}\|_{L^1(\mathcal{J};H^{m+1}(\Omega))}\right)\\ &+C\tau\left|\boldsymbol{\gamma}-\frac{1}{2}\right|\|D_t^3u\|_{L^1(\mathcal{J};L^2(\Omega))}\\ &+C\tau^4\left(\|D_t^5u\|_{C(\bar{\mathcal{J}};L^2(\Omega))}+\|D_t^3f\|_{C(\bar{\mathcal{J}};L^2(\Omega))}+\|D_t^6u(t)\|_{L^1(\mathcal{J};L^2(\Omega))}\right)\end{aligned}$$

for $\boldsymbol{\theta} = \frac{1}{12}$.

Proof. From the previous lemma, we have

$$\begin{aligned}\tau\sum_{r=1}^{N-1}\|\psi^r\| \leq C\Bigg[&h^{m+1}\left(\|f\|_{H^1(\mathcal{J};H^{m+1}(\Omega))}+\|u_{tt}\|_{L^1(\mathcal{J};H^{m+1}(\Omega))}\right)\\ &+\tau\left|\boldsymbol{\gamma}-\frac{1}{2}\right|\|D_t^3u\|_{L^1(\mathcal{J};L^2(\Omega))}+\tau^2\|D_t^4u\|_{L^1(\mathcal{J};L^2(\Omega))}\Bigg]\end{aligned}$$

for $\boldsymbol{\theta} \neq \frac{1}{12}$ and

$$\begin{aligned}\tau\sum_{r=1}^{N-1}\|\psi^r\| \leq C\Bigg[&h^{m+1}\left(\|f\|_{H^1(\mathcal{J};H^{m+1}(\Omega))}+\|u_{tt}\|_{L^1(\mathcal{J};H^{m+1}(\Omega))}\right)\\ &+\tau\left|\boldsymbol{\gamma}-\frac{1}{2}\right|\|D_t^3u\|_{L^1(\mathcal{J};L^2(\Omega))}+\tau^4\|D_t^6u\|_{L^1(\mathcal{J};L^2(\Omega))}\Bigg]\end{aligned}$$

for $\boldsymbol{\theta} = \frac{1}{12}$. Using triangle inequality, we can write

$$\max_{0\leq n\leq N-1}\|\Psi^n\| \leq \tau\max_{0\leq n\leq N-1}\left(\|\psi^0\|+\sum_{r=1}^{n}\|\psi^r\|\right) \leq \tau\|\psi^0\|+\tau\sum_{r=1}^{N-1}\|\psi^r\|.$$

From the estimates in Lemma 6.5.2 and previous estimates, we have

$$\begin{aligned}&\max_{0\leq n\leq N-1}\|\Psi^n\|\\ &\leq C\Bigg[h^{m+1}\left(\|u_t\|_{C(\bar{\mathcal{J}};H^{m+1}(\Omega))}+\|f\|_{H^1(\mathcal{J};H^{m+1}(\Omega))}+\|u_{tt}\|_{L^1(\mathcal{J};H^{m+1}(\Omega))}\right)\\ &+\tau\left|\boldsymbol{\gamma}-\frac{1}{2}\right|\|D_t^3u\|_{L^1(\mathcal{J};L^2(\Omega))}+\tau^2\left(\|D_t^3u\|_{C(\bar{\mathcal{J}};L^2(\Omega))}+\|f_t\|_{C(\bar{\mathcal{J}};L^2(\Omega))}+\|D_t^4u(t)\|_{L^1(\mathcal{J};L^2(\Omega))}\right)\Bigg]\end{aligned}$$

for $\boldsymbol{\theta} \neq \frac{1}{12}$ and

$$\max_{0\leq n\leq N-1} \|\Psi^n\| \leq C\Bigg[h^{m+1}\left(\|u_t\|_{C(\bar{\mathcal{J}};H^{m+1}(\Omega))} + \|f\|_{H^1(\mathcal{J};H^{m+1}(\Omega))} + \|u_{tt}\|_{L^1(\mathcal{J};H^{m+1}(\Omega))}\right) + \tau\left|\boldsymbol{\gamma} - \frac{1}{2}\right| \|D_t^3 u\|_{L^1(\mathcal{J};L^2(\Omega))} + \tau^4\left(\|D_t^5 u\|_{C(\bar{\mathcal{J}};L^2(\Omega))} + \|D_t^3 f\|_{C(\bar{\mathcal{J}};L^2(\Omega))} + \|D_t^6 u(t)\|_{L^1(\mathcal{J};L^2(\Omega))}\right)\Bigg]$$

for $\boldsymbol{\theta} = \frac{1}{12}$. Now the proof follows from the fact

$$\tau \sum_{n=0}^{N-1} \|\Psi^n\| \leq T \max_{0\leq n\leq N-1} \|\Psi^n\|$$

and Proposition 6.5.1. □

Now using Lemma 6.5.4, the following L^2 norm error estimate is obtained.

Theorem 6.5.1. *Let u^n and $\mathcal{U}^n$ solution of (6.1.1) and (6.4.1), respectively. For all $t \in (0, T]$, we have*

$$\max_{0\leq n\leq N} \|\mathcal{U}^n - u^n\| \leq C_1 h^{m+1} + C_2\tau^2$$

for $\boldsymbol{\theta} \neq \frac{1}{12}$ and

$$\max_{0\leq n\leq N} \|\mathcal{U}^n - u^n\| \leq C_3 h^{m+1} + C_4\tau^4$$

for $\boldsymbol{\theta} = \frac{1}{12}$, whenever $\boldsymbol{\gamma} = \frac{1}{2}$. For $\boldsymbol{\gamma} \neq \frac{1}{2}$, we have

$$\max_{0\leq n\leq N} \|\mathcal{U}^n - u^n\| \leq C_5 h^{m+1} + C_6\tau$$

for all $\boldsymbol{\theta}$. Here, the constants C_i, $i = 1 : 6$, are dependent on u_0, u, f and their derivatives and independent of mess size h and time step τ.

Proof. We divide the error as

$$\mathcal{U}^n - u^n := \xi^n + \eta^n,$$

where $\eta^n = R_h u^n - u^n$. By triangle inequality, Lemma 6.5.4 and Lemma 2.2.1, we get the desired results. □

6.6 Numerical Results

We illustrate some numerical experiments to verify the theoretical results discussed in the previous section. In particular, we will focus on the temporal orders of the proposed schemes (both two-level and three-level schemes) for the fully discrete approximation to the wave equation with high-order virtual element spatial discretization. For the spatial discretization, we have considered the Voronoi ($\mathcal{V}_h$) polygonal meshes. We show the three level scheme (6.4.1) for $\boldsymbol{\theta} = 1/12$ and $\boldsymbol{\gamma} = 1/2$ with initial approximation (6.4.6) produces a fourth-order accurate approximation, which is desired for higher order virtual element methods.

To ensure the order of convergence $O(h^{m+1})+O(\tau^s) = O(h^{m+1})$ in L^2 norm and $O(h^m)+O(\tau^s) = O(h^m)$ in H^1 semi-norm, we choose the time step $\tau = O(h^{\frac{m+1}{s}})$. Here, $m = 1, 2, 3$ is the polynomial degree of accuracy of the method and $s = 1, 2, 4$ is the order of the temporal scheme. In all the examples, we have consider the given model problem (6.1.1)-(6.1.2) with the coefficient $\sigma = I$, and the source function f and the data $\{u_0, v_0\}$ are chosen according to the choice of exact solution. The spatial domain Ω is considered as $(0, 1) \times (0, 1)$ and the temporal domain is taken to be $[0, 1]$.

Example 6.6.1. (**Two-level schemes**) We choose the exact solution to the model problem (6.1.1)-(6.1.2) as

$$u(x, y, t) = t^2 \sin(t) \sin(\pi x) \sin(\pi y).$$

We have considered the VEM algorithm with $m = 3$ for the spatial direction and the two-level schemes (6.4.8) with different value of $(\boldsymbol{\alpha}, \boldsymbol{\beta})$ for temporal discretization. We get a unconditionally stable second-order accurate (in time) implicit scheme for $(\boldsymbol{\alpha}, \boldsymbol{\beta})$=$(1/2, 1/2)$. Thus, for optimal convergence, we select the time step $\tau = h^2$ so that $O(h^4)+O(\tau^2) = O(h^4)$ for L^2 norm and $O(h^3) + O(\tau^2) = O(h^3)$ for H^1 semi-norm. For $(\boldsymbol{\alpha}, \boldsymbol{\beta}) = (0, 1)$ and $(\boldsymbol{\alpha}, \boldsymbol{\beta})$=$(1, 1)$, the scheme (6.4.8) is only first-order accurate in time and hence the time step τ is chosen to be $\tau = h^4$ for optimal convergence.

The history of errors and experimental orders of convergence (EOC) in both L^2 norm and H^1 semi-norm for different values of $(\boldsymbol{\alpha}, \boldsymbol{\beta})$ are shown in Table 6.6.1. It can be observed from the convergence plots in Figure 6.6.1 that the optimal convergence rates are obtained, that is, fourth-order in L^2 norm and third-order in H^1 semi-norm. This corroborates the theoretical prediction established in the last section.

Table 6.6.1: L^2 and H^1 errors at $T = 1$ for the two-level schemes in Example 6.6.1.

$(\boldsymbol{\alpha}, \boldsymbol{\beta})$	h	τ	$\|u - u_h\|$	EOC	$\|u - u_h\|_1$	EOC
$(0, 1)$	0.2500	$3.9000e-03$	$2.95789e-03$	-	$1.74835e-02$	-
	0.1768	$9.7656e-04$	$7.83219e-04$	3.8342	$5.53811e-03$	3.3171
	0.1250	$2.4414e-04$	$1.94802e-04$	4.0148	$1.78905e-03$	3.2604
	0.0884	$6.1035e-05$	$4.87774e-05$	3.9954	$6.27854e-04$	3.0214
	0.0625	$1.5259e-05$	$1.25016e-05$	3.9282	$2.16127e-04$	3.0771
$(1, 1)$	0.2500	$3.9000e-03$	$5.84773e-03$	-	$2.82509e-02$	-
	0.1768	$9.7656e-04$	$1.42758e-03$	4.0686	$7.65092e-03$	3.7692
	0.1250	$2.4414e-04$	$3.57158e-04$	3.9979	$2.23358e-03$	3.5525
	0.0884	$6.1035e-05$	$8.73198e-05$	4.0644	$7.08439e-04$	3.3133
	0.0625	$1.5259e-05$	$2.17715e-05$	4.0077	$2.30416e-04$	3.2408
$(1/2, 1/2)$	0.2500	$6.2500e-02$	$2.09897e-03$	-	$1.47766e-02$	-
	0.1768	$3.1200e-02$	$4.92310e-04$	4.1841	$4.82494e-03$	3.2295
	0.1250	$1.5500e-02$	$1.22349e-04$	4.0171	$1.66202e-03$	3.0752
	0.0884	$7.8000e-03$	$2.95606e-05$	4.0985	$6.03665e-04$	2.9222
	0.0625	$3.9000e-03$	$7.20311e-06$	4.0740	$2.11253e-04$	3.0295

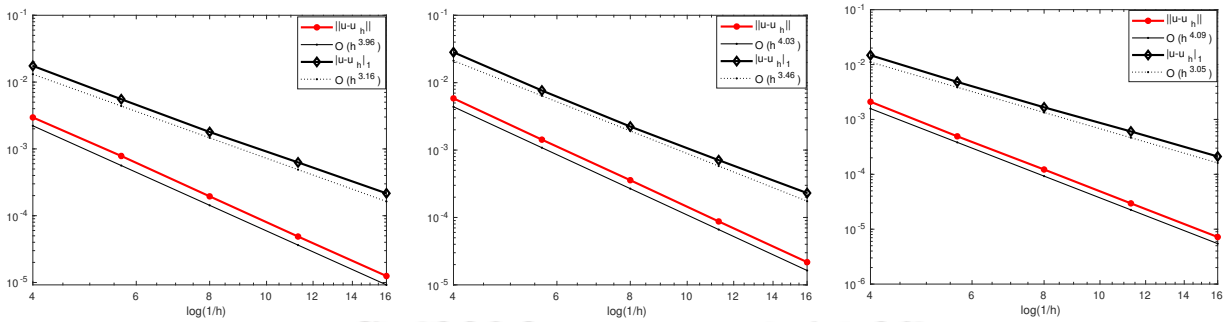

Figure 6.6.1: Log-log plots of the errors versus h at time $t = 1$ for $(\boldsymbol{\alpha}, \boldsymbol{\beta}) = (0, 1)$ (left), $(\boldsymbol{\alpha}, \boldsymbol{\beta}) = (1, 1)$ (center) and $(\boldsymbol{\alpha}, \boldsymbol{\beta}) = (1/2, 1/2)$ (right) in Example 6.6.1.

Example 6.6.2. (**Three-level schemes**) We consider the following smooth function as the exact solution to the model problem (6.1.1)-(6.1.2)

$$u(x, y, t) = t^4 \sin(t) \sin(\pi x) \sin(\pi y).$$

We have considered the VEM algorithm with $m = 3$ for the spatial direction and the three-level Newmark schemes (6.4.1) with different value of $(\boldsymbol{\gamma}, \boldsymbol{\theta})$ for temporal discretization. We get a unconditionally stable first-order accurate (in time) implicit scheme for $(\boldsymbol{\gamma}, \boldsymbol{\theta})$=$(3/2, 1)$. Thus, for optimal convergence, we select the time step $\tau = h^4$ so that $O(h^4) + O(\tau) = O(h^4)$ for L^2 norm and $O(h^3) + O(\tau) = O(h^3)$ for H^1 semi-norm. For $(\boldsymbol{\gamma}, \boldsymbol{\theta}) = (1/2, 0)$, the scheme (6.4.1) is conditionally stable second-order accurate in time and hence the time step τ is chosen to be $\tau = h^2/2$ for optimal convergence. For $(\boldsymbol{\gamma}, \boldsymbol{\theta}) = (1/2, 1/12)$, the scheme (6.4.1) is conditionally stable fourth-order accurate in time. We choose the time step to be $\tau = (0.1/48)h$ in order to satisfy the stability condition.

The history of errors and experimental orders of convergence (EOC) in both the L^2 norm and H^1 semi-norm for different values of $(\boldsymbol{\gamma}, \boldsymbol{\theta})$ are shown in Table 6.6.2. It can be observed from the convergence plots in Figure 6.6.2 that the optimal convergence rates are obtained, that is, fourth-order in L^2 norm and third-order in H^1 semi-norm. This corroborates the theoretical prediction established in Theorem 6.5.1.

Table 6.6.2: L^2 and H^1 errors at $T = 1$ for the three-level schemes in Example 6.6.2.

(γ, θ)	h	τ	$\|u - u_h\|$	EOC	$\|u - u_h\|_1$	EOC
	0.2500	$3.9000e-03$	$2.31231e-03$	-	$1.98548e-02$	-
$(3/2, 1)$	0.1768	$9.7656e-04$	$6.34597e-04$	3.7308	$7.02075e-03$	2.9996
	0.1250	$2.4414e-04$	$1.57872e-04$	4.0142	$2.44891e-03$	3.0390
	0.0884	$6.1035e-05$	$3.97882e-05$	3.9767	$9.07579e-04$	2.8641
	0.0625	$1.5259e-05$	$1.02001e-05$	3.9275	$3.23030e-04$	2.9807
	0.2500	$3.1500e-02$	$1.78212e-03$	-	$1.87559e-02$	-
$(1/2, 0)$	0.1768	$1.5500e-02$	$4.26714e-04$	4.1245	$6.70451e-03$	2.9683
	0.1250	$7.8000e-03$	$1.04393e-04$	4.0625	$2.39557e-03$	2.9695
	0.0884	$3.9000e-03$	$2.54335e-05$	4.0744	$8.97547e-04$	2.8326
	0.0625	$1.9000e-03$	$6.17970e-06$	4.0822	$3.21037e-04$	2.9665
	0.2500	$5.2083e-04$	$1.65991e-03$	-	$1.85333e-02$	-
$(1/2, 1/12)$	0.1768	$3.6828e-04$	$5.80883e-04$	3.0296	$6.92627e-03$	2.8399
	0.1250	$2.6042e-04$	$9.71528e-05$	5.1598	$2.38943e-03$	3.0708
	0.1000	$2.0833e-04$	$3.91559e-05$	4.0724	$1.23962e-03$	2.9410
	0.0625	$1.3021e-04$	$5.74314e-06$	4.0841	$3.20874e-04$	2.8755

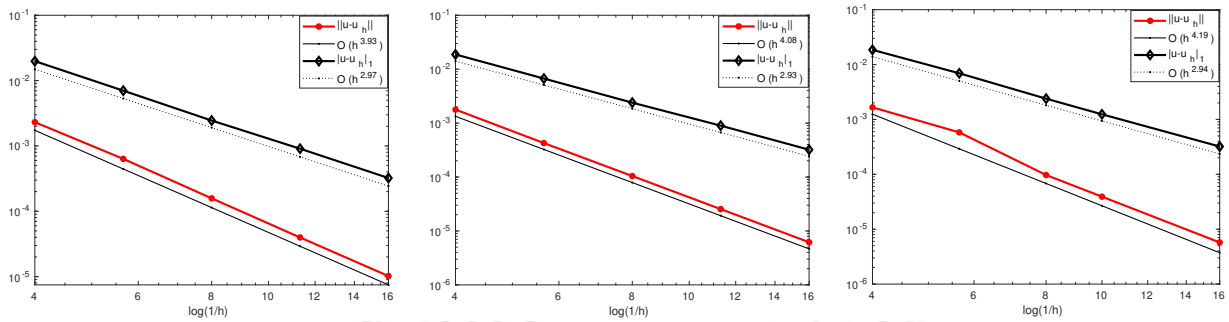

Figure 6.6.2: Log-log plots of the errors versus h at time $t = 1$ for $(\boldsymbol{\gamma}, \boldsymbol{\theta}) = (3/2, 1)$ (left), $(\boldsymbol{\gamma}, \boldsymbol{\theta}) = (1/2, 0)$ (center) and $(\boldsymbol{\gamma}, \boldsymbol{\theta}) = (1/2, 1/12)$ (right) in Example 6.6.2.

6.7 Conclusion

In this chapter, we have proposed a fully discrete virtual element method based on the general Newmark temporal discretization scheme for the wave equations. Optimal convergence results are derived for the semi-discrete virtual element approximation in both L^2 norm and H^1 semi-norm. We have presented both three-level and two-level Newmark based fully discrete schemes for the model problem and analysed the stability and convergence of the proposed schemes. Numerical experiments shows that the experimental order of convergence agrees with the theoretical results for all the proposed schemes. We have obtained a conditionally stable fourth-order algorithm by choosing $(\boldsymbol{\gamma}, \boldsymbol{\theta}) = (1/2, 1/12)$ in the three-level scheme (6.4.1). This will be helpful for higher-order VEM to preserve the accuracy obtained in the spatial direction.

7 Conclusion and Future Work

In this chapter, we highlight the significance of current thesis work and the corresponding results and techniques to derive them. We also provide information for the scope of possible extensions and future investigations.

7.1 Critical Review of the Results

In this work, we have presented newly introduced virtual element methods (VEMs) for various classes of problems obtained by choosing different values to the coefficients in the general linear second-order hyperbolic problems on polygonal meshes. The VEM for the general linear second-order hyperbolic problems can be constructed easily by following the ideas from the works presented in this thesis. We stress that the existing contributions on VEM dealing with hyperbolic problems with strong damping term either consider the damping coefficient to be constant or same as the diffusion coefficient. But, the case of variable coefficients when the damping coefficient is different from the diffusion coefficient, the standard elliptic projection operator is not sufficient to achieve an optimal convergence rate in L^2 norm as it can handle either the damping term or the diffusion term in the error analysis. Therefore, in this work, we have introduced a new non-standard projection operator which can handle the whole grad-grad part.

In Chapter 2, we have attempted to solve weakly damped wave equation with variable coefficients by introducing three discrete bilinear forms. The discrete bilinear forms in general do not satisfy the polynomial consistency and stability results. Additional analysis has been carried out to derive the consistency error estimates and the projection error estimate for the elliptic projection R_h . We have proved the stability of the semi-discrete solution

with respect to the initial data and the source function and derived the corresponding estimates which are very crucial to prove the optimal convergence rate of the fully discrete solution. Optimal order of convergence in both H^1 norm and L^2 norm is obtained for the semi-discrete approximation . For the fully discrete approximation, we have employed the Crank-Nicolson scheme to the first-order formulation of the model problem. It is shown that for the fully discrete scheme the discrete energy does not grow over time. Optimal convergence estimate is derived for the fully discrete approximation. Numerical examples with different types of domains and different types of polygonal meshes has been presented which shows the flexibility of the proposed method.

Chapter 3 deals with the virtual element approximation to the pulsed electric field model problems. These problems doesn't belongs to the well-known classes of partial differential equation and contains an additional strong damping term as compare to the Poisson problems. Optimal error estimates are derived for both semi-discrete and fully discrete schemes in L^2 and H^1 norms. The fully discrete scheme can be reinterpreted as the Crank-Nicolson discretization of the reformulation of the governing equation in the first-order system, as in Baker [13]. We have shown through some numerical examples that VEM is more cost-efficient than classical FEM by comparing the CPU time.

In Chapter 4, a new non-standard projection operator is defined in order to deal the whole grad-grad part of the second-order Sobolev equation. The new projection is motivated from the pulsed electric field problem and projection error estimate can be derived by following the idea of semi-discrete error analysis in the previous work. We have obtained optimal order of convergence, i.e., $O(h^m)$ in H^1 semi-norm and $O(h^{m+1})$ in L^2 norm, where m is the polynomial degree of the method, and h is the mesh size. For the optimal convergence estimate in L^2 norm the non-standard projection operator is used. For the temporal discretization, we have employed the second order Crank-Nicolson scheme and derived the optimal convergence estimates for the fully discrete scheme. We have illustrated some numerical experiments with various polynomial degree and shown that the experimental order of convergence agrees with the theoretical results.

Further in Chapter 5, we have extended the analysis in Chapter 4 to the viscoelastic wave equations and obtained optimal order of convergence for both the semi-discrete and fully discrete approximations. Numerical example with high-contrast coefficients is discussed.

In the last chapter, we have discussed a higher-order time stepping method for the standard wave equations along with virtual element discretization in spatial direction. We

have proposed the fully discrete schemes based on general Newmark method and detailed analyses on the stability and convergence of the proposed method has been carried out. The stability analysis is based on the energy method and we have shown that the discrete energy either converges or doesn't increase with time. The convergence analysis shows that we have up to forth-order convergence in time which is required for higher order methods. The theoretical results have been verified by numerical experiments.

7.2 Extensions and Remarks

In this section, we have mentioned some potential extensions of our findings. Here, we are briefly proposing some unexplored problems which can be considered as future scope of the thesis work.

VEM for Westervelt's quasi-linear acoustic wave equation: The Westervelt's wave equation, for the acoustic pressure u, is given by

$$(1-2ku)u_{tt} - c^2\Delta u - b\Delta u_t = 2ku_t^2. \tag{7.2.1}$$

In (7.2.1), the constant c denotes the speed of sound, b is the sound diffusivity, and $k = \beta_a/\lambda$, $\lambda = \varrho c^2$ is the bulk modulus, ϱ is the mass density and β_a the coefficient of nonlinearity of the medium. Our proposal is motivated by a increasing number of nonlinear ultrasound applications in medicine and industry. For more detailed discussion, we refer to [11, 95, 114] and references therein. Although substantial work has been dedicated to their analytical studies [58, 94] and their numerical treatment via finite element procedure (cf. [11, 58, 79, 114] just to name a few), rigorous error analysis for finite element methods of nonlinear acoustic phenomena is still largely missing from the literature. Recently, a priori error estimates for the classical finite element approximation of Westervelt's quasi-linear strongly damped wave equation (7.2.1) with linear elements have been discussed in [95]. Then, a high-order discontinuous Galerkin (DG) method for the equation (7.2.1) has been carried out in [11]. It is worthwhile to note that only the semidiscrete scheme (space discretization) has been discussed in [11, 95]. The fully discrete scheme (space-time discretization) error analysis is still open. In future, we would like to develop higher order virtual finite element schemes for the following initial boundary value problem (IBVP)

$$\begin{cases} u_{tt} - c^2\Delta u - b\Delta u_t = 2k(uu_{tt} + u_t^2), & \text{in } \Omega\times(0,T],\ T<\infty, \\ u = 0, & \text{on } \partial\Omega\times(0,T], \\ (u,u_t) = (u_0,u_1), & \text{on } \Omega\times\{t=0\}. \end{cases} \tag{7.2.2}$$

Here, $\Omega \subset \mathbb{R}^2$, is a convex polygonal domain with a Lipschitz boundary $\partial\Omega$.

A priori error analysis in [95] for the IBVP (7.2.2) heavily depends on a linearized problem

$$\begin{cases} \alpha(x,t)w_{tt} - c^2\Delta w - b\Delta w_t + \beta(x,t)w_t = f(x,t), & \text{in } \Omega \times (0,T],\ T < \infty, \\ w = 0, & \text{on } \partial\Omega \times (0,T], \\ (w, w_t) = (u_0, u_1), & \text{on } \Omega \times \{t = 0\}, \end{cases} \tag{7.2.3}$$

where $0 < \alpha_0 < \alpha(x,t) < \alpha_1$ in $\Omega \times (0,T]$ and f is a source function defined on $\Omega \times (0,T]$. For the linearized Westervelt's equation (7.2.3), we can borrow the error analysis that has been discussed in Chapter 5. Then, we can try to extend the convergence analysis technique that has been discussed in [95] for the IBVP (7.2.2).

Higher-order time stepping VEMs for time-dependent Maxwell's equations: In this thesis work, we primarily focus on scalar-valued problems. We can extend our methodologies and techniques to solve vector-valued problems as well. Consider the time-dependent Maxwell's equations of the following type (cf. [34]):

$$\varepsilon(\mathbf{x})\mathbf{E}_{tt} + \sigma(\mathbf{x})\mathbf{E}_t + \text{curl}\left(\frac{1}{\mu(\mathbf{x})}\text{curl }\mathbf{E}\right) = \mathbf{J}_t(\mathbf{x},t) \text{ in } \Omega \times (0,T]$$

with initial conditions

$$\mathbf{E}(\mathbf{x},0) = \mathbf{E}_0(\mathbf{x}) \quad \& \quad \mathbf{E}_t(\mathbf{x}.0) = \mathbf{E}_1(\mathbf{x}),$$

where $\mathbf{E}_1(\mathbf{x}) = \varepsilon(\mathbf{x})^{-1}\left(\mathbf{J}(\mathbf{x},0) + \text{curl }\mathbf{H}_0(\mathbf{x}) - \sigma(\mathbf{x})\mathbf{E}_0(\mathbf{x})\right)$ and boundary condition

$$\mathbf{E} \times \mathbf{n} = 0 \text{ on } \partial\Omega \times (0,T].$$

Here, $\mathbf{E}(\mathbf{x},t)$ is the electric field, $\varepsilon(\mathbf{x})$, $\sigma(\mathbf{x})$ and $\mu(\mathbf{x})$ are the dielectric coefficient, conductivity and magnetic permeability of the medium, respectively. Again, $\mathbf{J}(\mathbf{x},t)$ is the applied current density, $\mathbf{E}_0(\mathbf{x})$ and $\mathbf{H}_0(\mathbf{x})$ are the initial electric field and magnetic field, respectively. Maxwell's equations model many problems arising in science and industry, such as the diffraction of electromagnetic waves, microwave devices and plasma physics. The extension to vector-valued from scalar-valued will introduce additional complexities in both analysis and implementation.

Bibliography

[1] M. Abbaszadeh and M. Dehghan, *Interior penalty discontinuous Galerkin technique for solving generalized Sobolev equation*, Applied Numerical Mathematics, 154 (2020), pp. 172–186.

[2] D. Adak and E. Natarajan, *Analysis of nonconforming virtual element method for the convection diffusion reaction equation with polynomial coefficients*, arXiv preprint arXiv:1512.07359, (2015).

[3] D. Adak, E. Natarajan, and S. Kumar, *Convergence analysis of virtual element methods for semilinear parabolic problems on polygonal meshes*, Numerical Methods for Partial Differential Equations, 35 (2019), pp. 222–245.

[4] ——, *Virtual element method for semilinear hyperbolic problems on polygonal meshes*, International Journal of Computer Mathematics, 96 (2019), pp. 971–991.

[5] R. A. Adams and J. J. Fournier, *Sobolev spaces*, Elsevier, 2003.

[6] B. Ahmad, A. Alsaedi, F. Brezzi, L. D. Marini, and A. Russo, *Equivalent projectors for virtual element methods*, Computers & Mathematics with Applications, 66 (2013), pp. 376–391.

[7] K. Aki and P. G. Richards, *Quantitative seismology*, University Science Books, 2002.

[8] R. Alford, K. Kelly, and D. M. Boore, *Accuracy of finite-difference modeling of the acoustic wave equation*, Geophysics, 39 (1974), pp. 834–842.

[9] H. Ammari, D. Chen, and J. Zou, *Well-posedness of an electric interface model and its finite element approximation*, Mathematical Models and Methods in Applied Sciences, 26 (2016), pp. 601–625.

[10] H. Ammari, J. Garnier, L. Giovangigli, W. Jing, and J.-K. Seo, *Spectroscopic imaging of a dilute cell suspension*, Journal de Mathématiques Pures et Appliquées, 105 (2016), pp. 603–661.

[11] P. F. Antonietti, I. Mazzieri, M. Muhr, V. Nikolić, and B. Wohlmuth, *A high-order discontinuous galerkin method for nonlinear sound waves*, Journal of Computational Physics, 415 (2020), p. 109484.

[12] I. Babuška and J. Osborn, *Generalized finite element methods: Their performance and their relation to mixed methods*, SIAM Journal on Numerical Analysis, 20 (1983), pp. 510–536.

[13] G. A. Baker, *Error estimates for finite element methods for second order hyperbolic equations*, SIAM Journal on Numerical Analysis, 13 (1976), pp. 564–576.

[14] H. Bao, J. Bielak, O. Ghattas, L. F. Kallivokas, D. R. O'Hallaron, J. R. Shewchuk, and J. Xu, *Large-scale simulation of elastic wave propagation in heterogeneous media on parallel computers*, Computer Methods in Applied Mechanics and Engineering, 152 (1998), pp. 85–102.

[15] G. Barenblatt, Y. P. Zheltov, and I. Kochina, *Basic concepts in the theory of seepage of homogeneous liquids in fissured rocks*, Journal of Applied Mathematics and Mechanics, 24 (1960), pp. 852–864.

[16] L. Beirão da Veiga, F. Brezzi, A. Cangiani, G. Manzini, L. D. Marini, and A. Russo, *Basic principles of virtual element methods*, Mathematical Models and Methods in Applied Sciences, 23 (2013), pp. 199–214.

[17] L. Beirão da Veiga, F. Brezzi, L. D. Marini, and A. Russo, *The hitchhiker's guide to the virtual element method*, Mathematical Models and Methods in Applied Sciences, 24 (2014), pp. 1541–1573.

[18] ——, *Virtual element method for general second-order elliptic problems on polygonal meshes*, Mathematical Models and Methods in Applied Sciences, 26 (2016), pp. 729–750.

[19] L. Beirão da Veiga, K. Lipnikov, and G. Manzini, *Convergence analysis of the high-order mimetic finite difference method*, Numerische Mathematik, 113 (2009), pp. 325–356.

[20] R. C. Birkebak, W. Felts, and R. Harrison, *Heat transfer in biological systems*, International Review of General and Experimental Zoology, Volume 2, (1966), pp. 269–344.

[21] G. Böhme, *Non-Newtonian fluid mechanics*, Elsevier, 2012.

[22] J. Bonelle and A. Ern, *Analysis of compatible discrete operator schemes for elliptic problems on polyhedral meshes*, ESAIM: Mathematical Modelling and Numerical Analysis, 48 (2014), pp. 553–581.

[23] H. F. Bowman, E. G. Cravalho, and M. Woods, *Theory, measurement, and application of thermal properties of biomaterials*, Annual Review of Biophysics and Bioengineering, 4 (1975), pp. 43–80.

[24] S. C. Brenner, Q. Guan, and L.-Y. Sung, *Some estimates for virtual element methods*, Computational Methods in Applied Mathematics, 17 (2017), pp. 553–574.

[25] F. Brezzi, K. Lipnikov, and M. Shashkov, *Convergence of the mimetic finite difference method for diffusion problems on polyhedral meshes*, SIAM Journal on Numerical Analysis, 43 (2005), pp. 1872–1896.

[26] F. Brezzi and L. D. Marini, *Virtual element methods for plate bending problems*, Computer Methods in Applied Mechanics and Engineering, 253 (2013), pp. 455–462.

[27] C. R. Butson and C. C. McIntyre, *Tissue and electrode capacitance reduce neural activation volumes during deep brain stimulation*, Clinical Neurophysiology, 116 (2005), pp. 2490–2500.

[28] E. Cáceres and G. N. Gatica, *A mixed virtual element method for the pseudostress–velocity formulation of the Stokes problem*, IMA Journal of Numerical Analysis, 37 (2017), pp. 296–331.

[29] A. Cangiani, E. H. Georgoulis, and P. Houston, *hp-version discontinuous Galerkin methods on polygonal and polyhedral meshes*, Mathematical Models and Methods in Applied Sciences, 24 (2014), pp. 2009–2041.

[30] A. Cangiani, V. Gyrya, and G. Manzini, *The nonconforming virtual element method for the Stokes equations*, SIAM Journal on Numerical Analysis, 54 (2016), pp. 3411–3435.

[31] A. Cangiani, G. Manzini, and O. J. Sutton, *Conforming and nonconforming virtual element methods for elliptic problems*, IMA Journal of Numerical Analysis, 37 (2017), pp. 1317–1354.

[32] C. Cattaneo, *Sur une forme de l'equation de la chaleur eliminant la paradoxe d'une propagation instantantee*, Compte Rendus, 247 (1958), pp. 431–433.

[33] L. Chen and J. Huang, *Some error analysis on virtual element methods*, Calcolo, 55 (2018), pp. 1–23.

[34] P. Ciarlet, Jr and J. Zou, *Fully discrete finite element approaches for time-dependent maxwell's equations*, Numerische Mathematik, 82 (1999), pp. 193–219.

[35] B. Cockburn, W. Qiu, and M. Solano, *A priori error analysis for HDG methods using extensions from subdomains to achieve boundary conformity*, Mathematics of Computation, 83 (2014), pp. 665–699.

[36] G. Cohen and P. Joly, *Construction analysis of fourth-order finite difference schemes for the acoustic wave equation in nonhomogeneous media*, SIAM Journal on Numerical Analysis, 33 (1996), pp. 1266–1302.

[37] G. Cohen, P. Joly, J. E. Roberts, and N. Tordjman, *Higher order triangular finite elements with mass lumping for the wave equation*, SIAM Journal on Numerical Analysis, 38 (2001), pp. 2047–2078.

[38] D. Copeland, U. Langer, and D. Pusch, *From the boundary element domain decomposition methods to local Trefftz finite element methods on polyhedral meshes*, in Domain Decomposition Methods in Science and Engineering XVIII, Springer, 2009, pp. 315–322.

[39] L. C. Cowsar, T. F. Dupont, and M. F. Wheeler, *A priori estimates for mixed finite element approximations of second-order hyperbolic equations with absorbing boundary conditions*, SIAM Journal on Numerical Analysis, 33 (1996), pp. 492–504.

[40] L. C. Cowsat, T. F. Dupont, and M. F. Wheeler, *A priori estimates for mixed finite element methods for the wave equation*, Computer Methods in Applied Mechanics and Engineering, 82 (1990), pp. 205–222.

[41] L. B. Da Veiga, F. Brezzi, and L. D. Marini, *Virtual elements for linear elasticity problems*, SIAM Journal on Numerical Analysis, 51 (2013), pp. 794–812.

[42] L. B. da Veiga, F. Brezzi, L. D. Marini, and A. Russo, *Virtual element implementation for general elliptic equations*, in Building Bridges: Connections and Challenges in Modern Approaches to Numerical Partial Differential Equations, Springer, 2016, pp. 39–71.

[43] L. B. Da Veiga, K. Lipnikov, and G. Manzini, *Arbitrary-order nodal mimetic discretizations of elliptic problems on polygonal meshes*, SIAM Journal on Numerical Analysis, 49 (2011), pp. 1737–1760.

[44] L. B. da Veiga, K. Lipnikov, and G. Manzini, *The mimetic finite difference method for elliptic problems*, vol. 11 of MS&A. Modeling, Simulation and Applications, Springer, 2014.

[45] L. B. da Veiga and G. Manzini, *A higher-order formulation of the mimetic finite difference method*, SIAM Journal on Scientific Computing, 31 (2008), pp. 732–760.

[46] L. B. da Veiga and G. Manzini, *A virtual element method with arbitrary regularity*, IMA Journal of Numerical Analysis, 34 (2014), pp. 759–781.

[47] G. G. Dahlquist, *A special stability problem for linear multistep methods*, BIT Numerical Mathematics, 3 (1963), pp. 27–43.

[48] B. A. de Dios, K. Lipnikov, and G. Manzini, *The nonconforming virtual element method*, ESAIM: Mathematical Modelling and Numerical Analysis, 50 (2016), pp. 879–904.

[49] B. Deka and J. Dutta, *Convergence of finite element methods for hyperbolic heat conduction model with an interface*, Computers & Mathematics with Applications, 79 (2020), pp. 3139–3159.

[50] ——, *Finite element methods for non-fourier thermal wave model of bio heat transfer with an interface*, Journal of Applied Mathematics and Computing, 62 (2020), pp. 701–724.

[51] ——, *$L^\infty(L^2)$ and $L^\infty(H^1)$ norms error estimates in finite element methods for electric interface model*, Applicable Analysis, 100 (2021), pp. 1351–1370.

[52] B. Deka and P. Roy, *Weak Galerkin finite element methods for electric interface model with nonhomogeneous jump conditions*, Numerical Methods for Partial Differential Equations, 36 (2020), pp. 734–755.

[53] T. Dupont, *L^2-estimates for Galerkin methods for second order hyperbolic equations*, SIAM Journal on Numerical Analysis, 10 (1973), pp. 880–889.

[54] J. Dutta and B. Deka, *Optimal a priori error estimates for the finite element approximation of dual-phase-lag bio heat model in heterogeneous medium*, Journal of Scientific Computing, 87 (2021), pp. 1–32.

[55] J. Dutta, B. Deka, and N. Kumar, *Finite element methods for the electric interface model: Convergence analysis*, Mathematical Methods in the Applied Sciences, 43 (2020), pp. 4598–4613.

[56] R. E. Ewing, *Time-stepping Galerkin methods for nonlinear Sobolev partial differential equations*, SIAM Journal on Numerical Analysis, 15 (1978), pp. 1125–1150.

[57] T.-P. Fries and T. Belytschko, *The extended/generalized finite element method: an overview of the method and its applications*, International Journal for Numerical Methods in Engineering, 84 (2010), pp. 253–304.

[58] M. Fritz, V. Nikolić, and B. Wohlmuth, *Well-posedness and numerical treatment of the blackstock equation in nonlinear acoustics*, Mathematical Models and Methods in Applied Sciences, 28 (2018), pp. 2557–2597.

[59] A. L. Gain, C. Talischi, and G. H. Paulino, *On the virtual element method for three-dimensional linear elasticity problems on arbitrary polyhedral meshes*, Computer Methods in Applied Mechanics and Engineering, 282 (2014), pp. 132–160.

[60] F. Gao, J. Cui, and G. Zhao, *Weak Galerkin finite element methods for Sobolev equation*, Journal of Computational and Applied Mathematics, 317 (2017), pp. 188–202.

[61] F. Gao, J. Qiu, and Q. Zhang, *Local discontinuous Galerkin finite element method and error estimates for one class of Sobolev equation*, Journal of Scientific Computing, 41 (2009), pp. 436–460.

[62] F. Gao and X. Wang, *A modified weak Galerkin finite element method for Sobolev equation*, Journal of Computational Mathematics, (2015), pp. 307–322.

[63] F. Gardini and G. Vacca, *Virtual element method for second-order elliptic eigenvalue problems*, IMA Journal of Numerical Analysis, 38 (2018), pp. 2026–2054.

[64] E. Gekeler, *Linear multistep methods and Galerkin procedures for initial boundary value problems*, SIAM Journal on Numerical Analysis, 13 (1976), pp. 536–548.

[65] T. Geveci, *On the application of mixed finite element methods to the wave equations*, ESAIM: Mathematical Modelling and Numerical Analysis, 22 (1988), pp. 243–250.

[66] V. Giurgiutiu, *Structural health monitoring: with piezoelectric wafer active sensors*, Elsevier, 2007.

[67] O. Gorynina, A. Lozinski, and M. Picasso, *Time and space adaptivity of the wave equation discretized in time by a second-order scheme*, IMA Journal of Numerical Analysis, 39 (2019), pp. 1672–1705.

[68] W. M. Grill, *Modeling the effects of electric fields on nerve fibers: influence of tissue electrical properties*, IEEE Transactions on Biomedical Engineering, 46 (1999), pp. 918–928.

[69] M. J. Grote, A. Schneebeli, and D. Schötzau, *Discontinuous Galerkin finite element method for the wave equation*, SIAM Journal on Numerical Analysis, 44 (2006), pp. 2408–2431.

[70] M. J. Grote and D. Schötzau, *Optimal error estimates for the fully discrete interior penalty DG method for the wave equation*, Journal of Scientific Computing, 40 (2009), pp. 257–272.

[71] M. E. Gurtin and A. C. Pipkin, *A general theory of heat conduction with finite wave speeds*, Archive for Rational Mechanics and Analysis, 31 (1968), pp. 113–126.

[72] V. Gyrya and K. Lipnikov, *High-order mimetic finite difference method for dif-*

fusion problems on polygonal meshes, Journal of Computational Physics, 227 (2008), pp. 8841–8854.

[73] W. Hackbusch and S. A. Sauter, *Composite finite elements for the approximation of PDEs on domains with complicated micro-structures*, Numerische Mathematik, 75 (1997), pp. 447–472.

[74] G. H. Hardy, J. E. Littlewood, G. Pólya, G. Pólya, et al., *Inequalities*, Cambridge university press, 1952.

[75] J. S. Hesthaven, *High-order accurate methods in time-domain computational electromagnetics: A review*, Advances in Imaging and Electron Physics, 127 (2003), pp. 59–123.

[76] M. Ikawa, *Hyperbolic partial differential equations and wave phenomena*, vol. 189 of Translations of Mathematical Monographs, American Mathematical Society, 2000.

[77] E. W. Jenkins, B. Riviaere, and M. F. Wheeler, *A priori error estimates for mixed finite element approximations of the acoustic wave equation*, SIAM Journal on Numerical Analysis, 40 (2002), pp. 1698–1715.

[78] C. Johnson, *Discontinuous Galerkin finite element methods for second order hyperbolic problems*, Computer Methods in Applied Mechanics and Engineering, 107 (1993), pp. 117–129.

[79] Y. Kagawa, T. Tsuchiya, T. Yamabuchi, H. Kawabe, and T. Fujii, *Finite element simulation of non-linear sound wave propagation*, Journal of sound and vibration, 154 (1992), pp. 125–145.

[80] S. Kim and H. Lim, *High-order schemes for acoustic waveform simulation*, Applied Numerical Mathematics, 57 (2007), pp. 402–414.

[81] D. D. Kosloff and E. Baysal, *Migration with the full acoustic wave equation*, Geophysics, 48 (1983), pp. 677–687.

[82] P. Kumar, D. Kumar, and K. Rai, *A numerical study on dual-phase-lag model of bio-heat transfer during hyperthermia treatment*, Journal of Thermal Biology, 49 (2015), pp. 98–105.

[83] R. S. Lakes, *Viscoelastic solids*, vol. 9, CRC press, 1998.

[84] H. Li, Z. Zhao, and Z. Luo, *A space-time continuous finite element method for 2D viscoelastic wave equation*, Boundary Value Problems, 2016 (2016), pp. 1–17.

[85] Y. P. Lin, *A mixed type boundary problem describing the propagation of disturbances in viscous media I, weak solution for quasi-linear equations*, J. Math. Anal. Appl, 135 (1988), pp. 644–653.

[86] K.-C. Liu, Y.-N. Wang, and Y.-S. Chen, *Investigation on the bio-heat transfer with the dual-phase-lag effect*, International Journal of Thermal Sciences, 58 (2012), pp. 29–35.

[87] Q. H. Liu and Z. X. Zhang, *Traveling wave effect analysis on fabricated box girder bridge based on ansys*, in Applied Mechanics and Materials, vol. 587, Trans Tech Publ, 2014, pp. 1512–1517.

[88] K. J. Marfurt, *Accuracy of finite-difference and finite-element modeling of the scalar and elastic wave equations*, Geophysics, 49 (1984), pp. 533–549.

[89] K. Mitra, S. Kumar, A. Vedavarz, and M. Moallemi, *Experimental evidence of hyperbolic heat conduction in processed meat*, Journal of Heat Transfer, 117 (1995), pp. 568–573.

[90] A. Moiola, *Trefftz discontinuous Galerkin methods on unstructured meshes for the wave equation*, arXiv preprint arXiv:1505.00120, (2015).

[91] D. Mora, G. Rivera, and R. Rodríguez, *A virtual element method for the Steklov eigenvalue problem*, Mathematical Models and Methods in Applied Sciences, 25 (2015), pp. 1421–1445.

[92] L. Mu, J. Wang, and X. Ye, *Weak galerkin finite element method on polynomial meshes*, International Journal of Numerical Analysis & Modeling, 12 (2015), pp. 31–53.

[93] A. Narasimhan and S. Sadasivam, *Non-fourier bio heat transfer modelling of thermal damage during retinal laser irradiation*, International Journal of Heat and Mass Transfer, 60 (2013), pp. 591–597.

[94] V. Nikolić and B. Kaltenbacher, *On higher regularity for the westervelt equation with strong nonlinear damping*, Applicable Analysis, 95 (2016), pp. 2824–2840.

[95] V. Nikolic and B. Wohlmuth, *A priori error estimates for the finite element approximation of westervelt's quasi-linear acoustic wave equation*, SIAM Journal on Numerical Analysis, 57 (2019), pp. 1897–1918.

[96] K. Omrani, *The convergence of fully discrete Galerkin approximations for the Benjamin–Bona–Mahony (BBM) equation*, Applied mathematics and computation, 180 (2006), pp. 614–621.

[97] A. K. Pani and G. Fairweather, *H 1-Galerkin mixed finite element methods for parabolic partial integro-differential equations*, IMA Journal of Numerical Analysis, 22 (2002), pp. 231–252.

[98] H. Pascal, *Pressure wave propagation in a fluid flowing through a porous medium*

and problems related to interpretation of Stoneley's wave attenuation in acoustical well logging, International Journal of Engineering Science, 24 (1986), pp. 1553–1570.

[99] G. Pradhan and B. Deka, *High-order time stepping virtual element method for the wave equations on polygonal meshes*, Submitted, (2023).

[100] ——, *Optimal convergence analysis of the virtual element method for the second order Sobolev equations on polygonal meshes*, Submitted, (2023).

[101] ——, *Optimal convergence analysis of the virtual element method for the viscoelastic wave equations on polygonal meshes*, Submitted, (2023).

[102] ——, *Virtual element methods for pulsed electric field model problems on polygonal meshes*, AIP Conference Proceedings, 2819 (2023), p. 040006.

[103] G. Pradhan, J. Dutta, and B. Deka, *Virtual element methods for weakly damped wave equations on polygonal meshes*, Computational and Applied Mathematics, 42 (2023), p. 137.

[104] T. Qiu and C. Tien, *Short-pulse laser heating on metals*, International Journal of Heat and Mass Transfer, 35 (1992), pp. 719–726.

[105] P. Radu, G. Todorova, and B. Yordanov, *Higher order energy decay rates for damped wave equations with variable coefficients*, arXiv preprint arXiv:0811.2159, (2008).

[106] J. Rauch, *On convergence of the finite element method for the wave equation*, SIAM Journal on Numerical Analysis, 22 (1985), pp. 245–249.

[107] L. Rems, M. Ušaj, M. Kandušer, M. Reberšek, D. Miklavčič, and G. Pucihar, *Cell electrofusion using nanosecond electric pulses*, Scientific reports, 3 (2013), pp. 1–10.

[108] B. Riviere and M. F. Wheeler, *Discontinuous finite element methods for acoustic and elastic wave problems*, Contemporary Mathematics, 329 (2003), pp. 4–6.

[109] S. Rjasanow and S. Weisser, *Higher order bem-based fem on polygonal meshes*, SIAM Journal on Numerical Analysis, 50 (2012), pp. 2357–2378.

[110] J. C. Robinson, *Infinite-dimensional dynamical systems: An introduction to dissipative parabolic PDEs and the theory of global attractors*, vol. 28, Cambridge University Press, 2001.

[111] H.-G. Roos, M. Stynes, and L. Tobiska, *Robust numerical methods for singularly perturbed differential equations: convection-diffusion-reaction and flow problems*, vol. 24, Springer Science & Business Media, 2008.

[112] F. J. Sabadell, F. J. Serón, and J. Badal, *A parallel laboratory for simulation*

and visualization of seismic wavefields, Geophysical Prospecting, 48 (2000), pp. 377–398.

[113] K. H. Schoenbach, F. E. Peterkin, R. W. Alden, and S. J. Beebe, *The effect of pulsed electric fields on biological cells: Experiments and applications*, IEEE Transactions on Plasma Science, 25 (1997), pp. 284–292.

[114] I. Shevchenko and B. Kaltenbacher, *Absorbing boundary conditions for nonlinear acoustics: The westervelt equation*, Journal of Computational Physics, 302 (2015), pp. 200–221.

[115] D. Shi, *On the initial boundary value problem of nonlinear the equation of the moisture in soil*, Acta Mathematicae Applicatae Sinica, 13 (1990), pp. 33–40.

[116] D. Shi and Y. Zhang, *High accuracy analysis of a new nonconforming mixed finite element scheme for Sobolev equations*, Applied Mathematics and Computation, 218 (2011), pp. 3176–3186.

[117] G. R. Shubin and J. B. Bell, *A modified equation approach to constructing fourth order methods for acoustic wave propagation*, SIAM Journal on Scientific and Statistical Computing, 8 (1987), pp. 135–151.

[118] S. Singh, S. Singh, and Z. Li, *A high order compact scheme for a thermal wave model of bio-heat transfer with an interface*, Numerical Mathematics: Theory, Methods & Applications, 11 (2018), pp. 321–337.

[119] R. Sinkus, M. Tanter, T. Xydeas, S. Catheline, J. Bercoff, and M. Fink, *Viscoelastic shear properties of in vivo breast lesions measured by MR elastography*, Magnetic Resonance Imaging, 23 (2005), pp. 159–165.

[120] N. Sukumar and A. Tabarraei, *Conforming polygonal finite elements*, International Journal for Numerical Methods in Engineering, 61 (2004), pp. 2045–2066.

[121] O. J. Sutton, *The virtual element method in 50 lines of MATLAB*, Numerical Algorithms, 75 (2017), pp. 1141–1159.

[122] I. V. Suveyka, *Mixed problems for an equation for propagation of disturbances in viscous media*, Differentsial'nye Uravneniya, 19 (1983), pp. 337–347.

[123] A. Tabarraei and N. Sukumar, *Extended finite element method on polygonal and quadtree meshes*, Computer Methods in Applied Mechanics and Engineering, 197 (2008), pp. 425–438.

[124] C. Talischi, G. H. Paulino, A. Pereira, and I. F. Menezes, *Polygonal finite elements for topology optimization: A unifying paradigm*, International Journal for Numerical Methods in Engineering, 82 (2010), pp. 671–698.

[125] T. W. Ting, *A cooling process according to two-temperature theory of heat conduction*, Journal of Mathematical Analysis and Applications, 45 (1974), pp. 23–31.

[126] D. Tzou, *A unified field approach for heat conduction from macro-to micro-scales*, Journal of Heat Transfer, 117 (1995), pp. 8–16.

[127] D. Tzou and K. Chiu, *Temperature-dependent thermal lagging in ultrafast laser heating*, International Journal of Heat and Mass Transfer, 44 (2001), pp. 1725–1734.

[128] G. Vacca, *Virtual element methods for hyperbolic problems on polygonal meshes*, Computers & Mathematics with Applications, 74 (2017), pp. 882–898.

[129] G. Vacca and L. Beirão da Veiga, *Virtual element methods for parabolic problems on polygonal meshes*, Numerical Methods for Partial Differential Equations, 31 (2015), pp. 2110–2134.

[130] P. Vernotte, *Les paradoxes de la theorie continue de l'equation de la chaleur*, Compte Rendus, 246 (1958), pp. 3154–3155.

[131] M. Vohralík and B. I. Wohlmuth, *Mixed finite element methods: Implementation with one unknown per element, local flux expressions, positivity, polygonal meshes, and relations to other methods*, Mathematical Models and Methods in Applied Sciences, 23 (2013), pp. 803–838.

[132] E. L. Wachspress, *A rational finite element basis*, vol. 114 of Mathematics in Science and Engineering, Academic Press, Nework, 1975.

[133] X. Wang and J. Zou, *Identification of conductivity and permittivity in a pulsed electric field model*, Applicable Analysis, 95 (2016), pp. 2736–2749.

[134] H. Xia and Z. Luo, *Optimized finite difference iterative scheme based on POD technique for 2D viscoelastic wave equation*, Applied Mathematics and Mechanics, 38 (2017), pp. 1721–1732.

[135] Y. Xu, Z. Zhou, and J. Zhao, *Conforming virtual element methods for Sobolev equations*, Journal of Scientific Computing, 93 (2022), pp. 1–31.

[136] L. Yang, *Electrical impedance spectroscopy for detection of bacterial cells in suspensions using interdigitated microelectrodes*, Talanta, 74 (2008), pp. 1621–1629.

[137] Y. Yuan and H. Wang, *Error estimates for the finite element methods of nonlinear hyperbolic equations*, J Systems Sci Math Sci, 5 (1985), pp. 161–171.

[138] B. Zhang, J. Zhao, and S. Chen, *Virtual element method for the Sobolev equations*, Mathematical Methods in the Applied Sciences, 46 (2023), pp. 1266–1281.

[139] J. Zhao, B. Zhang, and X. Zhu, *The nonconforming virtual element method for parabolic problems*, Applied Numerical Mathematics, 143 (2019), pp. 97–111.